# GEOLOGY AND MINERAL RESOURCES OF THE ORTIZ MINE GRANT, SANTA FE COUNTY, NEW MEXICO

Open-file Report 560

By
Stephen R. Maynard

Consulting Geologist
1503 Central Ave., NW, Suite A
Albuquerque, NM 87104

New Mexico Bureau Geology & Mineral Resources
New Mexico Institute of Mining & Technology
Socorro, New Mexico 87801
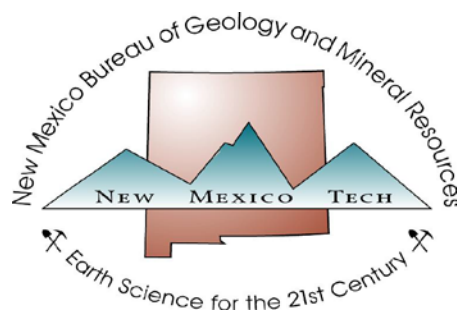
March 2014

ABSTRACT

The Ortiz Mine Grant, as defined by a patent issued by the US Congress in 1861, forms an approximately 10 mi x 10 mi tract centered on the old Ortiz Mine in the eastern part of the Ortiz Mountain range in the southwestern part of Santa Fe County, New Mexico. The Ortiz Mountains, physiographically and geologically, form part of a north-south trending mountain range known as the Ortiz Porphyry Belt that includes, from north to south, the Cerrillos Hills, the Ortiz Mountains, the San Pedro Mountains, and South Mountain.

Proterozoic basement rocks, consisting of amphibolite schist and quartzite, crop out in the southern part of the Little Tuerto Hills, in the southwestern part of the Ortiz Mine Grant. These rocks are similar to those exposed in the Monte Largo Hills, about 8 km (5 mi) to the south, and are believed to be approximately 1.6 billion years old.

Mississippian through Permian rocks are exposed in the northern part of the Little Tuerto Hills, in the San Pedro Mountains (on the Grant's southern margin), and on low ridges and in arroyo exposures in the area of Tuerto Arroyo, south of the Ortiz Mountains. Paleozoic rocks cumulative thickness is estimated at 745 m (2,450 ft).

Although somewhat obscured by faulting, intrusions of younger sills and stocks, and thermal metamorphism, there is a nearly complete section of Mesozoic rocks exposed in the Ortiz Mountains. Total thickness of the Mesozoic section measures about 2590 m (8515 ft).

The Paleocene Diamond Tail Fm and the Eocene Galisteo Fm. were deposited in a tectonic basin (the Galisteo Basin) that appears to have been controlled by Laramide movement on the Tijeras-Cañoncito Fault System (TCFS). More than 450 m (1500 ft) of the Paleocene Diamond Tail Formation is preserved in the Ortiz Graben. The Diamond Tail Fm is thickest in the Ortiz Graben, suggesting that the deepest part of the basin during the Paleocene lay in the Ortiz Mountains.

Igneous rocks on the Ortiz Mine Grant may be divided into an early calc-alkaline phase and a later slightly alkaline phase. The calc-alkaline phase is represented by extensive laccolithic intrusions of andesite porphyry that have been dated by $^{40}Ar/^{39}Ar$ at 34.29 – 35.79 Ma. The laccolithic intrusions occur at all stratigraphic levels. The alkaline phase is represented by stocks and dikes including augite monzonite, latite porphyry, and trachytic latite with $^{40}Ar/^{39}Ar$ ages ranging from 33.27 Ma to 31.68 Ma.

Volcanism associated with the igneous activity in the Ortiz Mountains is represented by the Dolores Gulch vent breccia or diatreme. Lavas and pyroclastic deposits of the Espinaso Fm are present only in the northeastern corner of the Grant; these represent the distal facies of volcanoes centered in the Ortiz Mountains, such as the Dolores Gulch vent, and others centered in the Cerrillos Hills and San Pedro Mountains . $^{40}Ar/^{39}Ar$ ages of the Dolores Gulch volcanic are 31.31 to 31.48 Ma, and thus correlate with the alkaline phase.

The major feature of the TCFS in the Ortiz Mountains, the Ortiz Graben, cuts the 34.29 – 35.79 Ma laccolithic intrusions, and is cut by the 33.27 Ma augite monzonite, the constraining its formation to a roughly 1 million-year period from 34.29 to 33.27 Ma. Mid-Tertiary movement resulted in left-lateral, down-to-the-north movement across the TCFS.

Mineralization in the Ortiz Mountains is mostly located along or adjacent to strands of the TCFS. Mineralization styles include skarn Au-Cu at Lukas Canyon and the Iron "Vein" prospect, open-space breccia fillings associated with a collapse breccia pipe at Carache Canyon and along margins of the Dolores Gulch volcanic vent or diatreme at the Cunningham Hill mine and Florencio prospect, veins at the old Ortiz and Candelaria mines, and porphyry Cu-Au

mineralization in upper Cunningham Gulch. Cross cutting relations at Carache Canyon suggest that the 31.56 – 32.20 Ma ^{40}Ar/^{39}Ar range of ages of adularia is the age of mineralization. This age is taken to be representative of all metallic mineralization in the Ortiz Mountains.

The Old Placers Mining District refers to placer and lode mineral deposits found in the Ortiz Mountains and its surroundings. Placer gold was discovered in Dolores Gulch, in the eastern part of the Ortiz Mountains, in the early 1820s. Lode deposits began to be developed by 1830. From the 1820s to the present (2014), artisanal prospecting, mineral exploration, and mining have resulted in the identification of several mineral prospects, identification of mineral resources at Lukas Canyon and Carache Canyon, and the extraction of 250,000 troy ounces of gold and about 50,000 troy ounces of gold at the Cunningham Hill and Old Ortiz Mines, respectively.

The old Ortiz Mine, on the northwest side of the Dolores vent breccia, was the original lode discovery in the area and is estimated to have produced about 50,000 troy ounces of gold at intervals from the late 1820s to the 1930s. The mine exploited a narrow magnetite/pyrite-filled fissure on 8 levels over 350 ft total depth.

At the Cunningham Hill mine gold and tungsten mineralization is hosted by open-space breccia formed principally in quartzite formed in sandstone of the Diamond Tail Fm immediately adjacent to a pyritic latite porphyry dike, and, to a lesser extent, in the Dolores Gulch volcanics. Gold occurs as fine, rarely visible, grains in fractures in pyrite. Tungsten occurs in scheelite in open spaces, along with pyrite, magnetite, hematite, and calcite gangue. The Cunningham Hill Mine operated from 1979 to 1987 and produced approximately 250,000 troy ounces of gold from 6 million short tons grading 0.055 oz/st. Tungsten was not recovered. About 12 million short tons of rock were removed as overburden or waste. Gold was extracted from the crushed ore by a cyanide leach - activated carbon adsorption - electroplating process.

Gold mineralization at Carache Canyon, outlined by an exploration campaign in the 1980s to early 1990s, occurs as coarse, commonly visible, grains with a gangue of pyrite, pyrrhotite, carbonate minerals, and lesser arsenopyrite, chalcopyrite, and sphalerite in open-space fractures along and outside of the southern and western margins of a collapse breccia pipe. Subsidence within the breccia pipe is estimated to be 120 to 240 m (400 to 800 ft).   The open spaces are best preserved in andesite porphyry sills and the Point Lookout sandstone, resulting in a series of "stacked" mineralized bodies separated by lower-grade Menefee and Upper Mancos shales.   A total resource of 1,169,000 troy ounces of gold contained in 16.7 million short tons at an average grade of 0.07 oz/st was published for Carache Canyon in 1991.

The gold-copper-bearing garnet-pyroxene skarn-altered Greenhorn limestone bed forms an east-dipping slope in the upper part of Lukas Canyon in the southwestern part of the Ortiz Mountains.   Resources of 180,000 troy ounces of gold and 15,000 short tons of copper contained in 5.44 million short tons grading 0.03 oz/st gold and 0.25% copper were published in 1991.

TABLE OF CONTENTS

LIST OF FIGURES

Introduction

Sedimentary rocks

Igneous rocks

Structural Geology

Economic Geology

Geophysics

Geological maps and cross sections (in pockets):

Plate 1: Geologic map of the Ortiz Mine Grant, Santa Fe County, New Mexico (1:24,000)

Plate 2: Ortiz Mine Grant cross sections (1:24,000)

Plate 3: Geologic map of the Cunningham Hill Mine

Maps generated by 1987 airborne geophysical survey (in pockets):

Plate 4: Pole-reduced total field magnetic, Ortiz Mine Grant.

Plate 5: First vertical derivative pole-reduced magnetics, Ortiz Mine Grant.

Plate 6: Apparent resistivity derived from electromagnetic survey, Ortiz Mine Grant.

Late 7: Very low frequency survey, Ortiz Mine Grant.

LIST OF TABLES

Introduction

Sedimentary rocks

Economic Geology

Geophysics

Isotopic dating

1) INTRODUCTION

LOCATION AND HISTORY

The Ortiz Mine Grant is located in southern Santa Fe County, New Mexico, about 20 miles south of the city of Santa Fe (**Figure 1-1**). The village of Golden, New Mexico, lies in the southwestern corner of the original Mine Grant. Madrid, New Mexico, lies within the northern part of the original grant. New Mexico state highway 14, runs from Tijeras to Santa Fe, cuts across the western part of the Ortiz Mine Grant from south to north, and links Golden and Madrid. Santa Fe County road 22 joins highway 14 about 5 miles north of Golden and meets Interstate Highway 25 at the Santo Domingo Pueblo exit, about 10 miles to the northwest.

This report refers to 1:24,000 geologic maps of the Golden, Captain Davis Mountain, Picture Rock, and Madrid 7.5-minute topographic maps (Maynard, 2000; Lisenbee and others, 2001; Maynard and others, 2001; and Maynard and others, 2002). These geologic maps have been produced by the StateMap program of the New Mexico Bureau of Geology and Mineral Resources. The position of these quadrangles relative to the Ortiz Mine Grant is indicated on **Figure 1-2**.

The Ortiz Mine Grant is one of the oldest mining areas in New Mexico and in the United States. Its legal status derives from the patenting of surface and mineral rights of an approximately 16-km by 16-km (10-mi by 10-mi) tract to the New Mexico Mining Company by the US Congress in 1861. Since the grant's original designation, the land comprising the grant has remained in private hands. Surface and mineral rights to parts of the grant were sold off, most notably the part of the Grant that overlaps the Mesita de Juana López Grant, which includes the Madrid area and its contained coalfields. Mineral estate owners sold surface rights to the rest of the Grant in 1947. The Ortiz Mine Grant includes the Old Placers and part of the New Placers mining districts as described by Elston (1967). This report covers the geology of the original Ortiz Mine Grant as delineated on U.S. Geological Survey topographic maps.

PURPOSE

This report on the geology of the Ortiz Mine Grant represents a compilation of work carried out by the exploration and development staff of LAC Minerals and Pegasus, along with studies done by the author, Gold Fields Mining Corporation, Conoco, Inc., and C.T. Griswold and G.R. Griswold, and others. The present describes the relationships of the mineral deposits with the stratigraphy and structural geology of the Grant, constrains timing and magnitude of movement on faults in the area, and places these relationships into the broader context of the geology of north-central New Mexico.

This report does not address matters of surface/mineral ownership, or legal descriptions of properties within or bordering the Ortiz Mine Grant.
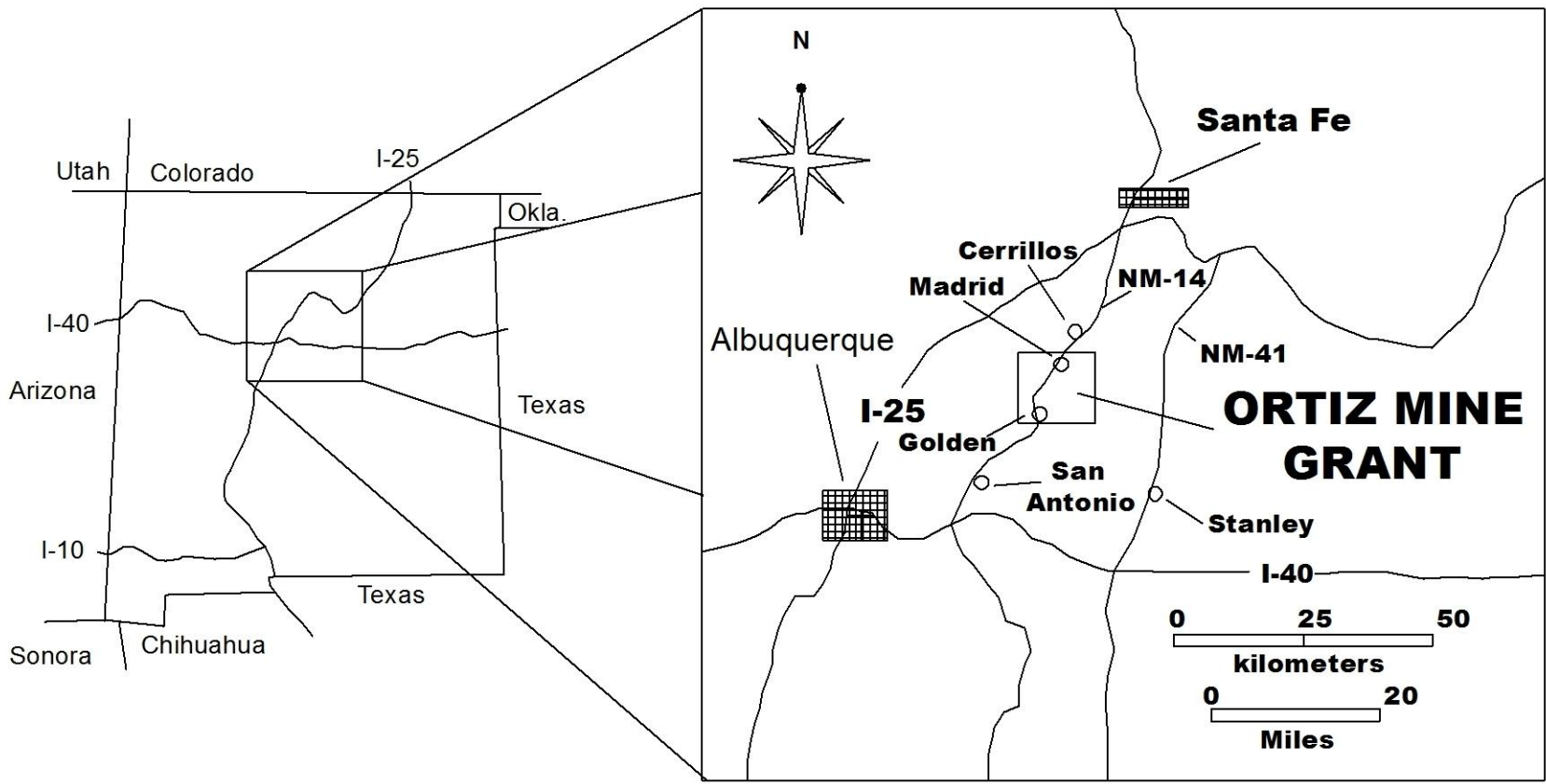
Figure 1-1. Location map of the Ortiz Mine Grant.
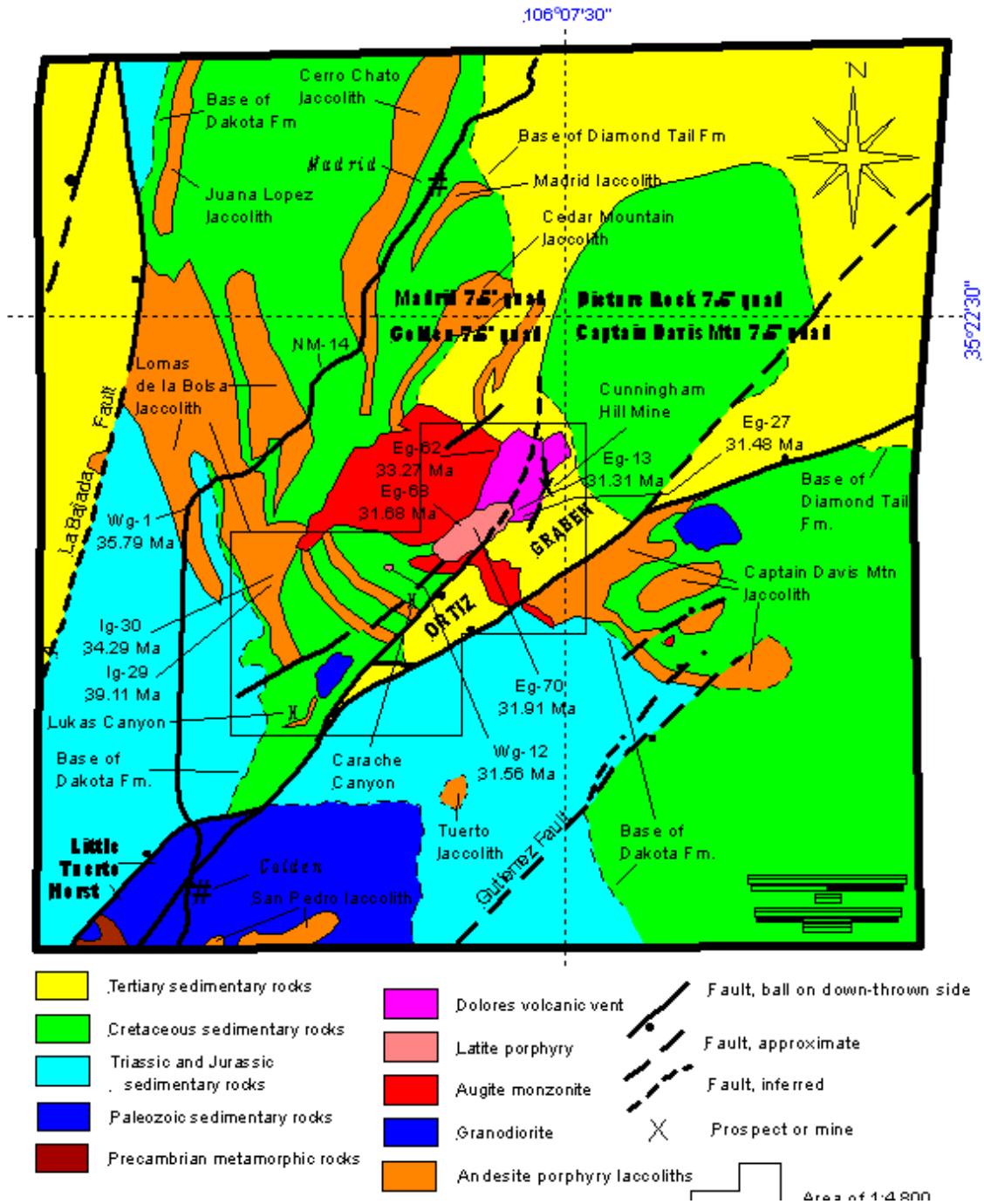
Figure 1-2. Simplified geologic map of the Ortiz Mine Grant

PREVIOUS WORK

Geological investigations pertaining to the Ortiz Mine Grant draw a great deal from comparison with studies in other parts of the Ortiz Porphyry Belt. These investigations, especially in the 19th century, owed their impetus to the work of prospectors and miners. Francisco Ortiz's discovery of lode gold in 1828 and his subsequent collaboration with a Spanish-trained mining engineer, Don Cano, started the modern era of focused investigation on the Ortiz Mine Grant. Townley (1968 and 1971), Milford (1995), and Baxter (2004) describe the events leading up to and following Ortiz's discovery.

Johnson (1903) presents a summary of 19th century investigators in the region of the Cerrillos Hills, many of whom also visited the Ortiz Mountains. Much of the early attention to the Ortiz Mountains focused on the placer and lode gold deposits in the Dolores Gulch area (Wislizenus, 1846; Abert, 1846; and Raymond, 1869 *a or b*). Further mining-related commentaries on the Ortiz Mountains during the latter half of the 19th century and first decades of the 20th century generally included descriptions of deposits in the San Pedro Mountains and the Cerrillos Hills. Jones (1904), Lindgren and Graton (1906) and Lindgren and others (1910) described the workings and production in the Dolores Gulch area. Yung and McCaffrey (1903) and Keyes (1909) described the copper-gold skarn mineralization at Lukas Canyon.

Several authors made detailed descriptions in unpublished reports of the Ortiz Mine and nearby prospects during the early part of the 20th century. Crane (1937) described the geology of Cunningham Hill. Jones (1935) and Perry and Moehlman (1938) reported on gold deposits on the Ortiz Mine Grant.

Academic descriptions of the geology of the region began with Marcou's expedition in 1853 (Marcou, 1858). Subsequently, Hayden (1869) described the red beds of the Galisteo "sands" and the Santa Fe Marl. Johnson (1903) was the first to describe laccoliths as being characteristic of the Ortiz Porphyry Belt. Ogilvie (1905, 1908) and Keyes (1909, 1918, and 1922) advanced the laccolith idea, though they did not distinguish between different intrusive rock types in the region. Ogilvie described the high-altitude conoplain (1905) and nepheline-bearing intrusive rocks (1908).

Stearns (1943, 1953a, 1953b, 1953c) formally described the Tertiary Galisteo and Espinaso Formations, and Tuerto Gravels; and the Upper Cretaceous rocks of the Galisteo-Tonque area surrounding the Ortiz Mine Grant. Stearns detailed different igneous rock types and proposed a non-laccolithic model in the Cerrillos Hills. Though Stearns' work did not specifically include the Ortiz Mine Grant, his stratigraphic and structural framework of the area laid much of the foundation for the present-day understanding of the geology of the Grant.

Coal deposits of the region, particularly those at Madrid attracted the attention of Johnson (1903) and Lee (1913), who described the Cerrillos (Madrid) coal field, as did Read and others (1950), Turnbull and others (1951), Beaumont (1964 and 1979), Bachman (1976), and Beaumont and others (1976). Gardner (1908) described more isolated coal fields in the region.

Griswold, in an unpublished report to Ortiz Mines, Inc., made the first systematic inventory of the mineral prospects of the Ortiz Mine Grant and placed them in a geologic framework (Griswold, 1950). C.T. Griswold and his son, G.R.Griswold, prepared the first geologic map of the Grant and described the occurrence of Paleozoic and Mesozoic rocks. They considered all the sandstone of the southern margin the of Ortiz Mountains to belong the Mesaverde Group. The Griswolds' work represented the first accurate resource estimates at

Lukas Canyon and Cunningham Hill, and recognized the potential for gold mineralization at Carache Canyon.

Bachman's (1975) map of the 1:62,500 Madrid quadrangle covered the entire Ortiz Mine Grant. Bachman's map grouped all the intrusive rocks of the Ortiz Porphyry Belt together as a laccolithic complex. Bachman indicated approximately 5 kilometers (3 miles) of left-lateral stratigraphic separation on the Tijeras-Cañoncito fault system in the Ortiz Mountains and showed outcrops of Mesaverde Group Galisteo Formation sedimentary rocks in a graben bounded by two principal strands of the fault system. Bachman and Mehnert (1978) presented the first published K-Ar dates on rocks of the region, establishing an Oligocene age for intrusive activity in the Ortiz Porphyry Belt.

Master's theses conducted on and near the Ortiz Mine Grant include Emerick's (1950) study of the Golden area, and Peterson's (1958) and McCrae's (1958) studies of the Ortiz Mountains. Kay (1986) studied gold mineralization in the area of the then-operating Cunningham Hill Mine. Kay's work included fluid-inclusion studies, and K-Ar age dating of the host rocks and mineralization and alteration. Coles (1990) examined the alteration and mineralization at Carache Canyon, and documented the petrologic distinctions of the calc-alkaline and alkaline intrusive rocks of the Ortiz Mine Grant. Schroer (1994) reported on the copper-gold skarn mineralization at Lukas Canyon. The latter three masters' theses benefited from sponsorship by the mining companies exploring the Grant and access to these companies' exploration data. This study relies heavily on data and many interpretations made by Coles (1990), Schroer (1994), and Kay (1986.)

Picha's (1982) descriptions of Phanerozoic stratigraphy of the Hagan Basin were used as a basis for correlations in the Ortiz Mountains. Gorham's (1979) and Lucas' (1982) work on the Galisteo Formation in the Hagan Basin and Cerrillos area led to recognition of the wide distribution of Tertiary sedimentary rocks in the Ortiz Mountains.

Other studies of mineralization and related intrusive complexes in the Ortiz Porphyry Belt considerably enhanced understanding of the Grant's geology. Atkinson (1961) and Disbrow and Stoll (1957) studied the geology of the San Pedro Mountains and Cerrillos Hills, respectively. Both studies described igneous successions similar to that observed on the Ortiz Mine Grant. Akright (1979) and Wargo (1964) reported on a gold-bearing copper porphyry deposit in the Cerrillos Hills. Thompson (1963) studied the geology of the South Mountain intrusive.

The Tijeras-Cañoncito fault system has been studied by many workers. Fulp and others (1982) documented the relationship of mineralization in Precambrian rocks to the Tijeras-Cañoncito fault system in the Manzanita-Northern Manzano Mountains. Woodward (1984) illustrated the relationship of the Tijeras-Cañoncito fault system to mid-Tertiary mineralization. Abbott (1995) studied exposures of the Tijeras-Cañoncito Fault System to the southwest and northeast of the Ortiz Mine Grant and documented its Laramide and Quaternary activity. Kelson and others (1998 and 1999) and Koehler and Kelson (2000) assessed seismic risk along the Tijeras-Cañoncito fault system.

Water supply and mine-working dewatering problems on the Ortiz Mine Grant have been addressed by Summers (1977) and Shomaker (1995).

GEOGRAPHIC SETTING

Physiography
The Ortiz Mine Grant lies in the Mexican Highland Section of the Basin and Range Physiographic Province (**Figure 1-3**).

The most important physiographic features of the Ortiz Mine Grant are the Ortiz Mountain Range and the surrounding gently sloping gravel-covered surface, known as the Ortiz Surface (Stearns, 1953b) (**Figures 1-3, 1-4, 1-5, 1-6, 1-7, 1-8**). The Ortiz Mine Grant occupies the lower, northern, foothills of the San Pedro Mountains along its southern edge. The Range and its outliers, Captain Davis Mountain, Lone Mountain, Las Lomas de la Bolsa and Cerro Chato, occupy approximately 40% of the Ortiz Mine Grant. Elevations in the Ortiz Mountains range from 1,964 m (6,500 ft) to 2,688 m (8,897 ft) at the summit of Placer Mountain. Numerous deep canyons incise the range and drain it in a roughly radial pattern.
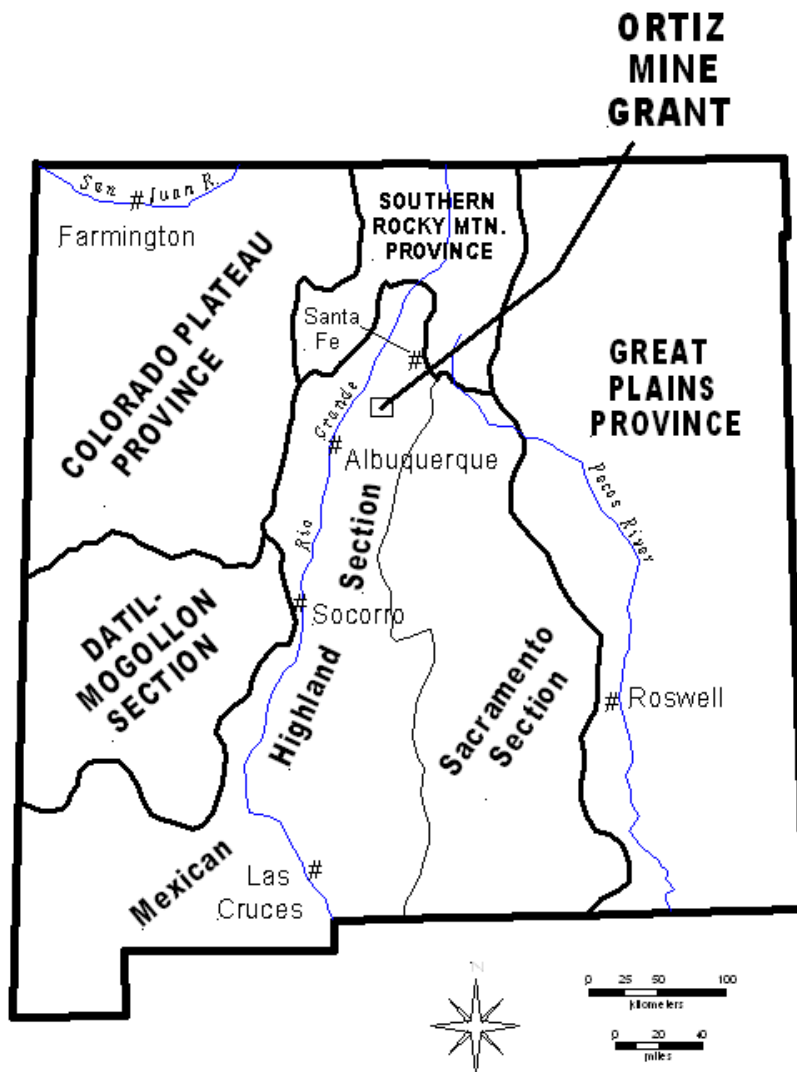
Figure 1-3. Map of New Mexico, showing major physiographic divisions. Modified after NM Geological Society (1982).

No perennial streams exist on the Ortiz Mine Grant, with the exception of Galisteo Creek, which crosses the northeastern corner of the Grant. Drainages that are fed from north-facing mountain slopes may have runoff for a few weeks in the late winter or spring. All arroyos and canyons are capable of heavy flow during summer downpours.

Drainages in the eastern and northern part of the Grant area incised and flow to the Galisteo River to the north. Tuerto Arroyo, which drains the southwestern part of the Grant, becomes progressively more incised to the west. It drains to Tonque Arroyo, which in turn empties into the Rio Grande on the San Felipe Indian Reservation.

The Ortiz Surface ranges in elevation from about 1,843 m (6,100 ft) in the northwestern part of the Grant to about 2,205 m (7,300 ft) on the southern flank of the Ortiz Mountains. The Ortiz Surface surrounds the Ortiz Mountains and slopes away from the range in all directions. To the southeast of the Ortiz Mountains, the Ortiz Surface merges with the surface of the Estancia Valley. The Plio-Pleistocene Tuerto Gravel, ranging from 0 to 30 m (0 to 100 ft) thick, covers the Ortiz Surface. Ogilvie (1905) coined the term "conoplain" to describe this geomorphic feature of the Ortiz Mountains.

Figure 1-4. Map of the Ortiz Mine Grant, showing principal geomorphic divisions and drainage pattern.

Figure 1-5. View of southern part of the Ortiz Mountains, as seen from NM-14 about 1.5 km south of Golden, NM. Pliocene-Pleistocene Tuerto Gravel covers gently sloping Ortiz Surface at foot of mountains.
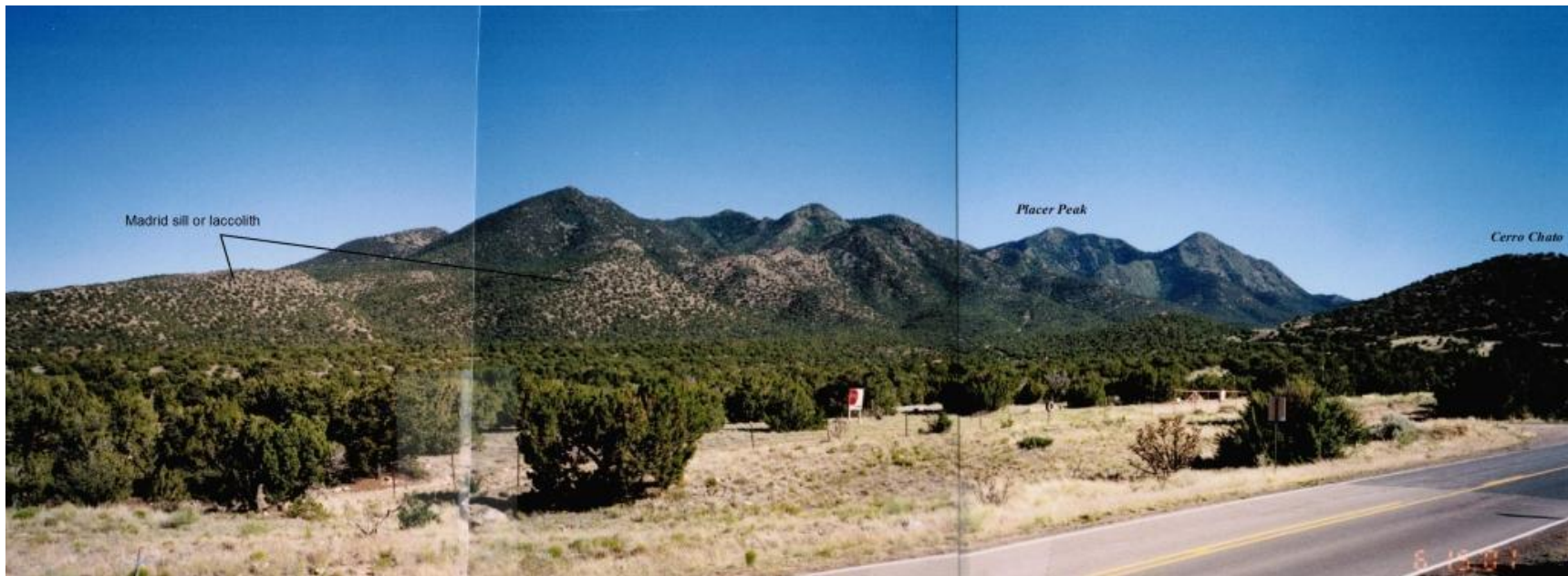
Figure 1-6. View of the northwestern part of the Ortiz Mountains, as seen from NM-14, about 1.5 km south of Madrid, NM. Highest peaks are composed of late Oligocene augite monzonite. High hill on left background is composed of Paleocene Diamond Tail Fm. Lower ridge in left middle ground, and Cerro Chato on right held up by Oligocene andesite porphyry.
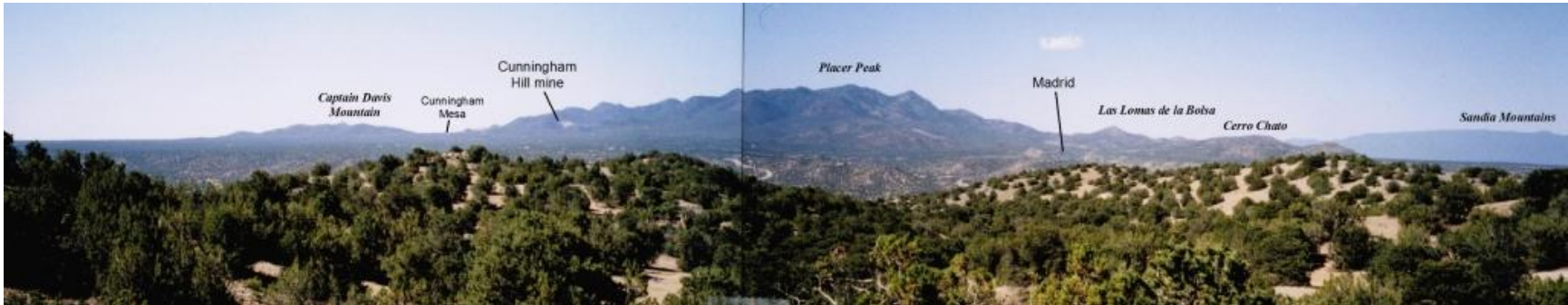
Figure 1-7. Ortiz Mountains as seen from Cerrillos Hills. Note plain sloping away from Ortiz Mountains ("conoplain" of Ogilvie, 1904).
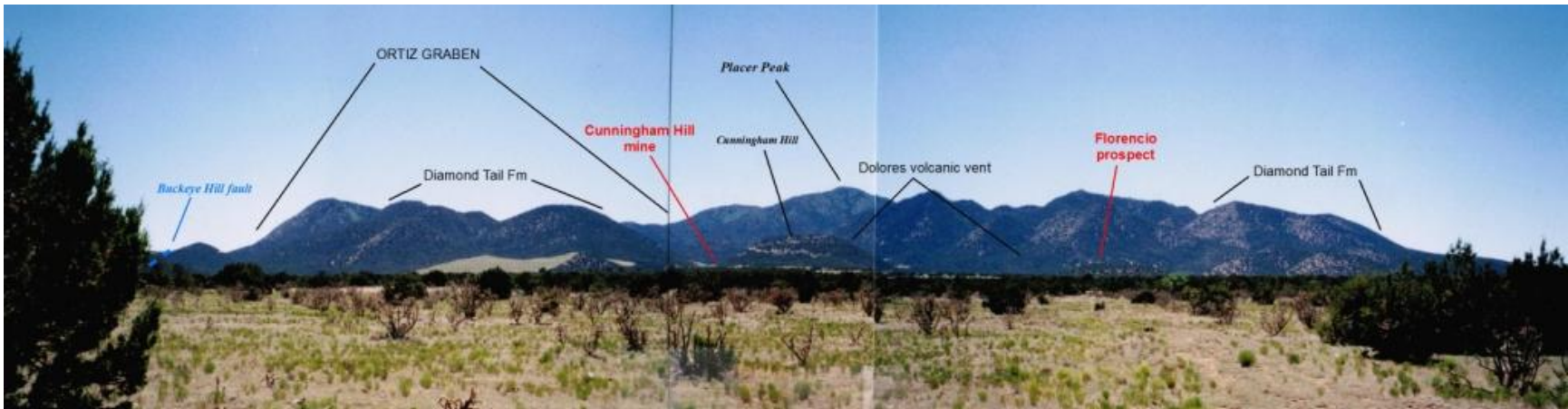
Figure 1-8. Northeastern part of the Ortiz Mountains from Cunningham Mesa. Light-colored hillside to left is reclaimed tailings pile from 1979-1987 mining operation at Cunningham Hill mine. Soil developed on Tuerto Gravel in foreground was partially scraped off for use in reclamation of the Cunningham Hill mine.

Climate

The Ortiz Mine Grant's weather is typical of the semi-arid central highlands of New Mexico. Precipitation is generally light with large variations in annual totals. Much of the precipitation occurs as late-summer thunderstorms. Climate data is recorded at Golden, New Mexico (Table 1-1). Winter precipitation usually occurs as snow. Typical snowfalls are a few inches, though storms have left as much as 18 inches with considerably higher accumulations at higher elevations. Snow pack on higher north-facing slopes in the Ortiz Mountains can exceed 5 feet in late winter.

Table 1-1. Average precipitation in inches at Golden, New Mexico. Data from Elliot (1991).

Month	1979 – 1989	1944-1981
January	0.89	0.61
February	0.86	0.66
March	1.18	0.86
April	1.25	0.58
May	1.54	0.98
June	1.37	0.74
July	1.54	2.28
August	1.76	2.44
September	2.40	1.18
October	1.85	0.92
November	0.99	0.56
December	0.79	0.69
Total	**16.42**	**12.50**

Vegetation and wildlife

Vegetation on the Ortiz Mine Grant occurs in six groupings, or plant communities (Table 1-2). The distribution of plant types reflects the general lack of surface water. Cottonwoods and willow grow near springs or where roots reach ground water along ephemeral streambeds. Isolated stands of aspens occur on a few talus-covered north-facing slopes at elevations above about 2,425 m (8,000 ft) in the Ortiz Mountains, indicating that the ground under the talus contains significant moisture.

Mule deer and coyotes are the most common large wild mammals in and around the Ortiz Mine Grant. Badgers, black bears, and mountain lions have been noted as well. Small mammals include various mouse and rat species, chipmunks, and squirrels. Reptiles include the western fence lizard and rattlesnakes. Common birds include the rufus-sided towhee, Bewick's wren, piñon jay, scrub jay, ash-throated flycatcher, house finch, mountain chickadee, white-breasted nuthatch, Stellar's jay, and western wood-peewee. Ravens are commonly sighted on the Ortiz Mine Grant, as are red-tailed hawks. Detailed studies of wildlife populations of the Ortiz Mine Grant were reported by Metric Corporation (1991).

Table 1-2.   Vegetation of the Ortiz Mine Grant (Elliot, 1991).

Plant Community	Dominant Species	Terrain
Blue Grama/Broom Snakeweed	Blue grama, broom snakeweed, galleta	Flat, lower elevations, southern and southeastern part of OMG.
Pinon/Gambel oak	Pinon, one-seed juniper, Gambel oak, muttongrass, junegrass.	North and east slopes at higher elevations,
Mixed confer/Gambel oak	Douglas fir, white fir, one-seed juniper, pinon.	Highest north and east slopes and narrow zones along certain incised drainage bottoms.
Pinon/one-seed juniper/ blue grama/muttongrass	Pinon, one-seed juniper, blue grama, yucca	Rolling and gently sloping terrain below 7500 feet elevation
One-seed juniper/ grama grasses	Yucca, prickly pear, cane cholla, one-seed juniper, and grama grasses.	Rocky southern exposures, 7,000 to 7,800 feet elevations
Rubber rabbitbrush/ sand dropseed	Rubber rabbitbrush (chamisa), sand dropseed, blue grama, cane cholla, kochia, cottonwood, Siberian elm, and coyote willow.	Flood plain terraces of ephemeral drainages

Land use

The steeper portions of the Ortiz Mountains are covered in forest and scrub and receive only light human impact. The effects of mineral exploration, mainly drill pads and access roads, have been largely mitigated by reclamation. At the Cunningham Hill Mine site, LAC Minerals, USA, Inc., has carried out larger-scale reclamation. Cattle are grazed on the Ortiz Mine Grant on the Lone Mountain Ranch, the Ortiz Mountain Ranch, and on some smaller parcels in the northeastern portion of the Mine Grant. Most of the acreage of the Ortiz Mine Grant lies within the Lone Mountain, Ortiz Mountain, and Dolores Ranches. Much of the remaining acreage has been subdivided into lots ranging from a few to a few tens of acres.

Griswold participated in the first systematic study of the Ortiz Mine Grant with his father, C.T. Griswold, in the late 1940s. Gil continued to represent the interests of Ortiz Mines until the early 1990s. His long-term efforts to promote the development of the Ortiz Mine Grant's mineral resources had a key role in the development of understanding of the Grant's geology.

2 SEDIMENTARY ROCKS

The entire stratigraphic section of north-central New Mexico appears on the Ortiz Mine Grant (Table 2-1). The Eocene Galisteo Formation is preserved in the northeastern part of the Mine Grant. The Ortiz Graben preserves about 300 m (1000 ft) of Paleocene(?)-Eocene Diamond Tail Formation. The Galisteo Monocline tilts Triassic and younger sedimentary rocks 10 to 30 degrees to the east north of the Tijeras-Cañoncito Fault System. Paleozoic sedimentary rocks are exposed in the San Pedro Mountains and in the northern portion of the Little Tuerto Hills. Precambrian metamorphic rocks core the Little Tuerto Hills; their descriptions are included in this section. Certain stratigraphic units are important host rocks for mineralization and thus may serve as guides for further exploration.
Faulting, intrusive activity, and metasomatic processes considerably complicate identification of sedimentary units in parts of the Ortiz Mine Grant. Oligocene intrusive rocks consist of laccoliths of andesitic composition of calc-alkaline affinity and later latitic to monzodioritic stocks and dikes of alkaline affinity. Laccoliths and sills are widespread and considerably inflate the stratigraphic section. The present synthesis derives from detailed core drilling and geologic mapping, and comparison of those findings to well-described and understood stratigraphic sections in the Hagan Basin (Black, 1979; Picha, 1982) and along Galisteo Creek (Bachman, 1975, 1976; Lucas and others, 1998; Lucas and others, 1999).

PRECAMBRIAN METAMORPHIC ROCKS

Precambrian rocks exposed on the Ortiz Mine Grant are limited to exposures in the Little Tuerto Hills southwest of the village of Golden. The rock types present, quartzite and amphibolite schist, are similar to rocks exposed in the Monte Largo Hills, about 6 km (4 mi) to the southwest and described by Huzarski (1971), Timmons and others (1995), and Ferguson and others (1999). The Precambrian outcrop in the Little Tuerto Hills forms the core of a northeast-trending horst block 760 m (2500 ft) and 3,600 m (12,000 ft) long.   The northern part of the horst block is expressed as a northeast-plunging anticline formed by the Madera Formation.

Amphibolite schist
Black, strongly lineated amphibolite schist crops out on the west flank of the Little Tuerto Hills near the south border of the Ortiz Mine Grant. Foliation strikes uniformly to the northeast and dips steeply northwest **(Figure 2-1)**.

Quartzite
White to tan, rarely micaceous quartzite with occasional iron-oxide-rich bands marking compositional layering is exposed in the southern part of the Little Tuerto Hills. The compositional layering indicated by iron-oxide bands strikes northeast and dips steeply to the northwest **(Figure 2-2)**.

Table 2-1. Stratigraphy of the Ortiz Mine Grant area.

Era	Period	Epoch/Series	Group	Formation	Member
CENOZOIC		QUATERNARY	Alluvium, colluvium, fan & terrace deposits		
CENOZOIC	TERTIARY	PLIOCENE	Santa Fe Group	Tuerto Gravel	
CENOZOIC	TERTIARY	PLIOCENE / MIOCENE	Santa Fe Group	Pre-Ortiz Surface Santa Fe Group sediments	Ogallala Formation?
CENOZOIC	TERTIARY	OLIGOCENE	Espinaso Formation – Ortiz Porphyry Belt Magmatism		
CENOZOIC	TERTIARY	EOCENE	Galisteo Formation		
CENOZOIC	TERTIARY	PALEOCENE	Diamond Tail Formation		
MESOZOIC	CRETACEOUS	UPPER	Mesaverde Group	Menefee Formation	Upper Menefee Member
MESOZOIC	CRETACEOUS	UPPER	Mesaverde Group	Menefee Formation	Harmon Sandstone Member
MESOZOIC	CRETACEOUS	UPPER	Mesaverde Group	Menefee Formation	Lower Menefee Member
MESOZOIC	CRETACEOUS	UPPER	Mesaverde Group	Point Lookout Sandstone	
MESOZOIC	CRETACEOUS	UPPER	Mancos Shale	Upper Mancos Shale Member	
MESOZOIC	CRETACEOUS	UPPER	Mancos Shale	Hosta-Dalton Sandstone Tongue	
MESOZOIC	CRETACEOUS	UPPER	Mancos Shale	Niobrara Member	
MESOZOIC	CRETACEOUS	UPPER	Mancos Shale	Juana Lopez Member	
MESOZOIC	CRETACEOUS	UPPER	Mancos Shale	Carlile Shale Member	
MESOZOIC	CRETACEOUS	UPPER	Mancos Shale	Greenhorn Limestone Member	
MESOZOIC	CRETACEOUS	UPPER	Mancos Shale	Graneros Shale Member	
MESOZOIC	CRETACEOUS	UPPER	Dakota Formation	Cubero Member	
MESOZOIC	CRETACEOUS	UPPER	Dakota Formation	Oak Canyon Member	
MESOZOIC	JURASSIC	UPPER	Morrison Formation	Jackpile Member	
MESOZOIC	JURASSIC	UPPER	Morrison Formation	Brushy Basin Member	
MESOZOIC	JURASSIC	UPPER	Morrison Formation	Salt Wash Member	
MESOZOIC	JURASSIC	MIDDLE	San Rafael Group	Summerville Formation	
MESOZOIC	JURASSIC	MIDDLE	San Rafael Group	Todilto Fomation	Tonque Arroyo Member
MESOZOIC	JURASSIC	MIDDLE	San Rafael Group	Todilto Fomation	Luciano Mesa Member
MESOZOIC	JURASSIC	MIDDLE	San Rafael Group	Entrada Sandstone	
MESOZOIC	TRIASSIC	UPPER	Chinle Group	Petrified Forest Formation	
MESOZOIC	TRIASSIC	UPPER	Chinle Group	Agua Zarca Formation	
MESOZOIC	TRIASSIC	MIDDLE	Moenkopi Formation		
PALEOZOIC		LOWER PERMIAN	San Andres Formation		
PALEOZOIC		LOWER PERMIAN	Glorieta Sandstone		
PALEOZOIC		LOWER PERMIAN	Yeso Formation		
PALEOZOIC		LOWER PERMIAN	Abo Formation		
PALEOZOIC		MIDDLE-UPPER PENNSYLVANIAN	Madera Formation		
PALEOZOIC		MIDDLE-UPPER PENNSYLVANIAN	Sandia Formation		
PALEOZOIC		LOWER-MIDDLE MISSISSIPPIAN	Arroyo Peñasco Group	Del Padre Sandstone?	
PALEOZOIC		PROTEROZOIC	Quartzite and amphibolite		

Figure 2-1. Amphibolite schist outcrop in Little Tuerto Hills.

Figure 2-2. Quartzite outcrop in the southern part of the Little Tuerto Hills. Note layering nearly parallel to hammer handle.

Figure 2-3. Del Padre(?) sandstone outcrop in Little Tuerto Hills. a) clean coarse sandstone overlying brownish conglomeratic sandstone. b) close up of conglomerate at base of outcrop. c) close up of coarse sandstone.

Figure 2-4. Madera Formation limestone, Little Tuerto Hills. Note chert nodules.

Figure 2-5. Abo Formation exposure in road cut on NM-14, about 200 m north of Golden, NM.

PALEOZOIC SEDIMENTARY ROCKS

Mississippian(?), Pennsylvanian, and Permian rocks crop out in the southwestern part of the Ortiz Mine Grant, in the Little Tuerto Hills, around the village of Golden, and in the San Pedro Mountains. In the Little Tuerto Hills, the base of the section is exposed. Exposures are small and isolated in the Golden area. The San Pedro Mountains afford continuous exposures, though the Pennsylvanian and Permian rocks are considerably affected by contact metamorphism.

MISSISSIPPIAN SYSTEM

Del Padre (?) Sandstone (Arroyo Peñasco Group)
White quartzite-pebble conglomerate nonconformably overlies metamorphic rocks and is overlain by shale and limestone of the Sandia Formation in the Little Tuerto Hills. The unit is approximately 15 m (50 ft) thick and is composed of medium to coarse sandstone and pebbles to cobbles of quartzite **(Figure 2-3)**. The quartzite pebbles bear strong resemblance to the underlying quartzite, suggesting local provenance. This unit was assigned to the Sandia Formation by Emerick (1950). Read and others (1999a and b) describe similar sandstone and pebble conglomerate in the Sandia Mountains and assign it to the Mississippian Del Padre Sandstone.

PENNSYLVANIAN SYSTEM

Sandia Formation
Shale and limestone overlies sandstone and conglomerate of the Del Padre Sandstone and underlies thick-bedded limestone of the Madera Formation in the Little Tuerto Hills. The unit is approximately 15 m (50 ft) thick and is assigned to the Sandia Formation.

Madera Formation
Gray, thick-bedded limestone of the Madera Formation crops out on the north end of the Little Tuerto Hills, in isolated overturned beds in an arroyo about 0.5 km (0.3 mi) south of the village of Golden, and in the northwestern foothills of the San Pedro Mountains **(Figure 2-4)**. No thickness was measured, but there appears to be in excess of 60 m (200 ft) exposed thickness of limestone in the Little Tuerto Hills. Emerick (1950) estimated the thickness of the Madera Formation in the Golden area at 300 m (1000 ft). In the San Pedro Mountains, Madera Formation limestone beds have been variously metamorphosed to garnet skarn and marble, and mineralized, in proximity to latite-porphyry intrusive rocks. Shales have been converted to hornfels.

PERMIAN SYSTEM

Permian rocks crop out in the southern part of the Ortiz Mine Grant. The lowermost formations, the Abo and Yeso Formations, are undifferentiated in the northern foothills of the

San Pedro Mountains. In the San Pedro Mountains these formations are commonly metamorphosed to a black to green hornfels.

Abo Formation

The Abo Formation is poorly exposed in isolated outcrops of reddish mudstone on the west side of the Little Tuerto Hills, along NM 14 about 1,200 m (4,000 ft) north of the village of Golden **(Figure 2-5)** and along Arroyo del Tuerto about 1,700 m (5,500 ft) east of NM 14. Atkinson (1961) estimated about 275 m (900 ft) of Abo Formation in the San Pedro Mountains.

Yeso Formation

The Yeso Formation crops out as brownish red sandstone and mudstone in isolated exposures northeast of the village of Golden and south of Arroyo del Tuerto. Atkinson (1961) estimated a thickness of about 120 m (400 ft) for the Yeso Formation in the San Pedro Mountains.

Glorieta Sandstone

The Glorieta Sandstone is a quartzose, white, medium-grained sandstone that crops out on the western slope of a north-trending ridge northeast of the village of Golden, and on the north flank of the San Pedro Mountains, about 2,100 m (7,000 ft) south-southwest of the Lone Mountain Ranch headquarters, and in a small exposure along Arroyo del Tuerto about 1,500 m (5,000 ft) east of NM 14. The Glorieta's thickness appears to be about 15 m (50 ft) on the ridge northeast of Golden and closer to 30 m (100 ft) in the San Pedro Mountains.   Glorieta sandstone has been mined for silica sand from an open cut in the San Pedro Mountains about 1,200 m (4,000 ft) south of the south boundary of the Ortiz Mine Grant.

San Andres Formation

Gray to yellowish limestone of the San Andres Formation crops out on the western slope of a north-trending ridge northeast of the village of Golden, and on the north flank of the San Pedro Mountains, about 2,100 m (7,000 ft) south-southwest of the Lone Mountain Ranch headquarters, and in a small exposure along Arroyo del Tuerto about 1,500 m (5,000 ft) east of NM 14. The San Andres Formation has not been measured but is estimated to be about 6 m (20 ft) thick on the ridge northeast of Golden.

MESOZOIC SEDIMENTARY ROCKS

TRIASSIC SYSTEM

Triassic rocks underlie much of the Tuerto Gravel-covered pediment west and south of the Ortiz Mountains. The best exposures of Triassic strata on the Grant are in the north-trending ridge northeast of the village of Golden and in the northeastern part of the San Pedro Mountains.

Moenkopi Formation
Red siltstone and sandstone form a recessive bench on the western slope of a north-trending ridge northeast of the village of Golden; and on the north flank of the San Pedro Mountains, about 2,100 m (7,000 ft) south-southwest of the Lone Mountain Ranch headquarters. The unit overlies San Andres Formation limestone and underlies the Agua Zarca Formation sandstone. The unit appears to be approximately 6 m (20 ft) thick. On the basis of lithology, thickness, and stratigraphic and geographic position, the unit is assigned to the Moenkopi Formation as defined by Lucas and Heckert (1995).

Chinle Group
Agua Zarca Formation
Coarse to locally conglomeratic sandstone of the Agua Zarca Formation forms prominent ridges northeast of the village of Golden; and on the north flank of the San Pedro Mountains, about 2,100 m (7,000 ft) south-southwest of the Lone Mountain Ranch headquarters. The minimum thickness of Agua Zarca Formation sandstone is estimated at 15 m (50 ft).

Chinle Group undifferentiated
No attempt has been made on the Ortiz Mine Grant to differentiate the Salitral Formation, Petrified Forest Formation, and Correo Sandstone of the Chinle Group. The Chinle Group is exposed in several isolated areas in the southwestern part of the Ortiz Mine Grant. Reddish brown mudstone and lesser sandstone exposed in Arroyo del Tuerto west of NM-14 and in Arroyo de la Joya east of the Lone Mountain Ranch headquarters probably correlate to the Petrified Forest Formation. Along the southern foothills of the Ortiz Mountains, in the low hills about 1,500 m (5,000 ft) northwest of the Lone Mountain Ranch headquarters and in the eastern part of the San Pedro Mountains, mudstone and sandstone of the Chinle Group has been metamorphosed to a mottled green to black and white hornfels and quartzite. Lucas and Heckert (1995) measured 390 m (1,280 ft) of Chinle Group rocks above the Agua Zarca Formation in the Hagan Basin. Chinle Group sedimentary rocks are extensively intruded by andesite porphyry laccoliths and sills in the south-central part of the Ortiz Mine Grant.

JURASSIC SYSTEM

Jurassic rocks are exposed on the Ortiz Mine Grant on the western margin of the Ortiz Mountains and along the southern side (footwall) of the Buckeye Hill Fault. Thicknesses encountered in drill hole ORT-126, in the southwestern part of the Ortiz Mountains, are depicted in **Figure 2-6**.

San Rafael Group

Entrada Sandstone
Sandstone overlying mudstone of the Chinle Group and overlain by the limestone member of the Todilto Formation is exposed in Arroyo del Tuerto 90 m (300 ft) east of NM-14, in several exposures along the southeastern and southwestern flanks of the Ortiz Mountains, and in Arroyo de la Joya about 1,800 m (6,000 ft) east of the Lone Mountain Ranch headquarters. Thickness of the Entrada sandstone was measured at 8.8 m (29 ft) in hole ORT-126. In the vicinity of the Iron Vein prospect, on the southern flank of the Ortiz Mountains, the Entrada sandstone is metamorphosed to quartzite.

Todilto Formation
Thin-bedded limestone of the Luciano Mesa Member of the Todilto Formation crops out in Arroyo del Tuerto approximately 45 m (150 ft) east of NM-14 **(Figure 2-7)** , and along the southwestern and southern flanks of the Ortiz Mountains. Hole ORT-126 intersected 3.4 m (11 ft) of the Todilto limestone. The gypsum (Tonque Arroyo) member of the Todilto is poorly exposed on the Ortiz Mine Grant and is considerably altered and brecciated in all known exposures. The limestone member is altered to magnetite-garnet skarn at the Iron Vein prospect. At the Iron Vein, and in one exposure in Arroyo del Tuerto, the gypsum member is replaced by a carbonate-matrix breccia with clasts of sandstone and andesite porphyry **(Figure 2-8)**.

Summerville Formation
The Summerville Formation is not mapped separately on the surface on the Ortiz Mine Grant, but instead is mapped with the Morrison Formation. In core drilling, sandstone and mudstone assigned to the Summerville Formation measures 21.2 m (86 ft) thick (**Figure 2-6**).

Morrison Formation
In the Ortiz Mine Grant, the Summerville Formation and the Salt Wash, Brushy Basin, and Jackpile members of the Morrison Formation were not distinguished in surface mapping. All sandstone and mudstone (and quartzite and hornfels derived from them) above the Tonque Arroyo gypsum member of the Todilto Formation and below the conglomeratic sandstone of the Dakota Formation were grouped together in the Morrison Formation. The lower part of the Morrison Formation is poorly exposed. Most of the Morrison Formation from the Ortiz Mountains is known from the 191 m (628 ft) thickness drilled in the southwestern part of the Ortiz Mountains (**Figure 2-6**). The kaolinitic sandstone exposed below the Dakota Formation on the west side of the hill known as El Punto, on the southwestern end of the Ortiz Mountains, is probably correlative with the Jackpile Member of the Morrison Formation, as described by Picha (1982) and Lucas and others (1999).
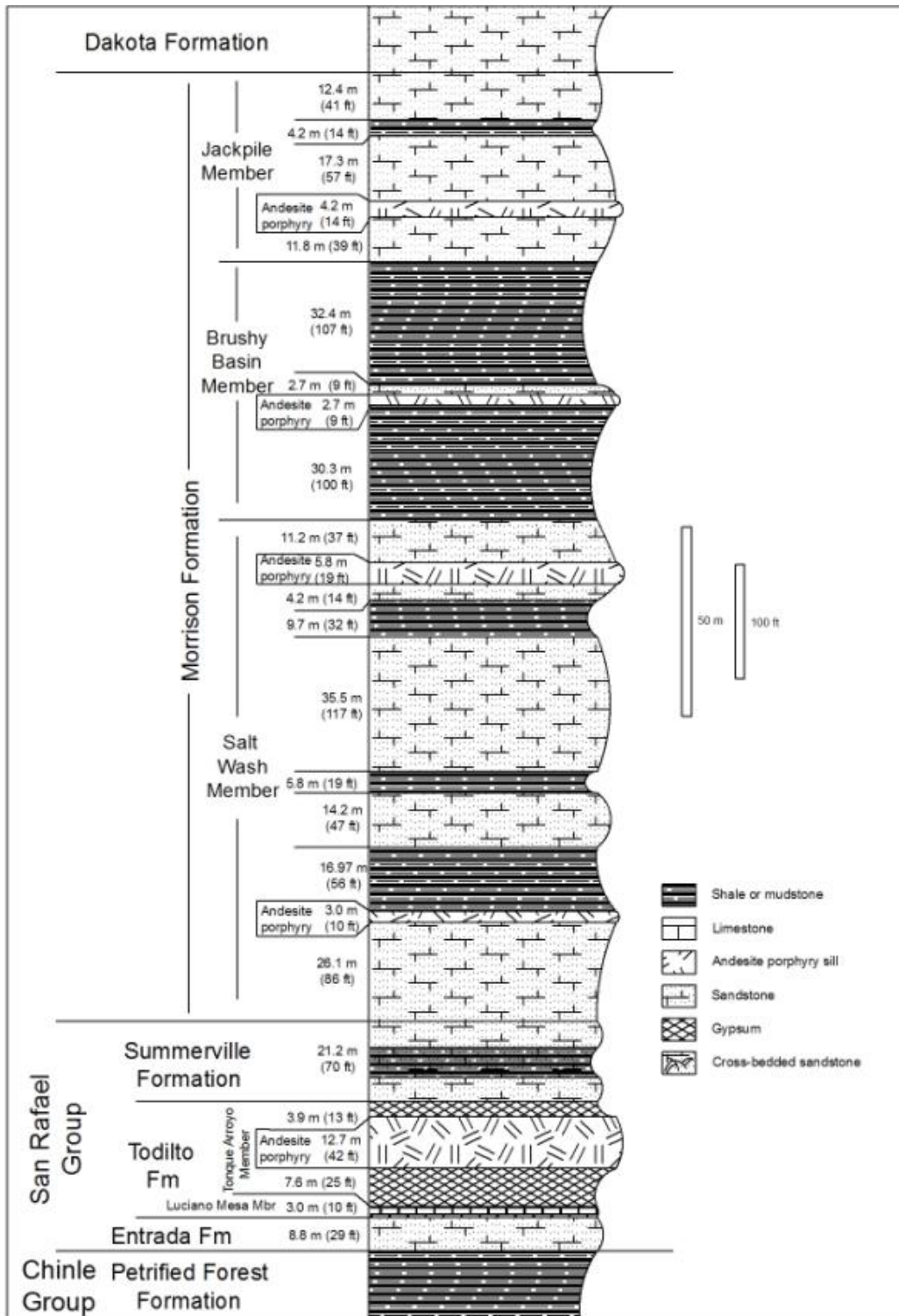
Figure 2-6. Stratigraphic column of Jurassic strata of the western part of the Ortiz Mountains. Based on core hole ORT-126.

Figure 2-7. Todilto Formation limestone (Luciano Mesa Member). a) Outcrops in Tuerto Arroyo. b) Close up of thin bedded limestone.
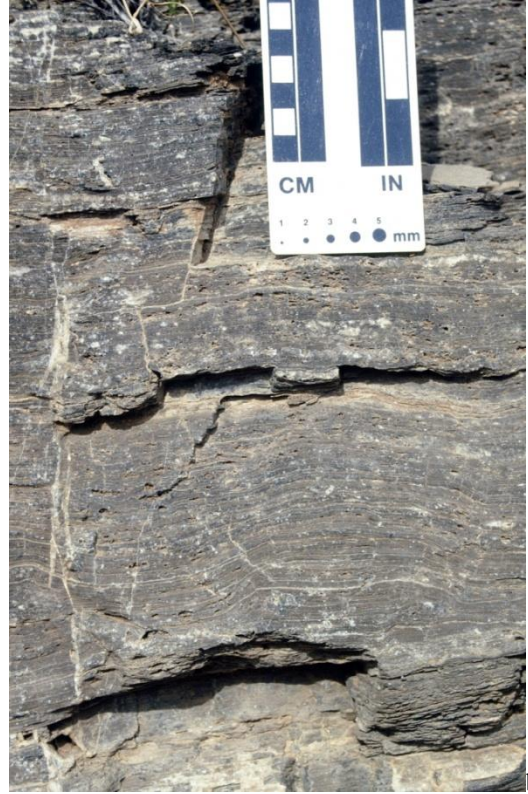
Figure 2-8.   Breccia developed in Todilto Formation gypsum (Tonque Arroyo Member). Outcrop in Tuerto Arroyo.

Figure 2-9. El Punto (center of photograph), viewed from highway NM-14. Highest point is capped by Dakota Formation sandstone.

CRETACEOUS SYSTEM

Cretaceous rocks are widespread on the Ortiz Mine Grant and host the principal laccolithic bodies in the Ortiz Mountains: the Lomas de la Bolsa laccolith and the Captain Davis Mountain laccolith. Cretaceous rocks occur in a broad band across the western part of the Ortiz Mountains and underlie much of the area of Captain Davis and Lone Mountain and the subdued topography of the southeastern part of the Ortiz Mine Grant.

Thicknesses of the Cretaceous units are derived from core drilling in the southern part of the Ortiz Mountains, from Lukas Canyon to Carache Canyon.

Dakota Formation

The Dakota Formation crops out on the top of El Punto Hill (**Figure 2-9**), on the southwest end of the Ortiz Mountains, and can be traced 1370 m (4500 ft) to the south and 600 m (2000 ft) to the north. Other smaller exposures of the Dakota Formation occur in the southeastern foothills of the Ortiz Mountains. The Dakota Formation has not been subdivided into members as it has been in the Hagan Basin (Picha, 1982), or at Galisteo Dam (Lucas and others, 1999). Coarse to conglomeratic sandstone with common worm burrows mark the

Dakota. Holes ORT-116 and ORT-126 drilled 32.8 m (108 ft) of Dakota sandstone and shale in the southwestern part of the Ortiz Mountains (**Figure 2-10**).

Mancos Shale

The Mancos Shale on the Ortiz Mine Grant has been subdivided into seven members with an aggregate thickness of 552.7 m (1,813 ft).   A complete section of the Mancos Shale is preserved in the Ortiz Mountains though it has been extensively intruded by laccoliths and sills of andesite porphyry. Contact metamorphism and metasomatism have strongly affected the Mancos Shale, in many places obscuring original sedimentary textures and structures.

Graneros Shale Member

Black shale underlying the Greenhorn Limestone Member and overlying sandstone of the Dakota Formation is assigned to the Graneros Shale Member. Drilling in the southwestern part of the Ortiz Mountains penetrated 38 m (126 ft) of marine shale below the Greenhorn Limestone Member and above sandstone of the Dakota Formation (**Figure 2-10**).

Greenhorn Limestone Member

The Greenhorn Limestone Member of the Mancos Shale serves as an important stratigraphic marker horizon regionally and locally (Molenaar, 1983). In the Ortiz Mine Grant, the Greenhorn is metamorphosed to a gold- and copper-bearing garnet-pyroxene-scapolite skarn in Lukas and Monte del Largo Canyons, in the southwestern part of the Ortiz Mountains (**Figure 2-11**). Extensive drilling of the Lukas Canyon deposit shows the metamorphosed Greenhorn beds to be 15 to 18 m (50 to 60 ft) thick (**Figure 2-10**). The skarn beds grade laterally into poorly exposed fresh limestone and shale (**Figure 2-12**). Other exposures of the Greenhorn limestone occur on and near Lone Mountain, a southeastern topographic outlier of the Ortiz Mountains.

The Greenhorn Limestone can be traced from the region of the Galisteo Dam southward into the northwestern part of the Ortiz Mine Grant. A small exposure of limestone in the northeastern portion of the Ortiz Mine Grant is likely to be either the Greenhorn limestone or the Juana López Member of the Mancos Shale.
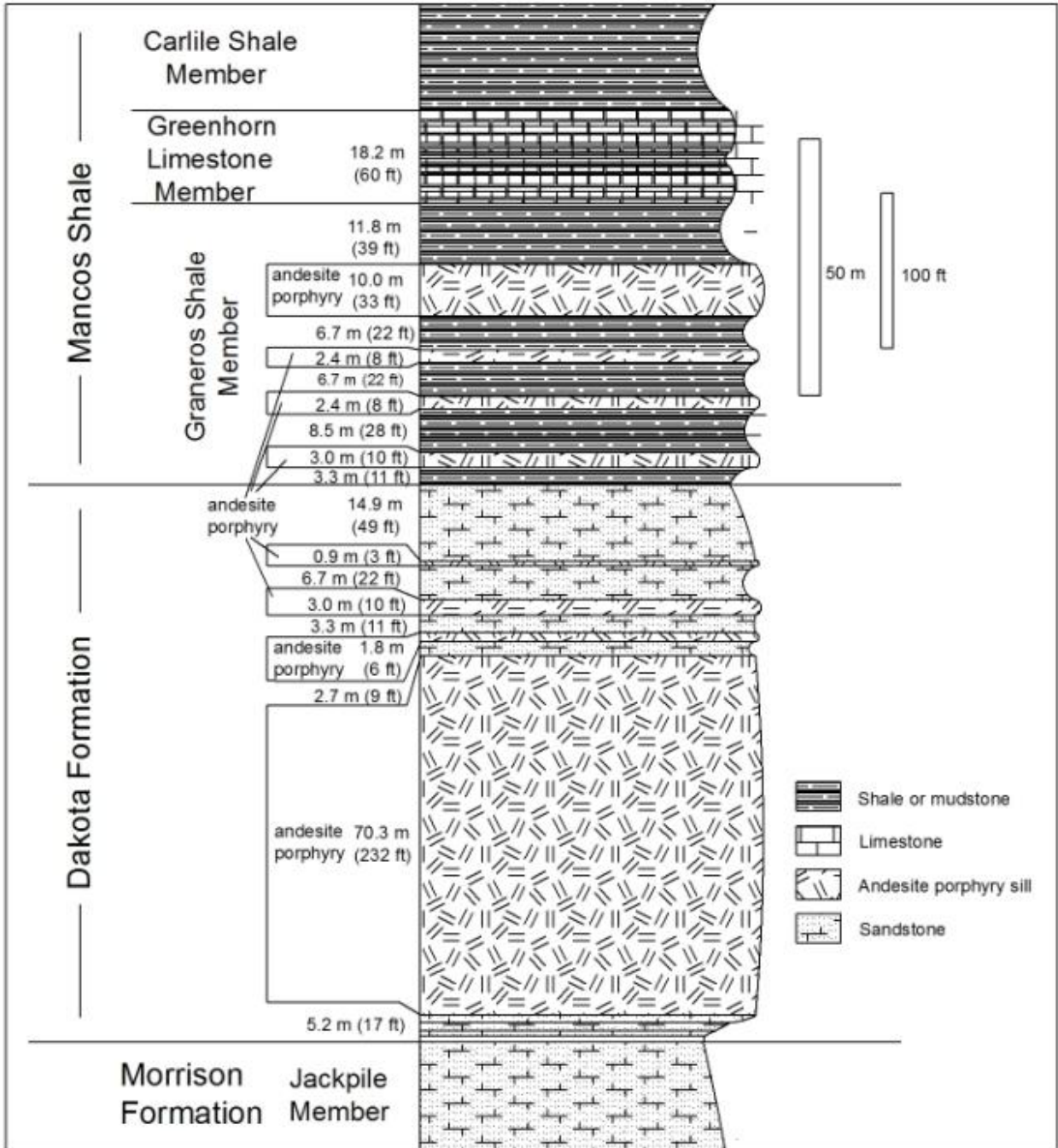
Figure 2-10. Stratigraphic column of the Dakota Formation – Greenhorn Limestone Member interval, southwestern part of the Ortiz Mountains.

Figure 2-12. Partially skarn-altered and copper-mineralized Greenhorn limestone outcrop near mouth of Lukas Canyon.

Figure 2-11. Lukas Canyon garnet skarn developed in Greenhorn Limestone. a) massive garnet-diopside skarn b)note layering interpreted as relict bedding.

Carlile Shale Member

The Carlile Shale crops out in the southwestern part of the Ortiz Mountains; and on Lone Mountain and Captain Davis Mountain, in the eastern part of the range. A third area of Carlile Shale exposure lies about 2,440 m (8,000 ft) west of the Bull Mill camp, in the southeastern part of the Ortiz Mine Grant. In the southwestern Ortiz Mountains, the Carlile Shale is 88 m (288 ft) thick, as measured by drilling (**Figure 2-13**). In outcrop in the southwestern Ortiz Mountains, the Carlile is commonly metamorphosed to a variegated brown, red, cream, and green hornfels. In the lower part of the Carlile section, near the skarn bed in Lukas Canyon, the Carlile hornfels commonly contains porphyroblasts of reddish brown garnet.

Juana López Member

In outcrop the Juana López Member is a fetid limestone about 1.5 m (5 ft) thick, overlying the Carlile Shale Member (Hook and Cobban, 1980). It crops out on the Ortiz Mine Grant on a low ridge about 8,000 feet (2,440 meters) west of the Bull Mill camp, in the southeastern part of the Ortiz Mine Grant. In this exposure it is comparable to its originally described exposure along Galisteo Creek west of Cerrillos (Rankin, 1944; Dane, 1960). In the southwestern part of the Ortiz Mountains, east of Lukas Canyon, it is strongly metamorphosed to a garnet porphyroblast-bearing hornfels. In core drilling in the southwestern Ortiz Mountains, 16.7 m (55 ft) of hornfels of the underlying Carlile member is included in the Juana López

Member (**Figure 2-13**). The Juana López is also present in poor exposures about 1.6 km (1 mi) east of Lone Mountain and in the northeastern portion of the Ortiz Mine Grant.

Niobrara Member

The Niobrara Member measures 245 m (804 ft) thick by drilling in the southern Ortiz Mountains (**Figure 2-14**). It is composed of interbedded calcareous sandstone, siltstone, and shale. Calcareous concretions are common in the Bull Mill Camp area and in Cañamo Arroyo, between Captain Davis Mountains and Lone Mountain. In the Ortiz Mountains the lower part of the Niobrara likely includes strata equivalent to the D-Cross Shale Member.

Hosta-Dalton Sandstone (Mesa Verde Group)

The Hosta-Dalton sandstone is the turn-around of the Cretaceous shoreline during and after Crevasse Canyon Formation deposition and therefore represents a regressive-transgressive cycle (R-3 – T-4 of Molenaar, 1983). It corresponds to the Cano Sandstone Member of Stearns (1953). In the Ortiz Mountains, the Hosta-Dalton is shown by drilling to be 46 to 64 m (150 to 210 ft) thick (**Figure 2-14**). Exposures in the Ortiz Mountains on the ridge east of Monte del Largo Canyon are poor, but considerable float of fine-grained sandstone covers the surface in this area. The Hosta-Dalton sandstone is not present in the eastern part of the Ortiz Mine Grant, nor has it been mapped in the region of the Galisteo Reservoir.   In the Cedar Crest area, the Hosta and Dalton sandstones are separated by the coal-bearing Crevasse Canyon Formation (Molenaar, 1983). The Hosta-Dalton sandstone overlies the Niobrara Shale Member and underlies marine shales of the Upper Mancos Shale Member. It may include part of the El Vado Sandstone in its basal part.

Upper Mancos Shale Member

Marine shales ranging from 104 to 113 m (340 to 371 ft) thick overlie the Hosta-Dalton sandstone and underlie the Point Lookout Sandstone in the Ortiz Mountains (**Figure 2-15**). The upper 15 m (50 ft) contain beds of bioturbated sandstone (**Figure 2-16**). These strata are equivalent to the Satan Tongue (Molenaar, 1983).
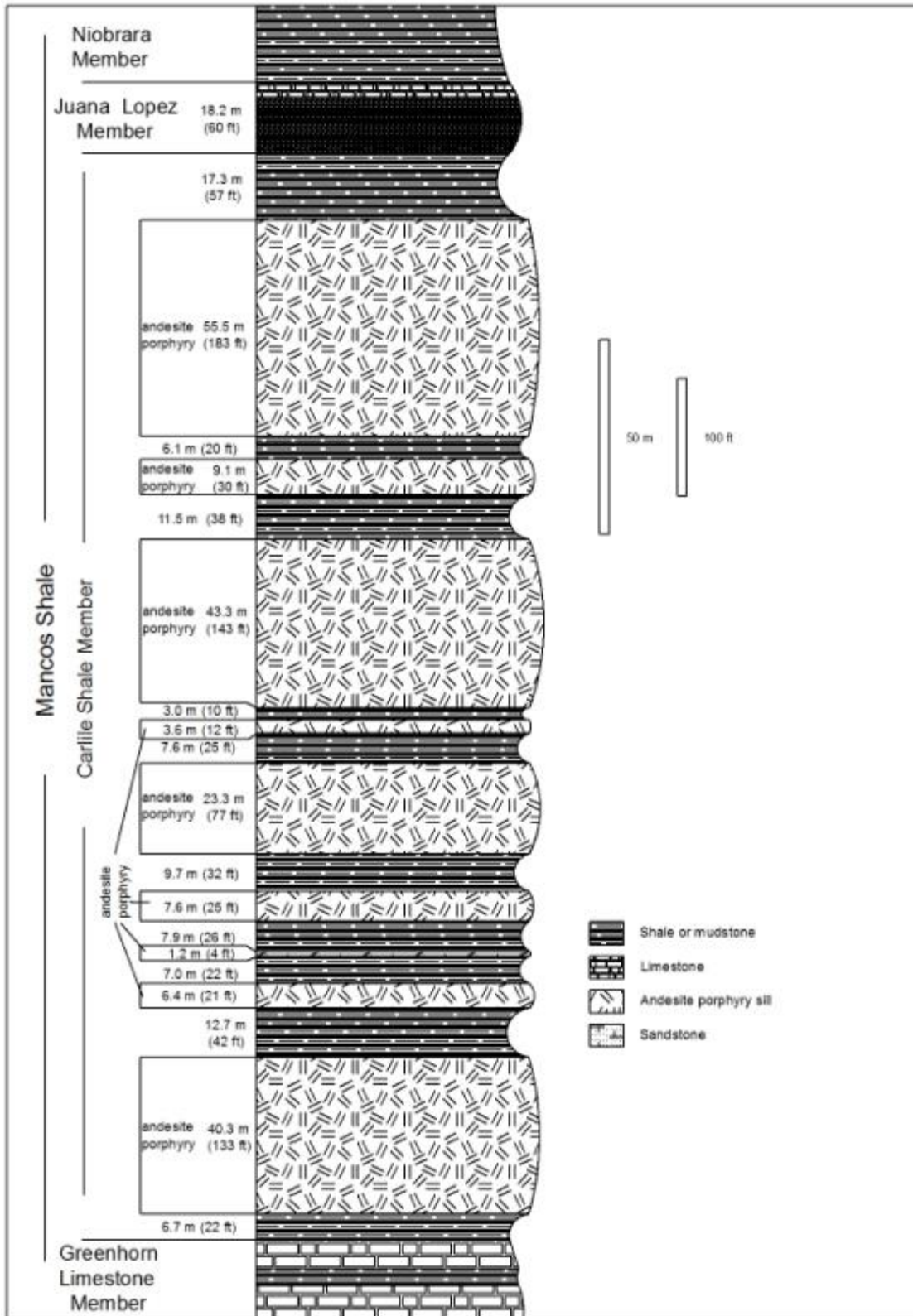
Figure 2-13. Stratigraphic column of the Carlile Shale – Juana López Member interval, southwestern part of the Ortiz Mountains.
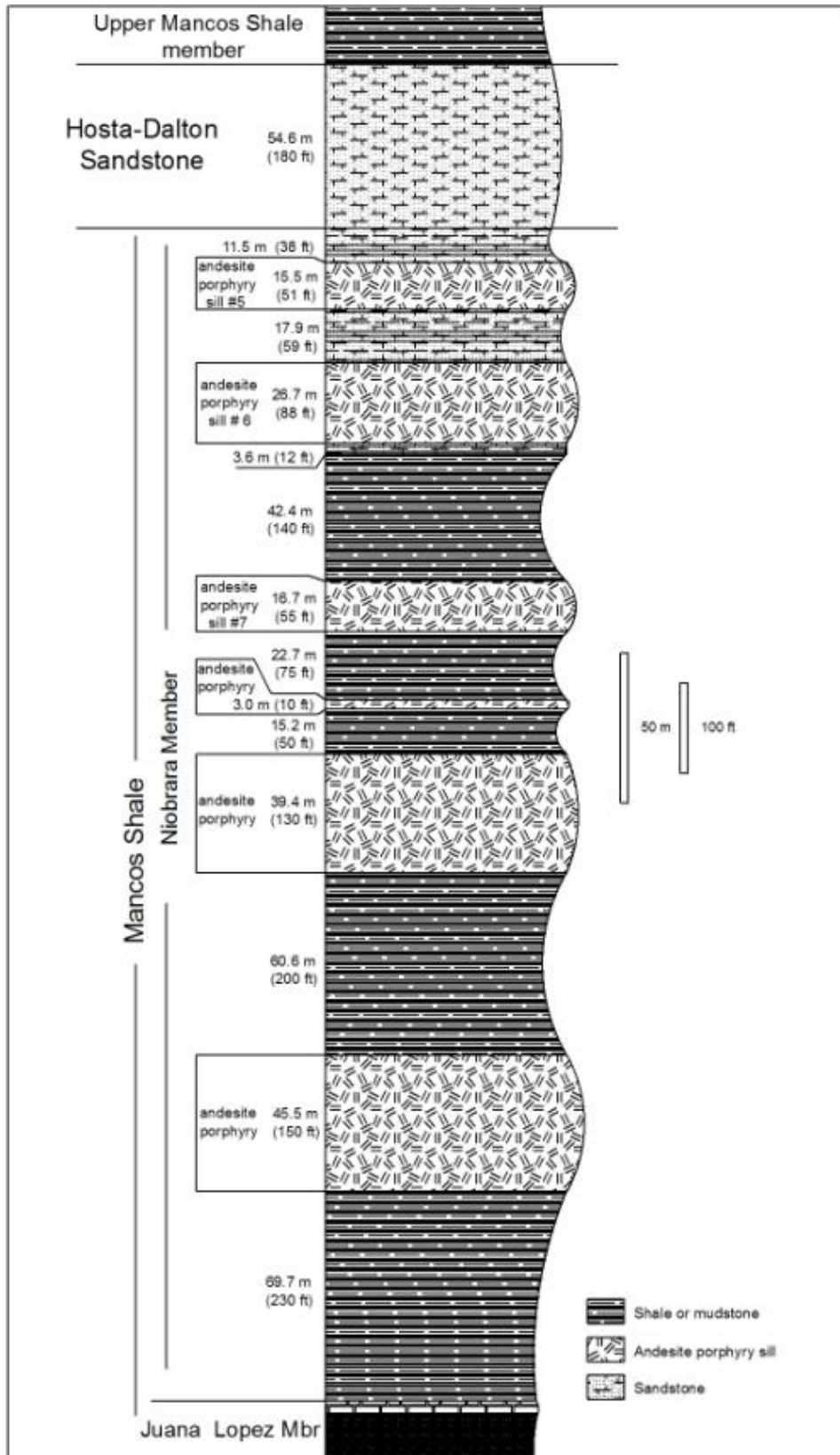
Figure 2-14. Stratigraphic column of the Niobrara Shale – Hosta-Dalton interval, southwestern part of the Ortiz Mountains.

Mesa Verde Group

Previous investigations in the Ortiz Mountains (Griswold, 1950; McRae, 1958; Peterson, 1958; Kay, 1986) assigned all sandstone-bearing units above the Mancos Shale to the Mesa Verde Formation or Group. Medium- to coarse-grained to pebbly sandstone present in the southern part of the Ortiz Mountains and exposed at the Cunningham Hill Mine was identified as lower Tertiary (Maynard, 1995). The remaining Mesa Verde Group sediments are divided into the Point Lookout Sandstone and Menefee Formation. Extensive core drilling in the Carache Canyon area has shown the indicated ranges in thickness.

Point Lookout Sandstone

White to tan, fine-grained, medium-bedded sandstone overlying the upper Mancos Shale member and underlying non-marine shale, sandstone, and coal of the Menefee Formation forms the ridge dividing Carache Canyon and the unnamed canyon to the west in the southern part of the Ortiz Mountains. The Point Lookout Sandstone can be traced northward in the Ortiz Mountains to the upper reaches of Crooked Canyon, where its trace is interrupted by the large augite-monzonite stock. The Point Lookout Sandstone resumes on the northwestern side of the augite-monzonite stock and can be traced along the west flank of Cerro Chato and into the southern reaches of Miller Gulch, west of the village of Madrid. The Point Lookout Sandstone also crops out in the eastern part of the Ortiz Mine Grant, southeast of the Tijeras-Cañoncito Fault System's trace, about 4 km (2.5 mi) east of Captain Davis Mountain.

The Point Lookout Sandstone on the Ortiz Mine Grant is best known at Carache Canyon, where it serves as both a convenient stratigraphic marker for evaluation of, and a host for, gold mineralization. At Carache Canyon, the Point Lookout Sandstone ranges from 25 to 31.4 m (82 to 103 ft) thick, as determined by core drilling (**Figure 2-15**).

Menefee Formation

Menefee Formation shale and sandstone are widely exposed in the Madrid area, where the formation hosts formerly exploited coal deposits. At Carache Canyon, the Menefee Formation can be divided into three informally named members.
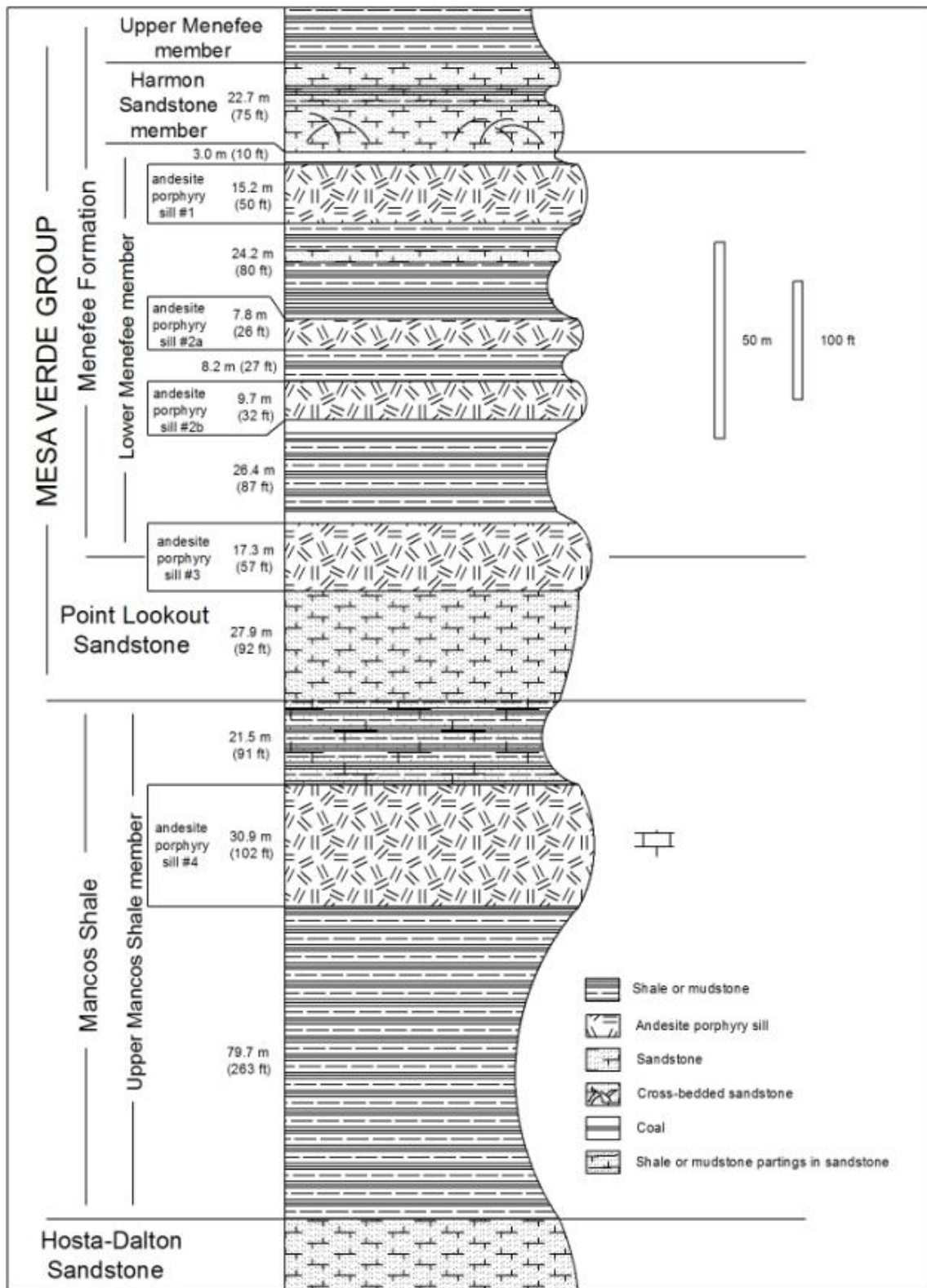
Figure 2-15. Stratigraphic column of the upper Mancos Shale – upper Menefee member interval, southern part of the Ortiz Mountains.
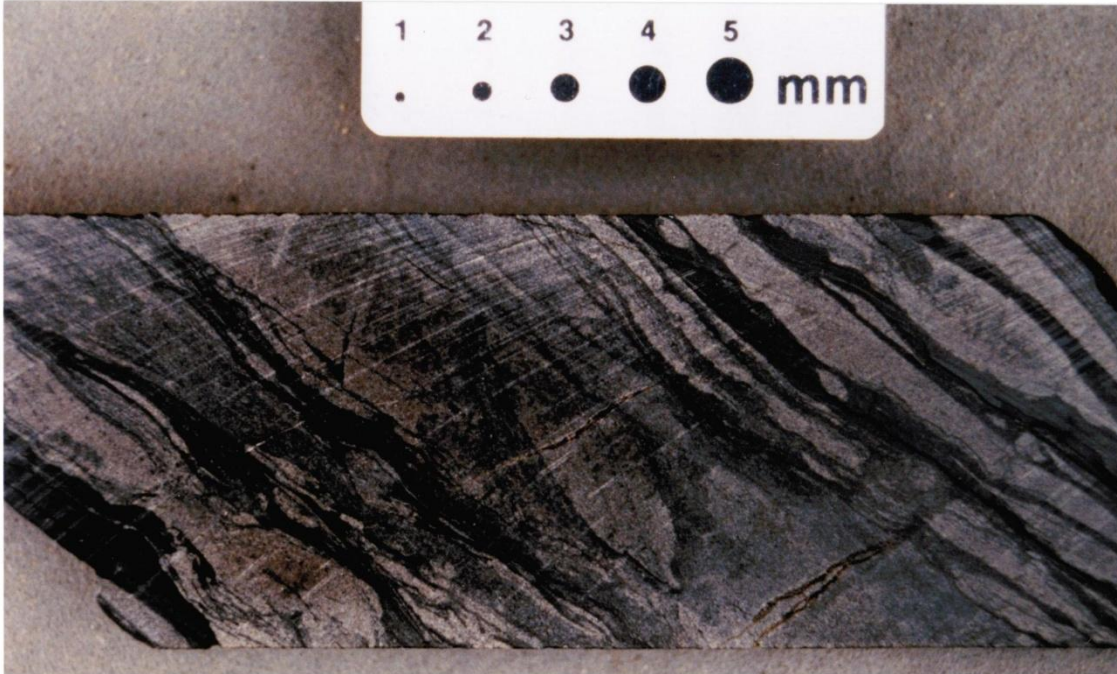
Figure 2-16. Sawed core sample of bioturbated sandstone of the upper Mancos shale.

Lower Menefee Member

At Carache Canyon, the lower Menefee member is composed of 52.7 to 91.5 m (173 to 300 ft) of shale, carbonaceous shale, sandstone, and coal (**Figure 2-15**). Detailed drilling shows that sandstone beds are not continuous over short distances.

"Harmon Sandstone" Member

A prominent, trough-crossbedded, laterally persistent sandstone in Carache Canyon corresponds to the "Harmon sandstone" in the Hagan Basin (Black, 1979; Picha, 1982) and in the Madrid coal field (Bachman, 1975; Maynard and others, 2001). At Carache Canyon, the Harmon sandstone is 22.7 m (75 ft) thick, on average (**Figure 2-15**).

Upper Menefee Member

Above the Harmon sandstone in Carache Canyon, up to 230 m (755 ft) of shale, carbonaceous shale, sandstone, and coal has been cut by drilling. The upper Menefee member is unconformably overlain by the Paleocene-Eocene Diamond Tail Formation.

CENOZOIC SEDIMENTARY ROCKS

TERTIARY SYSTEM

Paleocene-Eocene Diamond Tail Formation
Approximately 457 m (1,500 ft) of medium-grained to coarse to pebbly sandstone (**Figure 2-17**) metamorphosed to quartzite, and lesser amounts of black hornfels derived from mudstone are preserved in a graben on the southeastern margin of the Ortiz Mountains. These metasedimentary rocks and sandstones and mudstones overlying the Menefee Formation in the northern part of the Ortiz Mine Grant and in outcrops south of Peach Spring in the eastern part of the Ortiz Mine Grant are correlated with the Diamond Tail Formation of Lucas and others (1997). Lucas and others (1997) separated the lower dominantly sandstone Tertiary sediments from the Galisteo Formation in the Hagan Basin and on the east side of the Cerrillos Hills. The Diamond Tail Formation of Lucas and others (1997) is equivalent to the lower part of the Galisteo Formation as described by Gorham (1979) and Stearns (1953b). Earlier descriptions of the geology of the Ortiz Mine Grant referred to these rocks as Galisteo Formation (eg. Coles, 1990; Maynard, 1995), or grouped them with the Mesa Verde Group (eg. Griswold, 1950; Lindqvist, 1980; Kay, 1986). Bachman (1975) mapped a small part of the currently known Diamond Tail Formation as Galisteo Formation in the Ortiz Mountains.

In the Ortiz Mountains, typical exposures of the Diamond Tail Formation are medium- to coarse-grained, trough cross-bedded to massive, white to tan sandstone (**Figure 2-18**). Quartzite pebbles and pebble to cobble-size silicified wood fragments (**Figure 2-19**) are rarely abundant, though widely scattered. Mudstone beds, probably originally mudstone as described in the Hagan Basin (Lucas and others, 1997), are metamorphosed to gray to black hornfels. Quartzite breccia derived from Diamond Tail Formation sandstone hosts gold–tungsten mineralization at the Cunningham Hill Mine.

At exposures south of Peach Spring, along the Ortiz Mine Grant's eastern boundary, sandstone of the Diamond Tail Formation is well exposed without the effects of contact metasomatism. The Diamond Tail Formation's basal contact with the Menefee Formation can be traced for more than 760 m (2,500 ft). The base of the Diamond Tail here commonly has about 0.3 m (1 ft) of pebble conglomerate resting on Menefee Formation.
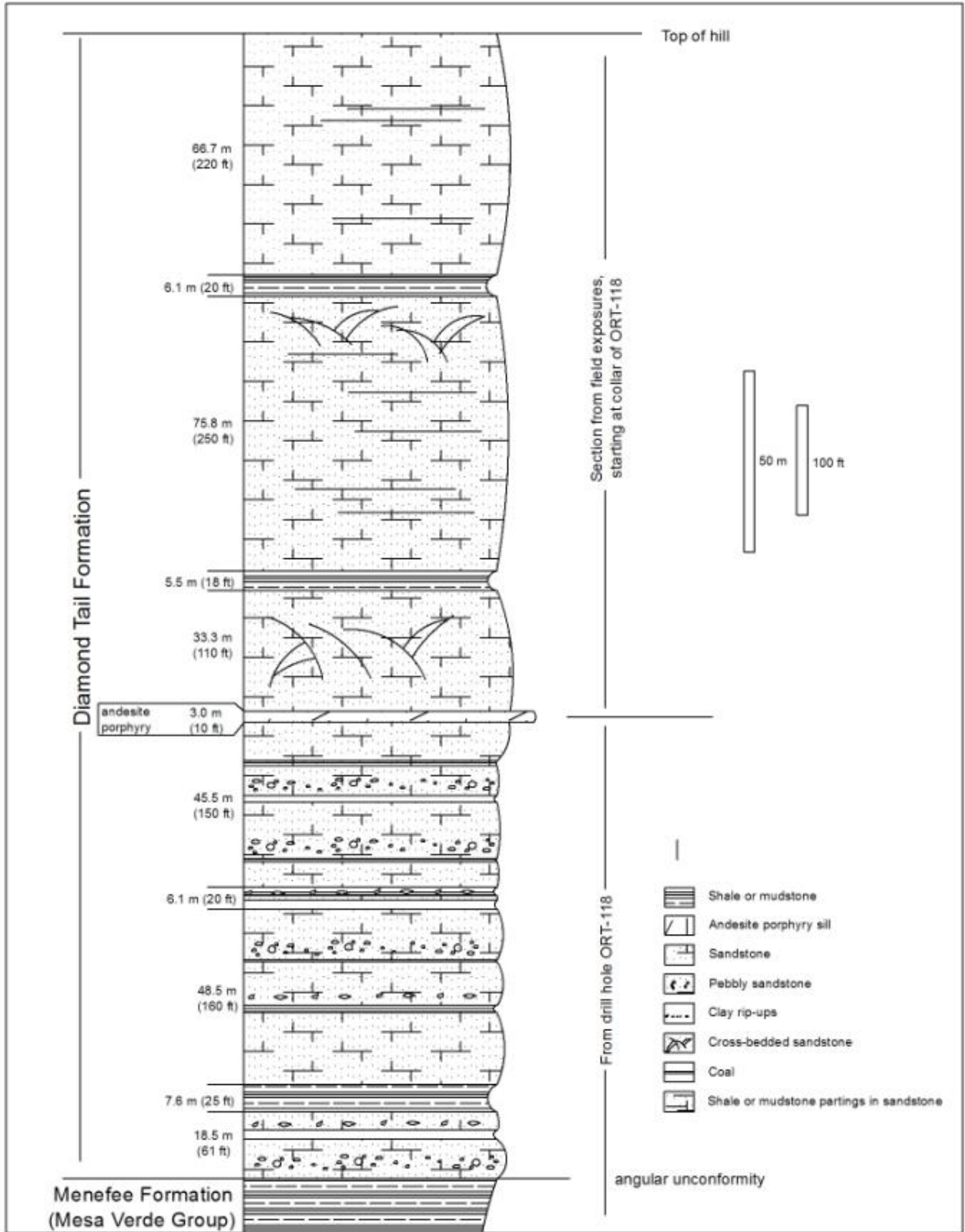
Figure 2-17. Stratigraphic section of the Diamond Tail Formation preserved in the Ortiz Graben in the southern part of the Ortiz Mountains.

Figure 2-18. Outcrop of Diamond Tail Formation sandstone in entrance to Carache Canyon, southeastern margin of the Ortiz Mountains. The author (in his salad days) for scale.

Figure 2-19. Petrified wood fragment, Diamond Tail Formation.

37

Eocene – Oligocene Galisteo Formation

Following the usage proposed by Lucas and others (1997), the Galisteo Formation comprises a lower mudstone and lesser sandstone member overlain by a dominantly sandstone member. Red mudstone and sandstone of the Galisteo Formation crops out in the Ortiz Mine Grant in the area around and north of Peach Spring and in the low hills south of the Galisteo River in the northeastern part of the Grant.

Oligocene Espinaso Formation

The Espinaso Formation consists of lavas, volcaniclastic sediments, and tuffs. In the Ortiz Mine Grant, well bedded Espinaso Formation is exposed in the northeastern corner, north of the Galisteo River (**Figure 2-20**). A fault block containing steeply dipping agglomerate beds of the Espinaso Formation lies in fault contact with Jurassic strata and Santa Fe Formation beds along the La Bajada Fault, in the northwest part of the Ortiz Mine Grant. A volcanic vent breccia lies in Dolores Gulch, north of the Cunningham Hill Mine, on the east side of the Ortiz Mountains. This unit is described in the section on igneous rocks. The Dolores Gulch volcanic vent is presumed to be a source of the Espinaso Formation volcanics. Other sources are possible, but not positively identified, in the Cerrillos Hills (Stearns, 1953b; and Disbrow and Stoll, 1957) and in the San Pedro Mountains.

Pliocene(?) gravel deposits

Light brown, pink, and buff-colored sandy gravel with a base that lies 20-30 m above the base of Tuerto gravels and a tread that preserves a 3-4 m thick stage IV-V calcic soil. A similar deposit consisting of boulders and cobbles of Ortiz Mountains-derived material caps Rich Hill, on the eastern side of the Ortiz Mountains, southeast of the Cunningham Hill Mine entrance gate. Placer gold is contained in this deposit as indicated by numerous workings whose roofs are supported by the thick calcic soil (F. Pazzaglia, written communication, 2001).
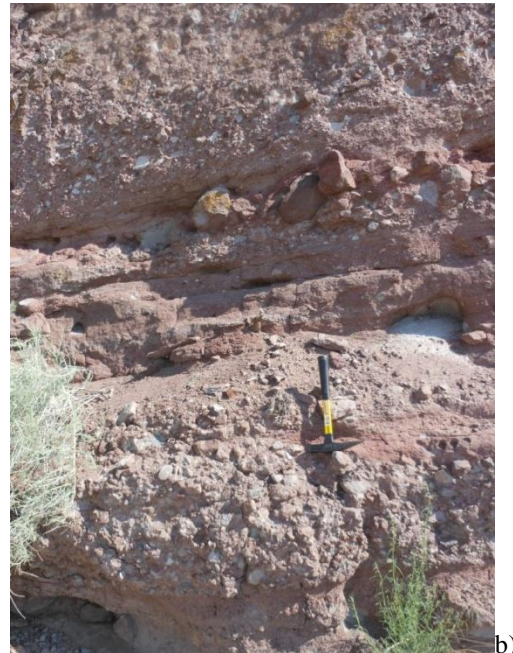
Figure 2-20. Espinaso Formation outcrops, northeastern part of the Ortiz Mine Grant. a) cliffs formed by bedded pyroclastics and volcaniclastic sediments. b) Coarse bedded pyroclastic sediments, partially reworked.

TERTIARY AND QUATERNARY

(latest) Oligocene-Pleistocene Santa Fe Group
The Santa Fe Group comprises the syntectonic sedimentary fill and associated volcanic rocks of basins within the Rio Grande Rift (Bryan, 1938; Chapin and Cather, 1994). On the Ortiz Mine Grant, the Santa Fe Group consists of two formations. The older formation consists of piedmont-slope deposits on the eastern part of the Santo Domingo sub-basin, west of the unnamed north-northeast-striking fault in the northwestern corner of the Grant. This older unit corresponds to the Blackshare Formation of Connell (2001). The younger unit, the Tuerto Gravel, is an unconformably overlying piedmont-slope deposit that was laid down on erosion surfaces outside the structural boundaries of the sub-basin.

Pliocene – Pleistocene Tuerto Gravel
The Tuerto Gravel is considered the uppermost member of the Santa Fe Group (Spiegel and Baldwin, 1963) and was first described by Stearns (1953b) from exposures in Tuerto Arroyo, about 3 km (2 mi) west of the western boundary of the Ortiz Mine Grant. Soil and rock material derived from the Ortiz Mountains, the San Pedro Mountains, and adjacent hills, partially cemented by caliche, deposited on the erosional Ortiz Surface constitute the Tuerto Gravel. The Tuerto Gravel lies on an angular unconformity on all older units, including the lower Santa Fe Group sediments. Tuerto Gravel may be distinguished from conglomerate of the Santa Fe Group by the presence of hornfels clasts in the Tuerto (Connell, 2001). The Tuerto Gravel extends several miles to the west of the Ortiz Mine Grant and ranges in thickness from 0 to 30 m (100 ft) thick. Post-Pleistocene erosion has cut numerous arroyos into the Tuerto Gravel, resulting in the gravel-capped mesas prominent in the eastern and northern parts of the Ortiz Mine Grant.

The age of the Tuerto Gravel is deduced from field relations and isotopic dating techniques. Spiegel and Baldwin (1963) suggested a correlation between the Ancha Formation and the Tuerto Gravel. Age dating of interfingering Cerros del Rio basalts (Bachman and Mehnert, 1978) and overlying lower Bandelier pumice (J. Winick, 1999, unpublished NM Geochronological Laboratory Internal Report, IR-78) indicates that the upper part of the Ancha Formation is between 2.8 and 1.6 Ma old. Both units rest unconformably on older tilted Santa Fe Group (Stearns, 1979).

QUATERNARY

Holocene alluvium, stream terraces, colluvium, fan deposits, and talus
Narrow bands of alluvium mark the area covered by water during seasonal runoff. Areas downslope movement of sediment are underlain by colluvium. Terrace deposits flank important drainages, such as Tuerto Arroyo, Arroyo de la Joya, Cunningham Gulch, and Cañamo Arroyo. Small alluvial fans are present at the headwaters of small tributaries. Talus deposits are locally significant at higher elevations of the Ortiz Mountains.

3   IGNEOUS ROCKS

INTRUSIVE ROCKS

Intrusive rocks on the Ortiz Mine Grant can be divided into an early group, consisting of quartz-bearing laccoliths and related sills and dikes, and a later group, consisting of quartz-poor and generally nepheline-normative stocks and dikes. These groupings are typical of the entire Ortiz Porphyry Belt (Stearns, 1953; Disbrow and Stoll, 1957; Atkinson, 1961). Isotopic dating, detailed in a later section of this report, shows that the first group ranges from 33.3 to 36.2 million years old (Ma). The second group cuts the laccolithic rocks; its oldest age is therefore constrained by the ages given for the laccoliths. Volcanics and a subvolcanic stock of the second group yield dates of 31.3 to 31.9 Ma. Base- and precious-metal mineralization occurs with the latest stages of the second group of intrusive rocks, at approximately 31 Ma.

Previous workers in the Ortiz Mountains have divided the intrusive rocks into aphanitic-porphyritic types and phaneritic types (McRae, 1958; Peterson, 1958; and Coles, 1991). Coles (1991) further divided the intrusives into early and late groups.

The following descriptions of the intrusive rocks from the Ortiz Mine Grant are taken from Coles (1991), and listed in order of decreasing age based on cross-cutting relations. Two hundred and one thin sections representing the various igneous phases were examined petrographically by Coles (1991). Classification of the rocks is based on a QAPF modal classification scheme for phaneritic rocks (**Figures 3-1a and 3-1b**) and on alkali-silica plots of whole-rock analytical samples including phaneritic and aphanitic to micro-phaneritic intrusives, and those containing very fine-grained isotropic material in the groundmass. Whole-rock analyses taken from Coles (1991) and Ogilvie (1908) are listed in **Appendix I**. Alkali-silica plots are presented for samples considered fresh on the basis of Coles' (1991) petrographic study (**Figure 3-2**). Using the criteria of MacDonald and Katsura (1965), the early group of intrusives falls into the subalkaline field and the later group mostly lies in the alkaline field (**Figure 3-3**).

EARLY INTRUSIVES – CALC-ALKALINE GROUP

Quartz andesite porphyry (Tap)

Andesite porphyry laccoliths, sills, and dikes constitute the oldest igneous rocks in the Ortiz Mountains area (Peterson, 1958; McRae, 1958; Kay, 1986, and Coles, 1991). Isotopic age determinations (K-Ar and ^{40}Ar/^{39}Ar) cluster in the range from 33.3 +/- 0.09 to 36.2 +/- 0.8 Ma (Mehnert and Bachman, 1979; Sauer, 1999; this study). Ogilvie (1908) and Keyes (1909) first regarded all the intrusive rocks of the Ortiz and San Pedro Mountains as parts of laccolithic masses (**Figure 3-4**). On the Ortiz Mine Grant, andesite porphyry occurs in 9 principal known laccolithic bodies, plus numerous smaller sills and dikes (**Figure 3-5 and 3-6**). Andesite porphyry forms laccoliths throughout the Ortiz Porphyry Belt. Andesite also occurs as dikes parallel to the Golden Fault, a part of the Tijeras-Cañoncito Fault System.
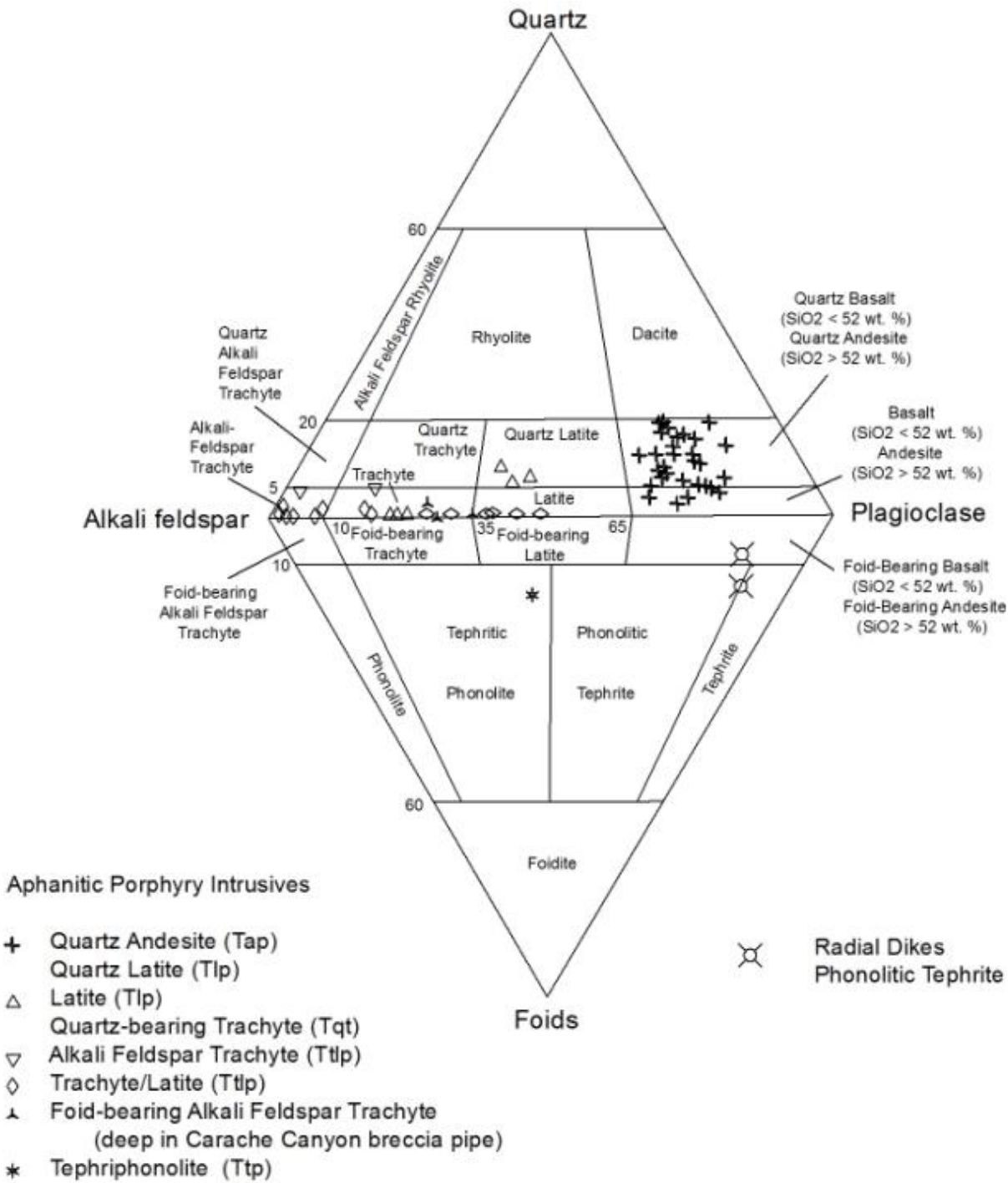
Figure 3-1a. QAPF plot of aphanitic intrusive rocks, including porphyries, of the Ortiz Mountains.

Figure 3-1b. QAPF plot of phaneritic intrusive rocks of the Ortiz Mountains.

Aphanitic intrusive rocks

X Quartz andesite porphyry (Tap)
△ Latite porphyry (Tlp)
▵ Quartz latite porphyry (Tlp)
◇ Quartz-bearing trachyte (Tqt)
⅄ Foid-bearing alkali feldspar trachyte
(deep in Carache Canyon breccia pipe)
＊ Tephriphonolite (Ttp)
⛣ Phonolitic tephrite
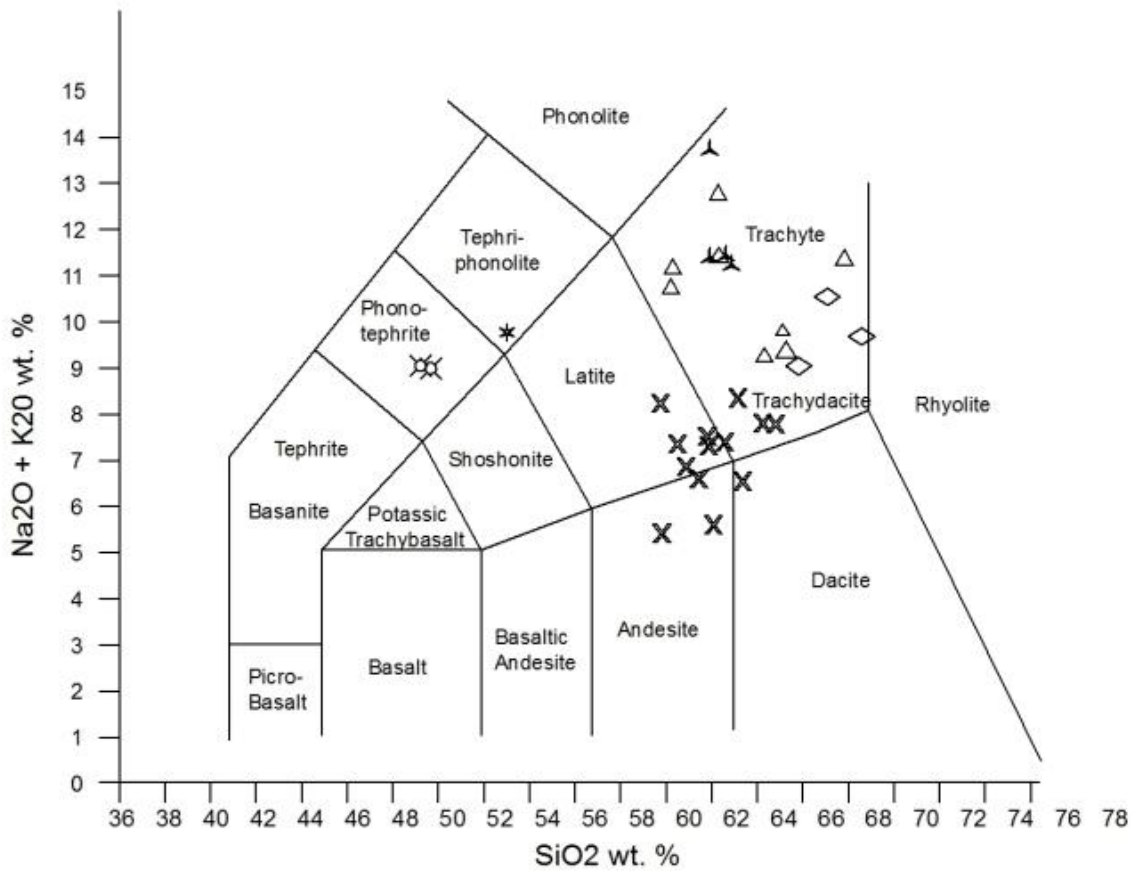
Figure 3-2. Total alkali-silica grid plot of intrusive rocks of the Ortiz Mountains.

Aphanitic intrusive rocks

X   Quartz andesite porphyry (Tap)
△   Latite porphyry (Tlp)
▲   Quartz latite porphyry (Tlp)
◇   Quartz-bearing trachyte (Tqt)
⊥   Foid-bearing alkali feldspar trachyte
      (deep in Carache Canyon breccia pipe)
∗   Tephriphonolite (Ttp)
⋈   Phonolitic tephrite

Phaneritic intrusive rocks

⊞   Quartz monzodiorite (Tqmd)
○   Hornblende-augite monzonite (Tam)
○   Augite monzonite (Tam)
⊖   Augite monzonite and hornblende monzonite
      (from Kay, 1986) (Tam)

Figure 3-3. Total alkali-silica diagram showing the line dividing the alkaline and subalkaline fields (MacDonald and Katsura, 1965). Modified from Coles (1991).

44
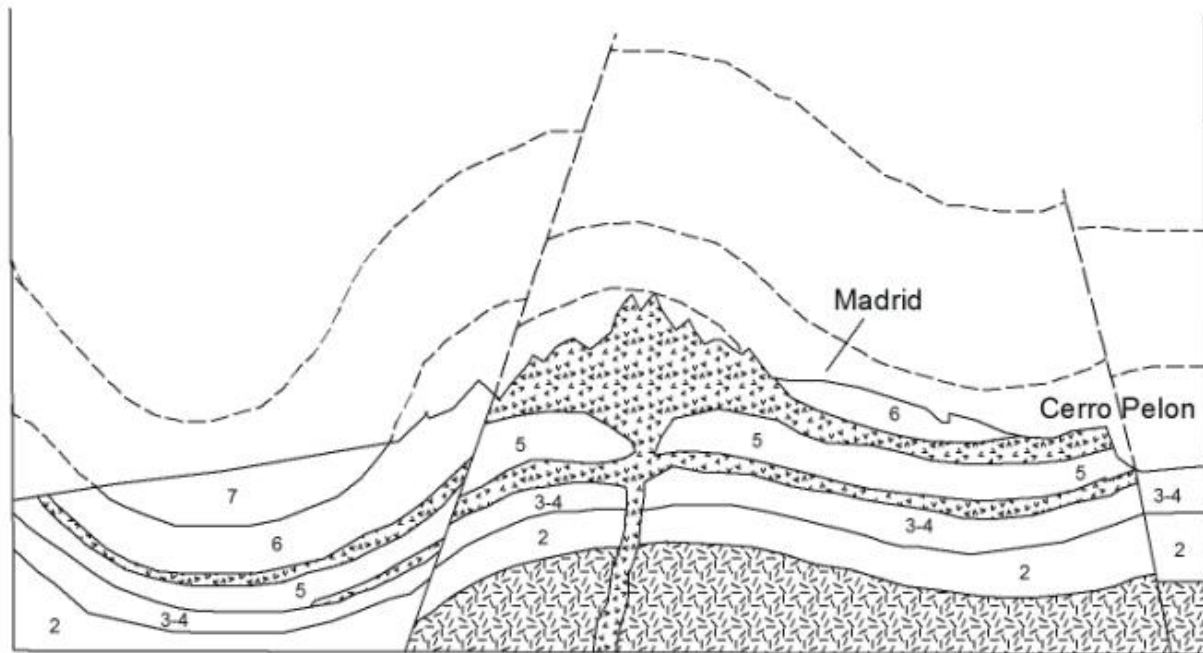
a)
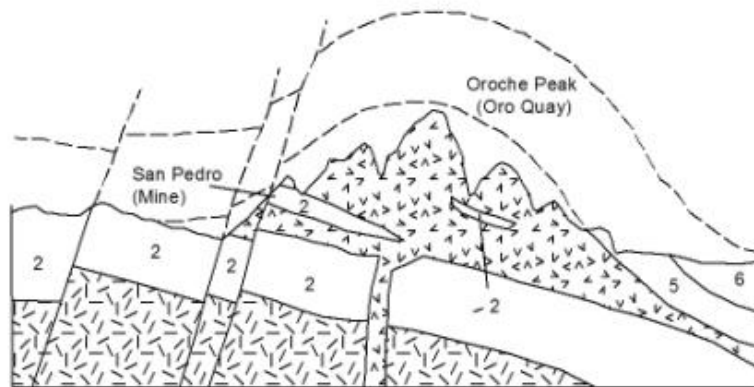
b)

EXPLANATION

 Laccolith

 Azoic schists

7. Tertiary marls and sands
6. Laramie (coal) shales and sandstones
5. Montana (coal) shales
4. Colorado shales
3. Mora sandstones
2. Carboniferous shales and limestones

Figure 3-4. Cross sections showing Keyes' (1909) models of laccoliths in the Ortiz Porphyry Belt. Keyes envisaged the igneous rocks of the San Pedro and Ortiz Mountains as monolithic laccolith complexes. a) Ortiz Mountains – Cerro Pelon. Note that the Cerro Pelon laccolith is shown connected to the mass of the Ortiz Mountains and that the Ortiz Mountains laccolith is shown extending into the Hagan Basin, offset by a basin-bounding fault. b) San Pedro Mountains.

45
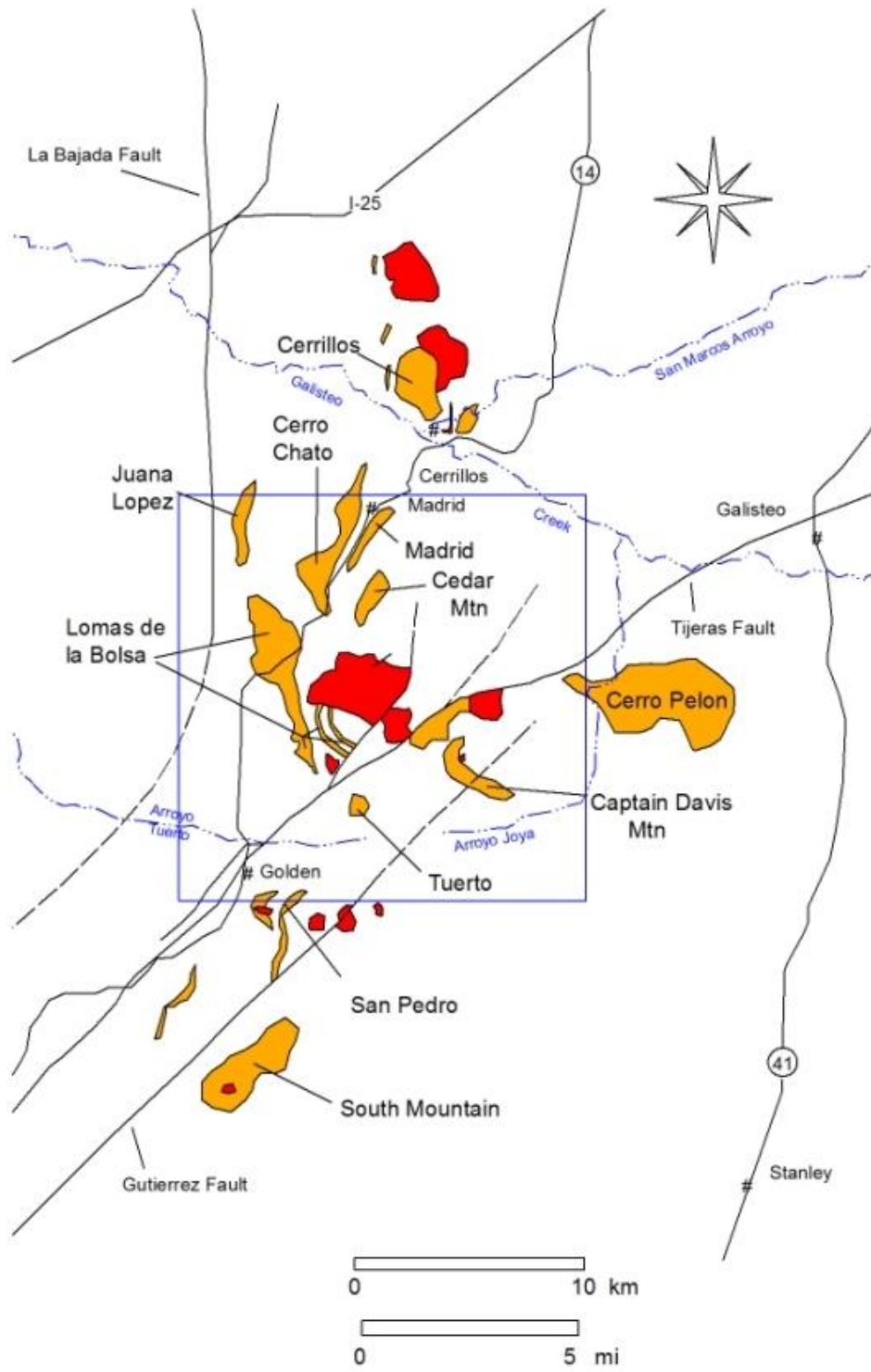
Figure 3--5. Exposed laccoliths (orange) of the Ortiz Porphyry Belt. Red indicates younger stock exposures. The Ortiz Mine Grant is outlined in blue.

Phenocrysts make up an average of 46% of the andesite porphyry with plagioclase dominating. Subhedral plagioclase phenocrysts (32%) are medium grained (1.4 mm average), and range in An content from 35 to 50%. Hornblende (12%) phenocrysts are euhedral, range from fine to medium grained (0.6-1.1 mm), and are black in fresh specimens. Quartz phenocrysts\ microphenocrysts average only 2% of the rock, and occur as groundmass to fine-grained (0.1-1.0 mm), clear, highly resorbed crystals. Augite, generally the least abundant phenocrystic phase, constitutes from 0 to 2% of the rock. It occurs as both distinct euhedral to subhedral, black phenocrysts\micro-phenocrysts (0.1-1.5 mm) and locally as cores to hornblende phenocrysts (Coles, 1991).

Andesite porphyry ranges from greenish gray to grayish green on fresh surfaces (Figure 3-6). Weathering produces surfaces that are olive drab to brownish green. Fractures in weathered rock locally contain coatings of iron and manganese oxide.

The microcrystalline groundmass makes up approximately 54% of the rock, with groundmass plagioclase averaging 29%, orthoclase 18%, and quartz 7%. The groundmass phases are anhedral and average 0.02 mm in size. Trace minerals include apatite and sphene, which locally make up more than 1% of the rock. They occur as euhedral microphenocrysts averaging 0.8 mm in size and as inclusions in hornblende. Allanite, zircon, and rutile occur as accessory minerals that make up less than 1% of the rock.

Figure 3-6. Andesite porphyry. a) Road-cut exposure of andesite porphyry sill on NM-14 on western flank of the Ortiz Mountains. b) Close up of lower sill contact. c) Hand specimen of andesite porphyry, note porphyritic texture and mafic inclusion in lower part of photo.

Lomas de la Bolsa Laccolith (Tap)

The Lomas de la Bolsa Laccolith comprises andesite porphyry masses that make up the bulk of Las Lomas de la Bolsa, the sills exposed on the western and south-central parts of the Ortiz Mountains, and in drilling at Lukas and Carache Canyons. In the western and south central Ortiz Mountains, the sills intrude Jurassic through Cretaceous sediments. Andesite porphyry sills and dikes in the Paleocene Diamond Tail Formation in the Ortiz Graben and near the Cunningham Hill Mine may represent the highest levels of the Lomas de la Bolsa Laccolith. In the vicinity of Las Lomas de la Bolsa and the adjacent part of the Ortiz Mountains (where NM-14 crosses the range at Stagecoach Canyon), andesite porphyry appears in map pattern to form a large irregular intrusive mass. Large sections of the Jurassic-Cretaceous stratigraphic succession are missing. In contrast, to the north and south, the andesite porphyry forms discrete concordant bodies and the stratigraphic section is complete, though "inflated" by the intrusive bodies. It is therefore inferred that the Stagecoach Canyon area is the central feeder zone of the Lomas de la Bolsa laccolith.

Captain Davis Mountain Laccolith (Tap)

A large faulted mass of andesite porphyry invading Cretaceous Mancos Shale lies adjacent to the Tijeras-Cañoncito Fault System (TCFS) at Captain Davis Mountain and Lone Mountain, to the east of the main mass of the Ortiz Mountains (this study; Lisenbee and Maynard, 2001). Faulting and the later intrusion of a granodiorite stock on the eastern end of Captain Davis Mountain and an augite monzonite plug on Lone Mountain obscure the original configuration of the andesite porphyry body in map pattern. Contacts of individual sills are commonly observed to be parallel to bedding, especially on the south and east sides of Lone Mountain. A central feeder system is likewise obscure, but may be inferred to lie along the TCFS, because of the greatest abundance of andesite porphyry in this area.

Cerro Chato, Madrid, Cedar Mountain and Juana López Laccoliths (Tap)

Three separate concordant andesite porphyry laccoliths intrude Mesa Verde Group sedimentary rocks and form prominent ridges, from the north flank of the Ortiz Mountains to the town of Madrid (**Figure 3-5**). A fourth laccolith, the Juana López Laccolith, intrudes the lower part of the Mancos Shale. No dikes or other feeder structures connecting the individual bodies have been observed. Such connecting structures may exist at depth, or they may have been eroded away. Johnson (1903) hypothesized that the laccoliths propagated from the Ortiz Mountains. However, the greatest thickness of each of these bodies appears to lie some distance away from the Ortiz Mountains, suggesting that the centers of the laccoliths (or feeding structure of a Christmas-Tree laccolith) lay away from the Ortiz Mountains.

San Pedro Laccolith (Tap)

The San Pedro laccolith, as mapped by Atkinson (1961), Ferguson and Osburn (2000), and Maynard (2000) is comprised of two concordant bodies of andesite porphyry in the western part of the San Pedro Mountains (**Figure 3-5**). Only one of the intrusive bodies is exposed. A lower sill is suggested by the high position of Pennsylvanian Madera Formation in the San Pedro Mountains with respect to Permian and Triassic strata exposed in Tuerto Arroyo to the north. Smaller, irregular masses of andesite porphyry also crop out in the eastern part of the range. Poorly exposed andesite porphyry intrudes Triassic strata in the valley between the San Pedro Mountains and the Ortiz Mountains. The two principal sills of the San Pedro laccolith intrude

limestone and shale of the Pennsylvanian Madera Formation and range in thickness from 0 to 60 m (0 to 200 ft). Strata and sills in the San Pedro Mountains are tilted to the east, except along the western flank of the range, where they are near horizontal (Atkinson, 1961; Ferguson and Osburn, 2000; Maynard, 2000).   Connecting feeder dikes between the sills have not been identified, though poor exposures of andesite porphyry southwest of the village of Golden, along a major strand of the TCFS, suggest a feeder there, with a "Christmas Tree", or half-"Christmas Tree" laccolith centered adjacent to the fault. The down-dip extent of the sills is not known.

Cerro Pelon Laccolith (Tap)

The Cerro Pelon Laccolith is exposed in the eastern-most part of the Ortiz Mine Grant. Mapping by Lisenbee (1967), Bachman (1975), Lisenbee (2000), and Lisenbee and Maynard (2001), show the Cerro Pelon laccolith as a body separated from the Ortiz Mountains by the Tijeras Cañoncito Fault System. The Cerro Pelon laccolith is comprised of a single 150 m- (500 ft-) thick concordant body invading Cretaceous Mesa Verde Group (Lisenbee, 1967; Lisenbee and Maynard, 2001; Lisenbee, 2000).

Tuerto Laccolith (Tap)

Andesite porphyry intrudes mudstone of the Chinle Group in the region between the Ortiz Mountains and Tuerto Arroyo in the south-central part of the Ortiz Mine Grant. Exposures are poor in this area, however it is postulated that a sizeable laccolith may have developed in the Triassic strata in this area.

Quartz-hornblende monzodiorite (Tqmd)

Quartz-hornblende monzodiorite crops out at Candelaria Mountain, in the southwestern part of the Ortiz Mountains. This rock is weather-resistant and forms steep slopes and cliffs with 0.2 to 5.0 meter diameter blocks at the base. The rock generally is medium to light gray, and hornblende crystals impart a black speckled appearance on fresh surfaces. Weathered surfaces are usually chalky gray to tannish brown, depending on the intensity of iron oxide staining. A similar intrusion is mapped on the eastern side of Captain Davis Mountain (Lisenbee and Maynard, 2001). K-feldspar from a single sample from Candelaria Mountain yielded a ^{40}Ar/^{39}Ar age of 31.1 Ma (this study).

The quartz-hornblende monzodiorite is commonly hypidiomorphic granular and rarely porphyritic. Plagioclase (An_{39}-An_{43}), the dominant constituent (51%), occurs as subhedral to euhedral, 0.8 mm crystals. Orthoclase (19%) is interstitial to the plagioclase and ferromagnesian minerals, as anhedral crystals that average 0.7 mm in their longest dimension. Hornblende constitutes 15% of the rock, is subhedral, averages 0.8 mm on its longest axis, and exhibits minor alteration to biotite chlorite, epidote, and quartz. Augite is rare and like hornblende, it exhibits minor alteration to biotite.   Primary biotite is present as a minor constituent in two samples, where it occurs as subhedral, 0.1 mm crystals. Quartz (13%) occurs as anhedral, 0.4 mm crystals, interstitial to plagioclase and hornblende.

Accessory minerals include magnetite, apatite, sphene and rutile. Magnetite locally constitutes from 1 to 2% of the rock where it occurs as subhedral, 0.15 mm crystals. Other accessories make up less that 1% of the rock and are typically euhedral.

The quartz hornblende monzodiorite forms roughly cylindrical stocks at both Candelaria Mountain and Captain Davis Mountain. Cross-cutting relations indicate that the quartz hornblende monzodiorite is younger than the andesite-porphyry laccoliths. However its

relationship to the Tijeras Cañoncito Fault System and to the augite monzonite stock is not known. Late trachyte dikes cut it, however.

LATE INTRUSIVES – ALKALINE GROUP

Augite monzonite, hornblende-augite monzodiorite, and hornblende monzonite (Tam)

Augite monzonite, hornblende-augite monzodiorite, and hornblende monzonite form the the core of the Ortiz Mountains and underlie its highest peaks. These rock types are grouped together for the sake of mapping as augite monzonite. K-Ar and ^{40}Ar/^{39}Ar age determinations range from 29.6 +/- 1.5 to 35.36 Ma. The age of the augite monzonite may be more tightly constrained by its cutting 33.3 +/- 0.09 to 36.2 +/- 0.8 34 Ma quartz andesite porphyry laccoliths and its being cut by the 31.1 to 31.91 Ma latite porphyry subvolcanic stock in Cunningham Gulch.

On fresh surfaces the rock ranges from light gray to deep gray or black (**Figure 3-7**). Locally, potassium feldspar imparts a pinkish tint to the rock. Weathered surfaces appear chalky gray white to tannish brown, depending on the presence and thickness of iron oxide stains.

Plagioclase (An$_{32}$-An$_{48}$) is usually the dominant phase in the augite monzonite, making up 43% of the rock. It occurs as subhedral crystals that average 0.6 mm in length. Orthoclase (37%) is found in subequal amounts to plagioclase and locally exceeds plagioclase in abundance. Orthoclase occurs as anhedral to subhedral, 0.6 mm, crystals that locally enclose plagioclase, augite, and hornblende giving the rock a poikilitic fabric. Quartz was observed in two samples as a trace mineral.

The presence or absence of nepheline is a subject of disagreement among the various investigators that have studied the Ortiz Mountains. Nepheline was identified in the augite monzonite by Ogilvie (1908).   McRae (1958) confirmed Ogilvie's observation, stating that some samples in his study area, in the northern portion of the Ortiz Mountains, contain as much as 10% nepheline, was not seen in any of the study samples but it may have been reported as clouded orthoclase and counted accordingly in the modes. Kay (1986) was unable to positively identify the presence of nepheline in his study area near the old Ortiz Mine. Coles (1991) also failed to identify nepheline in his study. Normative mineral calculations reported by Kay (1986) and Coles (1990) show that the augite monzonite contains between two and ten weight percent normative nepheline. It may be that modal nepheline occurs in discrete portions, or phases, of the augite monzonite, hornblende-augite monzodiorite, and hornblende monzonite stock. Kay (1986) focused most of his attention in the area around the Cunningham Hill Mine and Coles' (1990) samples came mainly from the central and southern part of the Ortiz Mountains.

Augite (8%) and hornblende (8%) are present in the Coles' (1991) study sample in sub equal amounts, with augite usually dominating. Subhedral augite is mantled by hornblende. In Ig-90, augite is successively rimmed by common hornblende and a green to emerald green pleochroic amphibole that may be arfvedsonite, but is too fine grained for accurate determination of its optical properties. Hornblende appears in part to have grown at the expense of augite and averages half the size (0.4 mm) of the augite crystals.   Biotite occurs as a trace mineral that, like hornblende, grew as a replacement of augite.
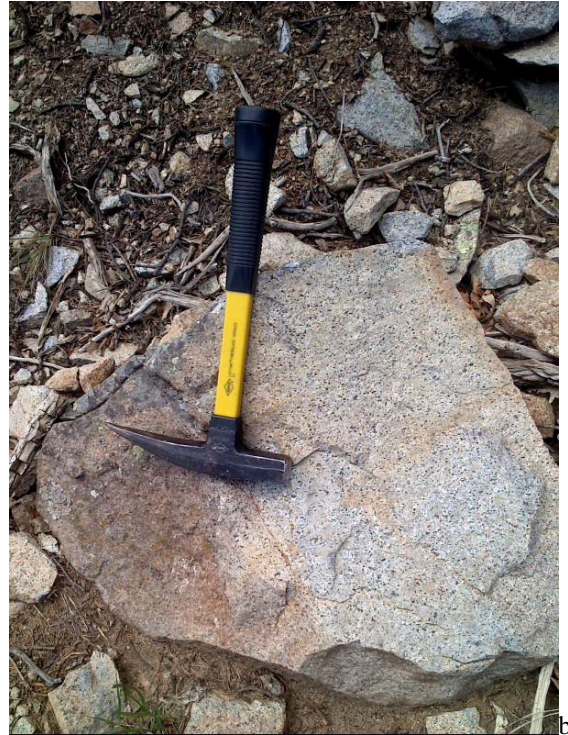
Figure 3-7. Examples of augite monzonite. a) Outcrop of augite monzonite on Placer Peak trail. Note sheeted fracturing.   b) Hand specimen of augite monzonite.

Biotite crystals are subhedral and are very small, averaging only 0.25 mm on their longest axis. McRae (1958) reports that biotite constitutes from 0 to 9% of this rock type.

Magnetite is the most abundant accessory mineral making up 3% of the rock on average and ranging from 2 to 4%. The 0.15 mm average diameter magnetite crystals are usually subhedral and in part appear to replace ferromagnesian minerals and sphene. Apatite, sphene, zircon, rutile, and allanite occur as accessory minerals that make up less than 1% of the rock.

Hornblende-augite monzodiorite is very resistant and tends to form steep slopes and cliffs, locally with large boulders strewn at the base. On fresh surfaces, the rock is generally gray to pale pink, with conspicuous black spots imparted by hornblende and augite. Weathering tends to produce a tannish brown to pinkish color caused by iron oxide stains. Texturally, the hornblende-augite monzodiorite is hypidiomorphic granular. In hand sample, it is very similar to augite monzonite from which it usually cannot be distinguished due to fine grain size. Hornblende-augite monzodiorite, therefore, was not mapped separately from the augite monzonite.

Plagioclase (An_{30}-An_{40}) is the most abundant constituent (55%) of the hornblende-augite monzodiorite. It occurs as subhedral, 0.9 mm length crystals. Anhedral orthoclase (26%) occurs as interstitial filling between earlier formed plagioclase and ferromagnesian minerals. Quartz constitutes 3% of the rock and, like orthoclase, is a late stage, anhedral, interstitial filling. The quartz crystals average 0.1 mm in their longest dimension. Augite (7%) occurs as subhedral to euhedral crystals that average 0.5 mm in length. Hornblende (4%) occurs as subhedral crystals that average 0.6 mm on their longest axis. Both augite and hornblende show minor alteration to biotite, chlorite, epidote, and magnetite, that represents late-stage deuteric effects.

Magnetite, sphene, apatite, zircon, and rutile constitute the accessory minerals in this rock. Magnetite (3%), the most abundant accessory mineral, occurs as subhedral 0.15 mm

crystals that in part appear to replace ferromagnesian minerals and sphene. Sphene, apatite, zircon, and rutile make up less than 1% of the rock.

Hornblende monzonite apparently is a phase of the augite monzonite (Maynard et al., 1989). It occurs southeast of a latite stock (Kay, 1986) and within the Ortiz graben (Maynard et al., 1989). Plagioclase and hornblende make up 40% and 15% of the hornblende monzonite, respectively. These early phases are enclosed by later interstitial cloudy orthoclase that makes up 30 % of the rock. Other phases that occur in minor amounts include augite (5%), biotite (3%), apatite (1.5%), sphene (1.5%), magnetite (2%), and epidote (2%) (Kay, 1986).

Kay (1986) reported a K-Ar date of 29.6 +/- 1.5 Ma for the hornblende monzonite and a K-Ar date of 30.3 +/- 1.2 Ma for the quartz latite/latite stock, which intrudes the hornblende monzonite. The overlapping data suggest that the intrusions are closely related temporally, as well as spatially.

Quartz latite and latite porphyry (Tlp)
The quartz latite and younger latite porphyries occur in the upper part of Cunningham Gulch in an elongate stock to the southwest of the Ortiz volcanic vent breccia and intrude the main augite monzonite stock (McRae, 1958; Kay, 1986). The rock types are grouped together on the geologic map. Isotopic dates range for the quartz latite and latite porphyry range from 29.9 +/- 1.2 to 35.1 +/- 1.4 Ma (Kay, 1986; this study). $^{40}Ar/^{39}Ar$ ages cluster in the range from 31.56 to 31.91 Ma (this study). Quartz latite is restricted to the southwestern end of the stock and forms the summit of Porphyry Hill. A small plug of latite porphyry also is present immediately to the northwest of Carache Canyon (**geologic map**). Weathering produces light gray to tannish brown iron oxide coatings on outcrops of both latites. Orthoclase phenocrysts are resistant to weathering relative to the groundmass and other phenocrysts, and stand out in relief on weathered surfaces (**Figure 3-8**).
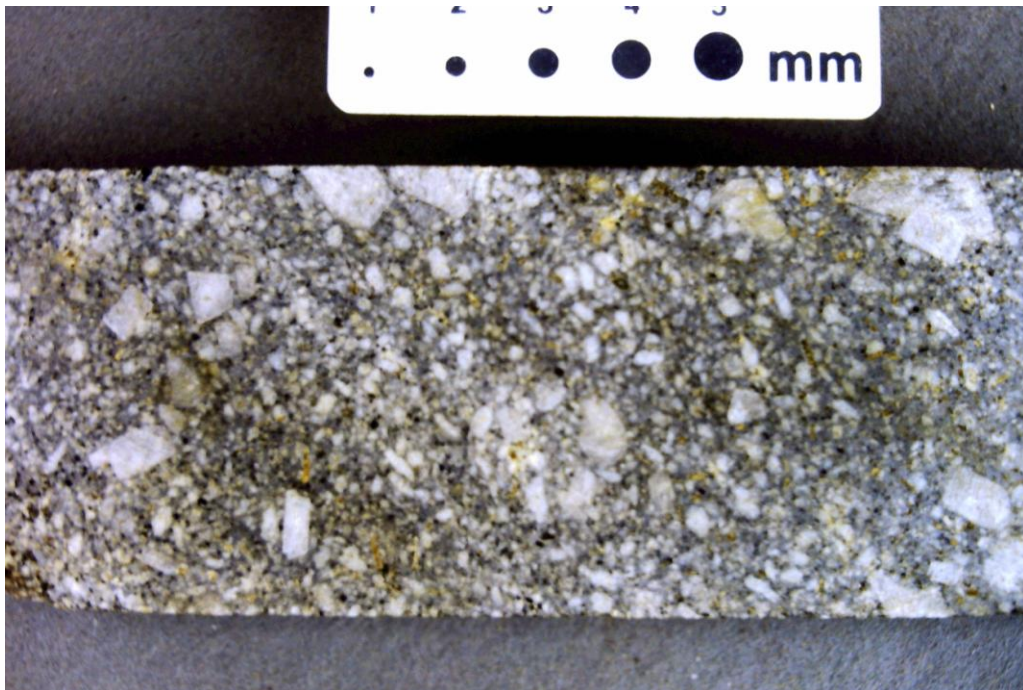
Figure 3-8. Sawed drill core of latite porphyry, Porphyry Hill - upper Cunningham Gulch.

The quartz latite samples studied from the Porphyry Hill-Cunningham Gulch area contain 38% plagioclase (An_{30} to An_{44}) phenocrysts. They are subhedral to euhedral, average 1.5 mm in size, and most are sodic-andesines. Orthoclase phenocrysts make up 10% of the rock on average, are subhedral, and average 3.0 mm in size. Ferromagnesian minerals make up approximately 6% of the rock and include hornblende, pyroxene, and biotite. Hornblende occurs as subhedral to euhedral, 0.8 mm phenocrysts. Pyroxene in OCN-10, 431' was identified by optical means as aegirine-augite but is too altered in other quartz latite samples to positively identify. Aegirine-augite occurs as euhedral to subhedral microphenocrysts that average 0.4 mm on their long axis and appears to predominate over hornblende. Biotite microphenocrysts (<1%) are subhedral to euhedral and average 0.2 mm on their longest axis.

The aphanitic microgranular groundmass (46%) consists of orthoclase, which is estimated, to make up 39% of the rock and quartz that makes up about 7%. The groundmass phases average 0.02 mm in size and are anhedral. Apatite and sphene occur as accessory minerals that make up less than 1% of the rock. Both minerals occur as euhedral crystals and average 0.08 mm on their longest axis.

The latite usually has smaller phenocrysts than the quartz latite; otherwise, they appear identical in hand specimen. Plagioclase phenocrysts (36%) are euhedral to subhedral and average 0.8 mm along their c-axes. Euhedral to subhedral orthoclase phenocrysts (12%) average 1/0 mm on their long axis. Augite, at Porphyry Hill, and aegirine-augite, at Rattlesnake Hill, are the only ferromagnesian phases in the latite. They occur as euhedral to subhedral phenocrysts that make up 6% of the rock and average 0.5 mm along the c-axis.

The aphanitic microgranular groundmass (46%) consists of orthoclase, which is estimated, to make up 39% of the rock and quartz that makes up about 7%. The groundmass phases average 0.02 mm in size and are anhedral. Apatite and sphene occur as accessory minerals that make up less than 1% of the rock. Both minerals occur as euhedral crystals and average 0.08 mm on their longest axis.

POST-VOLCANIC INTRUSIVES IN THE ORTIZ MOUNTAINS

Dikes of latitic to trachytic composition cut the volcanic vent breccia of Dolores Gulch and are therefore considered post-volcanic. Similar dikes cutting the Carache Canyon collapse breccia and the quartz monzodiorite stock at Candelaria Mountain are grouped with the post-volcanic intrusives on the basis of their similarity of chemistry and appearance.

Hornblende latite/trachyte porphyry (Thltp)
Hornblende latite/trachyte porphyry occurs as dikes parallel to the Tijeras-Cañoncito fault system within the Carache Canyon area, and to the southwest in upper Buckeye Canyon. This unit is more altered and more susceptible to weathering than other dike rocks at Carache Canyon and does not form extensive outcrops. Weathered samples of the latite/trachyte are grayish green and characterized by distinct light gray plagioclase phenocrysts and brown to brownish green altered hornblende phenocrysts.

Phenocrysts make up 45% of the average latite/trachyte with plagioclase dominating at 29%. Plagioclase phenocrysts are sericitized, subhedral and average 1.3 mm along the c-axis. Ferromagnesian mineral phenocrysts are the second most abundant phenocrystic phase constituting 16% of the rock. Pseudomorphic evidence indicates that both amphibole and

pyroxene were present, the amphibole having been dominant. These replaced phenocrysts average 1.3 mm and consist entirely of secondary minerals. Biotite phenocrysts are present in several specimens (OC-40, 314.5' and OC-53, 465.5') and may have been ubiquitous before alteration. The biotite averages 0.4 mm on its long axis and is subhedral to euhedral.

The groundmass has a weakly- to well developed trachytic to pilotaxitic texture and consists of sanidine, minor plagioclase, and trace amounts of biotite and apatite. Groundmass sanidine makes up 53% of the average latite\trachyte. It measures 0.06 mm on its c-axis, and is subhedral. Plagioclase makes up about 1% of the groundmass and crystals are much larger (0.3mm) than those of groundmass alkali feldspar. It may be closely related to the phenocrystal plagioclase. Apatite, and zircon are the only accessory minerals. Apatite occurs as subhedral, 0.09 mm crystals within the sanidine groundmass, and zircon occurs as 0.01 mm crystals.

Porphyritic alkali feldspar trachyte and trachyte/latite porphyry (Ttlp)

Porphyritic alkali feldspar trachyte occurs as dikes that crosscut hornblende latite/trachyte and the Carache Canyon breccia pipe. Like the hornblende latite/trachyte porphyry, the trachyte dikes lie parallel to the Tijeras-Cañoncito fault system. The trachyte dikes weather to conspicuous positive relief relative to host sediments and andesitic porphyry sills **(Figure 3-9)**. The trachyte is light tannish brown on weathered surfaces due to iron staining. Liesegang bands are prominent at some locations on the surface and in near-surface drill core, and apparently reflect a weathering phenomenon.

Phenocrysts make up 7% of the trachyte on average, although many samples contain no phenocrysts. Plagioclase phenocrysts (3%) are subhedral to euhedral, and average 1.2 mm along their c-axis. Commonly, thin sanidine rinds rim the plagioclase phenocrysts. Locally plagioclase cores sanidine phenocrysts.   Sanidine phenocrysts (4%) are more euhedral than the plagioclase phenocrysts, average 1.5 mm along the c-axis and generally occur as glomeroporphyritic arrays.

Groundmass sanidine constitutes approximately 87% of the rock, is euhedral, averages 0.3 mm on its long axis, and displays well-developed pilotaxitic to trachytic texture. Anhedral alkali feldspar (probably sanidine) occurs interstitially to sanidine laths and represents the last phase to crystallize. Altered ferromagnesian minerals and/or filled vesicles also occur interstitially to the sanidine laths. These sites make up 5% of the average sample, average 0.1 mm in diameter, and are now occupied by sericite and/or carbonates. Euhedral apatite and anhedral quartz are present in some samples as trace minerals interstitial to sanidine laths.

Trachyte/latite dikes crosscut the quartz latite/latite stock and thus clearly are younger. Texturally, these rocks closely resemble latite/trachyte in the stock at Rattlesnake Hill. Plagioclase (An_{34}-An_{37}) phenocrysts constitute 25% of the Carache trachyte/latite porphyry samples, are subhedral to euhedral and average 0.8 mm in length. Orthoclase phenocrysts (11%) are euhedral to subhedral, average 3.5 mm in length and locally occur as glomerophenocrysts. Exsolutions of albite-producing patchwork perthites are common. A phenocrystal ferromagnesian mineral made up 5% of the rock, but has been removed by hydrothermal alteration and weathering in all of the samples observed.

The groundmass consists of fine grained to aphanitic (0.08 mm) alkali feldspar that appears to by orthoclase based on its optical properties. Groundmass texture ranges from microgranular to weakly pilotaxitic. Apatite (1%), the only accessory mineral, occurs as 0.07 mm, euhedral crystals.
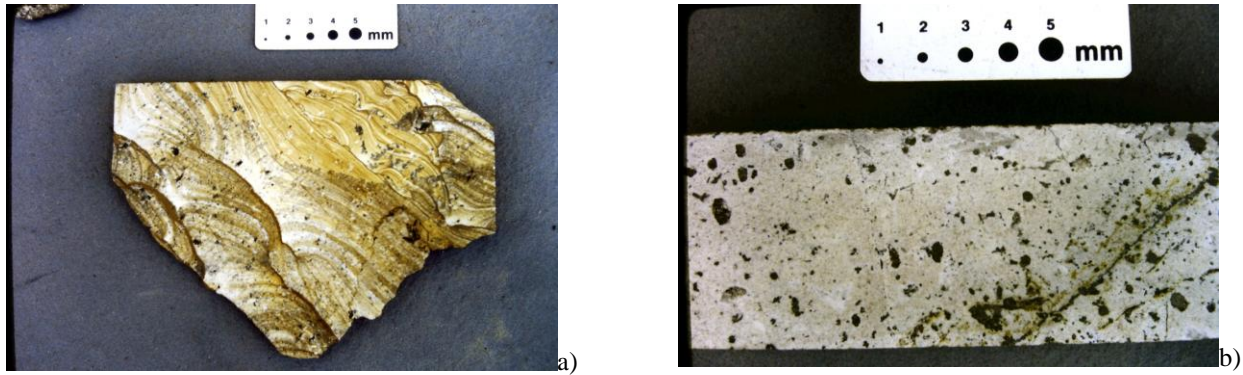
Figure 3-9. Sawed examples of porphyritic alkali feldspar trachyte, Carache Canyon. a) Surface sample with well-developed liesegang banding. b) core sample of unoxidized porphyritic alkali feldspar trachyte. Dark spots are blebs of pyrrhotite.

Porphyritic foid-bearing alkali feldspar trachyte

Porphyritic foid-bearing alkali feldspar trachyte was observed only in drill core at Carache Canyon; its temporal relationship to other intrusives is unclear. It is fresher than the other trachytes and is not sericitized suggesting that the foid-bearing alkali feldspar trachyte is younger than altered trachytes and latites in the area. Volumetrically this appears to be the least important of the Carache intrusives.

Small (0.4 mm) subhedral altered plagioclase phenocrysts make up 1% of the rock on average. Euhedral sanidine phenocrysts make up 11% of the rock, occur in glomeroporphyritic arrays, and are locally cored by plagioclase. Pseudomorphic gieseckite (probably after nepheline) indicates that nepheline once constituted 2% of this rock on average. The nepheline had occurred as (0.2 mm), euhedral microphenocrysts.

The groundmass is dominated by fine-grained (0.1 mm) euhedral to subhedral sanidine laths (78%) that have a prominent trachytic texture. Magnetite makes up 2% of the rock and is responsible for the black color of the less altered samples. The magnetite is at least in part secondary and tends to be euhedral. A ferromagnesian mineral (6%) was present as a groundmass phase; however, hydrothermal alteration has resulted in the complete replacement of this mineral without leaving pseudomorphs. Small vugs (1%) interstitial to the groundmass sanidine laths may have been vesicles. These vugs commonly are filled with secondary clays, calcite, and fluorite.

Porphyritic quartz-bearing trachyte (Tqt)

Porphyritic quartz-bearing trachyte crops out as dikes in the southwest and western Ortiz Mountains (geologic map). Outcrops commonly have strong positive relief, are brownish-tan and locally display liesegang iron oxide banding due to weathering. Although crosscutting relationships are not clear, this unit is considered to be temporally close to the other latite and trachyte dikes in the Ortiz Mountains.

Phenocrysts make up 8% of the rock on average, and range from 3 to 14%. Plagioclase, the most abundant phenocrystal phase (5%) occurs as euhedral to subhedral 0.7 mm crystals. Euhedral, 0.7 mm, sanidine phenocrysts constitute 3% of the rock.

Sanidine is the most abundant groundmass phase, making up 77% of the average sample. Groundmass plagioclase makes up 8% of the rock. Both plagioclase and sanidine are pilotaxitically to trachytically aligned, are subhedral to euhedral, and average 0.1 mm in their

longest dimension. A ferromagnesian mineral (2%) occurred interstitially to the feldspars, but has been weathered to goethite in all samples except Ig-96 where biotite is present as 0.05 mm subhedral crystals. Magnetite makes up 1% of the rock; it occurs as euhedral, 0.05 mm crystals interstitial to feldspars. Quartz (4%), the last phase to crystallize, occurs interstitially to the feldspars, is anhedral, and averages 0.05 mm in diameter.

Tephriphonolite porphyry (Ttp)

Tephriphonolite porphyry occurs as a dike on the hillside northeast of Buckeye Canyon. This unit is unique among the latite and trachyte suite dikes in not being hydrothermally altered, indicating it may be younger than the other alkaline dike rocks. However, it may merely have been shielded from the alteration that affected nearby trachyte and hornblende latite/trachyte dikes.

Light gray, medium grained (1.2 mm), subhedral plagioclase phenocrysts make up 25% of the rock. Euhedral nepheline phenocrysts (2%) average 0.4 mm in diameter. The nepheline is completely altered, leaving only pseudohexagonal outlines filled with gieseckite and traces of analcime. Black, medium grained (1.1 mm), euhedral augite phenocrysts make up 15% of the rock.

A weakly pilotaxitic groundmass constitutes 60% of the rock. Sanidine (33%) is the most abundant groundmass phase and its euhedral to subhedral crystals average 0.1 mm along the c-axis. Second in abundance is biotite (12%), which occurs as 0.1 mm subhedral crystals. An amphibole, probably hornblende (3%) occurs as 0.1 mm, subhedral, crystals. Late stage anhedral 0.05 mm analcime (10%) crystals occur interstitially to the groundmass feldspar and ferromagnesian minerals. Magnetite crystals (2%) are anhedral to subhedral and average 0.07 mm in diameter. The magnetite is at least in part secondary in origin and locally exhibits replacement of all the other phases. Very fine grained (0.01-0.1 mm) euhedral crystals of apatite, rutile, allanite, and zircon occur as accessory minerals that make up less than 1% of the rock.

RADIAL DIKES

Phonotephrite porphyry (Tpp)

Phonotephrite porphyry occurs as a dike at the extreme northeast corner of the Ortiz Mine Grant. On fresh surfaces the phonotephrite porphyry is black, but a brown iron oxide stain coats weathered surfaces.

Phenocrysts make up 33% of the rock, with plagioclase (An_{45}) dominating. Euhedral, 1.0 mm average length, calcic-andesine phenocrysts make up 30 % of the rock. Augite phenocrysts (3%) are subhedral, and average 1.0 mm in length. The groundmass displays weakly to moderately developed pilotaxitic texture and makes up 64% of the rock.   Subhedral plagioclase crystals (32%) average 0.1 mm in length and represent the dominant groundmass phase. Groundmass augite (10%)occurs as subhedral crystals that average 0.08 mm in length. Subhedral magnetite averages 0.05 mm in diameter and constitutes 4% of the rock. Biotite (3%) occurs as subhedral crystals that average 0.05 mm in length. Alkali feldspar occurs as anhedral fillings between groundmass plagioclase, augite and biotite. This feldspar constitutes 12% of the rock and averages 0.03 mm in diameter. Apatite and rutile make up less than 1% of the rock and are euhedral.

Hornblende-porphyry monzonite (Thpm)

Hornblende-porphyry monzonite occurs as dikes in the southeastern part of the Ortiz Mine Grant. In hand specimen it is dark purple-brown and aphanitic, with phenocrysts of pyroxene and feldspar. Dikes to 7 m (23 ft) width stand as bold walls along much of their lengths.

EXTRUSIVE ROCKS
Espinaso Formation (Te)

The Oligocene Espinaso Formation is composed of volcanic breccias, pyroclastic flows, tuffs, and reworked volcaniclastic sediments. The Espinaso Formation is present in two principal exposures in the Hagan Basin and east of the Cerrillos Hills. In the Hagan Basin and east of the Cerrillos Hills, the Espinaso Formation overlies the Galisteo Formation with a gradational contact. It is overlain in the Hagan Basin by the Tano Formation of Connell (2001) of the Santa Fe Group. The unit has been interpreted as the product of volcanism in the Ortiz Porphyry Belt, particularly in the Ortiz Mountains and in the Cerrillos Hills. Kautz and others (1981) reports K-Ar dates from the base, middle, and top of the Espinaso Formation in the Hagan Basin of 34.3 +/- 0.8, 34.6 +/- 0.7, and 26.9 +/- 0.6 Ma, respectively. The first two dates correspond to isotopic dates of the laccolithic rocks of the Ortiz Porphyry Belt, suggesting that they are their extrusive equivalent. Kautz and others' (1981) third K-Ar date is from an olivine basalt flow in sedimentary rocks in the lowest part of the Santa Fe Group. Connell (2001), in redefining the stratigraphy of the Santa Fe Group in the Hagan Basin area, places the olivine basalt flow in the lowest part of the Tano Formation. The 26.0 +/- 0.6 Ma age therefore constrains the younger limit of the Espinaso Formation.

On the Ortiz Mine Grant, pyroclastic flow deposits of the Espinaso Formation are exposed in two small areas. A faulted block of moderately dipping block-and-ash deposits is exposed on the western side of the La Bajada Fault in the extreme northwestern part of the Grant. The Grant covers a small portion of Espinaso Formation pyroclastic flows and volcaniclastic sediments in its extreme northeastern part **(Figure 3-10)**.

Figure 3-10. Outcrop of partially reworked pyroclastic flow deposit of the Espinaso Formation. Northeastern part of the Ortiz Mine Grant.

Volcanic vent of Dolores Gulch (Tv)

In the Ortiz Mountains, vent-facies volcanic rocks are preserved at Dolores Gulch, attesting to volcanic activity associated with the latter part of the second group of intrusive rocks. Various investigators (Stearns, 1953a, Disbrow and Stoll, 1957, Kautz and others, 1981, and Erskine and Smith, 1993) have noted compositional variations in the Espinaso volcanics suggesting that earlier intrusives may have contributed to the volcanic pile.

Volcanic rocks underlie a roughly elliptical area 1900 x 900 m (6200 x 3000 ft) in Dolores Gulch, in the eastern part of the Ortiz Mountains, immediately north of the Cunningham Hill Mine. Most exposures of the volcanic rocks, such as in the upper pit walls of the Cunningham Hill Mine, are a matrix-supported breccia composed of clasts of igneous and sedimentary rock in a tuffaceous matrix **(Figure 3-11)**. Lithic clasts vary in size and composition. In some exposures the vent breccia may be described as a lithic tuff. Fine-grained, water-lain sediments occur in the southeastern part of the vent breccia, suggesting a subsiding basin. Along the northwestern margin of the vent breccia, clasts are predominantly augite

monzonite. Along the southeastern margin, quartzite and other clasts of sedimentary origin dominate.

Core drilling shows that the volcanic rocks are at least 330 m (1000 ft) thick and that the body's contacts with the surrounding rocks are near vertical. This observation, coupled with the unsorted nature of much of the volcanic breccia, the intrusive contacts with sandstone of the Diamond Tail Formation, and the subvolcanic latite stock, lead to the interpretation of the Dolores Gulch volcanics being a vent facies.

Kay (1986) reports a K-Ar date on hornblende from the Dolores Gulch volcanic vent of 34.2 +/- 1.4 Ma. This date seems too old, given that the volcanic vent clearly is younger than the andesite porphyry and the augite monzonite. Two $^{40}Ar/^{39}Ar$ isochron dates on K feldspar from the volcanic vent (this study) yielded ages of 31.31 and 31.48 Ma. These dates are consistent with ages reported above for the subvolcanic quartz latite and latite porphyry stock.

a)

Figure 3-11. Field exposures of the Dolores Gulch volcanic vent. a) Lithic tuff-breccia, upper Dolores Gulch. b) Lithic tuff-breccia in wall of Cunningham Hill mine. Yellow color from oxidation of pyrite.

b)
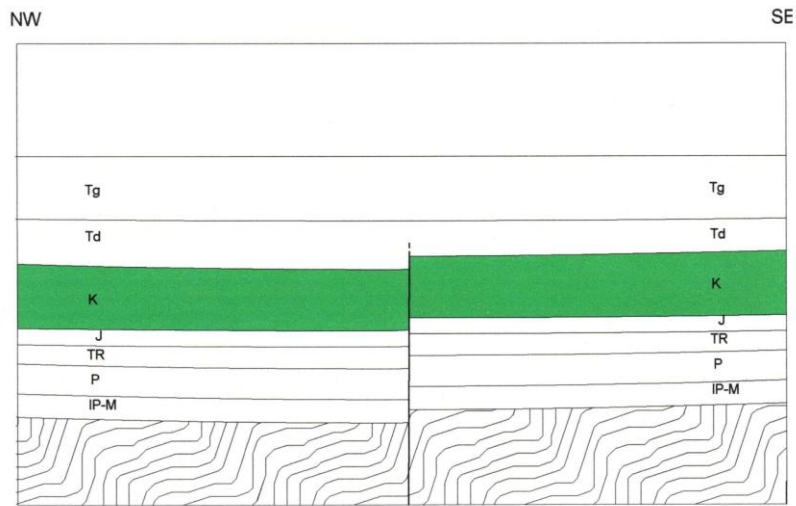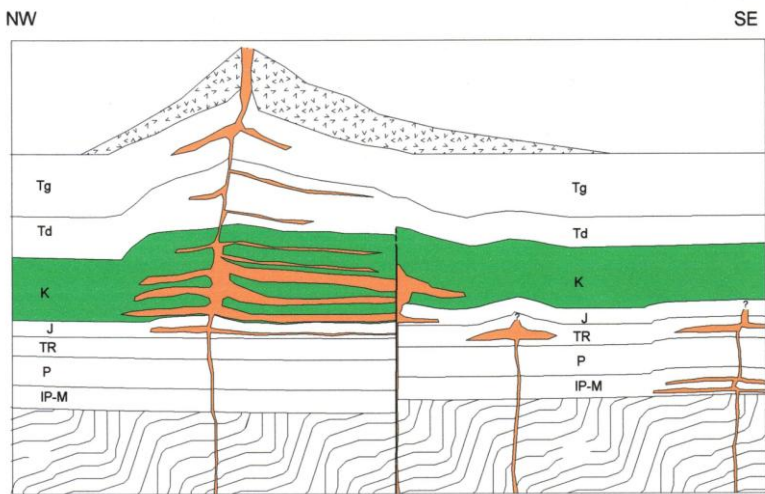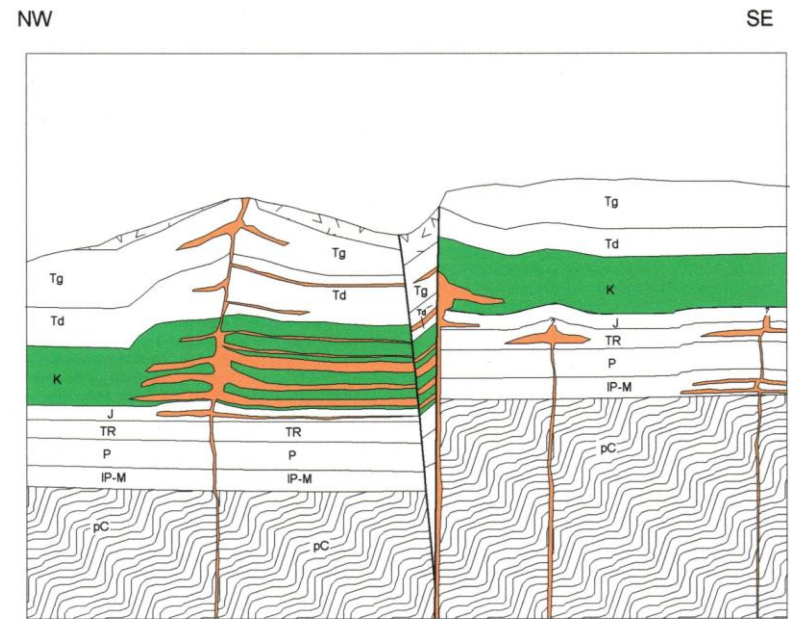
Figure 3-12. Schematic diagrams of the igneous succession of the Ortiz Mine Grant. 31.3 – 31.9 Ma. Explanation on page 63.   a) Pre-intrusive Galisteo Basin, about 36 Ma. Early Tertiary movement on the Tijeras – Cañoncito Fault System controlled basin subsidence. b) 33.3 to 36 Ma intrusions of quartz andesite porphyry laccoliths. May correspond to earliest stage of Espinaso volcanism. c) Major mid-Tertiary movement of the Tijeras-Cañoncito Fault System and formation of the Ortiz Graben.
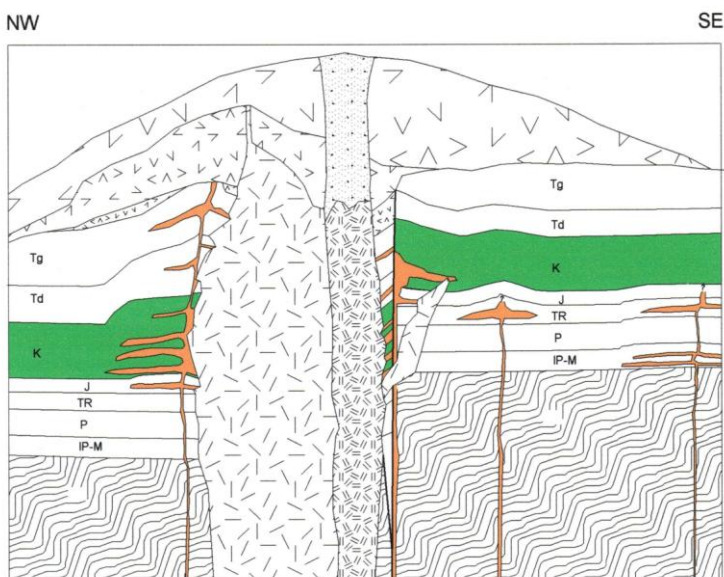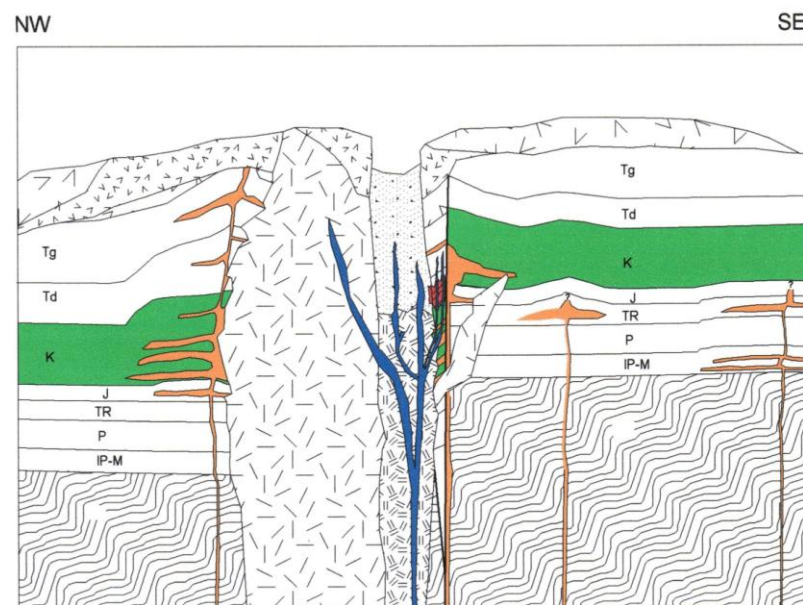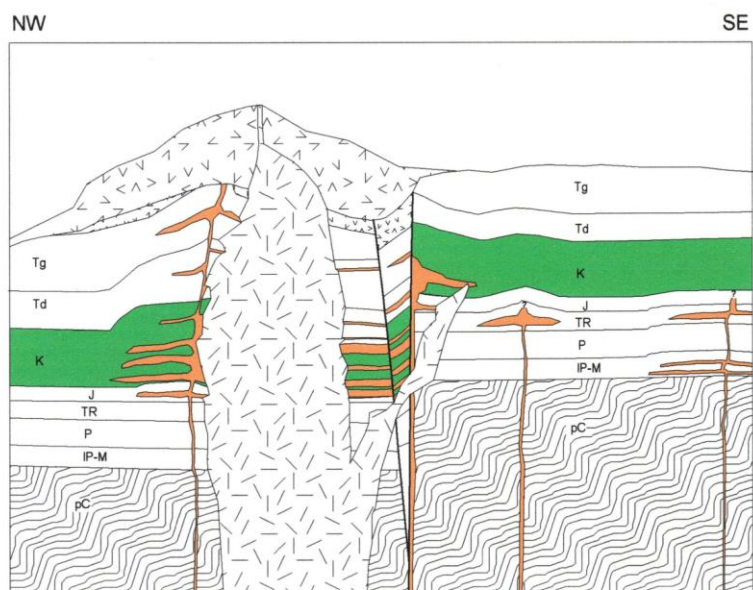
Figure 3-12 (continued). d) Intrusion of augite monzonite stock and corresponding volcanism. Augite monzonite cuts laccoliths and the Tijeras-Cañoncito Fault System, but is cut by the volcanic complex of Cunningham Gulch and Dolores Gulch. e) Cunningham Gulch - Dolores Gulch volcanic complex dated at 31.3 – 31.9 Ma. f) Intrusion of trachyte/latite dikes, formation of ore-hosting breccia, and subsequent mineralization. Best mineralization date appears to be about 31 Ma.
Explanation on page 63.
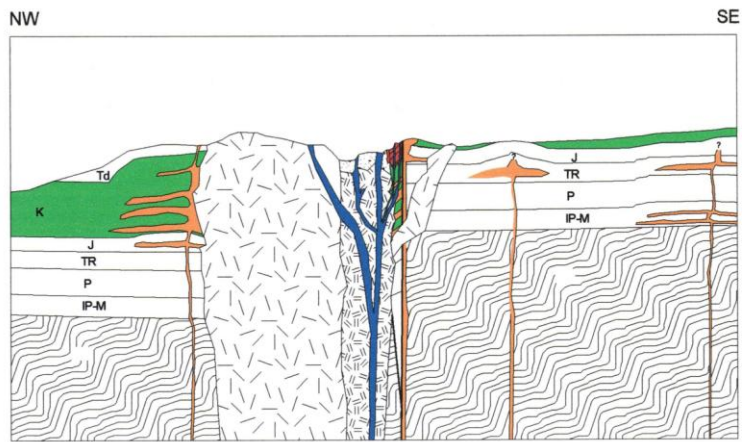
Figure 3-12 (continued). g) Modern erosion levels

g

Mineralized breccia

Flows and vent facies of Dolores Gulch

Volcanics associated with augite monzonite stock

Volcanics associated with andesite-porphyry laccoliths

} Espinaso Formation
34.3 - 31.48 Ma

Quartz latite and latite porphyry stock of Cunningham Gulch
(31.56 - 31.91 Ma), intruded by latite/trachyte dikes

Augite monzonite stock

Quartz andesite porphyry laccoliths
(33.3 - 36.2 Ma)

Precambrian basement

Tg   - Galisteo Formation

Tdt - Diamond Tail Formation

K   - Cretaceous

J   - Jurassic

TR   - Triassic

P   - Permian

IP-M - Pennsylvanian and Mississippian

4 STRUCTURAL GEOLOGY

TIJERAS-CAÑONCITO FAULT SYSTEM

The Tijeras-Cañoncito Fault System (TCFS) has been traced from the Manzanita Mountains, south of Albuquerque, to the Cañoncito area, east of Santa Fe (**Figure 4-1**). It appears to connect to the Pecos-Picuris Fault in the Sangre de Cristo Mountain Range. The structure as a whole maintains a relatively consistent N40E strike from Tijeras Canyon to the village of Golden. From Tuerto Arroyo to Cañoncito, the TCFS average strike is about N50E, though the fault system shows more variability in this zone. On the Ortiz Mine Grant, the TCFS has a general strike of about N60 E.
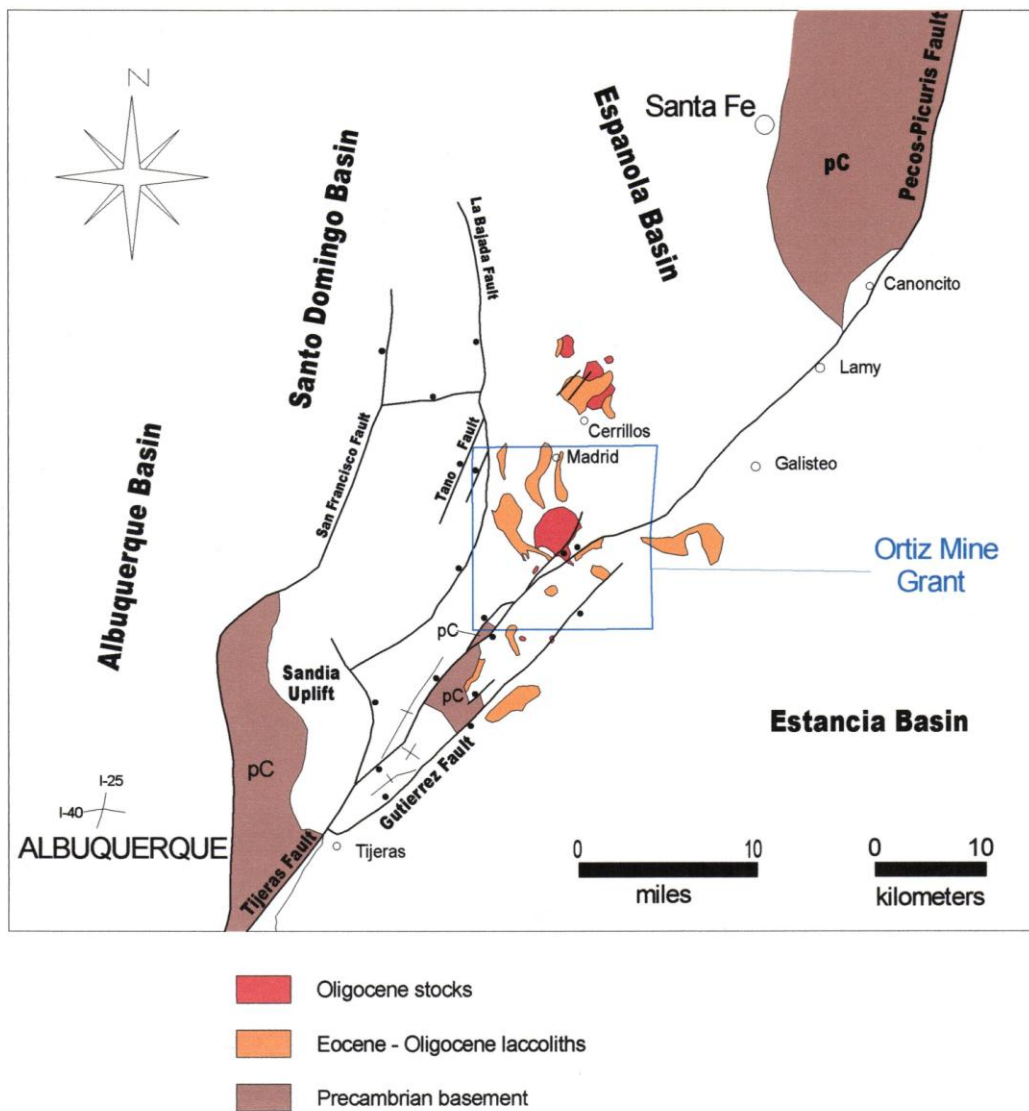
Figure 4-1. Tectonic setting of the Ortiz Mine Grant, showing the relationship of the Tijeras-Cañoncito Fault System to major structures of the Rio Grande Rift.

The TCFS links the southern boundary of the Hagan reentrant of the Rio Grande Rift with the southern boundary of the Española Basin of the Rio Grande Rift. Between these two zones, the fault crosses a structural high formed by the Ortiz Porphyry Belt. This section of the TCFS lies in the Ortiz Mine Grant.

On the Ortiz Mine Grant, the Tijeras-Cañoncito Fault System (TCFS) is traced from just southwest of the village of Golden, across the southeastern part of the Ortiz Mountains and the northern flank of Captain Davis Mountain, to the eastern boundary of the Grant, just east of Peach Spring (**Figure 4-2**). Lisenbee and others (1979) identified the TCFS as a regionally extensive, deep-seated structure with Precambrian to recent recurrent movement. Chapin and Cather (1982) postulated Laramide right-lateral movement on the TCFS. Fulp and others (1982), Woodward (1984; and 1987, unpub. report), and Maynard (1995) described the relationship of the TCFS to mineral deposits.

A subsiding Laramide basin has been invoked to explain southeastward thickening of Diamond Tail and Galisteo Formation sediments (Stearns, 1943 and 1953; Gorham, 1979; and Gorham and Ingersoll, 1979). Ingersoll and others (1990) suggested the TCFS acted as the southeastern boundary of the basin and was a control on the pattern of Paleogene sedimentation. Cather (1992) postulated that during the Paleogene, the TCFS acted as a releasing bend in the right-lateral strike-slip system and controlled extensional subsidence in a half-graben to the northwest of the fault system. Abbott and others (1995) showed that although the TCFS did not act as a boundary to Paleogene sedimentation, it exerted a control on the subsidence of the basin. Northeast and southwest paleoflow indicators suggest the fault system's control on sedimentation patterns. Paleogene dip-slip on the fault system is constrained to the stratigraphic thickness of the Diamond Tail and Galisteo Formations, or about 1300 m (4,300 ft).

In a summary paper on the on the TCFS, Abbott and others (2004) showed that minor fault patterns are identical in Precambrian and Phanerozoic rocks, indicating that their formation post-dates the younger rocks and suggesting no Precambrian history for the TCFS. Abbott and others (in press) further concluded that the Tijeras-Cañoncito Fault System was reactivated as a left-lateral strike-slip system during the transition between Laramide and Rio Grande rift-related tectonic settings, around 32 Ma and that left-lateral movement on the TCFS south of Golden continued into the Quaternary.

The Dakota Sandstone appears to be offset by about 8 km (5 mi) in a left-lateral sense across the Ortiz Graben in the Ortiz Mountains. The true nature of displacement is uncertain. Much of the apparent left-lateral separation across the TCFS in the Ortiz Mountains may be the result of net down-to-the north movement, followed by the Miocene eastward tilting that affects most of the Ortiz Porphyry Belt. Alternatively, significant pre-tilting left-lateral movement could have occurred, though it would not have been recorded by horizontal beds.
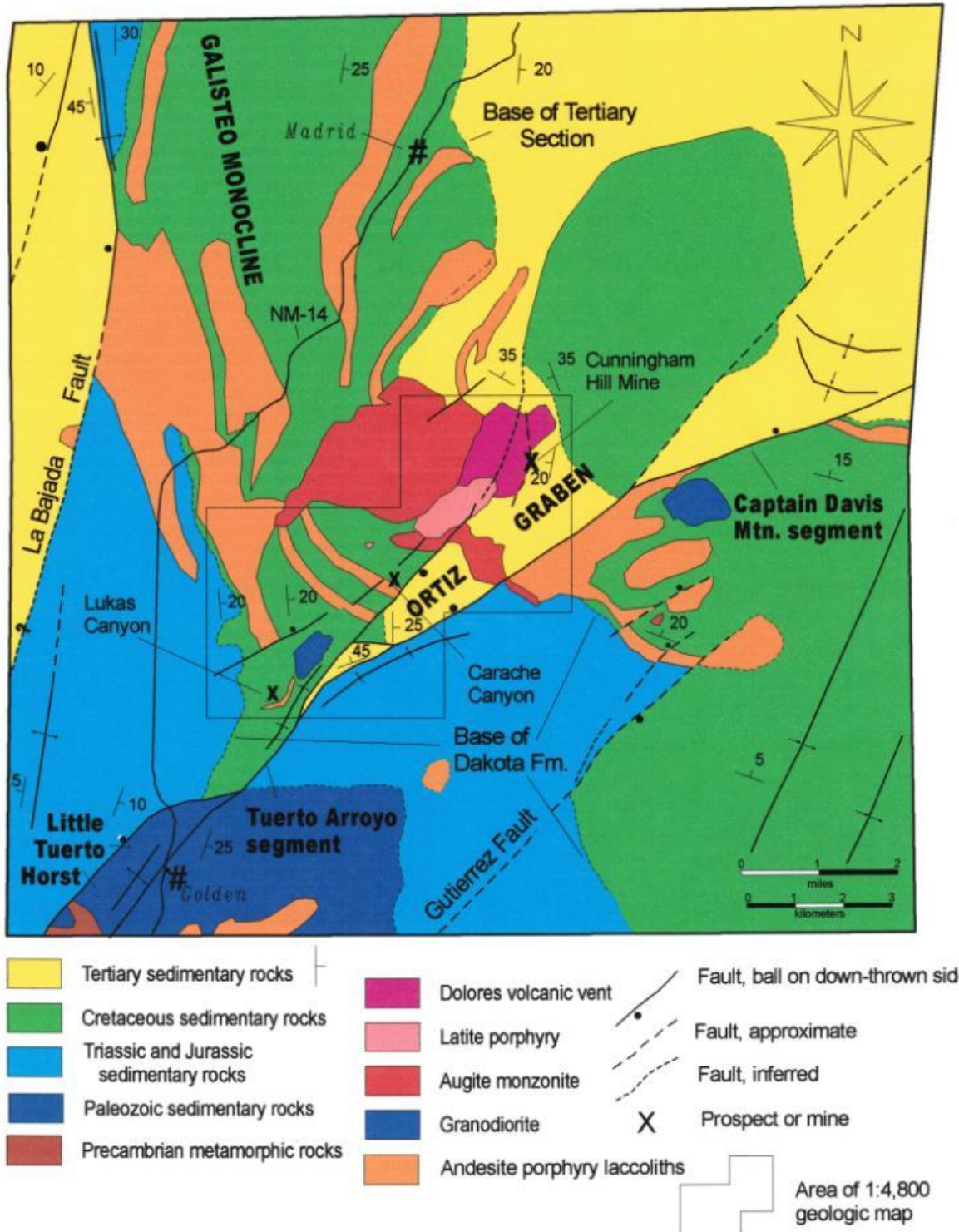
Figure 4-2. Tectonic elements of the Ortiz Mine Grant.

FAULT SEGMENTS

On the Ortiz Mine Grant the TCFS can be divided into four discrete segments. The segments have distinct amounts and sense of separation. In this report they are listed from southwest to northeast.

Little Tuerto Horst

Southwest of the intersection of NM-14 and Tuerto Arroyo, in the Little Tuerto Hills, the TCFS is manifested by a horst 760 m (2500 ft) wide cored by Precambrian metamorphic rocks. Emerick (1948) named the northwestern bounding fault the Aranta Fault and the southeastern fault the Golden Fault. The Aranta Fault juxtaposes Permian and Triassic sedimentary rocks against Precambrian metamorphic rocks and Mississippian(?) and Pennsylvanian sedimentary rocks. Steeply inclined to overturned limestone beds of the Pennsylvanian Madera Formation mark the Golden Fault to the southwest of the eponymous village. A north-northeast plunging anticline of Pennsylvanian Madera Formation limestone is exposed at the north end of the Little Tuerto Hills. Mapping to the southwest by Ferguson and Osborne (2000) indicates that the high-angle faults that bound the Little Tuerto horst are flower structures and therefore record both dip-slip and strike-slip motion.

Tuerto Arroyo Zone

Complex faulting is implied, but faults are poorly exposed, in the area northeast of the intersection of NM-14 and Tuerto Arroyo. Jurassic and Cretaceous sedimentary rocks on the northwestern side of the fault were faulted against Permian and Triassic rocks on the southeastern side, indicating an overall north-side-down stratigraphic separation of greater than 600 m (2000 ft).

Ortiz Graben

About 2150 m (7000 ft) south of Lukas Canyon, the TCFS splits into two principal strands that form a graben composed of several fault blocks. The fault blocks contain sandstone and quartzite of the Diamond Tail Formation and lesser exposures of the Menefee Formation. Both formations have been intruded by sills of andesite porphyry. Rocks preserved in the Ortiz Graben form a northeast-trending series of hills along the southeastern margin of the Ortiz Mountains (Figure 4-2). From cross-cutting relations, development of the Ortiz Graben post-dated the formation of andesite-porphyry laccoliths, and predated intrusion of the augite monzonite stock.

The Ortiz Graben's northwest bounding fault, the Golden Fault, is vertical to subvertical. For the section of the Golden Fault from Lukas Canyon to East Carache Canyon, Mancos Shale and Mesa Verde Group are juxtaposed with Diamond Tail Formation for a stratigraphic separation estimated at 760 m (2500 ft). Northeast of East Carache Canyon, the Golden Fault's trace is occupied by the Ortiz volcanic complex. The Golden Fault has not been traced along strike northeast of Dolores Gulch. A north- striking fault north of Dolores Gulch suggests that the pre-volcanic Golden Fault had a 50-degree curve near the center of the present volcanic vent. Several important mineral occurrences, prospects, and mines occur along or near the Golden Fault, including Lukas Canyon, Carache Canyon, Cunningham Gulch, and Cunningham Hill.

The Buckeye Hill fault forms the southeast margin of the Ortiz Graben. Its dip has not been measured directly, but must be near vertical because of its straight trace across rugged topography. From south of Lukas Canyon to Captain Davis Mountain, the Buckeye Hill fault juxtaposes Triassic to Cretaceous rocks on the south side with Cretaceous to Paleocene rocks on the north side, yielding a stratigraphic separation of approximately 1200 m (4000 ft). The northwestern flank of Captain Davis Mountain contains multiple strands of the Buckeye Hill Fault. Tuerto Gravel cover hinders estimation of stratigraphic separation on the Buckeye Hill Fault from Captain Davis Mountain to Peach Spring. In the vicinity of Peach Spring, on the eastern side of the Ortiz Mine Grant, a latite dike intruded the fault. In the Peach Spring area, the fault's vertical separation appears to have diminished considerably, faulting lower Galisteo Formation against Diamond Tail Formation. The Buckeye Hill Fault can be considered to be the principal strand of the TCFS in the Ortiz segment. It is also cut by the augite monzonite stock in the southeastern part of the Ortiz Mountains. Age dating of andesite porphyry sills and laccoliths (34 Ma), which are cut by the Buckeye Hill Fault, and the augite monzonite stock (32 Ma), which is cut by the Buckeye Hill Fault, constrain the age of major mid-Tertiary movement to the period 32 – 34 Ma. Mineralization at the Iron Vein prospect and the Red Outcrop prospect occurs along or adjacent to the Buckeye Hill Fault.

Captain Davis Mountain segment
The Buckeye Hill Fault can be traced from the northern flank of Captain Davis Mountain to just southeast of Peach Spring. Although concealed by Plio-Pleistocene Tuerto Gravel for most of the length of the Captain Davis Mountain segment, the fault juxtaposes Cretaceous sedimentary rocks and the mid-Tertiary Captain Davis Mountain laccolith on the southern side against the early Tertiary Diamond Tail(?) and Galisteo Formations. Proximity to the fault's trace is interpreted from isolated, arroyo-bottom exposures of vertical beds of sandstone, shale, and mudstone between Captain Davis Mountain and Peach Spring.

GUTIERREZ FAULT
The Gutierrez Fault forms the southeastern boundary of the Tijeras Syncline and Monte Largo Horst southwest of the Ortiz Mine Grant. It has been traced to the northeast, to the northern extremity of South Mountain (Ferguson and others, 1999). Bedrock exposures in the southern part of the Ortiz Mine Grant, north of the San Pedro Mountains, are poor. Airborne magnetic studies indicate a discontinuity that may correspond to the Gutierrez Fault in the southern portion of the Grant. In the vicinity of Oro Quay Peak in the eastern part of the San Pedro Mountains, Permian and Triassic sedimentary rocks, and an augite monzonite stock are offset along lies on projection of the Gutierrez Fault (Maynard, 2000; Ferguson and others, 1999).

LA BAJADA FAULT
The La Bajada Fault forms the eastern boundary of the Santo Domingo sub-basin of the Albuquerque Basin of the Rio Grande Rift (Figure 4-1). Segments of the La Bajada Fault are separated by junctions of the La Bajada Fault with northeast-striking faults that occur within the Santo Domingo sub-basin (Maynard and others, 2001). Along the La Bajada Fault, sedimentary rocks of Eocene Galisteo Formation and Miocene Santa Fe Group, and volcanic rocks of Oligocene Espinaso Formation are faulted against Mesozoic rocks. Quaternary activity on the northeast-trending Tano Fault is indicated by about 20 m (70 ft) of offset of the Tuerto Gravel

just north of the northwest corner of the Ortiz Mine Grant. In the southwestern part of the Madrid 7.5-quadrangle, just north of northwestern-most portion of the Ortiz Mine Grant the Tuerto Gravel is offset by about 12 m (40 ft) along the La Bajada Fault. This is the clearest indication of Quaternary movement on the La Bajada Fault. In the extreme south part of the quadrangle and on the adjoining Golden 7.5-minute quadrangle, offset of the Tuerto Gravel is not clear.

The La Bajada Fault appears to curve to the west and link with a northeast-trending fault in Tuerto Arroyo in the eastern part of the Hagan quadrangle. Steeply dipping Espinaso Formation volcaniclastic sediments and Galisteo Formation sediments lie between strands of the La Bajada Fault in the northwestern part of the Ortiz Mine Grant (Figure 4A).

In Tuerto Arroyo, continuous bedrock exposure between the Little Tuerto Horst and the La Bajada Fault shows occasional minor faults and a broad flexure of the exposed Triassic sedimentary rocks. The structural continuity of the Tuerto Arroyo section with Triassic rocks along the western flank of the Ortiz Mountains indicates that there is no major fault connecting the La Bajada Fault of the northwestern part of the Ortiz Mine Grant with the TCFS.

QUATERNARY SEISMIC ACTIVITY

Quaternary movement on the TCFS has been identified in Tijeras Canyon (Connolly, 1979; Lisenbee and others, 1979) and south of Golden (Abbott and Goodwin, 1995; and Kelson and others (1998, 1999). No Quaternary movement has been demonstrated along the TCFS north of Golden on the Ortiz Mine Grant (Koehler and Kelson, 2000).   The La Bajada Fault and the Tano Fault both show post-Tuerto Gravel movement in the northwestern part of the Ortiz Mine Grant.   Studies of stream terraces along Galisteo Creek suggest mid- to late-Pleistocene offset by the La Bajada Fault (Maynard and others, 2001). Quaternary movement on the TCFS south of Golden and on the La Bajada Fault indicates continued deformation of the Santo Domingo Basin – Hagan Reentrant.

5   ECONOMIC GEOLOGY

METALLOGENIC ASSOCIATION

North and McLemore (1986 and 1988) categorized the precious-metal deposits of New Mexico using criteria of age, tectonic setting, deposit type, and major metals. According to their scheme, the Old Placers, New Placers, and Cerrillos mining districts fall into the Great Plains Margin type, along with the Red River and Elizabethtown-Baldy districts of northeastern New Mexico, and the Gallinas, Jicarilla, White Oaks, Nogal, Orogrande, Chupadera, and Capitan Mountain districts of Torrance, Lincoln, and Otero Counties (**Figure 5-1**). All of these districts lie east of the Rio Grande Rift, near the margins of the Rocky Mountains or Basin and Range provinces and the Great Plains. Mid-tertiary alkalic rocks are found in each of the districts, except for those of Eocene age at Orogrande. Compared to other deposit types in New Mexico, precious metals are abundant relative to base metals in the Great Plains Margin types. North and McLemore (1988) note that Great Plains Margin type deposits account for about 1 million ounces of gold statewide (including placer production).
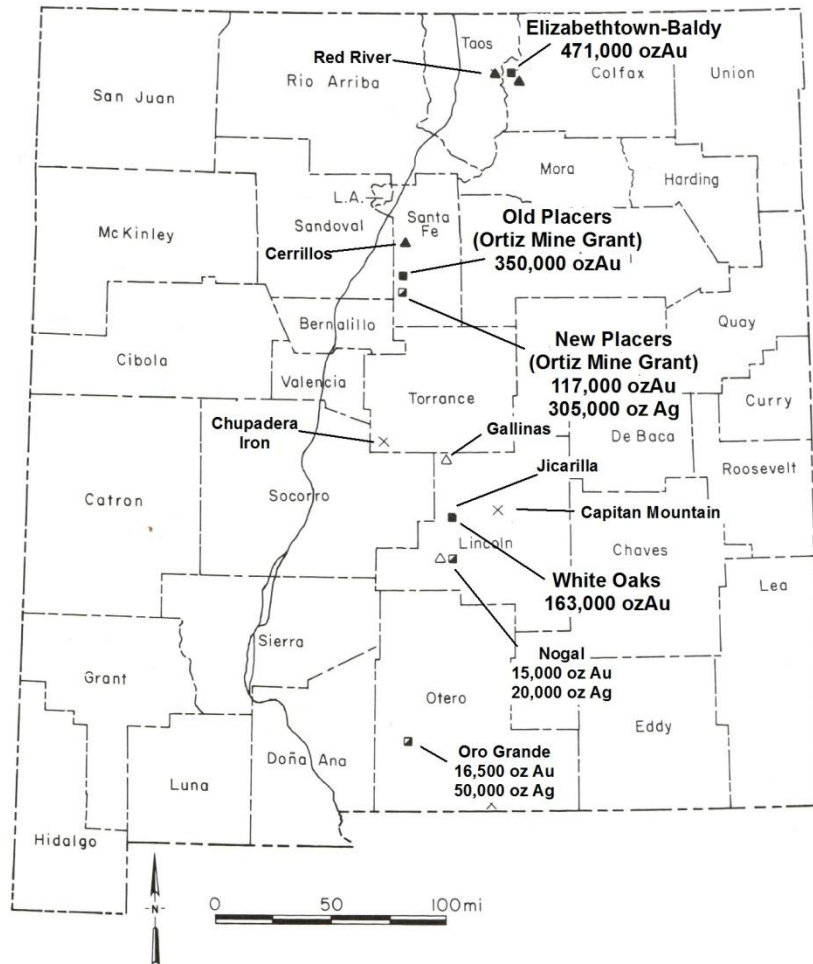
Figure 5-1. Great Plains Margin precious-metal districts of New Mexico, modified after North and McLemore (1988).

70

Mutschler and others (1988) reviewed precious-metal deposits related to alkaline rocks in the North American Cordillera. In the southern Rocky Mountains, these deposits typically occur east of the Rio Grande Rift and in some cases are concentrated along ancient linear crustal flaws such as the Colorado Mineral Belt. Precious-metal mineralization associated with alkaline rocks is found in the Front Range, Cripple Creek, and Rosita Hills districts of Colorado; Ortiz and Lincoln County Porphyry Belts of New Mexico; and the Trans-Pecos igneous province of west Texas.

MINERALIZATION IN THE ORTIZ PORPHYRY BELT

Metallic mineralization in the Ortiz Porphyry Belt occurs in the San Pedro Mountains, the Ortiz Mountains, and the Cerrillos Hills. In all three areas, metallic mineralization is spatially and genetically related to alkaline intrusive rocks that post-date the calc-alkaline laccoliths.

In the San Pedro Mountains, the most important mines and prospects are associated with base-metal skarn developed in limestone of the Pennsylvanian Madera Formation at the San Pedro, Carnahan, and Old Timer Mines (Yung and McCaffrey, 1903; Atkinson, 1961; Elston, 1967). A skarn prospect is also found in limestone of the San Andres limestone in the eastern part of the San Pedro Mountains. The skarns have a spatial association with latite-porphyry dikes and stocks that cross-cut the San Pedro andesite-porphyry laccolith. Skarns in the Madera Formation lie 1,820 to 2,425 m (6,000 to 8,000 ft) southeast of the Golden Fault. Skarn in the San Andres limestone is adjacent to the Gutierrez Fault strand of the Tijeras-Cañoncito Fault system (Atkinson, 1961; Maynard, 2000).

In the Cerrillos Hills, north-northeast- and northeast-striking lead-zinc-silver veins occur in two clusters and post-date porphyry copper-gold mineralization (Stearns, 1953; Disbrow and Stoll, 1956; Wargo, 1962; Bachman, 1975; Giles, 1991; Maynard and others, 2001).   The preferred direction of faults and veins in the Cerrillos Hills, like the Tijeras-Cañoncito Fault System, may be inherited from zones of basement weakness.

MINES AND PROSPECTS OF THE ORTIZ MINE GRANT

Gold, tungsten, and base-metal mineralization on the Ortiz Mine Grant falls into five groups: breccias, skarns, veins, porphyry-related stockworks, and placers (Tables 5-1, 5–2, 5–3, 5-4). Field relations, isotopic dating, and fluid inclusion studies indicate that the different lode mineralization types share a common origin. With the exception of the Lone Mountain copper skarn prospect and Crooked Canyon porphyry copper-gold prospect, all known metallic mineralization on the Ortiz Mine Grant lies in close proximity to strands of the Tijeras-Cañoncito Fault System (TCFS) (**Figure 5-2**). Alkaline intrusive rocks associated with the Ortiz volcanic complex were emplaced along the Golden Fault. Breccias, fractures, and stockworks associated with the volcanic and intrusive activity served as important hosts of mineralization. Skarns developed in calcareous units, in proximity to granodiorite bodies also intruded along the TCFS. Lode mineralization in the Ortiz Mountains was emplaced about 30 Ma. Placer gold deposits are found in the Plio-Pleistocene Tuerto gravel and in Quaternary stream alluvium.

Table 5-1. Ortiz Mine Grant breccia-associated prospects and mines.

Name	Cunningham Hill	Carache Canyon	Florencio
Type/ Origin	Breccia formed along contact of latite porphry dike in quartzite and volcanic breccia	Collapse breccia pipe, open-space fillings. Adularia-sericite epithermal.	Breccia formed along contact of latite porphry dike in quartzite and volcanic breccia
Metals	Au (W)	Au (Pb, Zn)	Au
Ore Minerals	Native gold, scheelite	Native gold, sphalerite, galena, chalcopyrite.	Native gold?
Gangue Minerals	Pyrite, specular hematite	Arsenopyrite, pyrrhotite, pyrite, calcite, mangano-siderite, adularia, sericite.	Pyrite, hematite
Host rock(s)	Eocene Diamond Tail Formation, Oligocene volcanic vent breccia.	Oligocene andesite-porphyry sills, Cretaceous Pt. Lookout Sandstone, Menefee Formation, and Mancos Shale.	Quartzite derived from Diamond Tail Formation
Structural Setting	On margin of Dolores volcanic vent, in Ortiz Graben, hanging wall of Golden Fault	Footwall of Golden Fault, faults parallel to Golden Fault control breccia pipe and mineralization	Northwest side of Dolores volcanic vent, footwall of Golden Fault
Resource	Mined reserves were 330,000 tr oz Au in 6 million st @0.055 oz/st. With ~75% Au recovery, 250,000 tr. oz. of Au were produced during 1979-1987. Ore graded about 0.05% WO_3, though tungsten was not produced.	1,169,000 tr. oz. gold in 16.7 million st @ 0.07 oz/st	60,000 tr. oz. Au in 3 million st @ 0.02 oz/st Au
Production/ years		None	Minor
References	Kay (1985), Maynard (1995)	Coles (1990), Schutz (1995)	Maynard (1995)

Table 5- 2. Ortiz Mine Grant skarn prospects.

Name	Lukas Canyon	Iron "Vein"	Lone Mountain
Type/ Origin	Skarn produced in limestone adjacent to intrusion of monzodiorite	Skarn developed in Todilto Formation	Skarn produced in limestone near intrusion of monzodiorite
Metals	Au, Cu	Au, Fe	Au, Cu
Ore Minerals	Native gold, chalcopyrite, chalcocite, digenite, covellite.	?	?
Gangue Minerals	Andradite garnet, diopside, scapolite, chlorite, actinolite, epidote, pyrite, biotite, calcite.	Magnetite, hematite, garnet, calcite, clay, gypsum, pyrite.	Pyroxene, epidote
Host rock(s)	Cretaceous Greenhorn Limestone, Graneros Shale, and Carlile Shale Members of the Mancos Shale; and Oligocene andesite-porphyry sills and dikes	Limestone and gypsum lithotypes of the Todilto Formation	Cretaceous Greenhorn Limestone
Structural Setting	Footwall of Golden Fault, mineralization occurs in metamorphic halo of granodiorite stock	Complex faulting and fracturing in footwall of Buckeye Hill Fault.	Northeast-trending faults, parallel to TCFS in Lone Mountain area.
Resource	180,000 tr oz Au in 6 million st @0.03 oz/st 0.13% Cu	Not determined	Not determined, small
Production/ years	Minor in 1930's	Minor in 1930's	None
References	Schroer (1994) Martin (1991) Griswold (1950)	Maynard (1995) Maynard (1988)	Griswold (1950). Lisenbee and Maynard (2001)

Table 5-3. Ortiz Mine Grant vein mines and prospects.

Name	(old) Ortiz Mine	English-Shoshone	Benton Mine/ New Live Oak	Red Outcrop	Candelaria Vein
Type/ Origin	Epithermal fissure vein	Epithermal fissure vein	Fissure vein in breccia	Hematite bodies and veins in Mancos Shale	Gold-bearing calcite vein
Metals	Au	Au	Au	Au, Fe	Au
Ore Minerals	Native gold	?	?	?	Native gold
Gangue Minerals	Magnetite, hematite	?	?	hematite	Calcite
Host rock(s)	Augite monzonite stock	Volcanic vent breccia	Diamond Tail Formation	Mancos Shale, andesite porphyry	Carlile Shale Member of Mancos Shale
Structural Setting	North side of Dolores volcanic vent, footwall of Golden Fault	North side of Dolores volcanic vent, footwall of Golden Fault	On margin of Dolores volcanic vent, in Ortiz Graben, hanging wall of Golden Fault	Footwall of Buckeye Hill Fault	Footwall of Golden Fault, close to its junction with Buckeye Hill Fault.
Resource	Not determined	Not determined, small	Not determined	Not determined, small	Not determined
Production/ years	Approx 20,000 oz Au intermittently from 1832 to 1940.	Small	Minor	None	Minor production in 1930s
References	Griswold (1950) Shorey (1935)	Griswold (1950)	Griswold (1950)	Gold Fields Mining Corp files (unpub)	Griswold (1950) Griswold (1951a,b)

Table 5-4. Ortiz Mine Grant porphyry-related stockwork prospects.

Name	Crooked Canyon	Cunningham Gulch
Type/ Origin	Porphyry Au-Cu mineralization	Porphyry-copper and gold mineralization around barren latite porphyry stock. Stockwork veinlets.
Metals	Au, Cu	Au, Cu, Mo
Ore Minerals	Chalcopyrite	Tenorite, chalcopyrite
Gangue Minerals	Magnetite, pyrite	Magnetite, fluorite, molybdenite
Host rock(s)	Augite monzonite, hornfels derived from Carlile Shale	Augite monzonite stock surrounding latite porphyry plug.
Structural Setting	Embayment in augite monzonite stock, far removed from TCFS	Peripheral to barren latite-porphyry stock, footwall of Golden Fault
Resource	Not determined, low grade	< 100,000 tr oz Au
Production/ years	None	None
References	Unpublished reports to LAC Minerals	Maynard (1995) Coles (1990)

Legend:

Ts	Tertiary sedimentary rocks
K	Cretaceous sedimentary rocks
Tr-J	Triassic and Jurassic sedimentary rocks
Pz	Paleozoic sedimentary rocks
pCm	Precambrian metamorphic rocks

Dolores volcanic vent

Latite porphyry

Augite monzonite

Granodiorite

Fault, ball on down-thrown side

Fault, approximate

Fault, inferred

X   Prospect or mine
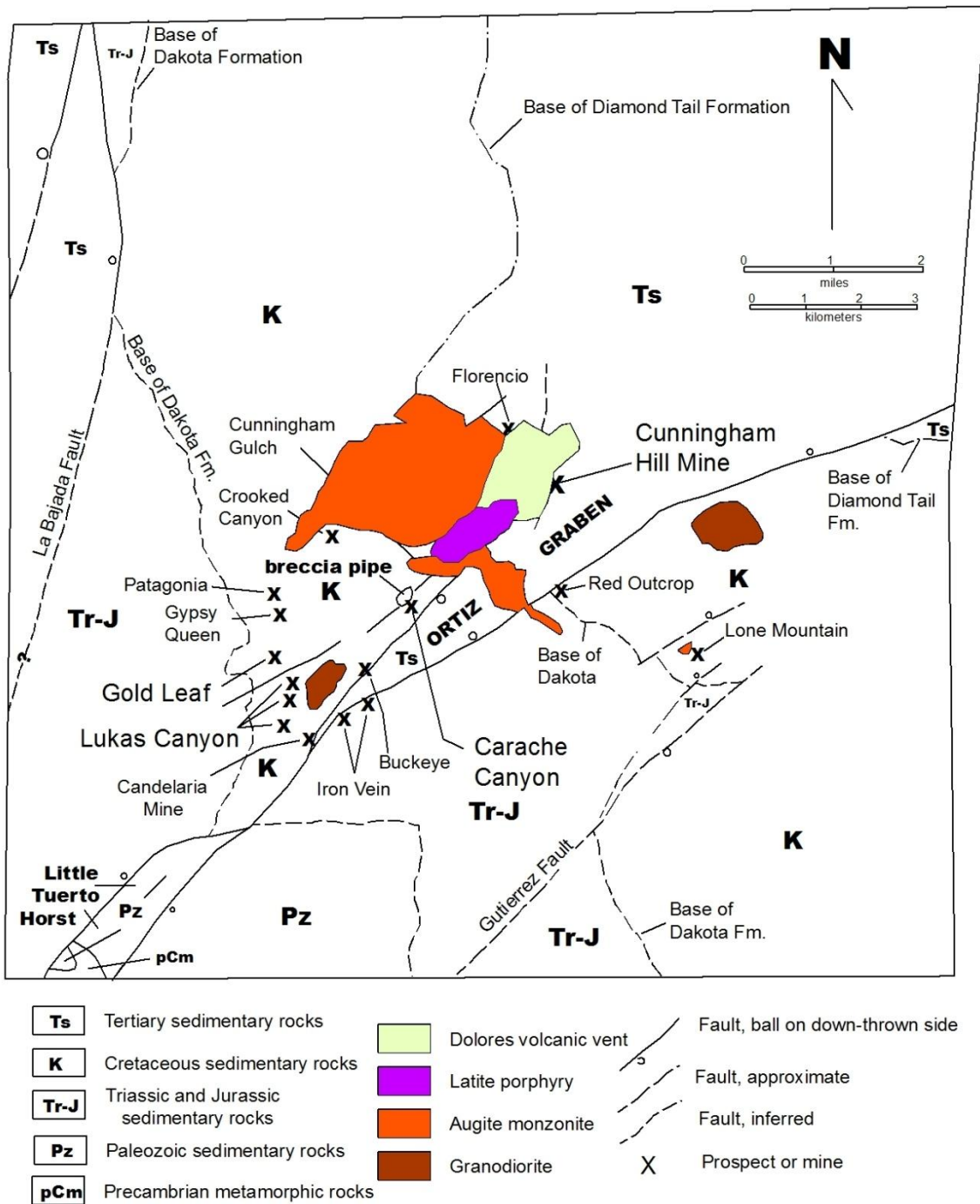
Figure 5-2. Map of the Ortiz Mine Grant, showing mines and prospects described in this report in relation to major tectonic elements. For simplicity, laccoliths and sills are not shown.

BRECCIA-RELATED MINERALIZATION

CUNNINGHAM HILL MINE

Cunningham Hill lies on the eastern side of the Ortiz Mountains, between Cunningham and Dolores Gulches. The Cunningham Hill Mine is referred to as the Ortiz Mine by authors associated with the Gold Fields effort, e.g.: Lindqvist (1980), Wright, (1980), Springett (1980), and Hickson (1981). In this report, the Cunningham Hill Mine refers to the Gold Fields operation and the Ortiz Mine refers to the smaller underground vein deposit that was the original lode discovery on the Grant.

Gold mineralization was known at Cunningham Hill in the mid-19th century (Raymond, 1870 and 1872). Raymond's comments (Raymond, 1870) on Cunningham Hill illustrate the difficulty early investigators had in describing what are now referred to a low-grade, bulk-mineable deposits:

> The difficulty in working the Cunningham as a quartz mine arises from its great size, and the manner in which the rich rock is scattered through it, in bunches and seams which it requires the eye of a Mexican to detect, and which cannot be extracted on a large scale by a regular system. The huge, irregular excavation or quarry, known as the Cunningham mine, has resulted from the 'coyoting' of the Mexicans to find and follow the rich rock. The width of the Cunningham outcrop is 600 feet; and its course can be traced for several miles. That it is a true fissure, one can scarcely doubt after examining the nature of the vein-matter, which is in many places, of the 'country', inclosed in a matrix of quartz. But the great dimensions of the fissure have prevented the formation, near the surface, of a defined 'pay-streak' of rich rock. By sinking along the footwall of the vein (which is a porphyry dike, while the hanging-wall is syenite) a narrower, more concentrated, and more regular vein-formation will doubtless be reached in depth.   This is, at least, in accordance with experience acquired in similar instances, in West-American practice.

Lindgren and others (1910) make no mention of mineralization in the breccia at Cunningham Hill.   Crane (1937), Perry and Moehlman (1938), and McKinnis (1938) described potentially economic resources at Cunningham Hill.   On the basis of churn drilling and from surface and underground sampling, C.T. Griswold (1950) calculated a resource at Cunningham Hill of 2,450,824 tons grading 0.077 troy ounces of gold per short ton. During the early 1950's US government concerns over strategic metal resources focused attention on the Cunningham Hill deposit for its tungsten content. Dale and McKinney (1959) quote a reserve calculation made by G.R. Griswold in 1955 as 2,901,616 tons containing 0.0711 ounces/ton Au and 0.0683 % WO_3 (Table 5-5). Consolidated Gold Fields' operation commenced during an historic run-up in the price of gold (exceeding US$800 per ounce in February 1980). Gold Fields mined a total of 6 million tons grading 0.055 ounces of gold per ton from 1979-1986 and recovered about 75 % of the contained gold, or 250,000 troy ounces (G. Griswold, personal communication, 1995). Gold Fields did not recover tungsten. Kay (1986) studied the geology of Cunningham Hill and the surrounding area.   Descriptions of mineralization, petrography, and fluid inclusions are taken from Kay (1986). In this report, Cunningham Hill is re-evaluated in the light of new interpretations of its stratigraphic and structural settings.

Table 5- 5. Summary of ore reserves at Cunningham Hill from G.R. Griswold report of 1955. Modified from Dale and McKinney (1959).

Category………………………….units	Oxide	Sulfide	Total	Weight-average grade
Overburden………………………..short tons	-	-	165,777	-
Ore………………………………….short tons	1,024,629	1,876,987	2,901,616	-
Gold……………….……ounces per short ton	0.0724	0.0704	-	0.0711
WO_3……………………………………percent	0.0566	0.0746	-	0.0683
Gold……………………………troy ounces	74,180.71	132,211.89	206,392.6	-
WO_3………………………………………pounds	1,159,880	2,949,665	4,109,545	-

Geologic setting

Cunningham Hill lies in the Ortiz Graben, on the southeast margin of the Dolores Gulch volcanic center.   Diamond Tail Formation sedimentary rocks exposed at Cunningham Hill and in hills to the northeast of Cunningham Hill dip into the volcanic vent (diatreme), suggesting a sagging of the sedimentary rocks into the volcanic center (**geologic map and Figure 5-3**). The Golden fault, the northwestern bounding structure of the Ortiz Graben, is occupied by the feldspar-porphyry latite of Porphyry Hill and Magnetic Hill, and the volcanic vent that they intrude.

Figure 5-3. Panoramic view of the Cunningham Hill, looking northeast. Note beds dipping to the left (northwest). Photo taken in fall of 1986.

A north-south striking, vertical fault crosses the open pit and juxtaposes volcanic vent breccia on the west from quartzite on the east side (**Cunningham Hill mine geologic map**). This fault appears to have been an important constraint on the distribution of mineralization and may postdate mineralization.

Breccia developed in quartzite of the Paleocene Diamond Tail Formation forms the principal host of economic mineralization at the Cunningham Hill Mine.   The quartzite is the

result of metamorphism of sandstone by fluids circulating from the adjacent volcanic and subvolcanic complex. Previous workers, e.g.: Griswold (1950), Lindqvist (1980), and Kay (1986) assigned the quartzite (sandstone) to the Mesa Verde Group. Comparing the mine exposures to descriptions from the Hagan Basin by Stearns (1943 and 1953c) and Picha (1982), and to exposures and drill core at Carache Canyon, Maynard and others (1990) and Maynard (1995) assigned the quartzite (sandstone) of Cunningham Hill to the lower part of the Galisteo Formation. The sandstone is now assigned to the Diamond Tail Formation, following the redefinition of Paleocene and Eocene rocks in the Hagan Basin by Lucas and others (1997).

Exposed in the open pit of the Cunningham Hill Mine is a section of quartzite and dark gray hornfels intruded locally by sills of andesite porphyry. The quartzite is medium to coarse grained, with rare quartzite pebbles. On the northeast end of Cunningham Hill, black silicified wood fragments occur as float. These wood fragments are typical of Diamond Tail exposures throughout the Ortiz Graben. The Diamond Tail Formation dips gently to the northwest, possibly in response to collapse into the Dolores Gulch volcanic vent.

Mesa Verde Group rocks do not crop out in the immediate area of the Cunningham Hill Mine. Because drill core samples from the Gold Fields program were destroyed, no re-examination was done. However, Gold Fields drill logs report coal (characteristic of the Menefee Formation) in deep drilling below the Cunningham Hill Mine. Menefee Formation crops out 1500 m (5000 ft) to the northeast of the Cunningham Hill Mine. No economic mineralization is reported in the Mesa Verde Group.

Andesite porphyry occurs as sills intruding the Diamond Tail Formation in the northeast high wall of the Cunningham Hill Mine and on the southeast side of Cunningham Hill, as well as in sills in the Diamond Tail Formation further removed from the open pit. The andesite porphyry is not an important ore host, though it displays the effects of sericitization associated with mineralization.

Northeast-trending dikes of latite porphyry intrude the Diamond Tail Formation and the quartzite breccia. The principal dike presently exposed in the open pit ranges from 24 to 50 m (80 ft to 160 ft) thick at the 6790' to 6900' levels, where it intrudes the remnants of the mineralized breccia. The dike maintains a width of about 30 m (100 ft) thick to the top of the northeast pit high wall. Latite porphyry dikes can be traced along the crest and flank of Cunningham Hill 450 m (1500 ft) to the northeast.

a   b
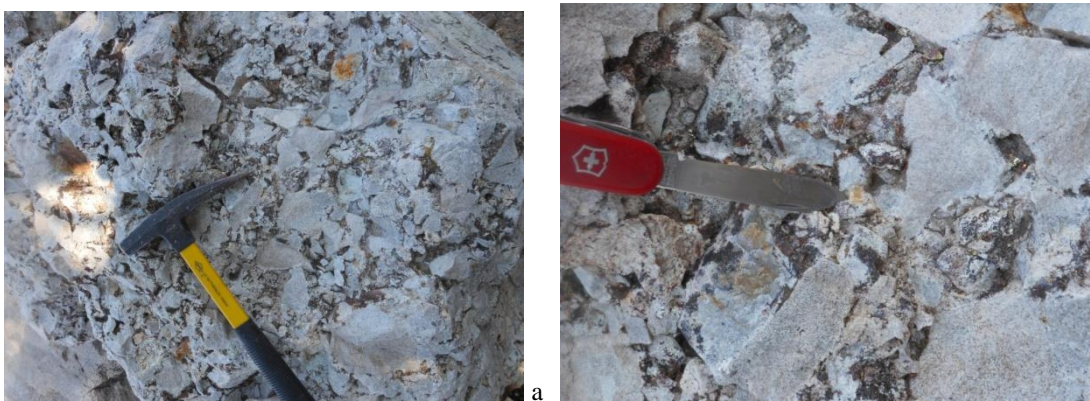
Figure 5-4. Quartzite breccia, Cunningham Hill Mine. a) Note dark sulfide filling of open spaces between quartzite clasts. b) Close up. Pale yellow mineral at blade tip is scheelite ($CaWO_4$).

The Cunningham Hill Mine lies on the southeast side of the volcanic vent breccia of Dolores Gulch. The vent breccia is a body 1500 m by 900 m (5000 ft by 3000 ft) in plan of lithic tuff, crystal tuff, volcaniclastic sediments, and volcanic breccia. Drilling near its eastern margins indicate its thickness to be greater than 1000 feet. The contacts of the vent breccia with the Diamond Tail Formation are mostly intrusive and fragments of Diamond Tail quartzite are commonly found in the vent breccia near its contacts. Likewise, contacts of the vent breccia with the augite monzonite are intrusive and fragments of augite monzonite are common in the area of the contact within the vent breccia. The latite porphyry stock at Magnetic Hill, 1200 m (4000 ft) to the southwest of Cunningham Hill, appears to intrude the vent breccia.

Mineralization

Gold-tungsten mineralization at Cunnningham Hill is hosted by open-space breccia mainly developed in quartzite and, to a lesser extent, in the Dolores Gulch vent breccia. The breccia at Cunningham Hill contains clasts of quartzite, hornfels, latite porphyry, andesite porphyry, and vent breccia. Clasts are subrounded to angular, and range from silt size to boulder size. The breccia is clast supported. Fine rock flour, alteration clay, sulfide and oxide gangue minerals, and open space constitute the breccia matrix. Vugs constitute up to 20% of the rock. Crystals of pyrite, magnetite, calcite, siderite, quartz, chalcopyrite, and scheelite commonly line the vugs. Vuggy zones contain the highest concentrations of gold, up to 0.3 ounces per short ton. Vugs are best developed in quartzite and are poorly developed in the volcanic vent breccia. Open-space mineralized breccia remains exposed in the bottom of the Cunningham Hill pit, intruded by a latite porphyry dike.

Prior to mining, the quartzite breccia at Cunningham Hill had a rounded triangular shape in plan view, and a steep southeasterly plunge. Its southern boundary followed a northeasterly trend (**Figures 5-5, 5-6, and 5-7**).

Ore minerals

Gold

Gold occurs in fractures or small voids in pyrite and siderite in the breccia matrix. Gold grains are usually less than 50 microns. The pyrite association dominates. In pyrite, the gold commonly shares the fractures with tetradymite, gold (silver) tellurides and chalcopyrite. Gold in siderite commonly occurs near the host mineral's boundaries with microcline or magnetite.

Small amounts of gold are occasionally found as inclusions or pore fillings in chalcopyrite as well (Gasparrini, 1984). The chalcopyrite-hosted gold is accompanied by bornite, gold telluride, or sulfosalt of copper, lead, and bismuth. Tiny amounts of gold occur as inclusions in hematite, magnetite, and clay.

Telluride minerals

Gasparrini (1984) showed that gold-silver tellurides occur in small quantities at Cunningham Hill. Studies of polished sections show calaverite ($AuTe_2$) and petzite (Ag_3AuTe_2) occurring in fractures in pyrite in association with chalcopyrite. Scanning electron microscopy shows tetradymite (Bi_2Te_2S) and tellurbismuth (Bi_2Te_3) also in pyrite fractures.

Sphalerite, galena, chalcopyrite, bornite, and sulfosalts

At Cunningham Hill, sphalerite and galena occur always as inclusions in pyrite. Chalcopyrite occurs as grains up to 2 mm in breccia cavities, as veinlet fillings with sphalerite, and as fine fracture fillings within pyrite. Bornite replaces chalcopyrite to varying degrees. Bornite is sometimes associated with a sulfosalt, tentatively identified as benjaminite ($CuPbBi_2S_4$).

Scheelite

Scheelite ($CaWO_3$) occurs as light tan subhedral to euhedral crystals averaging 0.5 mm in open spaces in the Cunningham Hill breccia. It usually is found on the margins of pyrite, hematite, or magnetite. Tungsten was not recovered from the Cunningham Hill ore, though resource calculations were made in the 1950's (Table 6.3.1A; Dale and McKinney, 1959).

Pyrite

Coarse- and fine-grained pyrite commonly occurs at the Cunningham Hill Mine. The coarse-grained pyrite dominates and forms aggregates of homogeneous grains that occupy open spaces in the mineralized breccia. Fine-grained pyrite, which apparently predates mineralization, occurs as disseminations in rocks within and outside of the mineralized breccia.
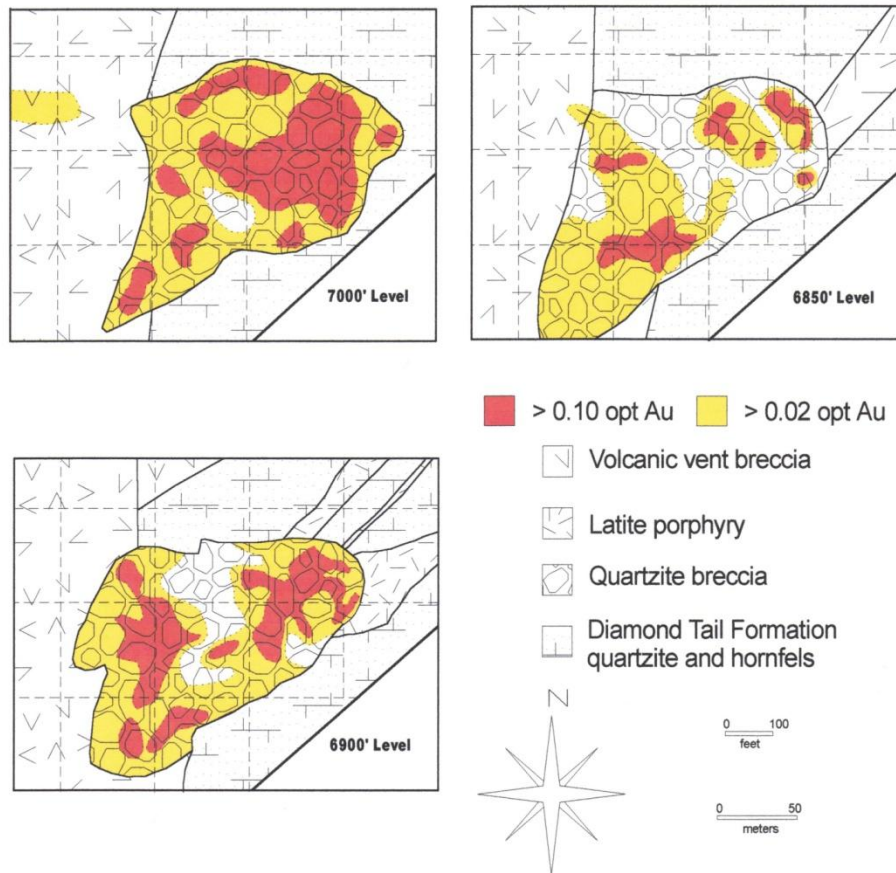
Figure 5-5. Geologic plans of 7000', 6900', and 6850' levels, Cunningham Hill Mine, showing gold grades in ounces per short ton.
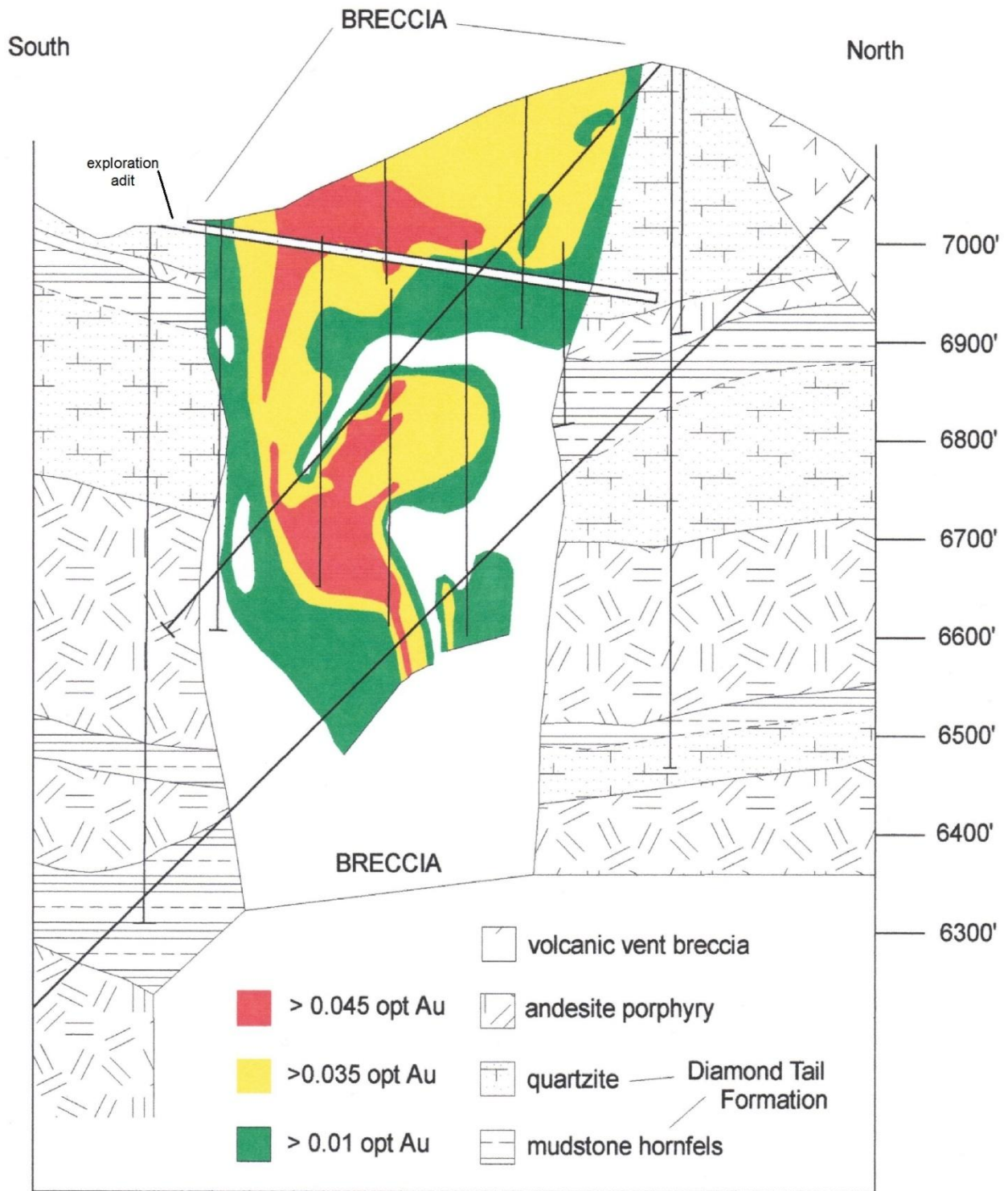
Figure 5-6. North-south cross section of Cunningham Hill ore body, prior to mining, showing distribution of gold grade. Modified after Kay (1986).
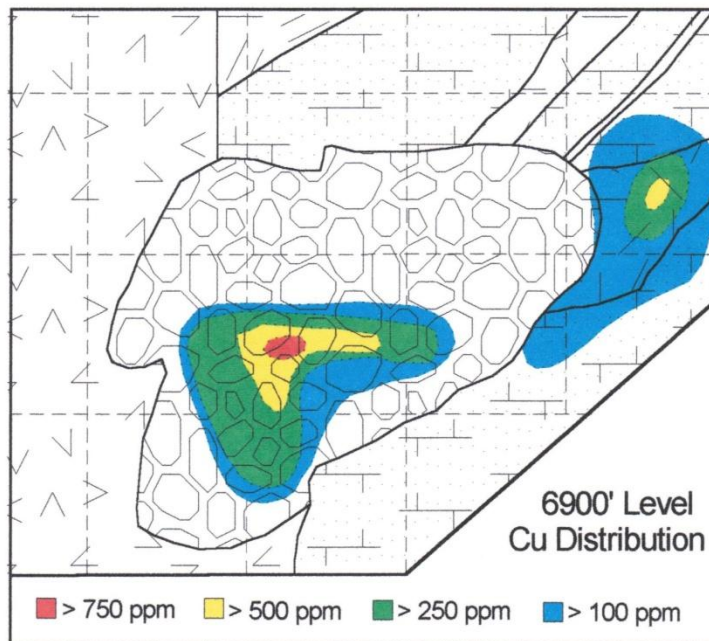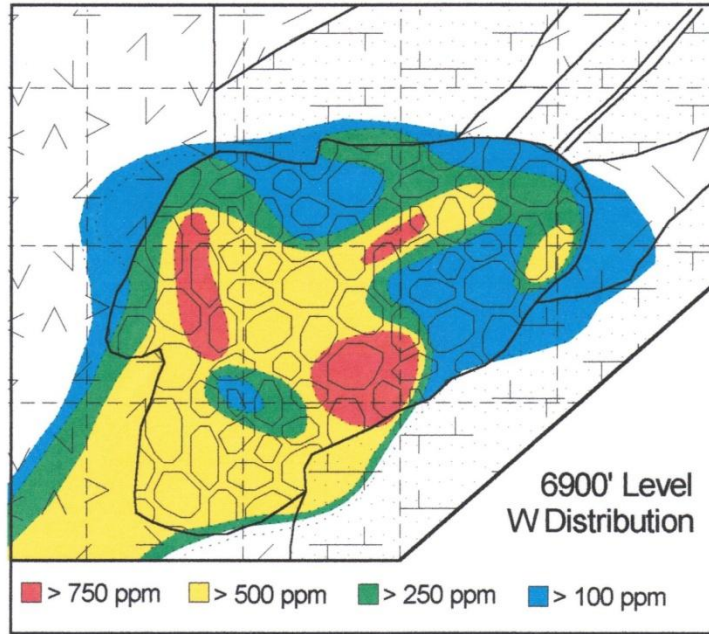
Figure 5-7. Tungsten oxide (WO_3) and copper distribution on the 6900' level, Cunningham Hill Mine. (Note that "W" in upper figure should read "WO_3".) Modified after Kay (1986).

Gangue minerals

Magnetite – hematite
Magnetite and hematite occur as open-space fillings in the mineralized breccia. Hematite forms bladed crystals up to 5 mm long. Magnetite commonly replaces the hematite and is intergrown with siderite.

Rutile
Prismatic to needle-like rutile crystals formed in open spaces on earlier-formed hematite and magnetite and constitutes 1-2% of most of the samples in Kay's study.

Carbonates
Siderite and calcite are the most common gangue minerals in the Cunningham Hill breccia. Siderite dominates and is closely associated with scheelite, occurring as masses and subhedral grains in the breccia matrix and as large euhedral crystals in veins. Small euhedral crystals of calcite line vugs in the breccia.

Quartz
Quartz as a gangue mineral is associated with calcite and sericite.

Sericite, kaolinite, and chlorite
Sericite is widespread at Cunningham Hill and is an alteration product mainly of plagioclase and, to a lesser extent, of sanidine and orthoclase. Sericite commonly occurs with kaolinite and quartz. Kaolinite is concentrated at the northeastern end of the breccia body and is present in north-striking shear zones. Chlorite is very minor, and occurs in gouge zones outside of the breccia body and in latite dikes.

Potassic feldspar
Fine-grained potassic feldspar occurs as filling of the breccia matrix.

Mineral Paragenesis

Kay (1986) proposed a tentative six-stage paragenetic sequence for mineralization at the Cunningham Hill Mine and the surrounding area (Table 5-6, **Figure 5-8**). Late supergene oxidation may be considered to be a seventh stage.

Fluid Inclusion Study
Kay (1986) studied fluid inclusions in fifteen samples from the Cunningham Hill Mine. Table 5-7 contains a summary of Kay's findings with regard to temperatures and salinities of hydrothermal fluids.

Table 5-6.   Paragenetic stages of mineralization at the Cunningham Hill Mine.   After Kay (1986).

Stage	Minerals	Comments
I	Pyrite, magnetite	Barren pyrite in veins and disseminations
II	Sphalerite - chalcopyrite +/-galena +/- pyrite +/-molybdenite	Veinlets or infillings of microfractures in vein pyrite. Unrelated to Cunningham Hill breccia.
III	Specular hematite	Fills open spaces of Cunningham Hill breccia and therefore post-dates it.
IV	Magnetite – magnetite-siderite - siderite	Replaces hematite at Cunningham Hill; forms matrix of intrusion breccias at Magnetic Hill
V	Coarse-grained pyrite +/- gold inclusions	Early stage of gold deposition; accounts for about 10% of the gold at Cunningham Hill.
VI	Gold +/- scheelite +/- chalcopyrite +/- tellurides	Deposition in fractures and voids. Principal stage of gold and tungsten deposition. Voids filled with siderite, calcite, and rutile late in Stage VI. Sericitic alteration.
VII	Supergene oxidation	Partial oxidation of Cunningham Hill orebody. Minor remobilization of gold.

Table 5-7. Summary of results of fluid inclusion study of Cunningham Hill Mine by Kay (1986).

Rock type	Mineral	% NaCl	Homogenization T (^{o}C)	Freezing T (^{o}C)	Remarks
Quartzite	Quartz	>40%	360 to 420	-	Stage I or Stage II in paragenetic sequence.
Breccia void fill	Siderite	10.9%	219 to 262; avg.: 240+/-15	-5.7 to –8.2; avg.: -7.4 +/-1.0	No separate CO_2 bubbles observed. Stages V and VI in paragenetic sequence.
Breccia void fill	Scheelite	Very high	324 to 445	-50	Stage VI in paragenetic sequence. May have high CaCl content.
Breccia void fill	Calcite	<1%	225	?	Late in Stage VI.
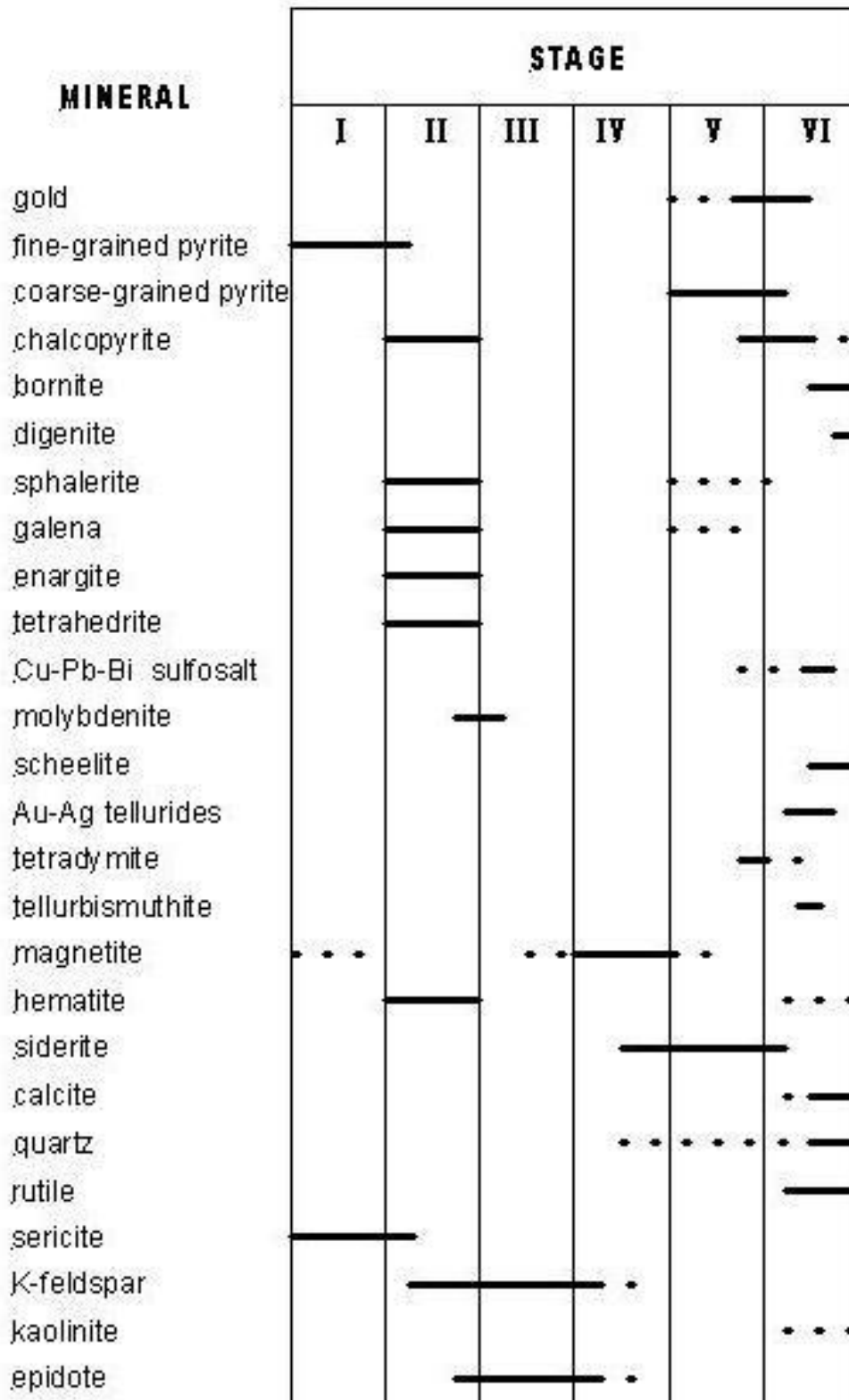
Figure 5-8. Paragenetic diagram, Cunningham Hill Mine. From Kay (1986). Note association of gold with scheelite, coarse grained pyrite, and carbonates late in paragenetic sequence.

CUNNINGHAM HILL MINE AND PLANT OPERATION

The Cunningham Hill mine produced 250,000 troy ounces of gold during the period 1979-1987. Mined reserves totaled 6 million short tons grading 0.055 oz/st. The cost of mine construction was $12 - $13 million. The per-ounce operating cost in 1980 was about $116. With the average price of gold of over $600 in that year, it was a highly profitable operation.

The Cunningham Hill Mine was Gold Fields Mining Corporation's first mining operation in the United States. Although prospectors had recognized the mineralization at Cunningham Hill more than a century earlier, the combination of low gold prices and inadequate technology prevented its being exploited. Cyanide heap leaching had been used to extract gold from ores as an auxiliary recovery method to milling in many gold-mining operations; however, the Cunningham Hill operation was one of the first in the world to use cyanide heap leaching as its sole method of recovering gold.   Design and operation of the mine was considered state-of –the-art at the time of its construction and initial years of operation. The traveling gantry method of placing ore on the leach pad and the on-off loading of ore were unique (McQuiston and Shoemaker, 1981). During 1980, production from the Cunningham Hill Mine represented 4% of the total gold produced that year in the United States, and it tripled New Mexico's gold production (Hickson, 1981). Since that time, numerous, much larger gold mines that operate exclusively by means of heap leaching have been constructed. Although technology has advanced considerably since 1980, the operation at the Cunningham Hill Mine represents a milestone in the development of cyanide heap-leaching of low-grade gold ores.

The following descriptions of the Cunningham Hill Mine are taken from McQuiston and Shoemaker (1981), Rubio (1984), Springett (1980) and Hickson (1981). **Figures 5-9 and 5-10** present flow sheets of the ore-processing operation.

Ore Estimation

Gold Fields utilized data from 74 core, churn, and hammer drill holes totaling 7,950.9 m (26,238 ft). About half of the drilling was represented by Gold Fields' own core drilling. In addition, 408 m (1,346 ft) of blasted tunnel rounds, as well as 210.6 m (695 ft) of slabbed tunnel walls, were sampled and used for ore estimation. Variogram analysis of the different sample types showed that the most representative (lowest nugget variances and relative standard deviations) samples were the bulk tunnel round samples, whereas grab samples of tunnel rounds and split-core samples were the least representative (with relative standard deviations greater than 50%). Open-hole drilling methods yielded dependable results, with variography indicating a lack of down-hole contamination of samples (Springett, 1980).

Reserve estimates were initially made in 1976 using a plan-polygon method, a cross-sectional method, and a rolling-mean method through a range of cut-off grades. The methods agreed within 10% for tonnage and grade, though the rolling mean was consistently lower. In 1979 a Kriging method was used to recalculate reserves on the basis of blocks corresponding to proposed benches (50 ft x 50 ft x 25 ft vertically, or about 5,000 short tons per block).   Block grade estimation standard deviations for individual blocks ranged from 16.7% to greater than 50 %. Blocks exceeding 50% standard deviation were not included in the reserve. Overall relative standard deviation for the deposit grade estimate was 2% and overall relative standard deviation for the deposit tonnage estimate was 3% (Springett, 1980). The Kriging study estimated about 6.8 million tonnes (7.5 million short tons) of ore at an average grade of 1.82 g/t Au (0.053 oz/st), with a strip ratio of 2:1.

Run of mine ore
↓
100 ton dump pocket
↓
Reciprocating feeder
↓
42" x 40" jaw crusher
↓
30" conveyor with magnet
↓
30" conveyor
↓
30" stacker
↓
3000 ton stockpile
↓
2 vibrating feeders
↓
30" conveyor -
magnetic head pulley
↓
6" x 17 " screen

-5/8"   -1 1/4"   +5/8"   +1 1/4"

5 1/2 " standard crusher
↓
30" scissors conveyors
↓
6' x 12' screen

+ 5/8"

5 1/2' short head
crusher
↓
30" conveyor
↓
sampler
↓

bucket elevator
↓
bin & feeder
↓
jaw crusher
↓
2 vezin samplers
↓
30 lb sample daily

Lime bin & feeder
Water

24" conveyor & scale
↓
24" conveyor & tripper on
rail-mounted stacker
↓
leach pad

Figure 5-9. Flowsheet of crushing procedure, Cunningham Hill Mine. Modified after McQuiston and Shoemaker (1981).

from crushing circuit

24" conveyor & tripper on
rail-mounted stacker

leach heap

trash screen

sand & gravel trap

barren
sump & pump   o'flow   1,500,000 gal.   o'flow   pregnant sump & pump
storage pond   750-800 gpm

30 mesh screen

0.8#/ton ore
NaCN
flo-bin

5#/ton ore
70 ton lime bin &
vibrating feeder

loaded carbon   5 adsorption columns   trash
8' phi x 6' high in series

mix tank

slaker

35 mesh screen

sampler

+35m   -35m

holding tank   holding tank

conditioning
tank

2-stripping vessels
5' phi x 9' high
4500 lb carbon each

stripped carbon
4500 / third day

propane-fired
solution heater

high-grade
pregnant solution

dewatering screw feeder

heat exchanger

solution

carbon reactivation
kiln 1100 F

-10 +28 mesh
makeup carbon

2 - 2' x 9'6"
electrolytic cells
in parallel

quench tank

35 mesh screen

+35m   -35m

ethanol 130#/day
NaOH 15#/day
NaCN 3#/day

barren

pump

holding tank

makeup tank

bag filter

pump

fine carbon
storage

CATHODES
TO REFINERY

Figure 5-10. Flowsheet of leaching and gold recovery process, Cunningham Hill Mine. Modified after McQuiston and Shoemaker (1981).

Mining and Grade Control

Six million short tons grading 0.055 troy ounces of gold per short ton was removed from the Cunningham Hill open-pit mine from 1979 to 1986. Overburden, or waste rock, totaled about 12 million short tons. The diameter of the final pit is 366 m (1200 ft) and its depth from the level of the primary crusher and main access road is approximately 190 m (625 ft). Waste rock was removed to a dump area on the north and northwest sides of the pit. Ore was blasted and taken to the primary crusher approximately 150 m (500 ft) east of the pit. Mine benches were 7.6 m (25 ft) high. A daily average of 2,722 tonnes (3,000 short tons) of ore was taken from the pit to the primary crusher (Hickson, 1981; Rubio, 1984).

Crushing

Crushing was accomplished in two independent stages. The first stage consisted of feeding the run-of-mine material to a primary jaw crusher, which reduced the ore to a size of approximately 140 mm (5 1/2 in). A conveyor carried this material to a 29,000 tonne (31,900 short ton) fine ore-storage pile. Ore was drawn as needed from the stockpile via feeders at the pile's bottom and carried by conveyors to secondary and tertiary cone crushers (Figure 5-12). The secondary cone crusher yielded 60% of the material passing 9.5 mm (3/8 in), which was sent directly to the leach pad. Oversize of the secondary crusher was sent to a tertiary cone crusher, which finished the job of reducing the ore to the 9.5 mm (3/8 in) size required for leaching. Crushed material was then conveyed to a traveling gantry, which loaded the ore onto the leach pad (**Figures 5-11, 5-12**). The entire crushing operation occupied an area 300 m x 45 m (1000 ft x 150 ft), between the open pit and the leach pad (Hickson, 1981; Rubio, 1984).
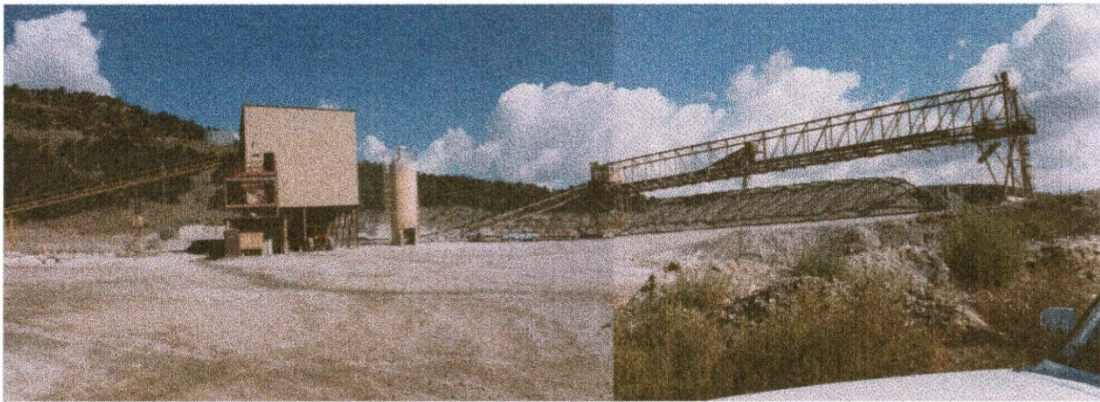
Figure 5-11. Secondary crusher and gantry, Cunningham Hill Mine. Coarsely crushed ore was fed to the secondary crusher from the primary crusher to the left of the photograph. Crushed ore was conveyed to the traveling gantry at right. Photograph taken in fall of 1986 by D. Irving.

Leaching and recovery of gold began in March 1980 and continued to 1987. In late 1986, the last ore from Cunningham Hill was placed on the leach pad. A small amount of ore from the old Ortiz Mine that was stockpiled near its shaft was trucked to the crushing facility and spread on the leach pad. The following description of the leaching and recovery of gold at the Cunningham Hill Mine is taken from Hickson (1981), unless otherwise noted.

Figure 5-12. Oblique aerial view of the Gold Fields Cunningham Hill mine and plant in the early 1980s. Photography and flying by Paul Logsdon. Photo from 1995 NM Geological Society Guidebook No 46.

Leaching

The leach slab was constructed of a lower 51 mm (2 in)-thick layer of impervious hydraulic asphalt and an upper 127 mm (5 in)-thick layer of asphalt with an impervious rubber membrane sandwiched in its middle. The slab was divided by 230 mm (9 in) curbs into eight 61 m (200 ft) by 49 m (160 ft) sections. Each section held a pile of 17,000 tonnes (18,750 short tons) of ore. The pad was loaded so that the tops of the piles were contiguous, even though their bases were separated by the curbs. The leach pad was constructed with a 4% slope.

Ore was loaded onto the sections by the traveling gantry. This eliminated the compaction (and reduced permeability) caused in some leaching operations by the use of heavy track- or rubber tire-mounted equipment to spread ore. This use of a gantry to spread ore for leaching was unique in the world in the early 1980s (McQuiston and Shoemaker, 1981).

Leaching was accomplished by the spraying a solution of sodium cyanide (NaCN) over the top of the crushed ore piles. Concentration of NaCN ranged from 0.05 to 1.5 mg/l depending on the sulfide content of the ore. Average NaCN content was 0.07%. pH was maintained at 10.2 +/- 1 by the use of lime additions to the solution. The solution was applied at a rate of 0.0018 l/m^2 (0.005 gallons/ft^2) by sprinklers similar to ordinary lawn sprinklers. As the solution percolated through the pile, gold was leached from the ore as per the chemical equation $4Au + 8NaCN + O_2 + H_2O = 4NaAu(CN)_2 + 4NaOH$. The gold-laden, or "pregnant" solution, then flowed by gravity along the surface of the pad to a system of ditches built into the pad, which in turn carried the solution to a lined holding pond.

Ore was subjected to cyanide leaching for an average of ten weeks, after which the piles were washed with water for three days to rinse out remaining cyanide. The piles were drained for another four-day period, then loaded onto trucks and taken to a tailings pile.

Gold Recovery

Adsorption - The pregnant solution was pumped into a series of five tower adsorption tanks. Each tank measured 2.44 m (8 ft) in diameter by 1.83 m (6 ft) high and contained 1,360 kg (3,000 lbs) of activated carbon granules (burnt coconut shells). The pregnant solution flowed upward through the carbon in each tank at a rate of 692 l/min per m^2. As the solution passed through the activated carbon, $NaAu(CN)_2$ was adsorbed to its surface, and the concentration of gold in the solution progressively dropped on its journey through the tanks. Solutions passed through the adsorption tanks in 7 minutes. Pregnant solutions typically contained about 1.0 g/t (0.03 oz/st) Au as it entered the first tank. The "barren" solution, exiting the last tank, had a gold concentration ranging from 0.14 to 0.34 g/t (0.004 to 0.010 oz/st). Thus, about 75% of the gold in the pregnant solution was adsorbed by the carbon. The barren solution was reused.

Desorption or "stripping" - Every two days the gold-laden carbon of the first tank was removed and the carbon of the each of the other tanks was advanced to the preceding tank. Reactivated carbon was placed in the last tank. The removed carbon was placed in a 1.52 m (5 ft)-diameter, 2.74 m (9 ft)-high desorption vessel. The laden carbon contained a minimum of 6850 g/tonne (200 oz/st) Au. In the desorption vessel, a caustic-cyanide "stripping solution" containing 1% sodium hydroxide and 5% ethanol was filtered up through the carbon at about 87°C. This solution reversed the adsorption process and put the gold, and any silver present, back into a cyanide solution. The desorption process took less than 24 hours. Heating the carbon it in a kiln at 600°C reactivated it. After reactivation, the carbon was placed in the fifth adsorption tank.

Electroplating - The gold-laden solution produced in the desorption process was passed through 316 stainless steel electrolytic cells. In these cells the gold was plated onto stainless steel wool cathodes measuring 685 mm x 585 mm x 76 mm (27 in x 23 in x 3 in). The loaded cathodes loaded 600 to 2000 g Au (20 to 65 troy ounces).

Gold Fields did not melt the steel wool cathodes to produce dore bullion. Instead, the loaded steel wool cathodes became anodes in a second tank and gold and silver were electroplated onto polished steel plate cathodes. The electroplated product was a foil generally containing about 83% gold and 14% silver. The foil was scraped by hand from the plate cathodes and shipped by armored courier to a precious metals refinery.

CARACHE CANYON

The Carache Canyon prospect lies in Carache Canyon, in the southern part of the Ortiz Mountains **(geologic map in pocket)**.

Exploration history

Gold mineralization at Carache Canyon has been the subject of exploration during several phases in the 20th century. The earliest recorded exploration of lode mineralization at Carache Canyon occurred during the 1930's. Charles McGinnis sank a 30 to 40 foot-deep inclined shaft during that time, with no recorded gold production (G. Griswold, personal communication, 1986). Griswold (1950) suggested that a small monzonite stock in Carache Canyon (Tia Bonita Canyon in his report) may be the source of gold for the Korache (Carache) placers. During the 1970s, Conoco, Inc. drilled at Carache Canyon and identified gold mineralization associated with a breccia pipe.

LAC Minerals, U.S.A., Inc. and the Ortiz Project Joint Venture focused on Carache Canyon and during the period 1983 – 1991. The key insight into gold mineralization at Carache Canyon was made in 1986, when it was realized that gold mineralization was concentrated in mid-Tertiary sills intruding the Cretaceous sedimentary rocks. The gently-dipping, tabular form of the mineralized hosts allowed for a significantly greater tonnage potential than the previously conceived high-angle vein interpretation.

Drilling at Carache Canyon totaled 85,254.3 m (281,339 ft) in 376 holes and is summarized in Table 5- 8. An exploration decline was begun in 1990 for the purpose of gaining underground access to mineralized rock for bulk sampling. The decline was halted at a total length of 515 m (1700 ft), about 215 m (700 ft) short of mineralization in the #3 sill. LAC Minerals and the Ortiz J.V. carried out detailed geologic investigations, including resource and reserve estimates and a prefeasibility mining study. The Ortiz Joint Venture announced a total resource of 1,169,000 troy ounces of gold in 16.7 million short tons of mineralized rock at an average grade of 0.07 troy ounces per short ton at Carache Canyon (Pegasus Mining Corporation, Annual Report, 1991).

A decline in gold prices led to the decision to halt exploration and development activities in 1993. LAC Minerals reclaimed all of the disturbed ground in the Carache Canyon project area and sealed off the decline portal.

Geologic setting

Upper Cretaceous Mancos Shale and Mesa Verde Group sandstone and shale dip 25° to 35° northeast at Carache Canyon (**Figure 5-13**). Deep drilling in two holes at Carache Canyon intersected lower parts of the Mancos Shale and possibly the Dakota and Jurassic Morrison Formations at depths exceeding 600 m (2000 ft). However, detailed information is available only for the upper parts of the Mancos Shale and Mesa Verde Group.
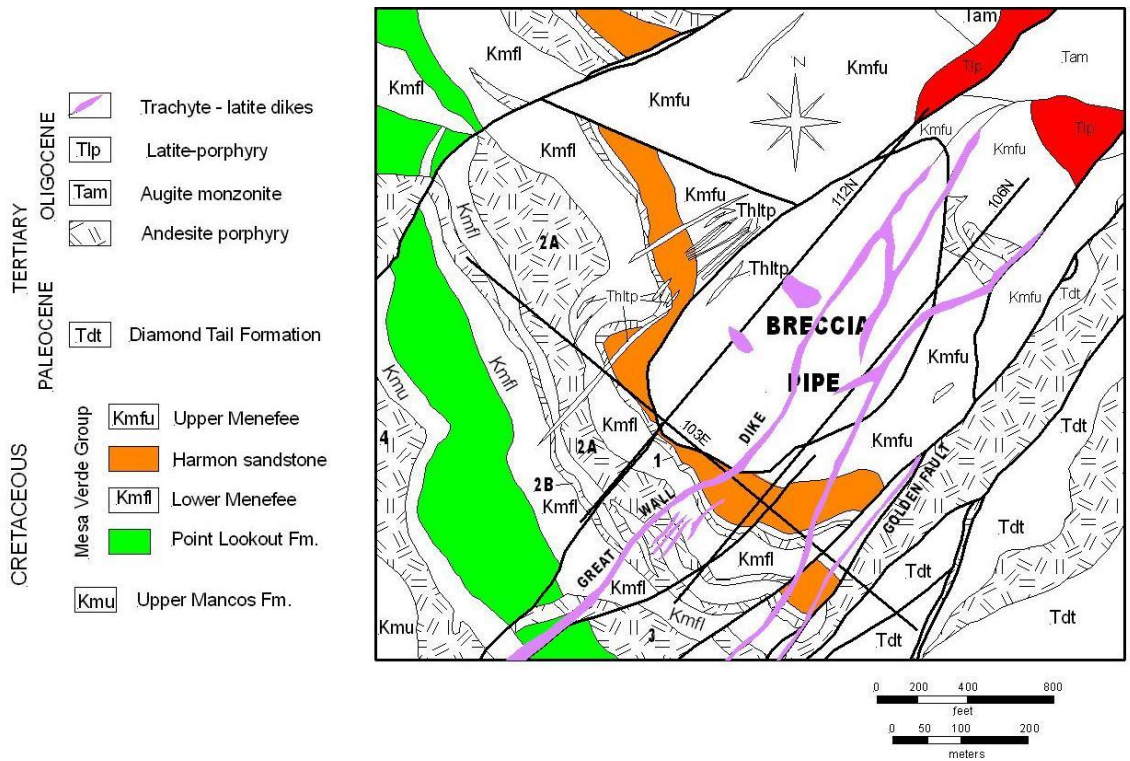
Figure 5-13. Carache Canyon geology. a) geologic map. Bold solid lines are cross section traces. The bold dashed line is the breccias pipe contact.
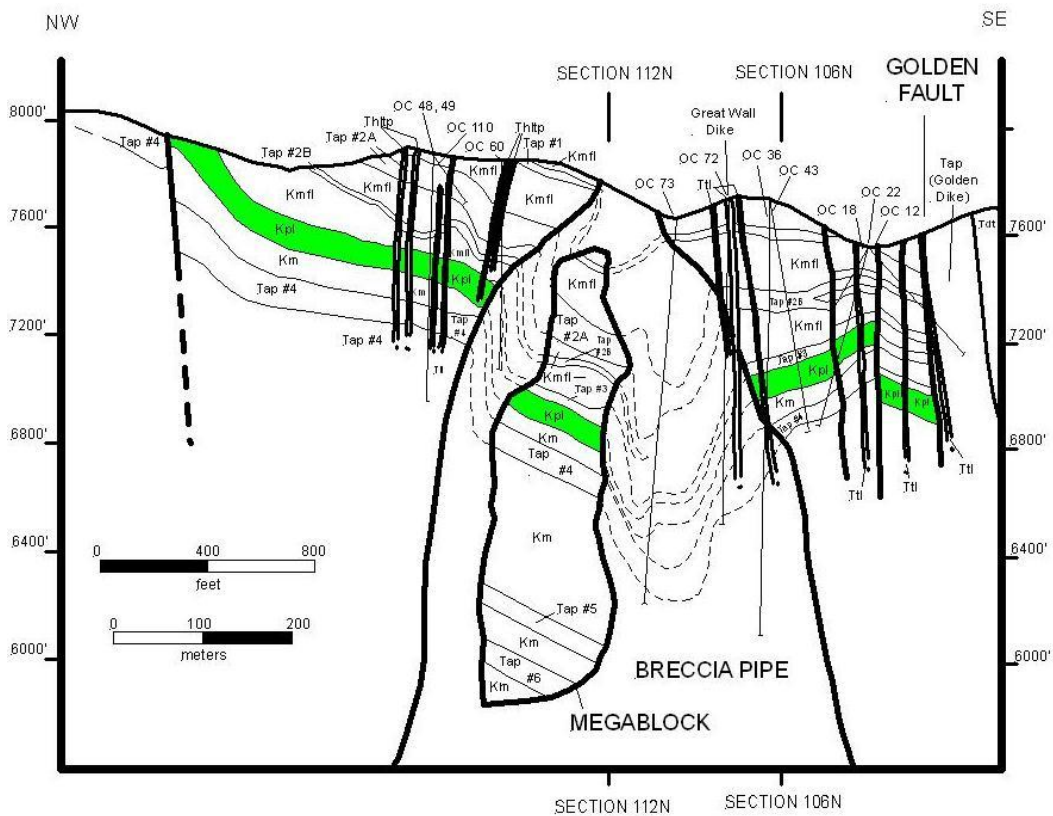
b) Geologic cross section 103E, facing northeast.
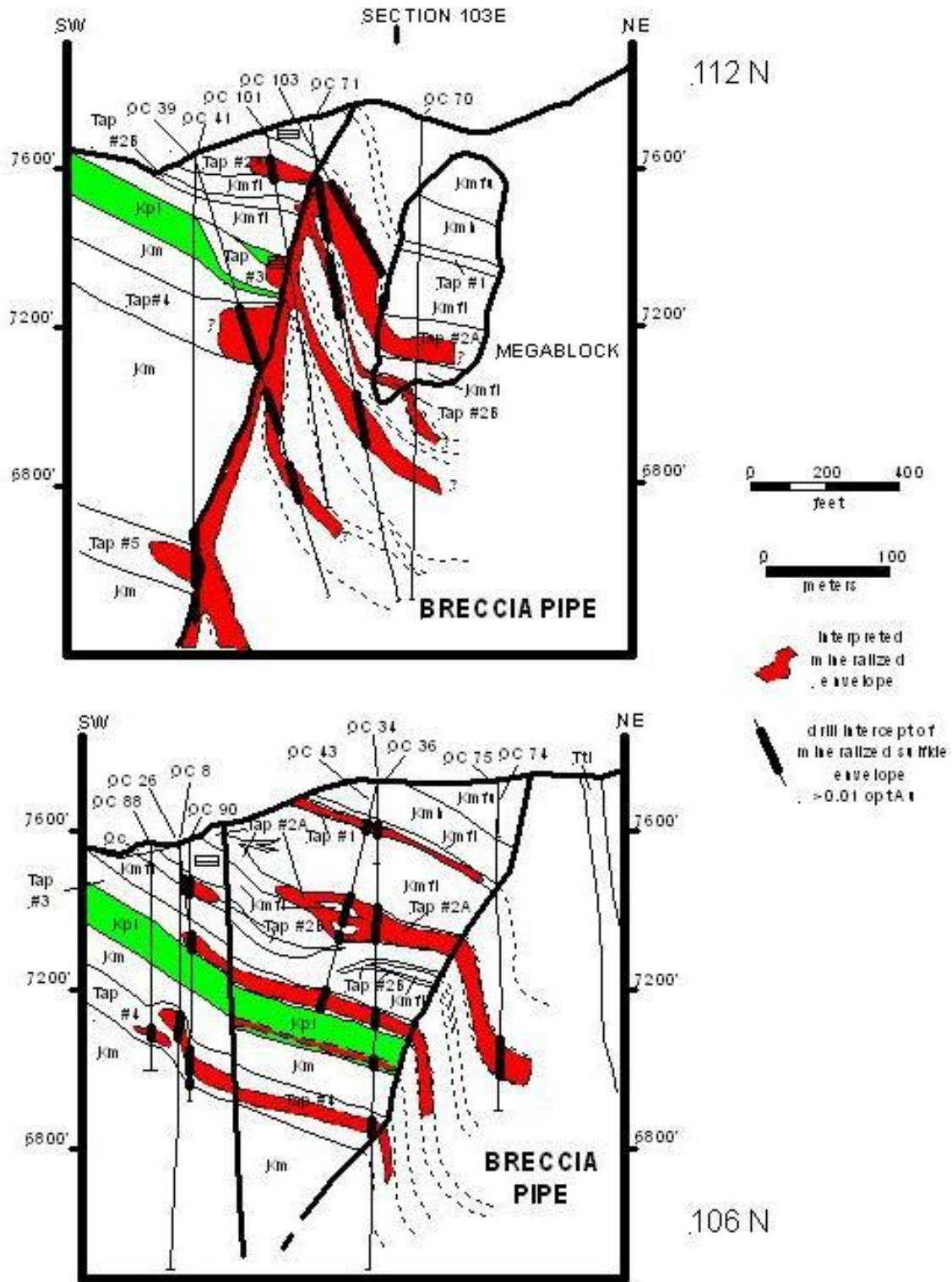
c) Geologic cross section 112N, facing northwest (top); d) Geologic cross section 106N, facing northwest (bottom). In cross sections, dashed lines represent brecciated, collapsed relict stratigraphy within the Carache Canyon breccia pipe. Drill holes are labeled with "OC" prefixes at collars. Green represents Point Lookout Sandstoe. From Schutz (1995).

Quartzite and minor hornfels of the Paleocene Diamond Tail Formation are preserved in the Ortiz Graben southeast of the Golden Fault.

Table 5-8. Summary of drilling in Carache Canyon. Includes drilling by Conoco, LAC Minerals, USA, Inc., and Ortiz Joint Venture. After Schutz (1991).

Exploration Campaign	Type of drilling	Number of holes	Meters	Feet
Pre 1989 Conoco and LAC	Core	128	39,903.9	131,683
1989 Ortiz JV	Core	12	3,890.6	12,839
	Reverse circulation	25	4,675.8	15,430
1990 Ortiz JV	Core	21	5,373	17,731
	Reverse circulation	117	21,353	70,465
	Condemnation reverse circulation	73	10,058	33,193
TOTALS		376	85,254.3	281,339

Seven andesite-porphyry sills intrude the Cretaceous sedimentary rocks at Carache Canyon. The upper four sills' relatively constant position in the mineralized area is depicted in a stratigraphic column in **Figure 5-14**. Although the sills are laterally continuous, they are modified by local pinch-outs, structural dams, bifurcations, and dike-like advances across bedding planes. Andesite porphyry dikes, volumetrically less important than the sills, invaded the Golden Fault and subsidiary structures (**Figure 5-13**). These dikes may originally have been feeders for the sills. Andesite porphyry sills constitute the major host of gold mineralization where they are fractured adjacent to the collapse breccia pipe. The andesite porphyry dike in the Golden Fault is also host to fracture-controlled mineralization.

Augite monzonite crops out in upper Cunningham Gulch 420 m (1,400 ft) northeast of the center of the Carache Canyon breccia pipe. Sedimentary rocks converted to hornfels produced by the augite monzonite have been intersected in deep parts of the breccia pipe.

Latite porphyry dikes with coarse euhedral feldspar phenocrysts are present along the northwest pipe margin. On the basis of compositional and textural similarities, the dikes apparently emanated from the Cunningham Gulch porphyritic quartz latite stock 2000 ft northeast of the breccia pipe (Maynard, 1995). Latite porphyry dikes cut the breccia pipe and are locally mineralized. Drill core evidence indicates the quartz latite plug is cut by trachyte dikes.

Trachyte dikes intruded fractures parallel to the Golden fault zone and locally cross-cut the breccia pipe margin. The most prominent of these, informally termed the Great Wall dike, has a strike length of more than 1600 m (5300 ft) and ranges from 5 to 12 m (15 and 40 ft) wide. It separates extensive sill-hosted gold mineralization southeast of the dike from limited sill-hosted mineralization to the northwest. Drill core evidence indicates that trachyte dikes locally truncate mineralization. However, the presence of mineralized trachyte dike breccias implies that Carache Canyon gold deposition closely followed brecciation and is bracketed within the late alkaline igneous episode.

The Golden Fault strand of the Tijeras-Cañoncito Fault System is the dominant structural feature of the Carache Canyon area and the Ortiz Mountains as a whole. Vertical stratigraphic separation across the fault at Carache Canyon measures about 600 m (1000 ft). The Carache Canyon breccia pipe is localized on a group of faults with lesser displacement that run parallel to

the Golden Fault. Fluids thought to be responsible for the development of the pipe are likely to have exploited these faults, as discussed in the following section.
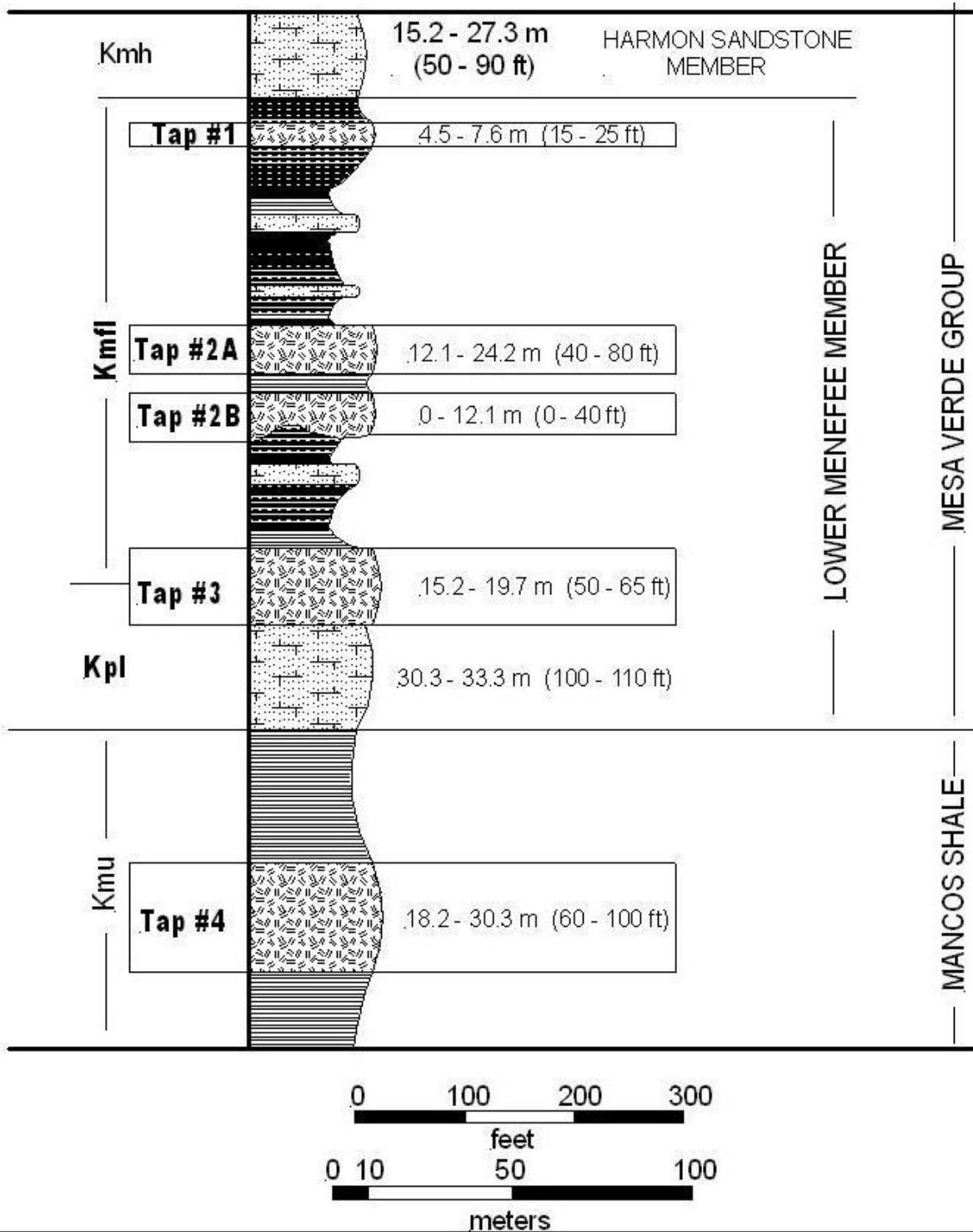
Figure 5-14. Stratigraphic section of the Carache Canyon prospect. Kmu = Upper Mancos shale is composed of calcareous marine shale, Kpl = Point Lookout sandstone. Kmfl = lower Menefee Fm carbonaceous shale, siltstone, sandstone, and minor coal. Tap #1 - #4 = andesite porphyry sills.

Carache Canyon Breccia Pipe

As noted above and depicted in **Figure 5-13**, the Carache Canyon breccia pipe's long axis lies along a fault parallel to the Golden Fault.   The following description of the configuration, composition, and internal structure of the pipe is quoted from Schutz (1995):

> The Carache Canyon breccia pipe possesses textural characteristics similar to hypabyssal breccia pipes defined by Baker et al(1986). It is tear-drop shaped in plan view, measuring 1900 ft by 1000 ft, with the long dimension parallel to the Golden Fault. The pipe plunges 70 $^{\circ}$ to 80° SW, has a distorted cylindrical cross-section shape and is present at drill depths greater than 3,255 ft. An exceptionally large breccia megablock measuring 1,800 ft vertical by 600 ft horizontal separated from the pipe margin and subsided 400 ft without significantly changing bedding attitude. The megablock proved instrumental in identifying collapsed relict stratigraphy throughout the pipe. Relict stratigraphy forms a "nested" series of attenuated andesite porphyry sill and sedimentary rock breccias that collapsed 400-800 ft (Schutz and Nelsen, 1990).
>
> The breccia pipe is typically clast-supported, consisting of angular to subangular fragments with gray to black rock flour matrix derived from comminuted sedimentary rocks. A second clast-supported breccia event resulted in open-space fractures and matrix voids that cross-cut primary black matrix breccia. Average matrix volume is 2-5% with a maximum of 10%. Clast size is poorly to moderately sorted near the pipe and megablock margins, grading to moderately sorted near the pipe center. Breccia clasts near the pipe margin average 0.5-5.0 ft and those near the pipe center average 0.5 to 2.0 ft in diameter. Large blocks measuring 30 to 100 ft long were commonly drilled near the pipe and megablock margins. Although mixed lithology breccias are located along relict contacts and near the pipe center, they are relatively minor and appear dominated by downward transport.

Although the bulk of identified mineralization lies in fractured sills and sandstone on the pipe's margins, significant mineralization was encountered in the pipe, especially in the area between the "megablock" and the southwestern margin of the pipe, northwest of the Great Wall dike (Schutz and Nelsen, 1990; Schutz, 1995).

An explanation of the origin of the breccia pipe must take into account the characteristics described by Schutz as cited above. Most importantly, the removal of material and creation of a void at the pipe's bottom that would allow for as much as 250 to 300 m (800 to 1000 ft) of collapse of a large volume of overlying rock must be considered. Schutz (1995) proposed that collapse was caused by the withdrawal of magma from a chamber underlying the pipe. This postulated withdrawal would have occurred during Dolores Gulch volcanism and emplacement of the latite porphyry and quartz-latite porphyry Cunningham Gulch stock. Coles (1990), citing McCallum (1985), Sillitoe (1985), and Burnham, (1979, 1985), considered three models (dissolution, phreatic, and magmatic hydrothermal) to explain the collapse.

Coles' (1990) dissolution model depends on dissolution of the gypsum (Tonque Arroyo) member of the Todilto Formation, and/or limestone of the San Andres and Madera Formations. The Todilto gypsum is easily dissolved and dissolution breccias are noted in Todilto exposures in and near the Ortiz Mountains. However, the Todilto gypsum's maximum thickness in the region is about 34 m (110 ft); its removal would not be sufficient to account for the collapse observed. The San Andres and Madera Formations are much lower in the stratigraphic section and are not known to develop major caverns in the area. Moreover, the stratigraphic section below the Dakota Formation is likely to be absent. Magnetic data suggest that the augite monzonite may underlie the Carache Canyon area at depths greater than 1000 m (3300 ft).

Coles (1990) considered that a phreatic model, in which magma encountering groundwater, with a subsequent steam explosion, could have fluidized and ejected enough material through a surface vent to allow for the collapse observed. However, phreatic eruptions are usually described in shallower environments.

The magmatic hydrothermal model proposed by Burnham (1979, 1985), and reviewed by Sillitoe (1985), is favored by Coles (1990):

> Burnham's (1979, 1985) model is based on the release of energy during exsolution of an aqueous phase during second boiling, and subsequent decompression during the crystallization of a hydrous magma at hypabyssal to shallow plutonic depths. Energy released during second boiling fractures the overlying rocks, resulting in decompression of the magma. With decompression, the fluids that have been exsolved expand and pressure quenching of a portion of the magma results. With pressure quenching the magma's remaining water is released. The release of energy is concentrated along fractures producing breccia bodies. In the center of the Carache prospect, fractures produced by second boiling may have reached a TCFS structure occupied by andesite and latite/trachyte dikes. Following second boiling the decompressional energy released could be concentrated on this structurally weak zone to produce the pipe. This structure could also explain the tear-drop shape in the upper portion of the pipe, as well as the orientation of dikes southwest of the pipe.
> In order to account for the tremendous volume expansion required by interstitial voids (now filled with hydrothermal minerals) and the down-dropped brecciated relic stratigraphic sequence, a large volume of material must have been removed from the pipe. Doming seems unlikely to explain this volume increase, since sill-like bodies of breccia leading off the pipe are not present and the host rocks do not dip away from the pipe. Probably, the interstitial space was created when the pipe reached the surface and much of the fine grained material was fluidized and erupted out the top. Exhaustion of the fluids responsible for the pipe formation would result in collapse, producing the down-dropped brecciated relic stratigraphic sequence.

The fluidizing event appears to have milled much of the sedimentary rock, mostly Mancos Shale, to rock flour and injected it into the spaces created between larger clasts (**Figure 5-15**). In addition, the black rock flour is injected into fractures in the pipes' margins.
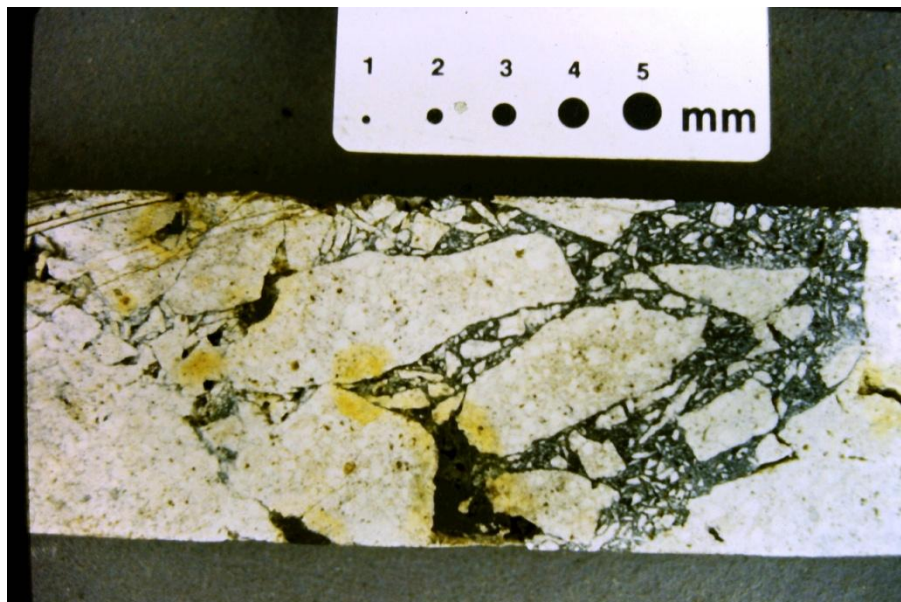
Figure 5-15. Black-matrix breccia in drill core. Clasts of altered andesite porphyry and matrix of rock flour derived from Cretaceous black shale.

The nearby movement of magma along shared, deep-seated structures is implied by the Dolores Gulch volcanic vent breccia and the subvolcanic intrusion of Cunningham Gulch. Withdrawal of magma during final stages of intrusion cannot be ruled out as a contributing factor in the formation of the collapse breccia. Magmatic hydrothermal fluids known from fluid inclusion studies were also present. Given the relatively small volume of hydrothermal minerals in the pipe and the pipe's size, it seems likely that mechanisms of magma withdrawal (Schutz, 1995) and hydrothermal activity (Coles, 1990) acted in concert to produce the collapse breccia.

Open-space breccia (see preceding excerpt from Schutz (1995)) is found in the pipe's wall rocks and cross cuts the black matrix breccia. Further hydrothermal activity is likely to be responsible for the second brecciation event, though secondary, small-scale collapse or settling of the pipe may have played a role as well. Open-spaces are best developed in the more competent rock types, andesite porphyry sills, and sandstone. Open-space is poorly developed in intervening shales of the Mancos Shale and Menefee Formation. Ore minerals are most abundant and gold grades are highest in areas of well-developed open-space breccia.

Mineralization

Continuing hydrothermal activity resulted in the subsequent deposition of gangue and ore minerals, and accompanying alteration of wall rocks. Minerals include native gold, sphalerite, galena, pyrrhotite, arsenopyrite, pyrite, cassiterite, scheelite, and wolframite. Native gold is the only mineral of economic importance at Carache Canyon. These minerals fill open spaces or crackle breccia in the walls of the breccia pipe, particularly on its west and southwest sides, and open-space breccia within the pipe itself.

Paragenesis

On the basis of petrographic examination of polished and thin sections, and detailed core logging, Coles (1990) described a five-stage mineral paragenesis for Carache Canyon (**Figure 5-16**). Schutz (1995) summarized Coles's findings as follows:

> Petrographic studies of Carache Canyon breccia and sill mineralization support a preliminary hypogene paragenetic interpretation, including an early gangue event (stage I) followed by tungsten minerals (stage II), base metal sulfides (stage III), and native gold-carbonate gangue-sulfide-iron oxides (stage IV) (Coles, 1990). Stage I gangue minerals coated open-spaced fractures and voids with a thin veneer of quartz, adularia, tourmaline, and minor barite, chlorite, sericite, and cassiterite. Deep breccia also contains abundant Stage I calcite and mariposite. Stage II scheelite and wolframite veins are rare. Their paragenetic position is based on limited cross-cutting mineral boundary relationships. Stage III minerals form the majority of open-space fillings and consist largely of pyrrhotite with minor chalcopyrite, sphalerite and galena. Stage IV minerals consist of marcasite, pyrite, magnetite, arsenopyrite, hematite, gold and gangue siderite, ankerite, dolomite, and calcite. Mineralized fractures outside the pipe are typified by distinctly zoned orange and green iron oxide selvages extending outward as much as three times the fracture vein width. Colorful oxide selvages are uncommon in the breccia pipe. Stage V supergene minerals include hematite, goethite, digenite, covellite, malachite, and jarosite (Coles, 1990).

Hydrothermal alteration

Schutz (1995) summarized Carache Canyon alteration as follows:

> Wall rock alteration is distributed in a broad zonal pattern relative to depth and open-space fracture and void frequency. Deep breccia (+1000 ft depth) igneous rock clasts were silicified, sericitized and locally potassic altered. Sedimentary rock clasts were decarbonized and

intensely silicified to pale brown and green hornfels. Deep breccia also contains a considerable amount of matrix-infill calcite, siderite, mariposite, pyrrhotite, and chalcopyrite, compared to shallow breccia. Deep level alteration probably reflects contact metamorphism near the augite monzonite stock, superimposed by hydrothermal alteration related to mineralization.

Shallow breccia alteration primarily developed in andesite porphyry and trachyte dike clasts as intense sericitic replacement of plagioclase phenocrysts and groundmass. Sedimentary rock fragments were not appreciably altered. Similar alteration occurred in sills outside the pipe, where sericitic alteration intensity is directly correlated with fracture frequency. As fracture frequency decreases outward from the pipe margin, alteration intensity in andesite porphyry sills decreases from strong sericitic alteration to pervasive propylitic and local biotitic alteration (Coles, 1990). Cross-cutting relationships imply several sericitic alteration events occurred.

Coles (1990) concluded that pervasive propylitic and biotitic alteration was the first alteration event, occurring within calc-alkaline sills and alkaline dikes. Intense pervasive sericitic alteration closely linked to breccia pipe formation followed as the main alteration event. Lastly, minor silicic, sericitic, K-feldspar, clays, and carbonate alteration developed during gold mineralization.

Fluid inclusions

Coles (1990) derived preliminary conclusions about the relationships of fluid chemistry to alteration and mineral paragenesis from fluid inclusions from hypogene mineral stages I, II, and IV. These conclusions are summarized by Schutz (1995):

Homogenization temperatures, trapping pressures, trapping temperatures, and salinity data suggest early gangue mineral fluids were relatively hot (275->400°C), saline (25-46 wt% eNaCl), and CO_2-rich and show evidence of boiling with variable fluid inclusion liquid:vapor ratios. Stage I and II fluids were interpreted as magmatic, occurring after breccia pipe formation and after intense sericitic alteration.

The gold-bearing stage IV fluids were considerably cooler (160-250°C), less saline (10.4-12.1 wt% eNaCl), CO_2-rich and also may have boiled. Stage IV fluids were of meteoric and/or magmatic origin and evolved to lower pH and higher oxygen activity coincident with gold deposition. These data imply that overall fluid conditions ranged between slightly acidic and slightly basic.

Coles (1990) classified Carache Canyon as an adularia-sericite epithermal gold deposit and compared Carache Canyon and Cunningham Hill (Kay, 1986) fluid inclusion data (Table 5-9) concluding that gold-bearing fluids at both breccia pipes were chemically and thermally similar.

Gold Distribution

As previously stated, mineralization lies in open-space breccia around the southwestern margin of the breccia pipe in relatively competent andesite porphyry sills and the Point Lookout Sandstone, as well as in the adjacent southwestern portion of the pipe. Less competent Menefee and Mancos shales did not allow well-developed open-space fractures and are therefore poorly mineralized. Two geometrically different gold distributions correspond to mineralization outside of and within the pipe.

Outside of the pipe, mineralization occurs in gently dipping, tabular, fractured, permeable sills and sandstone separated by impermeable barren Menefee Formation and Mancos Formation shales (**Figure 5-17**). This type of mineralization constitutes the bulk of the known and measured resource at Carache Canyon. The mineralized open-space breccia is often referred to as crackle breccia because of its apparently random orientation. However, a superimposed N35^o-45°E fracture pattern is suggested by drilling in the extensively mineralized region

southeast of the Great Wall dike. Concentric fractures around the southwest pipe margin may also control gold distribution (Schutz and Nelsen, 1990; Schutz, 1995).
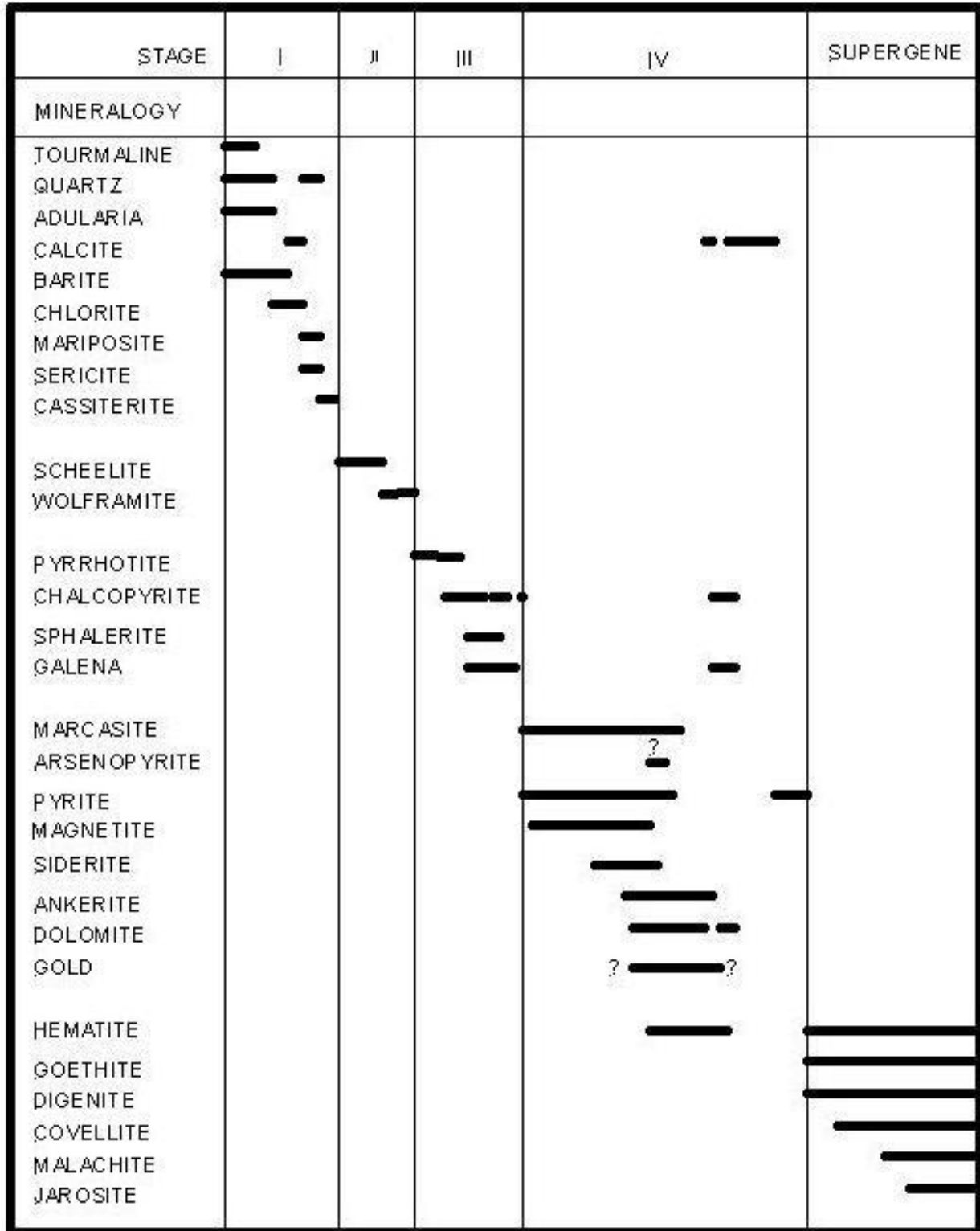
Figure 5-16. Mineral paragenetic diagram of Carache Canyon, from Coles (1990).

Table 5- 9. Comparison of fluids from inclusions in various minerals of similar paragenesis from the Cunningham Hill Mine and the Carache Canyon prospect. Th = degrees C, salinity = wt.% eNaCl; Para = paragenesis; Other = salts other than NaCl; VE = very early; E = early; L = late; VL = very late; H = high. From Kay (1986) and Coles (1990).

Mineral	Cunningham Hill Mine					Carache Canyon			
	Para	Th	Salinity	Other		Para	Th	Salinity	Other
Quartz	VE	>500	>40			VE	270>400	25-46	H $CaCl_2$ H $MgCl_2$ H KCl
Siderite	L	219-262	10.9			L	160-250	11	H $CaCl_2$ H $MgCl_2$, $CaCl_2$ H $MgCl_2$
Calcite	VL	225	<1			VL	175-220	<1	
Scheelite	VL	324-445	>56	H $CaCl_2$ H $MgCl_2$		E	303-370	31-40	H

Mineralization within shallow portions of the pipe is distributed in collapsed, near-vertical, sill and sandstone, relict-stratigraphy breccias separated by weakly mineralized or barren Menefee and Mancos shale breccia. Gold and sulfide mineralization is distributed between the megablock and pipe margin and locally within megablock sills (Figure 5R) (Schutz, 1995).

A third style of mineralization occurs in andesite porphyry and hornfels breccia below the #4 sill breccia.   Although details of deep breccia mineralization are scant due to limited drill data, it is known that at increasing drill depths below 300 m (1000 ft), Mancos shale and siltstone were progressively thermally metamorphosed to brittle hornfels, which gave the breccia matrix greater competency. Open-space fractures were better developed and gold was distributed among igneous- and sedimentary-fragment breccia matrix voids divergent from the relict stratigraphy control seen in shallow breccia Schutz, 1995).

Nugget effect
At Carache Canyon, native gold commonly occurs as equant grains up to 5 mm (0.2 in). The coarseness of the gold grains induced a significant nugget effect as quantified by metallic-screen fire-assay checks (Table 5-10). Large gold grains produce most of the assay variability, compared with small (drill hole) sample sizes (Pitard, 1988, unpub. report for LAC Minerals, USA, Inc.). Larger drill samples, taken in the reverse-circulation drilling campaign of 1990-1991, also failed to provide adequate sample size. Pitard's (1988) study indicated that bulk samples of mineralized rock were required to give adequate reproducibility to assays. A decline was driven to collect statistically accurate bulk samples and evaluate fracture pattern predictability. The decline advanced 515 m (1,700 ft) before it was idled in 1991.
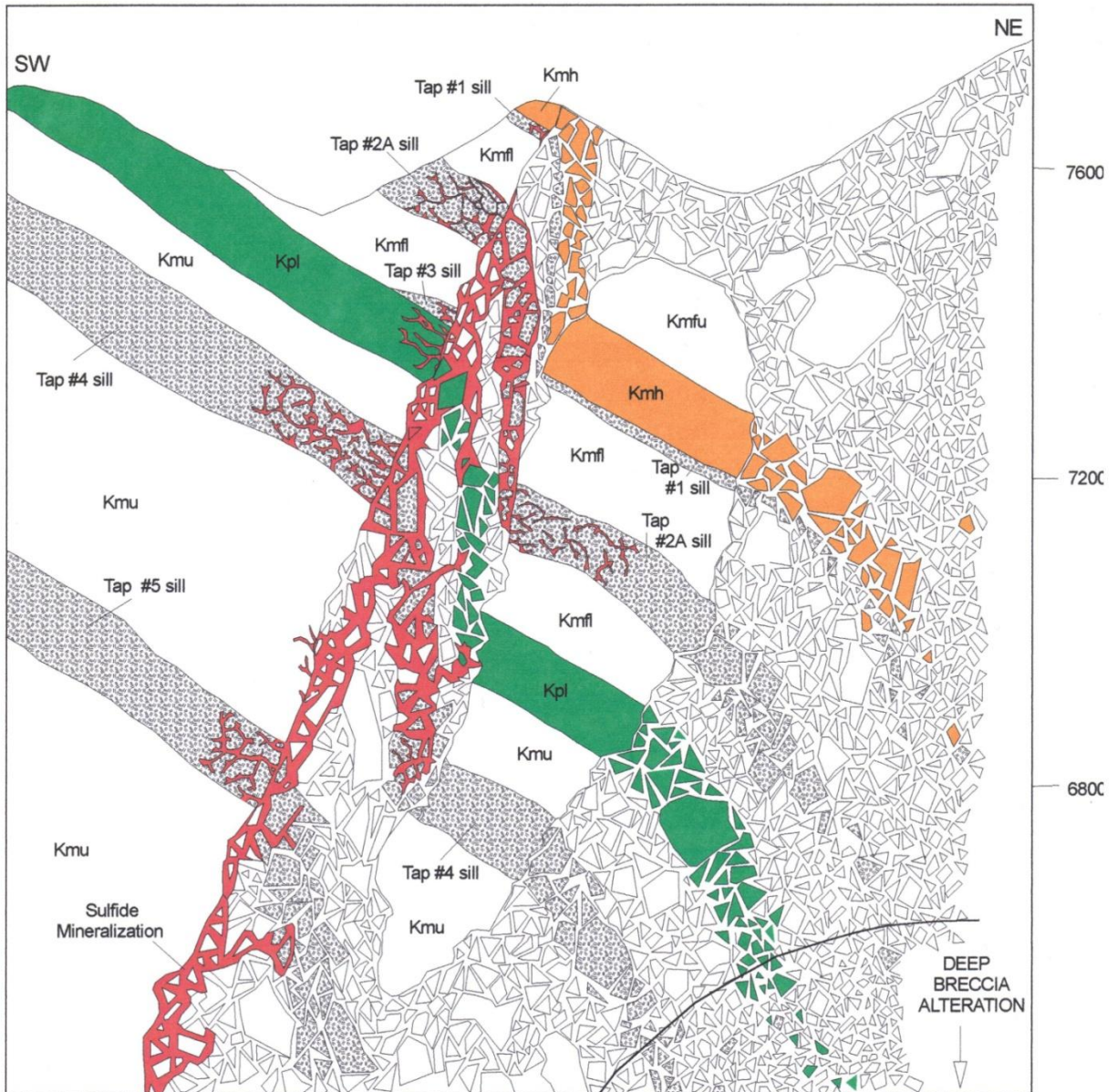
Figure 5-17. Schematic cross section of mineralization at Carache Canyon. Red represents area favorable to mineralization. Kpl=Point Lookout sandstone, which is roughly 30 m (100ft) thick. Mineralization is concentrated along margin of collapse breccia pipe, and in preferentially located in brittle lithologies such as sills and sandstone. Note down-dropped "mega block" with preserved stratigraphy.

Table 5- 10. Gold assay variability in metallic screen fire assay checks (Met 1-5) of drill hole OC-11 intersection of #4 sill. Five separate homogeneous splits of each sample interval were analyzed. Results imply a nugget effect indicated by erratic check assay values. Values are troy ounces of gold per short ton. After Schutz (1995).

Sample Interval (ft)	Met 1	Met 2	Met 3	Met 4	Met 5	Wt Avg
745-750	0.037	0.007	0.031	0.424	0.051	0.143
750-755	0.671	0.741	0.158	0.066	0.364	0.322
755-760	0.135	0.042	0.188	0.106	0.640	0.191
760-765	0.035	0.021	0.030	0.034	0.035	0.031
765-770	0.013	0.031	0.283	0.008	0.135	0.101
770-775	0.071	0.145	1.052	0.021	0.137	0.332
775-780	2.473	0.071	1.169	0.457	0.168	0.844
780-785	0.151	1.236	0.364	0.202	0.189	0.377
785-790	0.127	0.096	0.073	0.195	0.074	0.120
790-795	0.031	0.004	0.004	0.058	0.006	0.024
795-800	0.008	0.004	0.005	0.030	0.333	0.057
800-805	0.063	0.003	0.007	0.032	0.009	0.023
805-809	0.004	0.183	0.002	0.004	0.007	0.043
average	**0.294**	**0.199**	**0.259**	**0.126**	**0.165**	**0.204**

Resource Estimation

Mineral inventory totals 16.7 million short tons grading 0.070 oz/st at a cutoff grade of 0.020 oz/st, or 1.17 million ounces of gold (15.15 million tonnes grading 2.40 g/tonne gold or 36.34 tonnes of gold) for Carache Canyon (Pegasus Gold Corporation 1991 Annual Report). Different methods used for resource calculation can be described as follows.

Plan Polygon Method

Mineralization was measured separately by the plan polygon method in sills #1, #2a, #2b, #3, and #4, and the Point Lookout sandstone. This method was used only on the mineralized portions of the bodies that have a tabular and gently dipping geometry. Plan views of each body were constructed on separate maps. Structural geologic boundaries, including the breccia pipe margin, the edge of the megablock, the Great Wall trachyte dike, and major faults were plotted on the map. Midpoints of each drill intercept were plotted on the map. Polygons were constructed using perpendicular bisectors of lines between adjacent drill intercepts, with a 100 ft maximum radius of influence for each drill intercept. Polygons did not overlap structural boundaries.

Composite grade values for each polygon were derived from the arithmetic mean of all one-assay-ton fire assays, duplicate check assays, and metallic screen assays for each sample. A 0.020 oz/ton Au cutoff was applied to composited samples. Composite grade was then calculated as the sum of the products of sample thickness and grade divided by the intercept thickness.

The product of the sine of the drilling angle and intercept thickness gave the vertical thickness of the intercept. Vertical thickness multiplied by the polygonal area multiplied by the tonnage factor (ranged from 12.36 ft^3/ton to 13.75 ft^3/ton) gave the polygon's tonnage. Ounces per polygon were computed by multiplying tons by grade. Total ounces are computed as the sum of ounces for all polygons.

Cross Sectional Method

The resource contained in the breccia pipe examined mineralization in 27 separate rock units. Geologic boundaries, other than the boundary of the pipe itself, were not so easily defined as in the plan polygon method. Polygon boundaries were constructed equidistant from adjacent mineralized intercepts or projected 100 ft on either side of the midpoint intercept.

Compositing was carried out in a fashion identical to that used in the plan polygon method. Tonnage is the product of polygon area and section spacing (50 ft) divided by the tonnage factor. Ounces per polygon were computed by multiplying tons by grade. Total ounces are calculated as the sum of ounces for all polygons.

FLORENCIO PROSPECT

The Florencio Prospect lies on the northwestern side of the Dolores volcanic vent, about 1200 m (4000 ft) north-northwest of the Cunningham Hill Mine. Florencio lies on the northeast trend defined by the alignment of the old Ortiz Mine, and the English and Shoshone prospects. The contact of the augite monzonite stock and the Dolores volcanic vent follows this contact. Dikes of trachytic latite parallel this trend as well.

The Florencio mineralized breccia was determined by mapping and drilling to be a northeast-trending, tabular body of quartzite breccia (**Figure 5-18**).   In outcrop, the breccia body extends 450 m (1500 ft) and is typically 30 to 60 m (100 to 200 ft) wide. Drilling indicates that the breccia dips steeply to the northwest in its southwestern portion and steeply to the southeast in its northeastern part. In the northeastern part the breccia forms two separate bodies at the surface.   The breccia is a rotated-clast quartzite breccia developed at the contact of the Diamond Tail Formation and underlying Mesa Verde Group with the volcanic vent breccia. Gas explosions following magma crystallization are thought to have formed the breccia at Florencio, as at Cunningham Hill (Kay, 1986).

There are no records of production or other activity at the Florencio prospect.   Surface assays rarely exceeded a value of $2 per short ton (0.06 oz Au/st) at $35/tr oz Au, but irregular workings and an inclined shaft more than 100 ft deep suggested the presence of higher-grade zones (Griswold, 1950).   In the 1970s Gold Fields Mining Corporation cut a series of trenches and drilled 3,630.4 m (11,980.2 ft) in 20 core holes at Florencio and determined the general configuration of the mineralized body. In 1981 the company conducted an evaluation of near-surface mineralization by drilling 2,757.6 m (9,100 ft) in ninety-one 33 m (110 ft) air-track holes.   Gold Fields' preliminary estimate of the Florencio resource was 60,000 contained ounces of gold in 2.7 million tonnes (3 million short tons) grading 0.02 ounces per short ton.
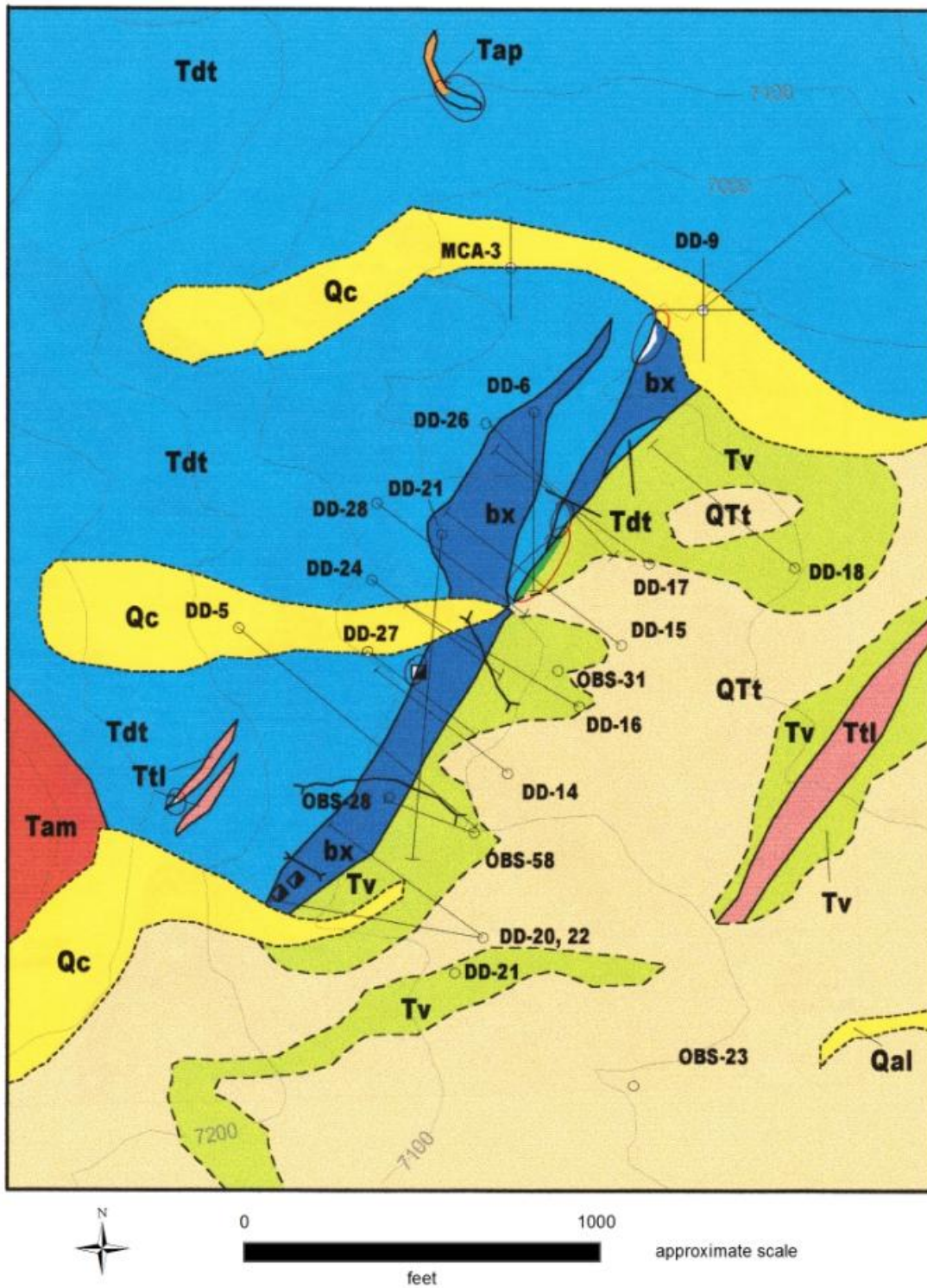
Figure 5-18. Geologic map of the Florencio prospect.

SKARNS

LUKAS CANYON

The Lukas Canyon prospect lies in Lukas Canyon (Alpine Gulch) and the lower part of Monte del Largo Canyon (Gold Leaf Gulch) in the southwestern part of the Ortiz Mountains (**geologic map in pocket**). The prospect has been also known as Old Reliable or Pat Collins. The Lukas Canyon prospect includes all gold-copper mineralization hosted by contact-metamorphic rocks developed in the Greenhorn limestone member of the Mancos Shale and adjacent rocks in the southwestern part of the Ortiz Mountains.

Gold and copper mineralization have been known from Lukas Canyon since at least 1900. (Keyes, 1909). Although no mention is made of the gold and copper mineralization in Lukas Canyon by Townley (1968), it seems likely that prospecting activity took place at the time of early mining at the Candelaria Mine, in the 1850s. Lindgren and others (1910) mention that ore from Lukas Canyon was treated at a 5-stamp mill in Tuerto Arroyo.

Lukas Canyon was known by the names of various small mines and prospects: Pat Collins, Old Reliable, Gold Leaf, Lime Area, and Alpine. Three mining claims had been excepted from the Ortiz Mine Grant in Lukas Canyon. These are known as the Black Prince, the Illinois, and the Ohio claims.

Investigation of the Lukas Canyon prospect in the late 1940s and early 1950s included detailed sampling and churn drilling. Griswold (1950) reported that there might exist 2 million tons of ore grading 0.08 ounces per ton gold and 0.3% copper.

Drilling conducted at Lukas Canyon from 1968 through 1990 is summarized on Table 5-11. As part of LAC and the Ortiz Joint Venture's study, Schroer (1994) performed a master's thesis study of the Lukas Canyon mineralization. The following description of the geology of Lukas Canyon, particularly the sections on mineralogy and geochemistry, are summarized from Schroer's work.

Table 5-11. Summary of drilling at Lukas Canyon. From Martin (1991).

Years and company	Type of drilling	Number of holes	Meters	Feet
1968 Molycorp	Core	1	214.0	702
1972-73 Conoco	Core	14	1,278.9	4,196
1984-85 LAC Minerals	Core	32	1,701.7	5,583
1988 LAC Minerals	Reverse circulation	60	3,478.8	11,480
	Core	2	361.5	1,186
1989-90 Ortiz JV	Reverse circulation	415	24,191.7	79,369
	Core	23	872.3	2,862
Total Reverse Circulation		**475**	**27,690.8**	**90,849**
Total Core		**72**	**4,428.4**	**14,529**
GRAND TOTAL DRILLING		**547**	**32,119.2**	**105,378**

Geologic setting

The Lukas Canyon prospect is hosted principally by skarn developed in the Greenhorn Limestone Member of the Upper Cretaceous Mancos Shale (**Figure 5-19**). The underlying Graneros Shale Member and the overlying Carlile Shale Member, as well as intrusive andesite porphyry sills and dikes, also host skarn mineralization. At Lukas Canyon, the sedimentary

rocks strike typically north to northeast and dip 25° to 35° to the east. The metamorphosed Greenhorn Limestone forms a dip slope on the western side of Lukas Canyon.

Sills and dikes of andesite porphyry intruded the Mancos Shale in discontinuous bodies of limited extent in the area of Lukas Canyon. The thick andesite porphyry sills of the Lomas de la Bolsa laccolith lie 1,500 to 2,000 meters to the north of Lukas Canyon.

A quartz-monzodiorite stock forms Candelaria Mountain, the prominent hill rising to an elevation of 7,912 feet (2412 m) on the east side of Lukas Canyon. The monzodiorite commonly contains zones of magnetite veining and magnetite-matrix breccia and is ringed by an aureole of strongly metamorphosed rocks of the Mancos Shale.

With metamorphism, the Graneros Shale Member's normal medium gray shale is converted to a blue gray hornfels. The Greenhorn Limestone Member, composed of interbedded limestones and calcareous shales, is metamorphosed to pyroxene-scapolite skarn interbedded with garnet tactite (**Figure 5-20**). The upper and lower portions of the skarn contain pyroxene-scapolite with orbicule garnets and garnet seams. The Carlile shale is commonly metamorphosed to a reddish-brown, green, and tan banded hornfels with garnet porphyroblasts (**Figure 5-21**).

Skarn at Lukas Canyon is exposed over 1.6 km of strike length of the outcrop of the Greenhorn limestone. The skarn grades into marble zones at its north and south ends. Strike is northeast and it dips 7°-35° to the southeast in the southern two-thirds of its exposure. In the northern third it strikes northwest and dips 11° to the northeast. The two zones are separated by the Gold Leaf fault. On the western side of Lukas Canyon the skarn forms a dip slope; on the eastern side of Lukas Canyon it is overlain by the hornfelsed Carlile shale member.   Drill information indicates that skarn of the Greenhorn limestone extends at least 2000 ft (610 m) down dip to the east.   Garnet tactite and pyroxene-scapolite skarn mimic the original interbedding of limestone and shale, respectively, in the Greenhorn limestone. Thickness of the skarn averages 50 ft (15.3 m) and ranges from 23 to 60 ft (7.0 to 18.3 m), reflecting variation in the original thickness of the Greenhorn limestone.

Skarn mineralogy and paragenesis

Prograde Alteration
The prograde exoskarn assemblage consists of garnet skarn (tactite) and pyroxene-scapolite skarn. Garnet skarn (tactite) replaces limestone beds of the Greenhorn limestone and forms interbeds with pyroxene-scapolite skarn. By definition, garnet skarn contains at least 50% garnet before retrograde alteration. Garnet dominates the assemblage, ranging from 50% to 99% of the rock and averages 79%, with subordinate pyroxene and scapolite. Pyroxene is found interstitial to and as inclusions within garnet.   Retrograde alteration attacked garnet skarn more readily than it attacked pyroxene-scapolite skarn.

Pyroxene-scapolite skarn contains less than 50% garnet and replaces shale beds of the Greenhorn limestone.   Pyroxene makes up from 1% to 50% of the rock and averages 19%. Scapolite makes up 0% to 85% and averages 32%. Garnet ranges from 0 to 45% and averages 23% of the rock. The pyroxene-scapolite skarn is commonly granoblastic and displays bands of pyroxene, scapolite and garnet. Garnet in particular forms bands and orbicular clots.
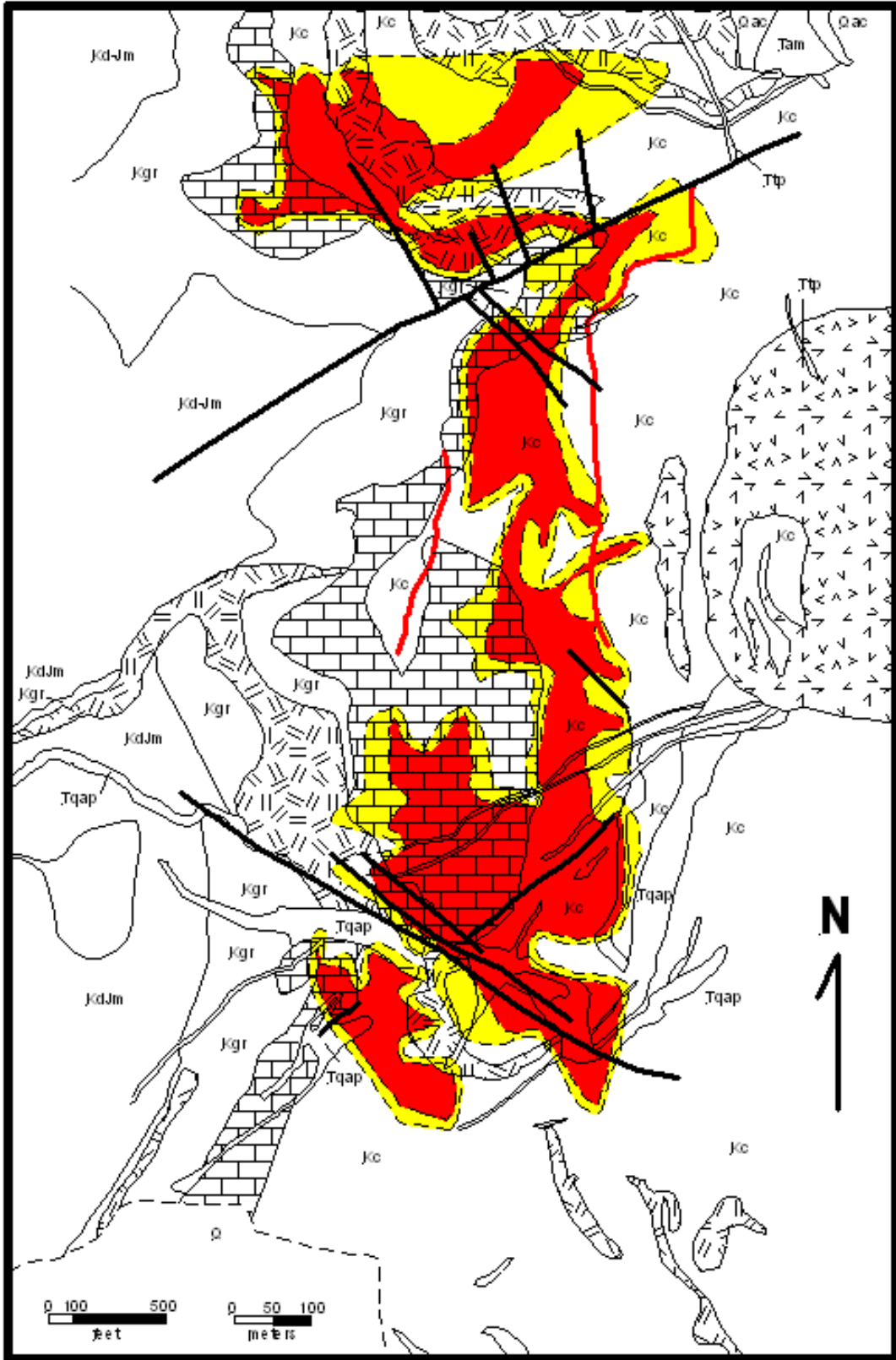
Figure 5-19. Geologic map of Lukas Canyon, showing outcrop distribution of Greenhorn Limestone member (brick pattern) and projection of gold values from 0.02 to 0.03 ounces/short ton (yellow) and more than 0.03 ounces/short ton (red).

Figure 5-20. Garnet skarn developed in Greenhorn limestone.

Garnet ranges from grossularite ($Ca_3Al_2Si_3O_{12}$) to andradite ($Ca_3(Fe^{+3},Ti)_2Si_3O_{12}$) and is zoned with isotropic cores; and iso- to anisotropic Fe^{3+} and Al^{3+} rims. Garnet replaces and hosts inclusions of scapolite and pyroxene, though deep red garnet occurring in late prograde stages overgrew earlier garnet and contains no inclusions of pyroxene or scapolite.   Pyroxenes range from diopside ($CaMgSi_2O_6$) to ferroan diopside and occur as equant grains ranging from 0.05 mm to 2.0 mm. Pyroxene replaces scapolite to a minor degree.   Scapolites are usually the Na-rich variety dipyre and form prismatic sub- to euhedral interlocking crystals with a granoblastic texture.   In the prograde phase, scapolite and pyroxene precede garnet in the replacement of the Greenhorn limestone.   Sphene and apatite are found as trace minerals but may comprise as much as 1% of the rock each.

Prograde endoskarn is minor at Lukas Canyon and is found in andesite porphyry in contact with the Greenhorn skarn. Garnet, pyroxene, epidote, and chlorite are alteration products of the endoskarn.

Retrograde Alteration

Retrograde alteration of skarn is associated with the cooling of the causative intrusive body and the resulting influx of meteoric water.   Meteoric water mixes with magmatic fluids and temperatures drop below 460°C.   Identified retrograde alteration minerals are actinolite, plagioclase, quartz, adularia, allanite, epidote, prehnite, biotite, paragonite, chlorite, calcite, hematite, magnetite, pyrrhotite, marcasite, pyrite, chalcopyrite, sphalerite, and molybdenite. Actinolite is common in the Lukas Canyon skarn and typically replaces pyroxene. It is commonly replaced by supergene clay and limonite. Plagioclase is found in most of the skarn body and replaces scapolite and garnet cores. Epidote replaces garnet, scapolite, and plagioclase and forms halos around opaque minerals.

Supergene Alteration

Clay formed from skarn silicate minerals, formation of limonite, and secondary copper sulfides, carbonates, and silicates constitute the suite of supergene minerals at Lukas Canyon. Clay minerals include smectite and kaolinite. Copper sulfides chalcocite, digenite, and covellite form replacements around hypogene sulfides, especially chalcopyrite and marcasite. Copper carbonates and oxides, chrysocolla, malachite, and azurite occur with secondary copper sulfides filling interstitial vugs. All visible gold studied occurs with supergene alteration. Although it seems most likely that gold originally entered the system during the retrograde event with sulfide minerals, no hypogene gold has been definitely identified. Copper and gold were redeposited at the paleo-water table during supergene alteration.

Geochemistry

Apart from the increases in base metals and gold, the conversion of limestone to skarn was accompanied by increases in Fe_2O_3, SiO_2, TiO_2, MnO, and P_2O_5 and a decrease in CaO (Schroer, 1994).

Resource estimation

Details of the resource estimate for Lukas Canyon are confidential but the methods used are here described. The geologic resource was calculated using a plan polygon method similar to that used for the mineralized sills at Carache Canyon. Resources were calculated for four rock units: Graneros shale, Greenhorn limestone, Carlile shale, and andesite porphyry. The Greenhorn limestone was found to contain nearly 90% of the contained gold.

The Ortiz Joint Venture calculated resources totaling 5.44 mt @ 1 g/t for 5.44 t Au (million short tons grading 0.03 oz/st gold (180,000 oz gold) and 0.25% copper (15,000 short tons copper)) with a strip ratio of 2.2:1 for Lukas Canyon.

IRON VEIN

A series of short adits and small prospect pits (Iron Vein, Italian workings, "O" workings, and the Lost workings) lies along the outcrop of the Jurassic Todilto Formation on the southeast side of the Ortiz Graben (**geologic map in pocket**). In this report, these workings are treated under the heading of the Iron Vein. The term "vein" is misapplied; mineralization is dominantly of the skarn/replacement type. Since the Iron Vein prospect has a history of usage in reports on the Ortiz Mountains, the use of the name is continued here. Although the earliest mention of the Iron Vein is in Raymond's 1860 report (Raymond refers to it as the Mammoth prospect), it seems likely that Spanish and Mexican prospectors investigated the area prior to the American occupation of New Mexico.

Investigation of the Iron Vein prospect consists of pits, trenches, and short adits that were dug prior to 1950 (most likely during the 1930s), plane-table mapping and sampling of the workings by Griswold in the early 1950s, and LAC's mapping, drilling, and sampling during the 1980s. LAC drilled 1,316 ft (401.1m) in eleven core holes and 8,059 ft (2456.4m) in seventeen reverse-circulation holes at the Iron Vein.

Geology

The geologic units present at the Iron Vein prospect include Triassic, Jurassic, Cretaceous, and Paleocene sedimentary rocks, plus andesite porphyry and a latite stock.   The rocks are strongly deformed by faulting along the Buckeye Hill Fault and subsidiary structures **(geologic map in pocket)**.

Triassic and Jurassic rocks lie in the footwall (south side) of the Buckeye Hill Fault. Maroon mudstone of the Triassic Chinle Group, probably correlative with the Petrified Forest Member, is commonly metamorphosed to a dark green hornfels in the area of the Iron Vein prospect. Jurassic Entrada Formation sandstone is thin (less than 50 ft thick) in the Iron Vein area, and is metamorphosed to quartzite. The Jurassic Todilto Formation is the most readily identified formation in the Iron Vein area. The upper member, the Tonque Arroyo gypsum member, is commonly brecciated and dissolved, and is probably tectonically thinned. Breccia in the Tonque Arroyo member contains clasts of sandstone and mudstone probably derived from the overlying Morrison Formation, as well as clasts of andesite porphyry **(Figure 5-21)**.   The Luciano Mesa limestone member is unaltered in some exposures, and converted to magnetite-hematite-garnet skarn in others. Most mineralization at the Iron Vein is associated with the Todilto Formation. Sandstone presumed to be of the Morrison Formation overlies the Todilto Formation gypsum member.

Cretaceous and Paleocene rocks prevail in the Ortiz Graben, on the hanging- wall (north side) of the Buckeye Hill fault. Float of coal and carbonaceous shale, as well as carbonaceous shale and sandstone intersected in drilling at the Iron Vein, are part of the Menefee Formation. Coarse to locally pebbly quartzite forming the hills immediately north of the Iron Vein prospect constitute the Diamond Tail Formation.

Figure 5-21. Breccia developed in Tonque Arroyo gypsum Mbr of Todilto Fm, Iron Vein prospect.

Mineralization

The Iron Vein prospect extends approximately 3040 m (10,000 ft) along the southern margin of the Ortiz Graben. Mineralization is contained in three environments in the Iron Vein prospect: 1) along the Buckeye Hill fault zone, 2) in massive pyrite veining in the contact zone of a subsurface granodiorite body, and 3) in replacement and skarn of the gypsum and limestone of the Todilto Formation.

Fractures that form the Buckeye Hill fault zone host gold mineralization, generally at grades less than 0.01 opt, though one 5.0-ft drill intercept intersected 0.08 opt gold. The Buckeye Hill fault zone may represent a substantial low-grade resource.

Massive pyrite occurs at the contact of a subsurface granodiorite body at its contact with the gypsum member of the Todilto Formation. The granodiorite is probably responsible for a northeast-trending magnetic high detected in the airborne geophysical study and the thermal metamorphism of most of the rocks in the Iron Vein area. Two drill intersections of the massive pyrite were 45.0 ft of 0.055 opt gold and 20.0 ft of 0.076 opt gold (**Figure 5-22**)

Gold mineralization is developed intermittently in the gypsum and limestone of the Todilto Formation. The highest grades come from hematite-magnetite skarn in the limestone member.
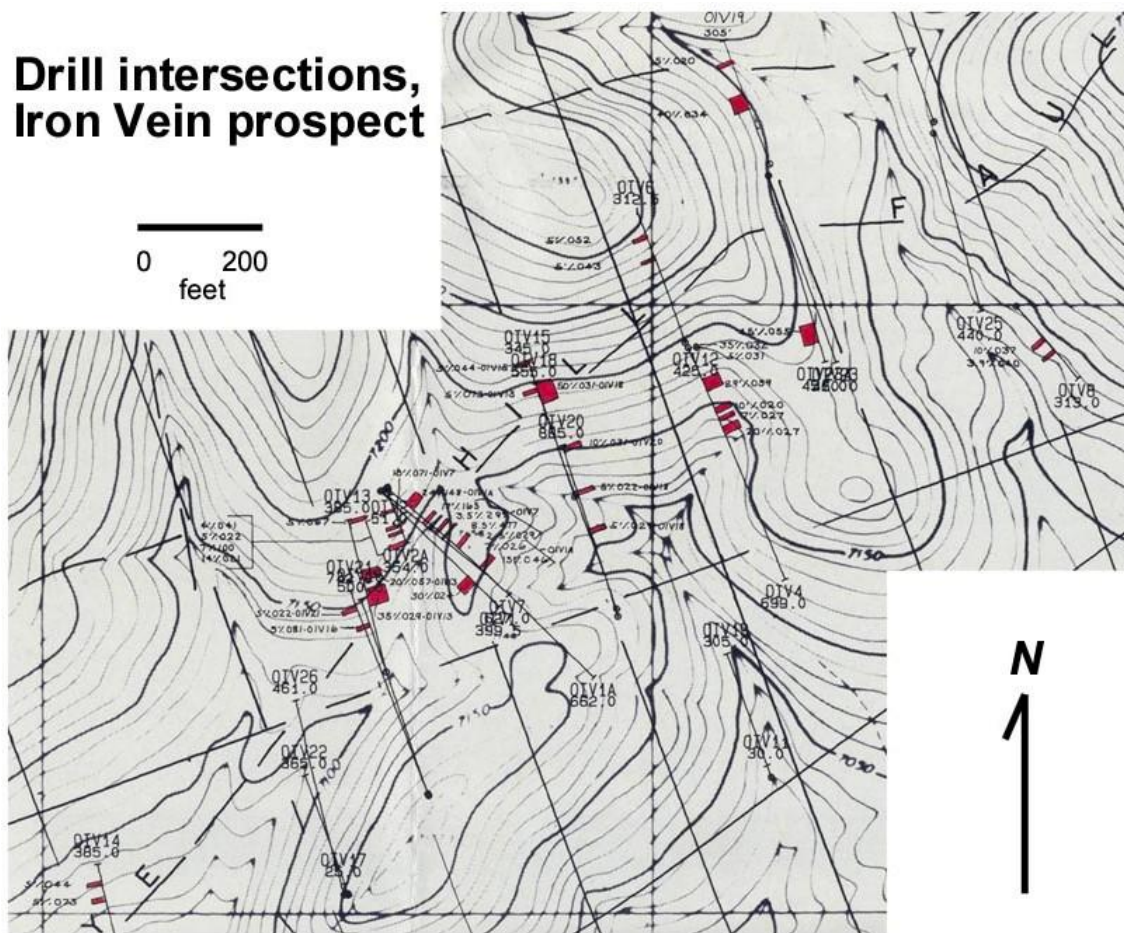
Figure 5-22. Drill intercept map of central part of Iron Vein prospect.

LONE MOUNTAIN

Pyroxene-epidote skarn developed in the Greenhorn limestone member of the Mancos Shale crops out on the south and west sides of Lone Mountain, about 45 m (150 ft) below its summit, (Griswold, 1950; Lisenbee and others, 2001). Short tunnels were driven on the mineralization, probably in the 1930s. Griswold (1950) reported that a single sample across 46 cm (18 in) of metamorphosed limestone assayed 0.04 oz/st Au.

VEIN MINERALIZATION

OLD ORTIZ (SANTO NIÑO) MINE

Location, history, and development

The Old Ortiz, or Santo Niño, Mine lies on the northwest side of the Dolores Gulch volcanic vent, about 4300 ft (1300 m) west of the Cunningham Hill Mine. The Ortiz Mine is the site of the first lode gold discovery in the Ortiz Mountains in 1828. The deposit was worked on a small scale during the 1830s and again more intensively during the 1850s and 1860s, and 1890s. Shorey (1948) stated that underground workings extended 400 ft (122m) along strike and 350 feet in depth.   Although Gold Fields did not mine any new ore at the Ortiz Mine, the company hauled a small tonnage of dump material to the leach pad for cyanide leaching, thus recovering a small amount of gold from the Ortiz Mine.

Gold production records for the Ortiz Mine do not exist, though it can be estimated that about 20,000 troy ounces of gold was produced from the Ortiz Mine during the 19th century.

Geologic setting

The Ortiz vein strikes N28[o]E and dips 76[o] to the northwest and lies within the augite monzonite, near and parallel to its contact with the Dolores Gulch volcanic vent breccia and the feldspar-porphyry latite stock that intrudes it (**geologic map in pocket, Figure 5-23**). The vein is oxidized to a depth of about 250 ft (76m) from the surface. Oxidized ore contained limonite, calcite, quartz, and specular hematite. Unoxidized ore consisted of pyrite, quartz, lesser calcite, minor chalcopyrite, minor galena, and magnetite. Underground sampling (Table 5-12) indicates an average gold grade of the vein at the 350 ft level to be 0.53 ounce per ton (Shorey, 1948). Assuming constant grade to the surface (no enrichment in the oxide zone) and leaving about 50% of the vein material as pillars, it can be estimated that about 20,000 troy ounce of gold was produced prior to Shorey's study.

Table 5-12. Gold values of samples from 350' level, Old Ortiz Mine. Locations of samples shown in Figure 5Ya. From Shorey, 1936.

Sample No.	Width (inches)	oz/st	Location
1	27	0.02	North breast
2	30	0.01	In back 10 ft south of no. breast
3	41	0.04	" 20 ft "
4	46	0.03	In bottom 38 ft south of no. breast
5	29	0.01	" 49 ft "
6	42	0.01	In back of raise above No. 5
7	42	0.02	" 59 ft so. of no. breast
8	24	0.18	" 68 ft so. of no. breast
9	46	0.01	" 79 ft so. of no. breast
10	30	1.20	11 ft. above back 92 ft south of no. breast
11	35	0.11	In back 5 ft south from br. northeast split
12	37	0.22	In back 19 ft south from br. northeast split
13	41	3.92	In bottom 107 ft. south of no. breast
14	46	2.91	In bottom 121 ft. south of no. breast
15	26	0.29	In back 143 ft. south of north breast
16	38	0.01	In back 151 ft. south of north breast
17	62	0.02	In back 162 ft. south of north breast
18	28	0.11	In back 177 ft. south of north breast
19	67	0.02	In back 186 ft. south of north breast
20	53	0.07	In back 201 ft. south of north breast
21	54	3.29	In back 213 ft. south of north breast
22	33	0.12	In back 221 ft. south of north breast
23	30	0.02	4 ft above back 233 ft south of north breast
24	52	0.10	In back 243 ft so. of no. breast
25	55	0.20	In bottom 254 ft so. of no. breast
26	40	0.13	In bottom 270 ft so. of no. breast
27	92	1.03	In back 292 ft so. of no. breast
28	53	0.10	In back 305 ft. so. of no. breast
29	61	0.08	In back 320 ft. so. of no. breast
30	58	0.03	In back 332 ft. so. of no. breast
31	67	0.12	In back 342 ft. so. of no. breast
32	54	0.02	In south breast
33	10 ft	0.01	Along hanging wall between #14 and #15
34	85	0.01	Along back 10 ft so of shaft
35	29	0.04	Along back 20 ft so. of shaft on west split
36	48	0.02	Along back 20 ft so. of shaft on east split Note: 31 in of dead rock between #35 and #36
37	44	0.16	In back 26 ft. so. of shaft
38	104	0.05	In back 40 ft. so. of shaft
39	54	0.02	In back 51 ft. so. of shaft
40	29	0.02	Across small split breast 4 ft. so. of #38
41	39	0.08	In back midway between #9 and #10
42	48	1.32	In bottom midway between #10 and #13
43	70	1.67	In bottom midway between #13 and #14
44	42	0.06	In back midway between #15 and #16
45	48	0.78	In back midway between #21 and #22
46	33	0.15	In bottom midway between #26 and #27
47	72	0.07	In back midway between #27 and #28
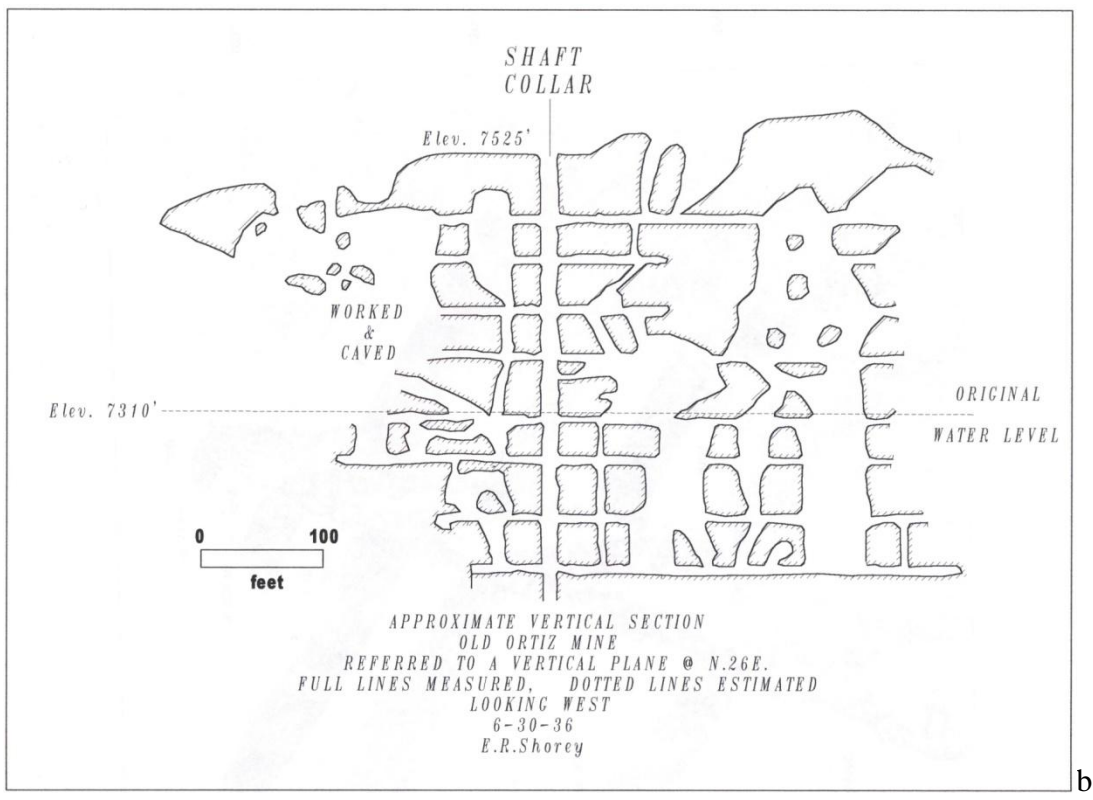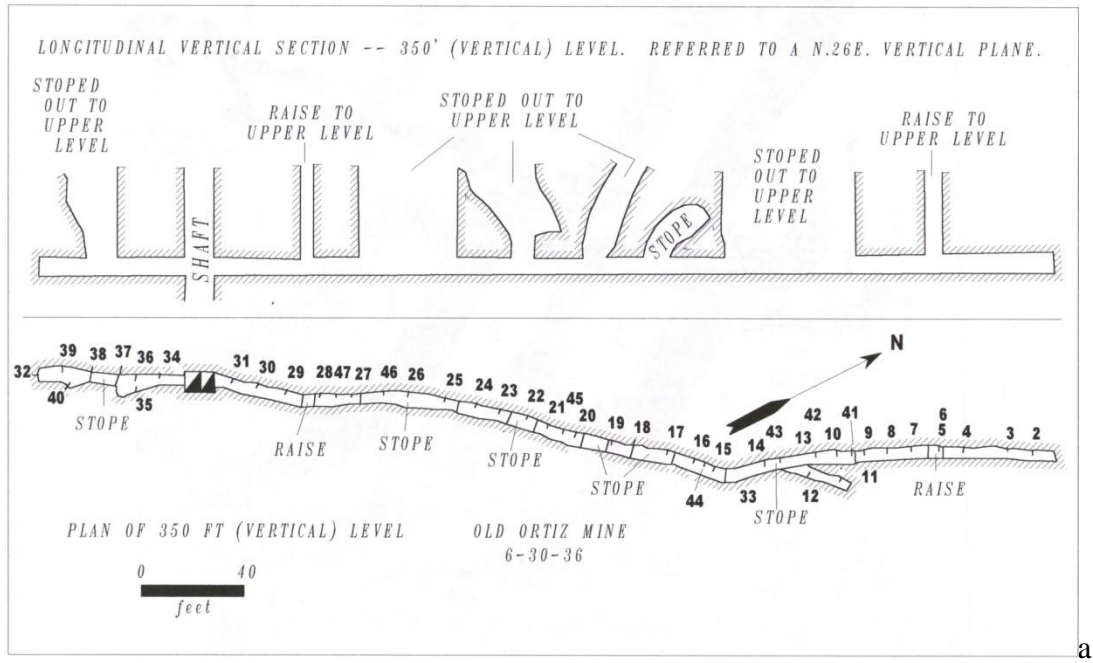
Figure 5-23. Old Ortiz (Santo Niño Mine) plan and section drawings, modified after Shorey (1936). a) Longitudinal section. b) Section and plan of 350' level. Assays presented in Table 5-12.

SHAFT
COLLAR

Elev. 7525'

OLD ORTIZ MINE
SHAFT ALIGNMENT
LOOKING NORTH
E.R.SHOREY
6-3-36

1st Level — 50'

2nd Level — 100'

3rd Level — 150'

4th Level

— 200'

ORIGINAL WATER LEVEL
5th Level

— 250'

6th Level

7th Level — 300'

8th Level — 350'
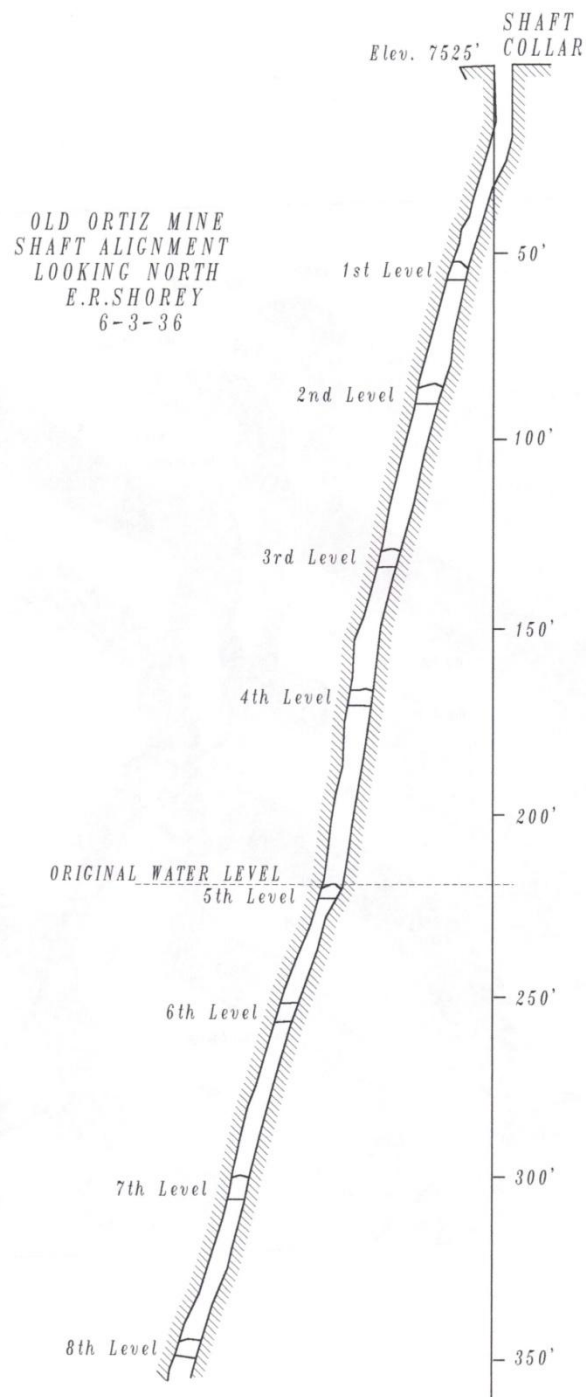
Figure 5-23. Old Ortiz (Santo Niño Mine) plan and section drawings, modified after Shorey (1936). c) Cross section through shaft.

118

CANDELARIA MINE

The Candelaria Mine lies on the southern end of the Ortiz Mountains, about 670 m (2200 ft) southwest of the Iron Vein prospect. Calcite veins cutting striped hornfels derived from the Carlile Member of the Mancos Shale were probably first prospected in the early 1800s. Raymond (1870) describes activity at the Candelaria Mine in 1869:

> The principal mines worked during the last year at Rio Del Tuerto are the Candelaria and Hutchinson, on the south side of the Old Placer Mountains,…..A stamp mill (10 stamps of 525 pounds each, dropping 10 inches and 36 times per minute, driven by a 20 horse-power engine) has been erected lately, which has crushed ore from the Ramirez and Candelaria lodes with satisfactory results. The mill was sold a short time ago to parties who work the Candelaria. On this lode they have started two tunnels, one 12 feet below the other. The vein strikes in this locality N7^o east, and dips west; at the breast of the upper tunnel, 30 feet in, the vein is faulted by a cross vein of kaoline, 1 foot wide, which courses N33^o east. Further north, toward the top of the hill, the lode has formerly been worked by an open cut, bearing north 23° east. It is 150 feet long, and at the deepest part of the excavation is 64 feet in depth. From this locality rich ore has been extracted, which yielded good results by mill process. In its southwest part the lode bears north 18° east, and dips 80° west. The tunnels are started about 150 feet below the old workings.

Raymond reported again in 1872 on activity at the Candelaria Mine in 1870:

> The Candelaria Company at Real Del Tuerto has worked eight men for ten months, and 1200 tons of quartz were mined by them. I am not informed of the yield of this ore; but as the company bought a ten-stamp mill last year, it may be expected that the business of the company was a paying one, though wages have been much higher in this part of New Mexico than elsewhere. The Candelaria has paid $83 per month to its hands, without board; and the New Mexico Mining Company about $60 with board.

A wooden headframe constructed in 1936 stood over the shaft until the early 1990s **(Figure 5-24)**, when it collapsed. The following description of the Candelaria Mine is excerpted from Griswold (1950):

> The Candelaria Mine was the best mine on the south side of the mountains. It is on the southeast slope of Candelaria Peak at an elevation of 7128'. Here are two fissure veins in striped shale; the main vein, 30" wide, is vertical and bears 25°E. It has been stoped from the surface down to the level of the new shaft, (i.e.) about 120'. The 12" vertical vein appearing at the northwest corner of the hoist house bears N3^{o}E and was drifted on for 70' with very little stoping. Mr. Charles McKinnis sank a shaft between these two veins in 1936 to a depth of 320' and did some exploratory diamond drilling before his money gave out. It is probable that he intended to sink the shaft to an intersection with the garnetized bed which Mr. Lucas had found profitable in Alpine gulch to the west. At I $^1/_8$ x 3 ½) there is a strong vein. On the north side of the arroyo a short cross-cut and an 80' drift bearing N30^{o}E explored a brecciated contact of dacite porphyry on the north with hornfels on the south. Across the arroyo a drift goes S27^{o}W on the vein in hornfels for 33' and a cross-cut bearing S67^{o}W finds the dacite at 49'. There is a shaft at least 50' deep on the vein at the junction of the vein and cross-cut. There workings were sampled and showed very low values.

Figure 5-24. 1930s-era Candelaria Mine headframe. The headframe collapsed in the early 1990s.

The underground and surface workings were mapped in detail by G.R. Griswold in 1951 (**Figures 5-25 and 5-26**). Griswold's (1951a and b) mapping shows important workings on four veins. The Candelaria shaft was sunk on the East vein. A drift runs along the east vein at the level (7128') of the shaft collar. A second level runs along the vein at the 6850' level. The West vein has no shafts and four adits at elevations ranging from 7128' to 7243'. The 50 ft-(15.2m-) deep Calcite Shaft and the 47 ft- (14.3 m-) deep Igneous Shaft were sunk on veins to the southwest of the Candelaria Mine Main shaft. Griswold collected samples during the mapping and analyzed them for tungsten and gold (Tables 5-13 and 5-14). Underground mapping showed that the east vein ranged from 10 to 127 cm (4 to 50 in) wide, with typical thickness between 50 and 75 cm (20 and 30 in). Gold values were only locally above 0.10 oz/st.

Following up on McKinnis' idea of intersecting the garnetized bed of Alpine Gulch (the metamorphosed Greenhorn Limestone of the Mancos Shale in Lukas Canyon) at depth, Molycorp, Inc. drilled a single core hole (MCA-5) at a site north of the Candelaria Mine in 1968. MCA-5 failed to intersect the Greenhorn Limestone. On the southeast flank of Candelaria Mountain, north of the Candelaria Mine, beds of the Carlile Shale Member dip steeply into the

Golden Fault, thus causing an increase in the Carlile Member's apparent thickness. The hole was abandoned on 24 December, 1968, probably because the drillers wanted to head home for Christmas.

LAC Minerals, USA, Inc., drilled 3 core holes at the Candelaria Mine in the late 1980s, in the hopes of encountering higher-grade or thicker vein material at depth, but failed to encounter significant mineralization.

Table 5-13. Tungsten values from samples at the Candelaria Mine.   Data from Griswold (1951a).

No	% WO$_3$	Description and Location
278-A	0.39	Calcite shaft dump
279-A	0.38	Igneous shaft dump, coarse & fines
280-A	1.28	High grade from Calcite shaft dump
281	0.18	3' vein NE bottom Calcite shaft
282	0.33	3' vein SW bottom Calcite shaft
283	0.22	2' vein SW bottom Igneous shaft
284	0.36	18" vein NE bottom Igneous shaft
285	0.20	40" vein NE bottom of 16' shaft, 100' SW of Calcite shaft
286	0.24	33" calcite vein, 85' SW of Calcite Shaft
287	0.10	70" gouge or caliche just N of #286
288	0.50	19" vein, 44' SW of Calcite Shaft
289	0.29	16" vein, 35' SW of Calcite Shaft
290	0.42	13" vein, 26' SW of Calcite Shaft
291	0.20	17" vein, 19' SW of Calcite Shaft
292	0.24	20" vein, 29' SW of Calcite Shaft

Table 5-14. Gold values from underground samples at the Candelaria Mine. Data from Griswold (1951b).

No	oz/st Au	Description and Location
294	0.02	W vein, 7128' level, 31" vein
295	0.42	W vein, 7128' level, high grade
296	trace	E vein, 6850' level, 50" vein
297	trace	E vein, " , 29" vein
298	0.16	E vein, " , 18" vein
299	0.38	E vein, " , 34" vein
300	?	E vein, " , 26" vein
301	nil	E vein, " , 28" vein
302	nil	E vein, " , 30" shear
303	nil	E vein, " , 22" vein
304	nil	E vein, " , 22" vein
305	trace	E vein, " , 18" vein
306	nil	E vein, " , 36" vein
307	trace	E vein, " , 6" vein
308	0.18	E vein, " , 31" vein
309	0.08	E vein, " , 27" vein
310	0.20	E vein, " , 21" vein
311	0.07	E vein, " , ? " vein
312	0.08	E vein, " , 18" vein
313	0.06	E vein, " , 18" vein
314	0.09	E vein, " , 4" vein
315	0.92	E vein, " , 4" vein
316	0.43	E vein, " , 4" vein
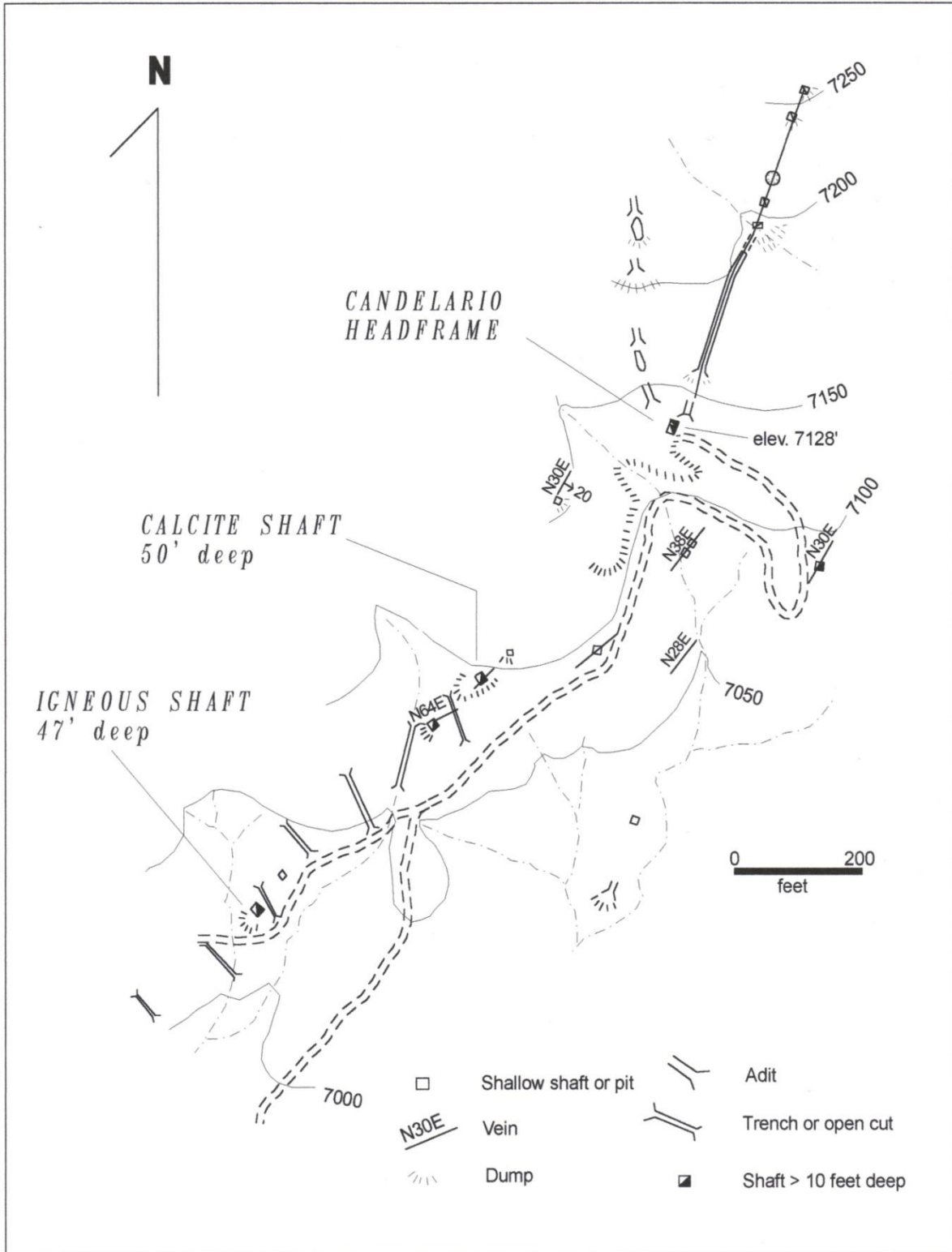
Figure 5-25. Candelaria Mine workings. Modified after Griswold (1950).

N

CANDELARIO
HEADFRAME

7250

7200

7150

elev. 7128'

N30E
20

CALCITE SHAFT
50' deep

N38E

N30E

7100

N28E

7050

IGNEOUS SHAFT
47' deep

N64E

0   200
feet

7000

☐   Shallow shaft or pit

N30E   Vein

Dump

Adit

Trench or open cut

Shaft > 10 feet deep
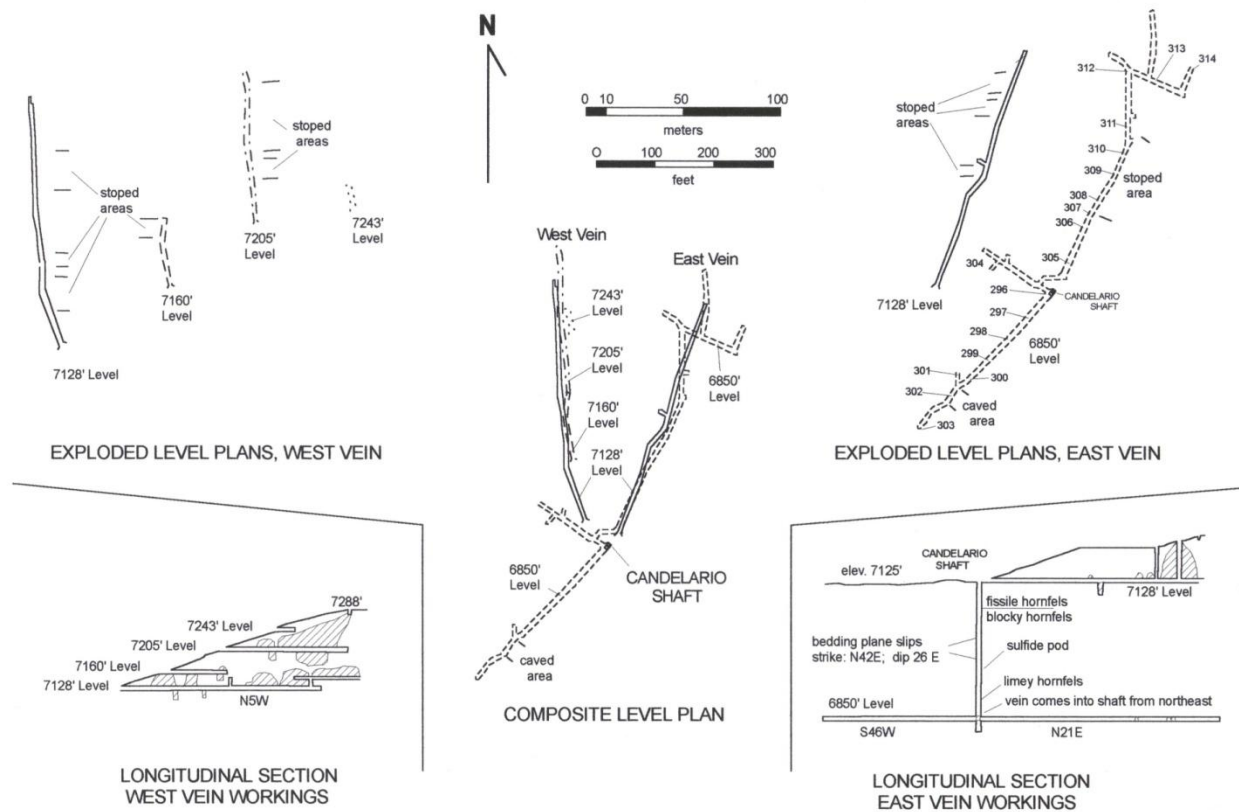
Figure 5-26. Level plans and longitudinal sections, Candelaria Mine. Shaded areas represent stopes. Three-digit numbers are sample identifiers; values are given in Table 5-14. Modified after Griswold (1951b).

BENTON MINE and OLD LIVE OAK MINE

The Benton Mine and the Old Live Oak Mine lie 600 m (2000 ft) southwest of the Cunningham Hill Mine. Griswold (1950) states that the Benton and Old Live Oak Mines were developed on a N73E-striking, 68°W-dipping fissure with a strike length of 250m (850 ft). The vein at the Benton Mine maintained a width of 76 cm (30 in) to a depth of 39 m (130 ft). Host rocks are vent-breccia volcanics in the eastern part (Benton) and latite porphyry in the western part (Old live Oak). Quartzite breccia similar to that encountered at Cunningham Hill is exposed in outcrop and float 60 m (200 ft) south of the Benton Mine. Sulfide ore was encountered at 250 ft below the surface. At the time of Griswold's investigation, only the upper 60 ft of workings were accessible. Two dump samples of sulfide material from the Benton Mine assayed an average $6.12 gold, or 0.17 opt gold (**Figure 5-27**, Table 5-15). No production records remain for the Benton-Old Live Oak workings. Griswold (1950) considered the Benton-Old Live Oak to be a good prospect.

Table 5-15. Assays of 5-ft channel samples shown on Figure 5ZB, Benton – Old Live Oak.

No.	Au	Ag	Pb	Remarks / vein width
	Ounce per ton		%	
B-1	0.69	0.15	tr	5" to 8"
B-2	0.29	0.10		5" to 6"
B-3	0.40	0.20		1" to 4"
B-4	2.13	0.50	tr	5" to 8"
B-5	2.62	0.60		4" to 8"
B-6	1.45	0.35		4" to 6"
B-7	0.32	0.30	tr	4" to 6"
B-8	0.11	0.30	tr	2" to 6"
B-9	0.46	0.10		6" to 7"
B-10	0.58	0.20		6" to 7"
B-11	0.43	0.35	tr	6" to 7"
B-12	0.29	0.20		at fault
B-13	0.01	trace		18"
B-14	0.06	0.10		22"
B-15	0.06	0.10		28"
B-16	0.01	trace		8"
B-17	0.41	0.50		6" to 7"
B-18	0.04	trace		6" to 7"
B-19	0.015	0.20		18" hanging wall
B-20	0.02	0.30		18" foot wall
B-21	0.98	0.45		16' level-shaft
B-22	2.42	0.60		16' level-shaft
B-A	0.26	trace		Benton dump
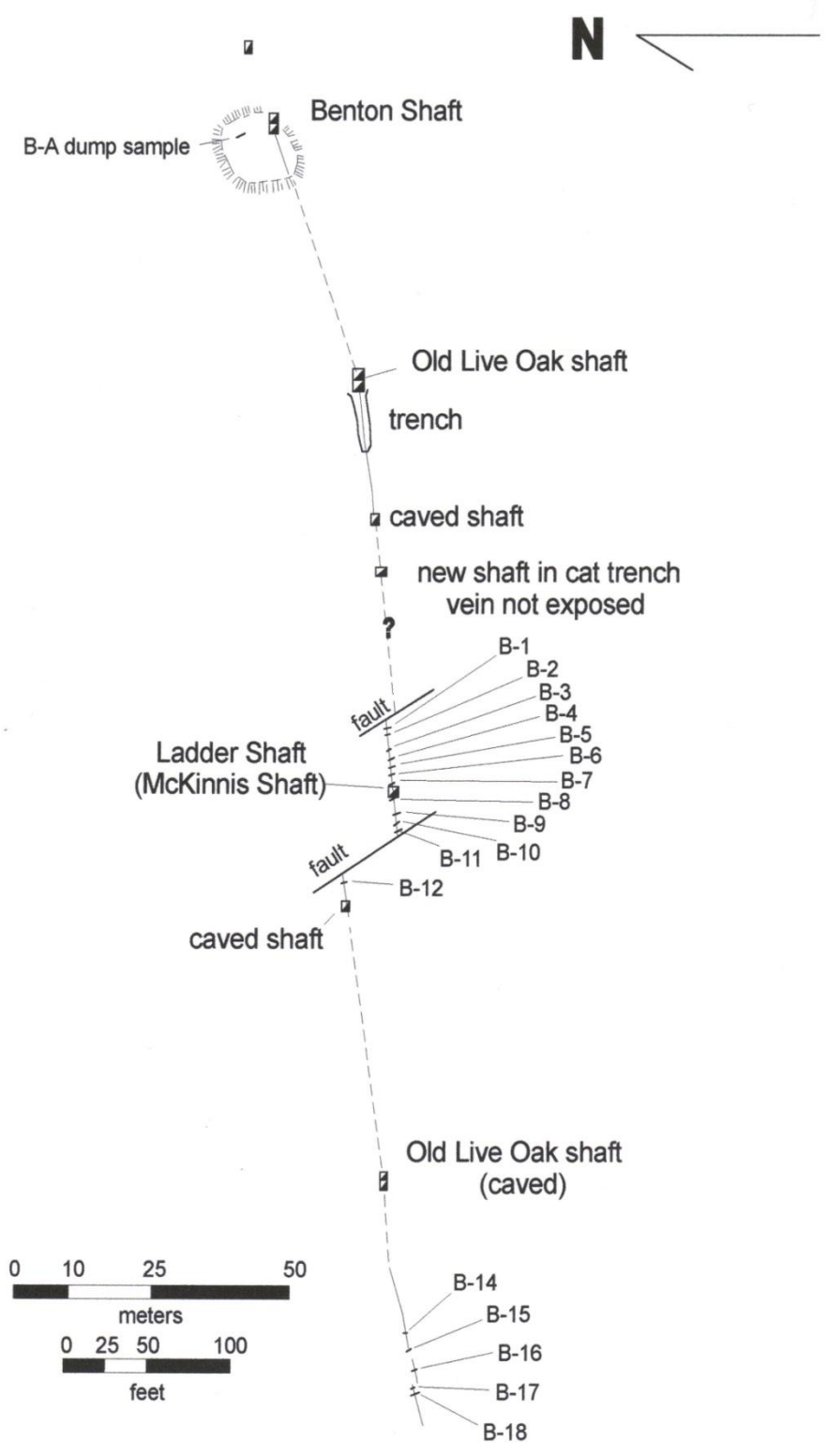
Figure 5-27. Map of Benton-Old Live Oak vein and sample locations. Gold values in samples presented in Table 5-15. Modified after Griswold (1950).

ENGLISH AND SHOSHONE MINES

The English and Shoshone Mines are two prospects on the northwest side of the Dolores volcanic vent.   The English Mine consists of three shafts located 515 m (1700 ft) northeast of the Ortiz Mine shaft. Citing uncertainty in its location, Griswold (1950) identified a shaft 379 m (1250 ft) northeast of the English Mine main shaft as the Shoshone Mine. There are no data on the mineral composition of the English and Shoshone veins. Griswold considered the veins to have considerable potential.

The English Mine workings were sunk on N25E-striking, 80°NW-dipping veins running parallel to a trachytic latite dike in volcanic vent breccia.   The vein was traced for 76 m (250 ft) along strike and 21 m (70 ft) down dip and ranged from 0.6 to 1.2 m (2 to 4 ft) thick. Gold values ranged from 0.11 oz/ton to 0.61 oz/ton ($4 to $22 per short ton) in samples from the surface to 21 m (70 ft).

The 1.2 m- (4 ft-) wide Shoshone Mine vein was visible to a depth of 9 m (30 ft) in the shaft at the time of Griswold's (1950) report. Like the English vein, the Shoshone vein strikes N25E, but it dips 70° to the SE.   A sample taken from a dump assayed 0.27 oz/short ton ($9.80 per short ton).

RED OUTCROP OR CAPTAIN DAVIS PROSPECT

The Red Outcrop prospect is a group of hematitic veinlets in rafts or xenoliths of sandstone and shale of the Mancos Shale surrounded by andesite porphyry in the southern part of the Ortiz Mountains. The prospect lies 60 to 240 m (200 to 800 ft) south of the Buckeye Hill Fault. Griswold (1950) described 15 cm (6 in) stringers striking N74W and dipping 68°S. Production of an unknown quantity of material from the prospect is indicated by a small caved stope reported by Griswold (1950). Gold Fields drilled 10 core holes at the Red Outcrop during the early 1980s.

PORPHYRY-RELATED STOCKWORK MINERALIZATION

CUNNINGHAM GULCH

The Cunningham Gulch prospect lies in the upper part of Cunningham Gulch, about 2550 m (8,400 ft) west-southwest of the Cunningham Hill open pit, and about 600 m (2000 ft) northeast of the center of the Carache Canyon breccia pipe. A soil-sampling campaign begun by LAC Minerals in 1986 led to the discovery of gold and copper mineralization in upper Cunningham Gulch. Detailed geologic mapping, sampling of road-cut exposures, and core drilling defined porphyry-type mineralization hosted by augite monzonite distributed around the western and southwestern margin of a barren feldspar-porphyry latite stock. Anomalous gold values from soil samples taken over the barren latite stock remain unexplained.

Augite monzonite intrudes shale and sandstone of the Menefee Formation in the upper reaches of Cunningham Gulch, baking and metamorphosing them to hornfels and quartzite, respectively. A coarse orthoclase-porphyry latite stock intrudes the augite monzonite on the northwest side of the Golden Fault. The Golden Fault and related fractures along with subsequent fracturing associated with the intrusion of the orthoclase-porphyry latite appear to have provided the plumbing for mineralizing fluids.

Near-surface mineralization consists of stockwork tenorite + magnetite +/- fluorite +/- molybdenite veinlets invading crackle breccia. Below the level of oxidation, mineralized material contains chalcopyrite rather than tenorite.

CROOKED CANYON

The Crooked Canyon prospect consists of pyrite – chalcopyrite stockwork veinlets and disseminations hosted by andesite-porphyry sills, Mancos Shale and augite monzonite in the upper part of Crooked Canyon, in the western part of the Ortiz Mountains.

PLACER DEPOSITS

Placer gold was probably known in the Ortiz Mountains by 1821 (Baxter, 2004), certainly by 1828. The largest known placer gold deposits on the Ortiz Mine Grant are concentrated on the eastern side of the range, at the mouths of Cunningham Gulch and Dolores Gulch, and along its southern boundary, east of the village of Golden. In both cases, most of the placer gold is contained in the Plio-Pleistocene Tuerto Gravel, though some may be reworked in recent stream alluvium. At Rich Hill, in the eastern part of the Ortiz Mountains, a coarse gravel deposit lies 30 to 40 ft above the Tuerto Gravel on nearby mesas and exhibits strong calcic soil development. The Rich Hill gravel is pocked with numerous placer workings. Smaller placer gold workings are known in several areas along the fronts of the Ortiz Mountains and the San Pedro Mountains, notably at Carache Canyon, near the Iron Vein prospect, and at Lukas Canyon. Griswold (1950) summarized the known placer gold potential of the Ortiz Mine Grant:

> In the early records reference is made to the Old Placer and the New Placers. These are classed as hill-side placers. The gold in the Cunningham Mesa placer, (Old Placer) was brought to its present location by flash floods from lodes in the Ortiz Basin. Due to the method of deposition the gold is erratically distributed both laterally and vertically within the outwash materials. Some re-concentration has resulted in especially rich gravel at the head of Las Viejo arroyo at the northwest corner of Cunningham Mesa. Here the original discovery was made in 1828, and here Thomas Edison tried his dry screening and electrostatic process of gold recovery in 1900. The Universal Placer Company operated here in 1937-38 with a dry process which was unsuccessful.
>
> Placer sampling to date on Cunningham Mesa and vicinity has proven some 17 million cubic yards of 30 cent gravel* and indicates an additional 17 million cubic yards of commercial gravel of somewhat lower value. A detailed report of the placer sampling in this area has been compiled by G.R. Griswold titled "Cunningham Mesa Placer", dated December 1949.
>
> In 1839 the New Placers east of Golden and along the south side of the Grant were discovered. The gold came from the weathering of many narrow veins on the north slope of the San Pedro Mountains. The Golden Placer at the mouth of Old Timer gulch covers 39 acres containing 1,800,000 cubic yards of 20 cent gravel. A dry land dredge using water from the Kelly well failed to show a profit here in 1935. Half a mile to the east, the Bonanza Placer covers 37 acres containing 1,855,000 cubic yards of 35 cent gravel. The ground has been intensively worked by dry washers. The gradient of this placer is about 15%.
>
> The Korache placer on the south side of the Ortiz Mountains is in a very narrow arroyo. The source of this gold has not been located. No systematic prospecting has been done in this area. It appears probable that there is a high-grade vein not far away which feeds this placer, or the gold might have come from the small monzonite stock near the head of Tia Bonita canyon.
>
> *Value of recoverable gold at $35/tr oz.

No effort has been made since the 1930s to mine placer gold in the area of the Ortiz Mine Grant, except on an artisanal or hobby scale. The chief function of the gold placers has been to point to the lode sources of gold in the Ortiz Mountains. Gold of the Cunningham Mesa Placers and smaller placers near the mouth of Dolores Gulch comes from Cunningham Hill, the Ortiz Mine, and other prospects in the eastern part of the Ortiz Mountains. Griswold's (1950) discussion of the source of the "Korache" placer is prophetic: the outcrop of the Carache Canyon breccia pipe was identified at that time as the Tia Bonita Canyon monzonite.

NON-METALLIC RESOURCES

COAL

The Cerrillos coal field, which includes the Miller Gulch, Waldo Gulch, and Madrid area mines, saw coal mining begin about 1835 and continue to 1953. The town of Madrid and the coal mines to the south lay in the original Ortiz Mine Grant. Total production of coal from the Madrid area is summarized in Table 1.

Table 5-16. Coal production from Cerrillos Coal Field. Data from Lee (1913) and Read and others (1950), as quoted by Beaumont (1979) and Elston (1967); and Beaumont (1979). Anthracite and bituminous are not distinguished in available production figures.

Years of production	Part of field	Production
1835 - 1882	Madrid area	Unknown but small. Coal sent to Dolores to run gold mill in 1835. Civil War–era production from Government Mine.
1882 - 1890	Entire Cerrillos field	408,568 short tons
1892 - 1897	Miller Gulch	15,000 short tons, bituminous coking coal
1897 – 1931	Entire Cerrillos field	> 3,000,000 short tons
1931 - 1940	Entire Cerrillos field	1,325,315 short tons
1940 - 1948	Entire Cerrillos field	577,700 short tons
1948 - 1953	Madrid area	150,000 short tons
Total production		**Approximately 5,500,000 short tons**

Bituminous and anthracite coal of the Cerrillos coal field occurs in the Cretaceous Menefee Formation (Mesa Verde Group).   The more valuable anthracite coal was produced by heat given off by the adjacent Madrid sill. Read and others (1950) estimated original reserves to have been 46.5 million short tons of bituminous coal and 11.4 million short tons of anthracite coal for a total of 57.9 million short tons. Beaumont (1979)

The Menefee Formation is exposed in the south-central Ortiz Mountains and has been drilled extensively at Carache Canyon. At Carache Canyon, drilling intersected seams of coal generally measuring less than 30 cm (1 ft) at various intervals in the lower and upper Menefee members. Coal quality at Carache Canyon was not tested; the complexities of faulting, brecciation, and intrusive activity, make it unlikely that economic quantities exist. Menefee Formation shales crop out on the eastern margin of the Ortiz Mine Grant, but coal has not been observed there.

AGGREGATE

Aggregate resources appear in the igneous rocks of the Ortiz Mountains and in the Tuerto Gravel. In particular, andesite porphyry laccoliths of the northwestern part of the Ortiz Mine Grant and the equigranular, medium-grained augite monzonite stock in the central part of the Ortiz Mountains represent potentially large resources of construction-grade material.   The Tuerto Gravel contains detritus shed from the Ortiz Mountains, much of it being cobble- to boulder-size andesite porphyry and augite monzonite clasts. Though the Tuerto Gravel is rarely greater than 30 m (100 ft) thick, it is extensive, and thus represents a large resource.

GYPSUM

The Tonque Arroyo Member of the Todilto Formation is composed principally of gypsum. The gypsum is a near-surface alteration (by hydration) of anhydrite. Regionally the Tonque Arroyo Member is an important source of commercially exploitable gypsum. On the Ortiz Mine Grant, most exposures and drill intersections of the Tonque Arroyo Member show considerable dissolution and brecciation. In the southern part of the Ortiz Mine Grant, about 1 mi (1.5 km) east of the Lone Mountain Ranch headquarters, outcrops of fresh Tonque Arroyo Member suggest the possibility of commercial quantities of gypsum.

6   GEOPHYSICS

Geophysical exploration techniques have been applied to the search for mineralized rock on the Ortiz Mine Grant since 1949 (Table 6-1).   These surveys were employed to detect contrasts in electrical, magnetic, and radiometric properties of the underlying rock. Rock bodies containing disseminated sulfides could be expected to yield induced polarization and /or resistivity anomalies. Magnetite-bearing bodies, such as the vein at the old Ortiz Mine would produce anomalies in the strength of the magnetic field. The most commonly used methods were ground-based induced polarization/ resistivity and ground-based magnetometry.   In 1987 LAC Minerals, USA, Inc. conducted a high-resolution airborne combination magnetic, electromagnetic, and very low frequency (VLF) survey of most of the Ortiz Mine Grant and adjacent parts of the San Pedro Mountains to complement its geologic study of the area.

GROUND-BASED STUDIES

MAGNETICS
The ground-magnetics survey conducted in 1949 in the Dolores Gulch-Cunningham Hill area was used to distinguish altered and unaltered intrusive rocks, dikes from sills, and to locate buried and potentially auriferous channels in the Tuerto Gravel (Stewart, 1949). LAC Minerals conducted a ground magnetic survey in the area of the Iron Vein prospect in 1985. A northeast-trending elongate magnetic high underlies the prospect area, probably corresponding to the granodiorite intrusion intersected in drilling. The magnetic high was confirmed by the airborne survey of 1987.

RADIOMETRICS
Griswold (1950) reported several Geiger counter traverses on the Ortiz Mine Grant. One dike, in the northeastern part of the Grant, gave anomalous readings, though it was not determined whether the anomaly was related to uranium or thorium minerals. The magnitude of the anomaly was not reported.

INDUCED POLARIZATION / RESISTIVITY
Several induced polarization (IP) / resistivity surveys have been conducted on the Ortiz Mine Grant.   Most studies concentrated on areas of known mineralization and were used to determine locations of specific structures, or bodies of sulfide-bearing rock. Interpretations of results from these studies have been made difficult by the influence of complex geometries of intrusive bodies, and local-scale variations in compositions of sedimentary rocks.
In 1969, Molycorp ran an induced polarization line across the breccia outcrop at Carache Canyon and concluded that the anomalous response was due to carbonaceous and graphitic material and not worth drilling.   Anomalies at Cunningham Hill that might have represented mineralization beyond what was then identified were drilled without success. The anomalies were explained as being related to gouge zones in faults or as carbonaceous material in sedimentary rocks (Cook, 1970). Conoco conducted a reconnaissance IP/resistivity study with large dipole spacing across the Ortiz Mountains during the 1970s, with inconclusive results.
More detailed IP/resistivity studies done by LAC Minerals at Carache Canyon (**Figure 6-1**) and Cunningham Gulch were also complicated by shale and coal of the Menefee Formation,

and by the high magnetite content of the augite monzonite (**Figure 6-2**). Other IP/resistivity surveys were done in the Iron Vein-Candelaria area, in Lukas Canyon, Crooked Canyon, and in the Dolores Gulch - Cunningham Hill Mine area.

Table 6-1. Geophysical surveys conducted on the Ortiz Mine Grant. Sources: Stewart (1948), Griswold (1950), Gay (1969), Hallof and Bell (1969), Cook (1970), Sadowski (1974, 1975), Wieduwilt (1980), Knox (1981), Anzman (1985, 1986), Bell (1987), Hallof (1986), de Carle (1987, 1988), and Smith and Nelsen (1988)

Year(s)	Type	Client	Contractor	Location
1948	Magnetic Resistivity – Wenner array	Potter and Sims	Stewart	Magnetics on Dolores Gulch-Cunningham Hill, Cunningham Mesa Resistivity on Cunningham Mesa
1950	Radiometric with Geiger counter	Potter and Sims	C.T. Griswold	Many traverses on Grant
1967 & 1969	IP/Resistivity, dipole-dipole variable frequency system	Molycorp	McPhar Geophysics and Mineral Systems	Candelaria Mine-Lukas Can., Dolores Gulch-Cunningham Hill, and Carache Canyon
1974-1975	IP/Resistivity Frequency and time domain Dipole-dipole, Dipole length 1000 ft	Conoco	In house	Crooked Canyon, Buckeye Canyon, and Carache Canyon
1975?	Airborne magnetic survey Fixed-wing aircraft Average altitude 500 ft above ground	Conoco	In house?	Western ½ of Ortiz Mountains
1981	IP/Resistivity, dipole-dipole dipole length 100 - 200 ft	Gold Fields	?	Dolores Gulch – Cunningham Hill area
1986	Magnetic	Gold Fields	In house	Dolores Gulch – Cunningham Hill-Cunningham Mesa, Captain Davis Mtn.
1985	Magnetic	LAC	Western Geo Surveys	Iron Vein area Lukas Canyon
	IP/Resistivity	LAC		Carache Canyon
1989	Phase IP/Resistivity Dipole-dipole Dipole length 200 ft	LAC	Phoenix Geophysics, Inc.	Crooked Canyon Cunningham Gulch
	IP/Resistivity			Iron Vein – Candelaria
1987	Airborne magnetics, electromagnetics, very low frequency	LAC	Aerodat, Ltd.	Entire Ortiz Mine Grant and San Pedro Mountains
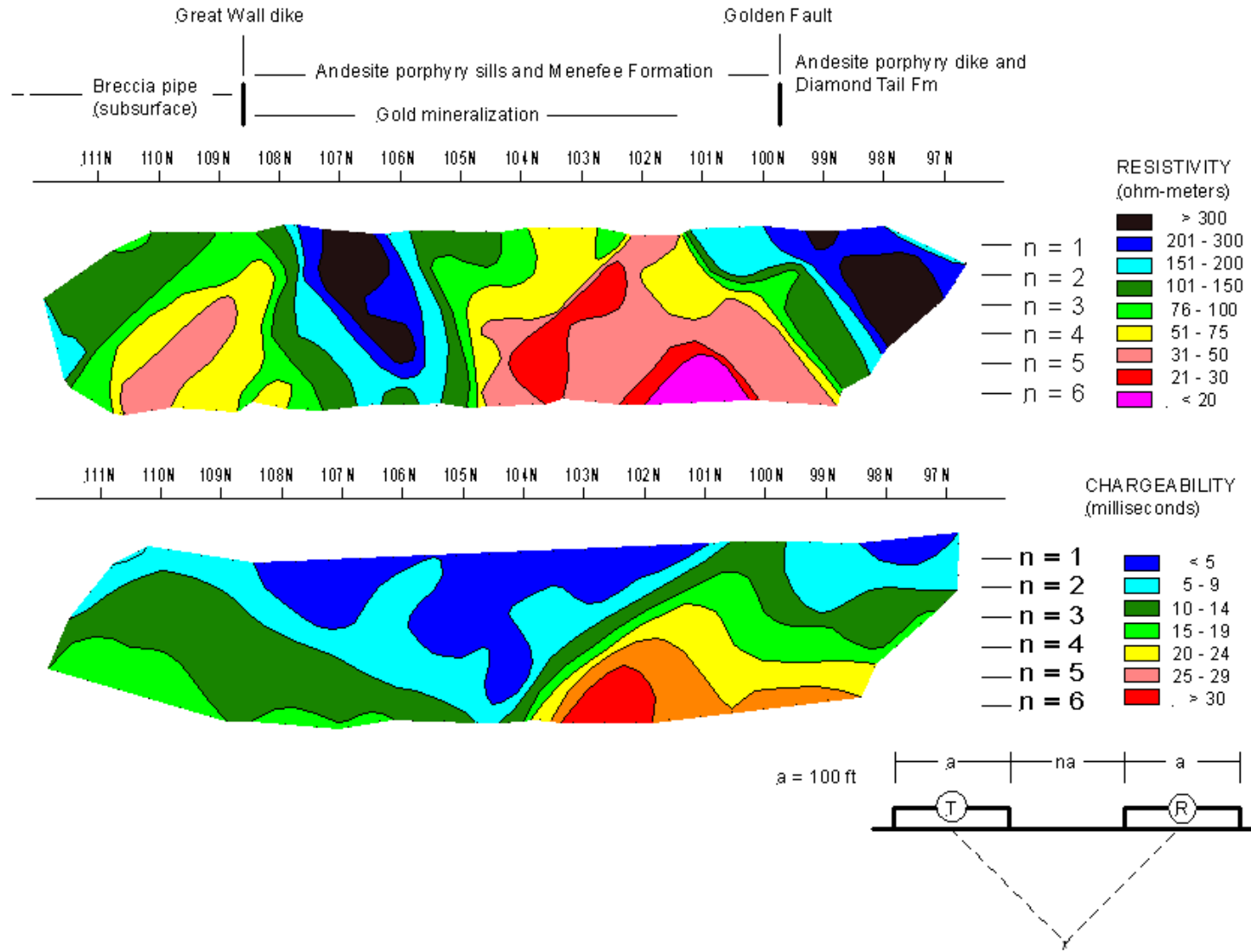
Figure 6-1. Pseudosection of time-domain IP/resistivity study of Carache Canyon, line 102E. View to northeast. Time domain measurement, dipole-dipole array. Resistivity low / chargeability high in 101 - 103 N area probably corresponds to carbonaceous shale and coal of the Menefee Formation and northeast-trending faults. Location of survey line is plotted on Figure 5Na. Modified after Anzman (1986).
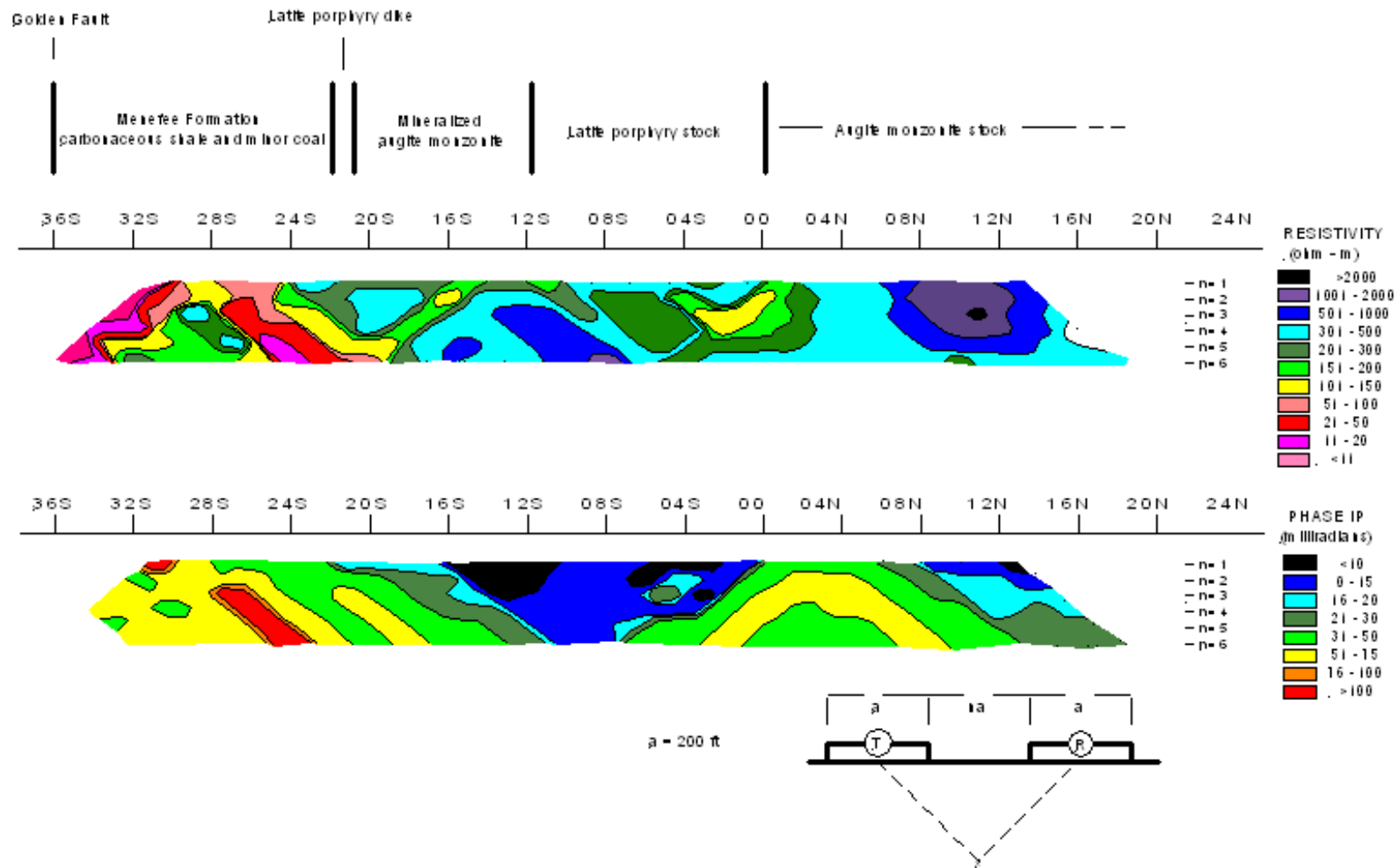
Figure 6-2. Pseudosection of phase IP/resistivity study of Cunningham Gulch prospect, line 3W. View to west. Dipole-dipole array. Resistivity low / chargeability high in 36S - 22S. Response of mineralized augite monzonite may be masked by contrast between conductive shales and resistive latite porphyry stock. Modified after Phoenix Geophysics (1987).

AIRBORNE GEOPHYSICAL SURVEYS

     In the mid 1970s Conoco, Inc., conducted a fixed-wing airborne magnetic survey over the western part of the Ortiz Mountains. Airborne surveys resumed in 1987 when LAC Minerals contracted Aerodat, Ltd. to carry out a high-resolution helicopter-borne geophysical survey of the entire Ortiz Mine Grant area. The surveyed area included the land of the Mesita de Juana López Grant that overlaps the Ortiz Mine Grant, and the San Pedro Mountains. The helicopter towed on a cable an electromagnetic (EM) system, a magnetometer, and a very low frequency (VLF) receiver. The helicopter maintained a nominal height of 61 m (200 ft) above the terrain and readings were taken at intervals of 0.1 to 0.2 seconds. Flight lines were spaced at a nominal 100 m (330 ft). The following descriptions of the Aerodat airborne survey are taken from Smith and Nelsen (1989) and de Carle (1987) (Table 6-2).

     The helicopter-borne survey was a considerable aid to geologic mapping, especially with regard to identification of buried intrusive bodies, the nature of subsurface contacts of stocks versus laccoliths, distribution of conductive sedimentary rocks, and locations of faults.

Magnetics

     The cesium magnetometer measured the strength of the total magnetic field at any given sample point. Readings, measured in nanoteslas, from a continuously recording base-station magnetometer, timed with the airborne system, were used to eliminate diurnal and secular variations from the data. Results were rendered as line plots and contour maps. Magnetic data was further reduced to the magnetic pole, a process by which the effects of the inclination of the earth's magnetic field were eliminated (maps in pocket).

     Magnetic field strength values over the surveyed area ranged from 51,890 to 54,955 nanoteslas. The survey detected magnetic anomalies in excess of 54,000 nanoteslas corresponding to the augite monzonite, latite porphyry, and quartz monzodiorite stocks. Andesite-porphyry laccoliths produce weaker anomalies, rarely exceeding magnetic field strength values of 52,400 nanteslas. Areas underlain by Mesozoic and Cenozoic sedimentary rocks north and west of the Ortiz Mountains yielded magnetic field strengths of 51,890 to 53,000 nanoteslas. Much of the southeastern part of the Ortiz Mine Grant shows magnetic field strengths of 52,300 to 52,400 nanoteslas, suggesting the presence of a large, unexposed intrusive body or bodies. A ridge of high magnetic field strength values extends 4500 m (15,000 ft) east-northeastward from the eastern end of the San Pedro Mountains. The Precambrian basement high contained within the Little Tuerto Horst gives magnetic field strength values of 52,350 nanoteslas.

     The main traces of the Tijeras-Cañoncito fault system are manifested by the strong magnetic field contrasts of adjacent bodies. In the region of the Iron Vein prospect, and north and east of Captain Davis Mountain, magnetic highs are elongate parallel to the fault trends, suggesting a primary structural control on the geometry of the intrusive bodies.

Electromagnetics (EM)

     Electromagnetic fields were generated by coil pairs (vertical coaxial at 935 and 4600 Hz, and horizontal coplanar at 4175 Hz). A receiver measured the strengths of the electromagnetic fields and recorded the data. High-frequency (4175 Hz and 4600Hz) electromagnetic fields are useful for analysis of surficial deposits and near-surface bedrock. The low-frequency field (935 Hz) penetrates more deeply and indicates resistivity of bedrock formations. Results are expressed as apparent resistivity, in ohm-meters. Line plots of variation in field strength were

produced, as well as contour maps of apparent resistivity for high- and low-frequency fields. The EM study served to identify resistivity anomalies, such as low-resistivity shale, mudstone, or coal, and fault and fracture systems with clay and/or water. (map in pocket).

Apparent resistivity was calculated by assuming a 200-meter thick conductive layer over resistive bedrock. Using nomograms for the modeled layer, the computer generated resistivity consistent with the sensor's elevation and recorded amplitude for the coaxial 4600 Hz channels.

Very Low Frequency (VLF)

Powerful military radio transmitters that operate at 15 to 25 kHz are termed very low frequency (VLF) transmitters. These radio signals induce electric currents in conductive rocks thousands of miles away from their source. The secondary magnetic fields produced by the electric currents in turn produce deviations in the primary VLF field.   VLF surveys are typically used to identify buried faults in exploration programs. Transmitters are usually selected to lie roughly on strike with suspected faults (Klein and Lajoie, 1988).   In the Aerodat survey of the Ortiz Mine Grant, readings were taken from two VLF transmitting stations: NAA at Cutler, Maine (24.0 kHz), and NPG at Jim Creek, Washington (24.8 kHz). Because the dominant structural grain in the survey area is northeasterly, the Cutler transmitter functioned as the line station. The Jim Creek transmitter served as the orthogonal station. For the purposes of data presentation, Cutler data were used. Results were given as line plots, and as contour maps. Data is expressed as percentage of the strength of the total VLF field.

Table 6 - 2. Aerodat geophysical survey specifications.

AIRCRAFT		
	Aerospatiale 315B Lama helicopter	
	Aircraft nominal height above terrain: 61 m (200 ft)	
GEOPHYSICAL EQUIPMENT		

Electromagnetic System (EM)	Aerodat 3-frequency system:
	     Two vertical coaxial pairs at 935 Hz and 4600 Hz
	     One horizontal coplanar coil pair at 4175 Hz
	     Transmitter-receiver separation: 7 m (23 ft)
	     Sensor container towed 30 m (100 ft) below helicopter	

Very low frequency (VLF) Receiver	Herz Totem 2A, receiving two transmitters, towed 8 m (25 ft) below helicopter	

Magnetometer	Scintrex Model VIW-2321 H8 cesium, with 0.1 nanoTeslas sensitivity
	     at a 0.2 second sample rate; towed 15 m (50 ft) below
	     helicopter.	

Magnetic Base Station	IFG-2, clock synchronized with airborne system.	
DATA RECORDING		
Analog Recorder	RMS dot-matrix real time recording of 14 traces, plus manual and time fiducial markers	
Digital Recorder	DGR 33 recording on magnetic tape	
	Recording intervals:	
	Equipment	*Interval in seconds*
	EM system	0.1
	VLF	0.2
	Magnetometer	0.2
	Altimeter	0.2
	Navigation	1.0
NAVIGATION AND LOCATION EQUIPMENT		
Navigation Equipment	Motorola Mini-Ranger	
Radar Altimeter	Hoffman HRA-100, measuring height of helicopter.	
Flight Path Tracking	By video camera.	

7   ISOTOPIC AGE DETERMINATIONS

Based on field relations, igneous rocks of the Ortiz Porphyry Belt are younger than the Eocene Galisteo Formation, which they intrude in the Ortiz Mountains and in the Cerrillos Hills. Because the Galisteo Formation grades upward into the Espinaso Formation, which is assumed to be age equivalent of rocks of the Ortiz Porphyry Belt, an Oligocene age has been inferred for the Ortiz Porphyry Belt igneous activity. However, a younger limit on the age of intrusive activity or on mineralization is imposed only by the Plio-Pleistocene Tuerto Gravel.

Timing of movement on Tijeras-Cañoncito Fault System is constrained by the prior emplacement of calc-alkaline andesite porphyry laccoliths and sills, and by subsequent intrusion of alkaline augite monzonite stocks. Movement on the Tijeras-Cañoncito Fault thus represents a magmatic break, as well a tectonic one. Dating of the suite of igneous rocks of the Ortiz Mountains was designed to determine the absolute ages of the rocks and their related mineralization, and to constrain major mid-Tertiary movement on the Tijeras-Cañoncito Fault System.

K-Ar Age Determinations

Several workers have made age determinations on rocks from the Ortiz Mountains and nearby areas using the potassium-argon method (Table 7-1). Armstrong (1976) collected two samples from the augite-monzonite stock that forms the core of the Ortiz Mountains. Hornblende and feldspar were dated from one sample, 113-55-59, which yielded ages of 55.7 +/- 2.0 Ma and 44.7 +/- 1.6 Ma, respectively. Both of these Eocene ages seemed too old, since the Galisteo Formation was being deposited at the same time. Sample 1222155-61 yielded a date of 33.9 +/- 1.2 Ma on hornblende.

Bachman and Mehnert (1978) reported two hornblende dates from andesite porphyry from the Ortiz Porphyry Belt. A sample taken from the Cerrillos Hills yielded a date of 47.1 +/- 3.2 Ma. Another sample, taken from a road cut on highway NM-14 on the western side of the Ortiz Mountains, gave an age of 34.0 +/- 2.2 Ma.

Kautz and others (1981) reported three dates from samples from the base, middle, and top of the Espinaso Formation outcrop in the Hagan Basin.   Clasts from the base and middle gave ages of 34.3 +/- 0.8 Ma and 34.6 +/- 0.7 Ma, respectively. The nepheline latite flow reported to be from the top of the Espinaso Fm. yielded an age of 26.9 +/- 0.6 Ma. Field inspection of the nepheline latite flow shows that it is in the lowest part of the Santa Fe Group sediments (S. Connell, personal communication, 2001). Texturally it resembles limburgite dikes of the western part of the Cerrillos Hills.

Kay (1986) collected 13 samples from his study area around the Cunningham Hill mine in the eastern part of the Ortiz Mountains. Hornblende from an andesite porphyry sample taken from a mine dump (OR-6) gave an age of 43.2 +/- 2.3 Ma.   Sample OR-3, taken from drill hole NM-010 at 600 feet depth, was of hornblende monzonite, part of the central stock of the Ortiz Mountains. Hornblende from OR-3 yielded an age of 29.6 +/- 1.5 Ma. Feldspar and biotite taken from the subvolcanic latite plug and (trachytic) latite dikes in Cunningham Gulch yielded seven ages ranging from 29.9 to 35.1 Ma (Table 7-1). Kay dated feldspar in two samples of the volcanic rocks of Dolores Gulch.   Sample OR-4 gave an age of 52.1 +/ 1.5 Ma and sample OR-5 gave an age of 34.2 +/- 1.4 Ma. Kay also dated alteration sericite from the mineralized quartzite breccias at Cunningham Hill and the Florencio prospect. Sample OR-1 (Cunningham Hill) gave an age of 39.6 +/- 1.5 Ma, and sample OR-2 (Florencio) gave an age of 32.0 +/- 1.2 Ma.   The K-

Ar dates determined by previous workers showed considerable scatter and included several dates that were clearly too old (Eocene). Discarding the dates greater than 40 Ma, the andesite porphyry laccoliths dated at about 34 Ma and the augite (hornblende) monzonite stock in the range of 29.6 to 33.9 Ma. The latite porphyry and trachytic latite dikes range from 29.9 to 35.1 Ma, and the volcanic rocks of Dolores Gulch gave a range from 26.9 to 34.2 Ma. Mineralization dates were 32.0 and 39.6 Ma.

While the K-Ar dates allow for a general confirmation of the observed field relations, they do not establish with sufficient precision the ages of magmatism, major movement on the Tijeras Fault System, and mineralization. In order to more finely tune understanding of the chronology of the tectonic and magmatic development of the Ortiz Mountains, a suite of samples was submitted to the ^{40}Ar/^{39}Ar lab at New Mexico Tech for this study.

^{40}Ar/^{39}Ar Age Determinations

Age determinations and analytical data for fifteen samples submitted to the ^{40}Ar/^{39}Ar laboratory at New Mexico Tech are listed on Table 7-1.   Included in Table   are ^{40}Ar/^{39}Ar dates determined by the U.S. Geological Survey Denver lab (Sauer, 2000).

Andesite Porphyry

Ages of three samples of andesite porphyry sills were determined from step-heating of hornblende and yielded fair to poor isochrons. Sample Ig-30, with a fair isochron, gave an age of 34.29 Ma. Sample Wg-1, with a poor isochron, gave an age of 35.79 Ma. Sample Ig-29, also with a poor isochron, gave an age of 39.22 Ma.

Augite monzonite stock

Two samples of the augite monzonite stock were analyzed by the hornblende step-heating method. Sample Eg-62, with an irregular spectrum, gave an age of 33.27 Ma. Sample Ig-26, with a poor isochron, gave an age of 35.26 Ma.

Subvolcanic latite stock

Feldspar crystals from two samples were analyzed by step heating and yielded fair to good isochrons and ages of 31.68 Ma (Eg-68) and 31.91 Ma (Eg-70).   Sanidine from a similar plug located NW of Carache Canyon (sample Wg-12) yielded a well-behaved SCLF age of 31.83 Ma.

Volcanics of Dolores Gulch

Feldspar crystals from two samples were analyzed by step heating and yielded fair to good isochrons and ages of 31.31 Ma (Eg-13) and 31.48 Ma (Eg-27).

Granodiorite stock of Candelaria Mountain

A feldspar crystal from sample Ig-68, analyzed by step heating, gave an age of 31.10 Ma.

Adularia associated with gold mineralization at Carache Canyon

Two adularia specimens from drilling in Carache Canyon (OC-43, 564' and 554') were analyzed by the plateau method and yielded ages of 32.2 Ma and 31.56 Ma, respectively.   A third specimen (OCC-200, 566') turned out not to be adularia on the basis of its K/Ca ratio. Its date of 36.21 Ma therefore cannot be trusted.

DISCUSSION

Previous reviews of K/Ar data (Maynard and others, 1990; Maynard, 1995) indicated a gap between calc-alkaline magmatism occurring between 36 Ma and 34 Ma and alkaline magmatism occurring between 30 Ma and 26 Ma. New ^{40}Ar/^{39}Ar dates suggest tighter constraints on Ortiz magmatism and mineralization, and on major movement on the Tijeras-Cañoncito Fault System (**Figure 3-15**).

Taking the ^{40}Ar/^{39}Ar age determinations of displaying fair or better quality, the following ages can be assigned:

- Laccoliths, sills, and dikes of andesite porphyry, dated at 34.29 Ma.

- Augite (hornblende) monzonite, dated at 33.27 Ma.

- Volcanic rocks of Dolores Gulch, dated at 31.31 Ma to 31.48 Ma.

- Subvolcanic latite plugs and trachytic latite dikes dated at 31.56 Ma to 31.91 Ma.

- Granodiorite stock of Candelaria Mountain dated at 31.1 Ma.

- Gold mineralization-associated adularia from Carache Canyon dated at 31.56 Ma to 32.2 Ma.

34.29 Ma andesite porphyry laccoliths, sills, and dikes are widespread in the Ortiz Porphyry Belt. They intruded at all stratigraphic levels (Pennsylvanian to Eocene), they are dominantly concordant with respect to bedding, and they are quartz bearing. Because the andesite porphyry laccolithic bodies preferred to intrude as concordant bodies, it is likely that they were intruded into relatively undisturbed layered rocks. The distribution of sills intruding the Cretaceous section on the Ortiz Mine Grant show a center in the western part of the Ortiz Mountains, north of the Tijeras Fault, and another in the area of Captain Davis Mountain, south of the Tijeras Fault. This "offset" in sill distribution mimics the offset of the Cretaceous section as a whole, suggesting that major movement on the fault occurred after emplacement of the laccoliths.

33.27 Ma augite (hornblende) monzonite cuts the laccolithic bodies and the Ortiz Graben, with minor subsequent movement. Thus the augite monzonite stock emplacement post dates major movement on the Tijeras Fault and major movement on the Tijeras-Cañoncito Fault System on the Ortiz Mine Grant occurred during the period 34.29 Ma to 33.27 Ma.

Younger intrusions, with the exception of the granodiorite of Candelaria Mountain, are quartz poor. 31.56 Ma to 31.91 Ma subvolcanic latite plugs slightly predate the 31.31 Ma to 31.48 Ma volcanic rocks of Dolores Gulch. The somewhat greater degree of uncertainty in the ages of the volcanic rocks allows for the interpretation that the volcanics and subvolcanic intrusions are essentially coeval. The 31.1 Ma granodiorite stock at Candelaria Mountain appears to be coeval with the subvolcanic latite plugs as well.

31.56 Ma to 32.2 Ma adularia from Carache Canyon suggests that Carache Canyon mineralization is somewhat older than the subvolcanic latite intrusions of Cunningham Gulch and Rattlesnake Hill. The collapse breccia pipe at Carache Canyon predates mineralization.

Table 7-1. Summary of isotopic dates of rocks from the Ortiz Porphyry Belt. Units are listed from oldest to youngest, based on field relations. Samples yielding dates greater than 40 Ma are excluded.

Unit	Study/Sample	Age (Ma)	Method, type	Comment
Andesite Porphyry Ortiz Mountains	Bachman and Mehnert (1978)	34.0 +/- 2.2	K/Ar hornblende	
	This study/Ig-30	34.29	$^{40}Ar/^{39}Ar$, hornblende, isochron	fair isochron
	This study/Wg-1	35.79	$^{40}Ar/^{39}Ar$, hornblende, isochron	poor isochron
	This study/Ig-29	39.11	$^{40}Ar/^{39}Ar$, hornblende, isochron	poor isochron
	Sauer (1999)/K97-9-25F/3/KD9	34.3 +/- 0.3	$^{40}Ar/^{39}Ar$, hornblende, isochron	
	Sauer (1999)/K97-9-25C/2/KD9	35.9 +/- 0.09	$^{40}Ar/^{39}Ar$, hornblende, isochron	
	Sauer (1999)/K97-9-25E/8/KD9	36.2 +/- 0.8	$^{40}Ar/^{39}Ar$, hornblende, isochron	
	Sauer (1999)/K97-9-25B/4/KD9	33.3 +/- 0.09	$^{40}Ar/^{39}Ar$, hornblende, plateau	
Augite (hornblende) monzonite, Ortiz Mountains	Armstrong (1975)/1222155-61	33.9 +/- 1.2	K/Ar hornblende	
	Kay (1986)	29.6 +/- 1.5	K/Ar hornblende	
	This study/Eg-62	33.27	$^{40}Ar/^{39}Ar$, hornblende	irregular spectrum
	This study/Ig-26	35.36	$^{40}Ar/^{39}Ar$, hornblende	poor isochron
	Sauer (1999)/O-4-BS/14/KD9	31.3 +/- 0.3	$^{40}Ar/^{39}Ar$, hornblende, Tmax?	
Augite (hornblende) monzonite, San Pedro Mountains	Sauer (1999)/SP-1-BS/20/KD9	30.6 +/- 0.5	$^{40}Ar/^{39}Ar$, hornblende, isochron	
	Sauer (1999)/SP-1-BS/7/KD9	30.94 +/- 0.06	$^{40}Ar/^{39}Ar$, hornblende, plateau	
Volcanic rocks of Dolores Gulch	Kay (1986)/NMO-13,1072'	34.2 +/- 1.4	K/Ar hornblende	
	This study/Eg-13	31.31	$^{40}Ar/^{39}Ar$, K spar	fair to good isochron
	This study/Eg-27	31.48	$^{40}Ar/^{39}Ar$, K spar	fair to good isochron
Espinaso Volcanics, Hagan Basin	Kautz and others (1981)/base	34.3 +/- 0.8	K/Ar	
	Kautz and others (1981)/middle	34.6 +/- 0.7	K/Ar	
	Weber (1971)/ middle	36.9 +/ 1.2	K/Ar	
	Kautz and others (1981)/top	26.9 +/- 0.6	K/Ar	
Subvolcanic latite plug and trachytic latite dikes	Kay (1986)/ OR-9	35.1 +/- 1.4	K/Ar feldspar	
	Kay (1986)/ OR-10	30.7 +/- 1.2	K/Ar feldspar	
	Kay (1986)/ OR-12	30.3 +/- 1.2	K/Ar biotite	
	Kay (1986)/ OR-11	29.9 +/- 1.2	K/Ar whole rock	
	Kay (1986)/ OR-8	33.1 +/- 0.8	K/Ar feldspar	
	Kay (1986)/ OR-13	35.1 +/- 1.4	K/Ar feldspar	
	Kay (1986)/ OR-7	31.6 +/- 1.2	K/Ar biotite	
	This study/ Eg-68	31.68	$^{40}Ar/^{39}Ar$, K spar	fair to good isochron
	This study/ Eg-70	31.91	$^{40}Ar/^{39}Ar$, K spar	fair to good isochron
	This study/ Wg-12	31.56	$^{40}Ar/^{39}Ar$, sanidine	well behaved

Table 7-1 (cont.). Summary of isotopic dates of rocks from the Ortiz Porphyry Belt. Units are listed from oldest to youngest, based on field relations. Samples yielding dates greater than 40 Ma are excluded.

Unit	Study/Sample	Age (Ma)	Method, type	Comment
Granodiorite stock of Candelaria Mountain	This study/ Ig-68	31.1	$^{40}Ar/^{39}Ar$, K spar	fair to good isochron
Mineralization-associated minerals	Kay (1986)/ OR-1	39.6 +/- 1.5	K/Ar sericite	
	Kay (1986)/ OR-2	32.0 +/- 1.2	K/Ar sericite	
	This study/ OC-43, 564'	32.2	$^{40}Ar/^{39}Ar$, adularia	
	This study/ OC-43, 554'	31.56	$^{40}Ar/^{39}Ar$, adularia	

8 REFERENCES

Abbott, J.C., 1995, Constraints on the deformational history of the Tijeras-Canoncito fault system, north-central New Mexico [M.S. Thesis]: New Mexico Institute of Mining and Technology, 161 pp.

Abbott, J.C., Cather, S.M., and Goodwin, L.B., 1995, Paleogene synorogenic sedimentation in the Galisteo basin related to the Tijeras-Canoncito fault system: New Mexico Geological Society Guidebook 46, p. 271-278.

Abbott, J.C., and Goodwin, L.B., 1995, A spectacular exposure of the Tijeras fault, with evidence of Quaternary motion: New Mexico Geological Society Guidebook 46, p. 117-126.

Abbott, J., Goodwin, L.B., Kelley, S., and Maynard, S., 2004, The anatomy of a long-lived fault system: Structural and thermochronologic evidence for Laramide to Quaternary activity on the Tijeras Fault, New Mexico: Cather, S., McIntosh, W.C., and Kelley, S. (eds) *Tectonics, Geochronology, and Volcanism of the Southern Rocky Mountains and Rio Grande Rift*, New Mexico Bureau of Geology and Mineral Resources Bulletin.

Abert, J.W., 1846, Senate Executive Document, No. 23, 30th Congress, 1st Session.

Akright, R.L., 1979, Geology and mineralogy of the Cerrillos copper deposit, Santa Fe County, New Mexico: New Mexico Geological Society, Guidebook 30, pp. 257-260.

Amindyas, C.A., and Brookins, D.G., 1988, Geochemical study of hydrothermally altered rocks, Cerrillos porphyry copper deposit, Santa Fe County, New Mexico: New Mexico Journal of Science, v. 28, no. 2, p. 125-137.

Anzman, J.R., 1985, Interpretation of geophysical surveys, Carache Canyon area, Ortiz Project, Santa Fe County, New Mexico: unpublished report for Long Lac Mineral Exploration Limited, 6 p.

Anzman, J.R., 1986, Synopsis interpretation, induced polarization survey Ortiz Project, Santa Fe County, New Mexico: unpublished report for Long Lac Mineral Exploration Limited, 2 p., maps.

Atkinson, W.W., 1961, Geology of the San Pedro Mountains, Santa Fe County, New Mexico: New Mexico Bureau of Mines and Mineral Resources, Bulletin 77, 49 p.

Aubele, J.C., 1979, The Cerros del Rio volcanic field: New Mexico Geological Society, Guidebook 30, pp. 243-252.

Bachman, G.O., 1975, Geologic map of the Madrid Quadrangle, Santa Fe and Sandoval Counties, New Mexico: U.S. Geological survey Geologic Quadrangle Map GQ-1268, scale 1:62,500.

Bachman, G.O., 1976, Cretaceous rocks in the area of the Madrid coal field, New Mexico: New Mexico Bureau of Mines and Mineral Resources, Circular 154, p. 41-43.

Bachman, G.O., and Mehnert, H.H., 1978, New K-Ar dates and the late Pliocene to Holocene geomorphic history of the central Rio Grande region, New Mexico: Geological Society of America, Bulletin, v. 89, p. 283-292.

Baldridge, W.S., Damon, P.E., Sahfiqullah, M., and Bridwell, R.J., 1980, Evolution of the central Rio Grande Rift, New Mexico: New potassium-argon dates: Earth and Planetary Science Letters, v. 51, p. 309-321.

Baltz, E.H., 1967, Stratigraphy and regional tectonic implications of part of the Upper Cretaceous and Tertiary rocks, east-central San Juan Basin, New Mexico: U.S. Geological Survey Professional Paper 552, 101 pp.

Baltz, E.H., 1978, Resume of Rio Grande depression in north-central New Mexico: New Mexico Bureau of Mines and Mineral Resources, Circular 163, p. 210-228.

Bauer, P., and Giles, D.L., 1995, Turquoise: *minipaper in* Bauer, P.W., Maynard, S.R., Smith, G.A., Giles, D.L., Lucas, S.G., Barker, J.M., Smith, E.W., and Kottlowski, F.E., Third-day road log, from Santa Fe to the Cerrillos Hills, Cerrillos and the Ortiz Mountains: New Mexico Geological Society Guidebook, 46th Field Conference, Geology of the Santa Fe Region, pp 60-61.

Bauer, P.W., Maynard, S.R., Smith, G.A., Giles, D.L., Lucas, S.G., Barker, J.M., Smith, E.W., and Kottlowski, F.E., 1995, Third-day road log, from Santa Fe to the Cerrillos Hills, Cerrillos and the Ortiz Mountains: New Mexico Geological Society Guidebook, 46th Field Conference, Geology of the Santa Fe Region, pp 60-61.

Baxter, W., 2004, The gold of the Ortiz Mountains, a story of New Mexico and the west's first major gold rush: Lone Butte Press, Santa Fe, NM, 154 pp.

Beaumont, E.C., 1964, Geology of the anthracite coal deposits of the Madrid area, New Mexico: unpublished report, 21 pp.

Beaumont, E.C., 1979, Geology of the Cerrillos coal field, Santa Fe County, New Mexico: New Mexico Geological Society, Guidebook 30, p. 269-274.

Beaumont, E.C., Shomaker, J.W., Stone, W.J., and others, 1976, Guidebook to the coal geology of northwest New Mexico: New Mexico Bureau of Mines and Mineral Resources, Circular 54, 58 pp.

Bell, B.S., 1987, Report on the induced polarization and resistivity survey in the Ortiz Mountains, New Mexico: unpublished report for Long Lac Minerals Exploration (Texas) Inc., by Phoenix Geophysics, Inc.,

Black, B.A., 1979a, Structure and stratigraphy of the Hagan embayment: a new look: New Mexico Geological Society, Guidebook 30, p. 101-106.

Black, B.A., 1979b, Oil and gas exploration in the Santa Fe – Galisteo - Hagan area of New Mexico: New Mexico Geological Society, Guidebook 30, p. 275-279.

Black, B.A., 1982, Oil and gas exploration in the Albuquerque basin: New Mexico Geological Society, Guidebook 33, p. 313-324.

Burnham, C.W., 1979, Magmas and hydrothermal fluids, in Barns, H.L., ed.s Geochemistry of hydrothermal ore deposits: New York, John Wiley and Sons, p. 71-136.

Burnham, C.W., 1985, Energy release in subvolcanic environments: implication for breccia formation: Economic Geology, v. 80, p. 1515-1522.

Burns, S.G., 1897, Ortiz Mine Grant: a report to Thomas A. Edison.

Cather, S.M., 1992, Suggested revisions to the Tertiary tectonic history of north-central New Mexico: New Mexico Geological Society, Guidebook 43, p. 109-122.

Chapin, C.E., and Cather, S.M., 1981, Eocene tectonics and sedimentation in the Colorado Plateau – Rocky Mountain area: Arizona Geological Society Digest, v. 14, p. 173-198.

Chenowith, W.L., 1979, Uranium in the Santa Fe area, New Mexico: New Mexico Geological Society, Guidebook 30, p. 261-264.

Coles, D.W., 1990, Alteration and mineralization of the Carache Canyon gold prospect, Santa Fe County, New Mexico [MS Thesis]: Fort Collins, Colorado State University, 183 p.

Connolly, J.R., 1981, Geology of the Precambrian rocks of Tijeras Canyon, Bernalillo County, New Mexico [M.S. Thesis]: Albuquerque, University of New Mexico, 147 pp.

Cook, W., 1970a, An evaluation of the Ortiz Basin No. 2 breccia and Candelaria-Lime anomalies of the Ortiz Mine Grant, Santa Fe County, New Mexico: unpublished report to Molybdenum Corporation of America, 48 pp.

Cook, W., 1970b, Results of sampling the Cunningham placer, Ortiz Mine Grant, Santa Fe County, New Mexico: unpublished report to Molybdenum Corporation of America, 48 pp.

Crane, G.W., 1937, Geological report on the Cunningham Mine, a portion of the Ortiz Mine Grant, Santa Fe County, New Mexico: unpublished report.

Corry, C.E., 1988, Laccoliths; mechanics of emplacement and growth: Geological Society of America, Special Paper 22, 110 pp.

Dale, V.B., and McKinney, W.A., 1959, Tungsten deposits of New Mexico: U.S. Bureau of
      Mines, Report on Investigations, 5517, 72 p.

Dane, C.H., 1946, Stratigraphic relations of Eocene, Paleocene, and latest Cretaceous formation
      of eastern side of San Juan basin, New Mexico: U.S. Geologic Survey, Oil and Gas
      Investigations, Preliminary Chart 24.

Dane, C.H., 1960, The boundary between rocks of Carlile and Niobrara age in San Juan Basin,
      New Mexico and Colorado: American Journal of Science (Bradley volume), v. 258-A, p.
      46-56.

de Carle, R.J., 1987, Report on the combined helicopter magnetic, electromagnetic, and VLF
      survey, Ortiz Mountain Range area, for Long Lac Mineral Exploration (Texas) Inc.:
      Private report by Aerodat, Ltd., 50 pp.

de Carle, R.J., 1988, Report on the combined helicopter magnetic, electromagnetic, and VLF
      survey, Ortiz Mountain Range area extension survey, for Long Lac Mineral Exploration
      (Texas) Inc.: Private report by Aerodat, Ltd., 26 pp.

Disbrow, A.E., and Stoll, W.C., 1957, Geology of the Cerrillos area, Santa Fe County, New
      Mexico: New Mexico Bureau of Mines and Mineral Resources, Bulletin 48, 73 pp.

Elliot, J.C., 1991, Vegetation baseline study for the Ortiz Project Joint Venture: Unpublished
      report for Pegasus Gold Corporation, 39 pp.

Elston, W.E., 1967, Summary of the mineral resource of Bernalillo, Sandoval, and Santa Fe
      Counties, New Mexico: New Mexico Bureau of Mines and Mineral Resources, Bulletin
      81, 81 pp.

Emerick, W.L., 1950, Geology of the Golden area, Santa Fe County, New Mexico [M.S. Thesis]:
      Albuquerque, University of New Mexico, 66 pp.

Erskine, D.W., and Smith, G.A., 1993, Compositional characterization of volcanic products from
      a primarily sedimentary record: Geological Society of America Bulletin, v. 105, p. 1214-
      1222.

Ferguson, C., and Osbourn, R., 2000, Preliminary geologic map of the San Pedro 7.5-minute
      quadrangle: New Mexico Bureau of Mines and Mineral Resources, Open-File Report,
      OM- .

Fulp, M.S., Connolly, W.J., and Woodward, L.A., 1982, Mineralization in Precambrian rocks in
      the Manzanita-North Manzano Mountains, central New Mexico: New Mexico
      Geological Society, Guidebook 33, p. 303-304.

Gardner, J.H., 1908, Isolated coal fields in Santa Fe and San Miguel Counties, New Mexico:
      Contributions to Economic Geology, 1908, Part II, p. 447-451.

Gay, S.P., 1969, Report on induced polarization surveys, Ortiz Mine Grant project, Santa Fe County, New Mexico: unpublished report by Mineral Surveys, Inc. to Molybdenum Corporation of America, 9 pp.

Gierzycki, G.A., 1984, Carache Canyon, Ortiz Mine Grant, Santa Fe County, New Mexico: report to Long Lac Mineral Exploration, 26 pp.

Gierzycki, G.A., 1985a, Carache Canyon, Ortiz Mine Grant, Santa Fe County, New Mexico – Summary report: report to Long Lac Mineral Exploration, 10 pp.

Gierzycki, G.A., 1985b, Crooked Canyon geology report, Ortiz Mine Grant, Santa Fe County, New Mexico: report to Long Lac Mineral Exploration, 13 pp

Gierzycki, G.A., 1985c, Iron Vein, Ortiz Mine Grant, Santa Fe County, New Mexico: report to Long Lac Mineral Exploration, 18 pp.

Gierzycki, G.A., and Martin, K., 1985, Eagle Canyon geology report, Ortiz Mine Grant, Santa Fe County, New Mexico: report to Long Lac Mineral Exploration, 10 pp.

Giles, D.L., 1995, Cerrillos Mining District: *minipaper in* Bauer, P.W., Maynard, S.R., Smith, G.A., Giles, D.L., Lucas, S.G., Barker, J.M., Smith, E.W., and Kottlowski, F.E., Third-day road log, from Santa Fe to the Cerrillos Hills, Cerrillos and the Ortiz Mountains: New Mexico Geological Society Guidebook, 46th Field Conference, Geology of the Santa Fe Region, pp 61-62.

Gilbert, G.K., 1877, Geology of the Henry Mountains, Utah: U.S. Geographical and Geological Survey of the Rocky Mountain Region, 170 p.

Gorham, T.W., 1979, Geology of the Galisteo Formation, Hagan Basin, New Mexico [M.S. Thesis]: Albuquerque, University of New Mexico.

Gorham, T.W., and Ingersoll, R.V., 1979, Evolution of the Eocene Galisteo Basin, north-central New Mexico: New Mexico Geological Society, Guidebook 30, p. 219-224.

Gregg, J., 1954, Commerce of the prairies: University of Oklahoma Press, Norman, OK.

Griswold, C.T., 1950, Report on the mineral possibilities of the Ortiz Mine Grant: private report prepared for G.W. Potter of Joplin, Missouri.

Griswold, G.R., 1948, Report on the Ortiz Mine Grant, Santa Fe County, New Mexico: private report.

Griswold, G.R., 1951a, Calcite vein and Candelario veins, the Ortiz Mine Grant, Santa Fe County, New Mexico, scale 1"=200': unpublished map for Potter and Sims.

Griswold, G.R., 1951b, Underground workings of the Candelaria Mine, the Ortiz Mine Grant, Santa Fe County, New Mexico, scale 1"=50': unpublished map for Potter and Sims.

Hafenfeld, S.R., and Anderson, O.J., 1995: History and engineering aspects of Galisteo Dam and Reservoir, Santa Fe County, New Mexico: *minipaper in* Bauer, P.W., Maynard, S.R., Smith, G.A., Giles, D.L., Lucas, S.G., Barker, J.M., Smith, E.W., and Kottlowski, F.E., Third-day road log, from Santa Fe to the Cerrillos Hills, Cerrillos and the Ortiz Mountains: New Mexico Geological Society Guidebook, 46th Field Conference, Geology of the Santa Fe Region, p 64.

Hallof, P.G., 1986, Review of geophysical results from Ortiz project: unpublished report to Long Lac Mineral Exploration, 5 pp.

Hallof, P.G., and Bell, R.A., 1969, Report on the induced polarization and resistivity survey of the Ortiz basin grid, Santa Fe County, New Mexico: unpublished report by McPhar Geophysics, Inc. to Molybdenum Corporation of America, 7 pp.

Harrison, E.P., 1949, Geology of the Hagan coal basin [M.S. Thesis]: University of New Mexico.

Hayden, F.N., 1869, Third annual report of the United States geological survey of the territories embracing Colorado and New Mexico, including a report by Persifor Frazer, Jr., titled "On mines and minerals of Colorado": Department of the Interior, Washington, D.C.

Hickson, R.J.., 1981, Heap leaching practices at Ortiz Gold Mine, Santa Fe County, New Mexico: Society of Mining Engineers of AIME, preprint, No. 81-347.

Hook, S.C, and Cobban, W.A., 1980, Reinterpretation of type section of Juana Lopez member of Mancos Shale: New Mexico Geology, vol. 2, No. 2.

Hunt, C.B., Averitt, P., and Miller, R.L., 1953, Geology and geography of the Henry Mountains region, Utah: U.S. Geological Survey Professional Paper 228.

Huzarski, J.R., 1971, Petrology and structure of the eastern Monte Largo Hills, New Mexico [M.S. Thesis]: Albuquerque, University of New Mexico, 45 pp.

Independent Mining Consultants, Inc., 1992, Reserve audit prepared for Pegasus Gold Corporation, Ortiz Project Joint Venture.

Ingersoll, R.V., Cavazza, W., Baldridge, W.S., and Shafiqullah, M., 1990, Cenozoic sedimentation and paleotectonics of north-central New Mexico: implications for initiation and evolution of the Rio Grande Rift: Geological Society of America Bulletin, v. 102, p. 1280-1296.

Ingersoll, R.V., and Kelley, V.C., 1979, Stratigraphy and paleoenvironments of the Hagan Basin, north-central New Mexico: New Mexico Geological Society Guidebook, 30th Field Conference, p. 197-200.

Jackson M.D., and Pollard, D.D., 1988, The laccolith-stock controversy: New results from the southern Henry Mountains, Utah: Geological Society of America Bulletin, v. 100, p 177-139.

Johnson, A.M., and Pollard, D.D., 1973, Mechanics of growth of some laccolithic intrusions in the Henry Mountains, Utah, Part I, Field observations, Gilbert's model, physical properties, and flow of the magma: Tectonophysics, v. 18, no. 3-4, p. 261-309.

Johnson, D.W., 1903, The geology of the Cerrillos Hills, New Mexico: School of Mines Quarterly, Vol. 24, pp. 173-246, 303-350, 456-500; vol. 25, 00. 69-98.

Johnson, C.H., 1943, San Pedro Mine, Santa Fe County, New Mexico, U.S. Bureau of Mines, War Minerals Report 143.

Jones, F.A., 1904, New Mexico mines and minerals: World's Fair edition: New Mexico Printing Co., Santa Fe, New Mexico.

Jones, F.A., 1935, Occurrence of gold on the Ortiz Mine Grant, Santa Fe County, New Mexico: unpublished engineering manuscript, Albuquerque, New Mexico.

Kautz, P.F., Ingersoll, R.V., Baldridge, W.S., Damon, P.E., and Shafiqullah, M., 1981, Geology of the Espinaso Formation (Oligocene), north-central New Mexico, part 2: Geological Society of America, Bulletin, v. 92, pp. 2318-2400.

Kay, B.D., 1986, Vein and breccia gold mineralization and associated igneous rocks at the Ortiz Mine, New Mexico, USA [M.S. Thesis]: Golden, Colorado School of Mines, 179 p.

Kelley, V.C., 1963, Geologic map of the Sandia Mountains and vicinity, New Mexico: New Mexico Bureau of Mines and Mineral Resources, Geologic Map 18.

Kelley, V.C., and Northrup, S.A., 1975, Geology of the Sandia Mountains and vicinity: New Mexico Bureau of Mines and Mineral Resources, Memoir 29, 136 pp.

Kelson, K.I., Hitchcock, C.S., and Harrison, J.B.J., 1998, Paleoseismologic assessment of the southern Tijeras Fault, Central New Mexico, final technical report: U.S. Geological Survey, National Earthquake Hazards Reduction Program.

Kelson, K.I., Hitchcock, C.S., and Harrison, J.B.J., 1999, Paleoseismology of the Tijeras fault near Golden, New Mexico: New Mexico Geological Society, 50th annual Field Conference Guidebook, pp. 201-209.

Keyes, C.R., 1909, Garnet contact deposits of copper and the depths at which they are formed: Economic Geology, v. 4, p. 365-372.

Keyes, C.R., 1918, Mechanics of laccolithic intrusion [abs.],: Geological Society of America Bulletin, v. 29, p. 75.

Keyes, C.R., 1922, New Mexican laccolithic structures: Pan-American Geologist, v. 37, no.2, p. 109-120.

Klein, J., and Lajoie, J.J, 1988, Electromagnetics: *in* Van Blaricom, R., compiler, Practical geophysics for the exploration geologist: Northwest Mining Association, pp. 239-290.

Knox, W.P., 1981, I.P. report on Florencio prospect: unpublished report for Gold Fields Mining Corporation, 2 p., with maps.

Koehler, R.D., and Kelson, K.I., 2000, Paleoseismologic assessment of the northern Tijeras-Cañoncito Fault System, Central New Mexico, final technical report: U.S. Geological Survey, National Earthquake Hazards Reduction Program.

Lamb, G.M., 1968, Stratigraphy of the lower Mancos shale in the San Juan Basin: Geological Society of America, Bulletin, v. 79, p. 827-854.

LeBas, M.J., LeMaitre, R.W., Streckeisen, A., and Zanettin, B., 1986. A chemical classification of volcanic rocks based on the total alkali silica diagram. J. Pet. 27:745-750.

Lee, W.T., 1913, The Cerrillos coal field, Santa Fe County, New Mexico: U.S. Geologic Survey, Bulletin 531e, pt. II, p. 285-312.

Lindgren, W., and Graton, L.C., 1906, A reconnaissance of the mineral deposits of New Mexico: U.S. Geologic Survey, Bulletin 285, p. 74-86.

Lindgren, W., Graton, L.C., and Gordon, C.H., 1910, The ore deposits of New Mexico: U.S. Geologic Survey, Professional Paper 68, 316 pp.

Lindqvist, W.F., 1980, The exploration of the Ortiz gold deposit, New Mexico – geology and exploration: Colorado Mining Association, 1980 Yearbook, p. 106-112.

Lisenbee, A.L., 1967, Geology of the Cerro Pelon – Arroyo de la Jara area, Santa Fe County, New Mexico [M.S. Thesis]: Albuquerque, University of New Mexico, 112 pp.

Lisenbee, A.L., 1976, Shale diapirism and the structural development of Galisteo Syncline, Santa Fe County, New Mexico; *in* Woodward, L.A., and Northrup, S.A., eds., Tectonics and Mineral Resources of Southwestern North America: New Mexico Geological Society Special Publication No. 6, pp. 88-94.

Lisenbee, A.L. and Maynard, S.R., expected 2001, Geology of the Captain Davis Mountain 7.5-min. quadrangle, Santa Fe County, New Mexico, New Mexico Bureau of Mines and Mineral Resources, Open-file Geologic Map OF-GM 48 , scale 1:12,000.

Lisenbee, A.L., Maynard, S.R., and Rogers, J. , 2001, Preliminary geologic map of the Picture Rock 7.5-minute quadrangle: New Mexico Bureau of Mines and Mineral Resources, Open-File Report, OM- .

Lisenbee, A.L., Woodward, L.A., and Connolly, J.R., 1979, Tijeras-Cañoncito fault system – a major zone of recurrent movement in north-central New Mexico: New Mexico Geological Society, Guidebook 30, p. 89-99.

Locke, A., and Perry, E.H., 1915, The Santa Fe Mine, report of geological examination: report to Santa Fe Gold & and Copper Mining Company, 100 pp.

Long, R.C., 1985, Progress report, Lukas Canyon area, Ortiz Mine Grant, Santa Fe County, New Mexico: unpublished report to Long Lac Mineral Exploration, 39 pp.

Long, R.C., 1986a, Ortiz Mine Grant, summary report: unpublished report to Long Lac Mineral Exploration, 24 pp.

Long, R.C., 1986b, Second progress report for Lukas Canyon, Ortiz Mine Grant: unpublished report to Long Lac Mineral Exploration, 32 pp.

Lucas, S.G., 1980, Stratigraphy and age of the Galisteo Formation and the structural history of the Rio Puerco fault zone (abstract): Geological Society of America, Abstracts with Programs, v. 12, p. 279.

Lucas, S.G., 1982, Vertebrate paleontology, stratigraphy, and biostratigraphy of Eocene Galisteo Formation, north-central New Mexico: New Mexico Bureau of Mines and Mineral Resources, Circular 186, 34 pp.

Lucas, S.G., 1984, Correlation of Eocene rocks of the northern Rio Grande rift and adjacent areas: implications for Laramide tectonics: New Mexico Geological Society, Guidebook 35, p. 123-128.

Lucas, S.G., and Hayden, S.N., 1991, Type section of the Permian Bernal Formation and the Permian Triassic boundary in north-central New Mexico: New Mexico Geology, v. 13, p. 9-15.

Lucas, S.G., and Heckert, A.B., 1995, Triassic stratigraphy around the Sandia Uplift, central New Mexico: New Mexico Geological Society, Guidebook, 46th Field Conference, pp. 233-241.

Lucas, S.G., and Kues, B.S., 1979, Vertebrate biostratigraphy of the Eocene Galisteo Formation, north-central New Mexico: New Mexico Geological Society, Guidebook 30, p. 225-229.

Lucas, S.G., Cather, S.M., Abbott, J.C., and Williamson, T.E., 1997, Stratigraphy and tectonic implications of Paleogene strata in the Laramide Galisteo Basin, north-central New Mexico: New Mexico Geology, November, 1997.

Lucas, S.G., Anderson, O.J., and Estep, J.W., 1998, Stratigraphy and correlation of Middle Cretaceous rocks (Albian-Cenomanian) from the Colorado Plateau to the southern High Plains, north-central New Mexico: *in* Lucas, S.G., Kirkland, J.I., and Estep, J.W., eds., 1998, Lower and Middle Cretaceous Terrestrial Ecosystems: New Mexico Museum of Natural History and Science Bulletin No. 14, p. 57-66.

Lucas, S.G., Estep, J.W., and Anderson, O.J., 1999, Correlation of Jurassic strata from the Colorado Plateau to the High Plains, across the Rio Grande rift, north-central New Mexico: New Mexico Geological Society Guidebook, 50th Field Conference, Albuquerque Geology, pp. 317-326.

Marcou, J., 1858, Geology of North America, with two reports on the prairies of Arkansas and Texas, the Rocky Mountains of New Mexico, and the Sierra Nevada of California, originally made for the United States Government: Zurcher and Furrer, Zurich, 144 p.

Martin, K.W., 1991, Summary of drilling exploration and geologic resource evaluation of the Lukas Canyon deposit: unpublished report for Ortiz Joint Venture.

Maynard, S.R., 1995, Gold mineralization associated with mid-Tertiary magmatism and tectonism, Ortiz Mountains, Santa Fe County, New Mexico: New Mexico Geological Society, Guidebook 46, p. 161-166.

Maynard, S., 2000, Geology of the Golden 7.5-min. quadrangle, Santa Fe County, New Mexico, New Mexico Bureau of Mines and Mineral Resources, Open-file Geologic Map OF-GM 36, scale 1:12,000.

Maynard, S., Rogers, J. and others, 2001, Geology of the Madrid 7.5-min. quadrangle, Santa Fe County, New Mexico, New Mexico Bureau of Mines and Mineral Resources, Open-file Geologic Map OF-GM 40, scale 1:12,000.

Maynard, S.R., Nelsen, C.J., Martin, K.W., and Schutz, J.L., 1990, Geology and gold mineralization of the Ortiz Mountains, Santa Fe County, New Mexico: Mining Engineering, August 1990, p. 1007-1011.

Maynard, S.R., Woodward, L.A., and Giles, D.L., 1991, Tectonics, intrusive rocks, and mineralization of the San Pedro-Ortiz porphyry belt, north-central New Mexico: New Mexico Bureau of Mines and Mineral Resources, Bulletin 137.

McCallum, M.E., 1985, Experimental evidence for fluidization processes in breccia pipe formation: Economic Geology, v. 80, p. 1523-1543.

McQuiston, F.W., and Shoemaker, R.S., 1981, Gold and silver cyanidation plant practice, Volume II: Society of Mining Engineers of American Institute of Mining, Metallurgical, and Petroleum Engineers, Inc., New York, 263 pp.

McRae, O.M., 1958, Geology of the northern part of the Ortiz Mountains, Santa Fe County, New Mexico [M.S. Thesis]: Albuquerque, University of New Mexico, 112 pp.

Metric Corporation, 1991, Late summer and winter wildlife baseline studies and wildlife impact analysis of the Ortiz Mountains, Santa Fe County, New Mexico: Unpublished report for Pegasus Gold Corporation.

Milford, H.E., 1994, History of the Los Cerrillos mining area: New Mexico Abandoned Mine Land Bureau Report 1994-2.

Milford, H.E., 1995, Mining history of the Cunningham deposit and Ortiz Mine Grant, Santa Fe County, New Mexico: *minipaper in* Bauer, P.W., Maynard, S.R., Smith, G.A., Giles, D.L., Lucas, S.G., Barker, J.M., Smith, E.W., and Kottlowski, F.E., Third-day road log, from Santa Fe to the Cerrillos Hills, Cerrillos and the Ortiz Mountains: New Mexico Geological Society Guidebook, 46th Field Conference, Geology of the Santa Fe Region, pp 65-67.

Molenaar, C.M., 1977, Stratigraphy and depostional history of upper Cretaceous rocks of the San Juan Basin area, New Mexico and Colorado, with a note on economic resources: New Mexico Geological Society, Guidebook 28, p. 159-166.

Moore, J.C., 1979, Uranium deposits in the Galisteo Formation of the Hagan Basin, Sandoval County, New Mexico: New Mexico Geological Society, Guidebook 30, p. 265-267

Mudge, R.M., 1968, Depth control of some concordant intrusions: Geological Society of America Bulletin, v. 79, p. 315-322.

Mutschler, F.E., Griffin, M.E., Stevens, D.S., and Shannon, S.S. Jr., 1985, Precious metal deposits related to alkaline rocks in the North American cordillera – an interpretive review: Transactions of the Geological Society of South Africa, v. 88, p. 355-377.

Mutschler, F.E., Mooney, T.C., and Johnson, D.C., 1990, Precious metal deposits related to alkaline igneous rocks—a space-time trip through the Cordillera:

Myers, D.A., and McKay, E.J., 1976, Geologic map of the north end of the Manzano Mountains, Tijeras and Sedillo quadrangles, Bernalillo County, New Mexico: U.S. Geological Survey, Map I-968.

New Mexico Geological Society, 1982, New Mexico highway geologic map, scale 1:1,000,000.

North, R.M., and McLemore, V.T., 1986, Silver and gold occurrences in New Mexico: New Mexico Bureau of Mines and Mineral Resources, Resource Map 15, 32 pp.

North, R. M., and McLemore, V.T., 1988, A classification of the precious metal deposits of New Mexico: *in* Bulk mineable precious metal deposits of the western United States, Symposium Proceedings, Geological Society of Nevada.

Ogilvie, I.H., 1905, The high-altitude conoplain: a topographic form illustrated in the Ortiz Mountains: American Geologist, v. 36, p. 27-34.

Ogilvie, I.H., 1908, Some igneous rocks from the Ortiz Mountains, New Mexico: Journal of Geology, v. 16, p. 230-238.

Perry, V.D., and Moehlman, R.S., 1938, Report on the Ortiz Mine Grant, Santa Fe County, New Mexico: unpublished report.

Peterson, J.W., 1958, Geology of the southern part of the Ortiz Mountains, Santa Fe County, New Mexico [M.S. Thesis]: Albuquerque, University of New Mexico.

Picha, M.G., 1982, Structure and stratigraphy of the Montezuma salient – Hagan Basin area, Sandoval County, New Mexico [M.S. Thesis]: Albuquerque, University of New Mexico, 248 pp.

Pitard, F.F., 1988, Study of the heterogeneity of the Ortiz gold ore: Confidential report to LAC Minerals, USA, Inc., 72 pp.

Pollard, D.D., Muller, O.H., and Dockstader, D.R., 1975, The form and growth of fingered sheet intrusions: Geological Society of America Bulletin, v. 86, p. 351-363.

Raymond, R.W., 1870, Report on the mineral resources of the states and territories west of the Rocky Mountains: 40th Congress, 3rd session, Ex. Doc. No. 54., Ch LVII, p. 404-407.

Raymond, R.W., 1870 (for the year 1869), Statistics of mines and mining: House of Representatives Document 207, p. 407.

Raymond, R.W., 1872 (for the year 1870), Statistics of mines and mining: House of Representatives Document 10, p. 283.

Read, A.S., Karlstrom, K.E., and Ilg, B., 1999a, Mississippian Del Padre Sandstone or Proterozoic quartzite?: *minipaper in* NM Geological Society Guidebook, 50th Field Conference, Albuquerque Geology, 1999, pp 41-45.

Read, A.S., Karlstrom, K.E., Connell, S., Kirby, E., Ferguson, C., Ilg, B., Pazzaglia, F., Osburn, G., and Van Hart, D., 1999b, Geology of the Sandia Crest 7.5-minute quadrangle, Bernalillo and Sandoval Counties, New Mexico: New Mexico Bureau of Mines and Mineral Resources, Open-file Digital Geologic Map OFDM 6, scale 1:12,000.

Read, C.B., Duffner, R.T., Wood, G.H., and Zapp, A.D., 1950, Coal resources of New Mexico: U.S. Geological Survey, Circular 89, 24 pp.

Robinson, P., 1957, Age of Galisteo Formation, Santa Fe County, New Mexico: American
Association of Petroleum Geologists, Bulletin, v. 41, p. 757.

Sadowski, R.M., 1974, Ortiz Mine Project – geophysical report: Conoco, Inc., unpublished
report.

Sadowski, R.M., 1975, Ortiz Mine Project – geophysical report: Conoco, Inc., unpublished
report.

Schroer, G., 1994, Geology of the Greenhorn Au-Cu skarn deposit, Lukas Canyon, Ortiz mining
district, New Mexico [M.S. Thesis]: Colorado State University, 115 pp.

Schutz, J.L., 1988, Gold mineralization in the #1, #2A, #3, and #4 sills and Point Lookout
Sandstone: confidential report for LAC Minerals, USA, Inc.

Schutz, J.L, 1991, Ortiz Mine Grant, Santa Fe County, New Mexico, summary report, gold
resource evaluation of the Carache Canyon prospect: unpublished report for the Ortiz
Project JV.

Schutz, J.L., 1995, Gold mineralization associated with alkaline intrusives, Carache Canyon
breccia pipe prospect, Ortiz Mountains, New Mexico: New Mexico Geological Society,
Guidebook 46, p. 167-174.

Schutz, J.L, and Nelsen, C.J., 1990, Geology and gold mineralization of the Carache Canyon
breccia pipe, Ortiz Mountains, New Mexico: _in_ Gold '90, Proceedings of the Gold '90
Symposium, Salt Lake City, Utah, D.M. Hausen, editor, p. 65-81.

Seay, M., and Armstrong, D., 1974, Geology of the southwest Ortiz Mountains: unpublished
report, Continental Oil Company, Mineral Exploration Dept.

Sillitoe, R.H., 1979, Some thoughts on gold-rich porphyry copper deposits: Mineralium
Deposita, v. 14, pp 161-174.

Sillitoe, R.H., 1985, Ore-related breccias in volcano-plutonic arcs: Economic Geology, v. 80, p.
1467-1514.

Smith, D.A., and Nelsen, C.J., 1989, High-resolution helicopter mag-em survey of the Ortiz
Mountains, Santa Fe County, New Mexico: Mining Engineering.

Smith, G.A., 1995, Supplemental road log 3, Cerrillos to I-25 via Waldo: New Mexico
Geological Society Guidebook, 46th Field Conference, Geology of the Santa Fe Region,
pp 77-79.

Smith, G.A., Larsen, D., Harlan, S.S., McIntosh, W.C., Erskine, D.W., and Taylor, S., 1991, A
tale of two volcaniclastic aprons: Field guide to the sedimentology and physical
volcanology of the Oligocene Espinaso Formation and Miocene Peralta Tuff, north-

central New Mexico: New Mexico Bureau of Mines and Mineral Resources, Bulletin 137, p. 87-103.

Smith, J.F., and others, 1945, San Pedro and Carnahan Mines, New Placers mining district, Santa Fe County, New Mexico: U.S. Geological Survey, File Report.

Spiegel, Z., and Baldwin, B., 1963, Geology and water resources of the Santa Fe area, New Mexico, with contributions by F.E. Kottlowski and E.L. Barrows, and with a section on geophysics, by H.A. Winkler: U.S. Geological Survey Water-Supply Paper 1525, 258 p.; U.S. Geological Survey Open-File Report, 403 p., 1958.

Springett, M., 1980, The exploration of the Ortiz gold deposit, New Mexico – sampling and ore reserves: Colorado Mining Association, 1980 Mining Yearbook.

Stearns, C.E., 1943, The Galisteo Formation of north-central New Mexico: Journal of Geology, v. 51, p. 301-319.

Stearns, C.E., 1953a, Early Tertiary vulcanism in the Galisteo-Tonque area, north-central New Mexico: American Journal of Science, v. 251, p. 415-452.

Stearns, C.E., 1953b, Tertiary geology of the Galisteo-Tonque area, north-central New Mexico: Geological   Society of America, Bulletin, v. 64, p. 459-508.

Stearns, C.E., 1953c, Upper Cretaceous rocks of the Galisteo-Tonque area, north-central New Mexico: American Association of Petroleum Geologists, Bulletin, v. 37, p. 961-974.

Stearns, C.E., 1979, New K-Ar dates and the late Pliocene to Holocene geomorphic history of the central Rio Grande region, New Mexico: Discussion: Geological Society of America Bulletin, Part I, v.90, p. 799-800.

Sun, M-S., and Baldwin, B., 1958, Volcanic rocks of the Cienega area, Santa Fe County, New Mexico: New Mexico Bureau of Mines and Mineral Resources, Bulletin 54, 80 pp.

Thompson, T.B., 1964, The geology of the South Mountain area, Bernalillo, Sandoval, and Santa Fe Counties, New Mexico [M.S. Thesis]: University of New Mexico, 69 pp.

Thompson, T.B., 1964, The geology of the South Mountain area, Bernalillo, Sandoval, and Santa Fe Counties, New Mexico (abs.): New Mexico Geological Society Guidebook, 15th Field Conference, p. 188.

Timmons, J.M., Karlstrom, K.E., and Kirby, E., 1995, Geology of the Monte Largo Hills area, New Mexico: structural and metamorphic study of the eastern aureole of the Sandia pluton: New Mexico Geological Society Guidebook, 46th Field Conference, Geology of the Santa Fe Region, pp. 227-232.

Townley, J.M., 1968, History of mining activity in New Mexico, prehispanic to 1920 [M.A. Thesis]: University of Nevada, Reno.

Townley, J.M., 1971, El Placer: A New Mexico mining boom before 1846: Journal of the West, v. 10, no. 1, p. 102-115.

Turnbull, L.A., Toenges, A.L., Davis, J.E., Reynolds, D.A., and Parks, B.C., 1951, Miller Gulch and Cook and White coal beds, near Cerrillos, Santa Fe County, New Mexico – reserves, coking, petrographic, and chemical properties: U.S. Bureau of Mines, Report of Investigations 4814, 29 pp.

Wargo, J.G., 1964, Geology of a primary disseminated copper deposit near Cerrillos, New Mexico: Geological Society of America Special Paper 76, p.296.

Widdecomb, R., 1976, Geology of the Madrid coal mines, Cerrillos coal field, Santa Fe County, New Mexico (unpublished field project): Albuquerque, University of New Mexico, 22 pp.

Wieduwilt, W.G., 1980, Induced polarization and resistivity survey, Ortiz property, Santa Fe County, New Mexico: unpublished report for Gold Fields Mining Corporation by Mining Geophysical Surveys, Inc., 4 p.

Wilson, E.D., 1956, Mineralization in the Alpine, Gold Leaf, and Gypsy Queen areas of the Ortiz Mountains, New Mexico: unpublished report for Potter and Sims of Joplin, Missouri, 36 pp.

Wislizenus, A., 1848, Memoir of a tour to northern Mexico: Senate Miscellaneous Document, No. 26, 30th Congress, 1st Session.

Woodward, L.A., 1979, Tectonics of central-northern New Mexico: New Mexico Geological Society, Guidebook 30, p. 101-106.

Woodward, L.A., 1982, Tectonic framework of Albuquerque country: New Mexico Geological Society, Guidebook 33, p. 141-146.

Woodward, L.A., 1984, Basement control of Tertiary intrusions and associated mineral deposits along Tijeras-Cañoncito fault system, New Mexico: Geology, v. 12, p. 531-533.

Woodward, L.A., 1987, Tectonic map of the Ortiz porphyry belt and Tijeras fault system: unpublished report for Long Lac Mineral Exploration.

Woodward, L.A., and Ingersoll, R.V., 1979, Phanerozoic tectonic setting of Santa Fe Country: New Mexico Geological Society, Guidebook 30.

Woodward, L.A., Ingersoll, R.V., Fitch, D.C., and Hutchinson, P., 1979, Second day optional road log number 2, New Mexico highway 14 to Gold Fields Mining Corporation's Ortiz Mine: New Mexico Geological Society, Guidebook 30, p. 27-28.

Wright, A., 1983, The Ortiz gold deposit (Cunningham Hill) – geology and exploration: Nevada Bureau of Mines and Geology, Report 36, p. 42-51.

Yung, M.B., and McCaffrey, R.S., 1903, The ore deposits of the San Pedro district, New Mexico: American Institue of Mining and Metallurgical Engineering Transactions, v. 33, p. 350-362.

APPENDIX I. Major oxide and trace element analyses, Ortiz Mountains (from Coles, 1990).

	Sample ID	Rock Type	Altera-tion	SiO2 %	TiO2 %	Al2O3 %	Fe2O3 %	FeO %	MnO %	MgO %	CaO %	Na2O %	K2O %	P2O5 %	LOI %	Totals %	CO2 %	H20+ %	S %	Ag (ppm)	As (ppm)	Au (ppb)	B (ppm)	Ba (ppm)
Trachytic latite porphyry	OC-49 722	Ttlp	S/C	62.50	0.38	19.60	0.88	0.60	0.08	0.32	0.61	5.55	5.68	0.29	1.60	98.09	0.51	1.10	0.59	0.1	5.6	<2	17	1800
	OC-49 763.7	Ttlp	S/C	57.90	0.38	18.50	1.41	0.60	0.07	1.36	2.47	3.60	7.51	0.28	3.80	97.88	3.40	0.36	1.04	0.1	19.0	8	18	2100
	OC-58 714.5	Ttlp	S/C	57.50	0.37	18.40	0.24	0.65	0.09	1.43	3.32	4.73	6.06	0.26	4.40	97.45	4.10	0.25	0.33	0.1	2.5	<2	19	1700
	OC-55 136	Ttlp	A/S	64.00	0.40	20.90	0.02	0.15	<.02	0.12	0.38	6.20	4.95	0.26	1.10	98.48	<.02	0.94	<.02	0.6	2.0	3	18	1800
	DJ-62	Ttlp	S/W	59.00	0.58	21.20	3.09	0.20	0.19	0.23	0.23	5.40	5.69	0.33	1.90	98.04	<.02	1.70	<.02	0.1	2.6	<2	51	1100
	DJ-82	Ttlp	S/C	56.90	0.45	19.30	0.91	0.65	0.10	0.40	4.66	4.41	5.16	0.28	4.80	98.02	3.70	1.01	0.19	0.9	<.5	<2	81	1000
Trachyte porphyry	OC-12 506.8	Ttp	S/A	56.43	0.25	19.70	0.51	0.60	0.23	0.30	3.69	3.55	8.54	0.24	3.90	97.94	2.96	0.58	0.03	1.9	3.3	<2	72	980
	OC-27 2158	Ttp	S/A	61.00	0.17	19.20	1.55	0.25	0.02	0.29	1.89	5.26	7.14	0.20	2.20	99.17	1.46	1.15	1.08	1.4	182.0	13	26	1200
	OC-36 1927	Ttp	S/A	62.00	0.17	18.20	0.44	0.40	0.03	0.19	1.84	2.53	10.80	0.24	1.70	98.54	1.53	0.42	0.35	0.2	5.3	<2	16	1700
	OC-44 85	Ttp	S	60.40	0.49	20.60	2.70	0.25	<.02	0.22	0.12	5.17	6.54	0.25	2.40	99.14	<.02	2.13	1.76	2.8	153.0	588	57	1500
	OC-45 152.6	Ttp	S	60.60	0.44	22.60	0.52	0.15	<.02	0.22	0.23	4.37	5.88	0.21	3.30	98.52	<.02	2.19	0.02	2.3	16.0	<2	33	1400
Tephri-phonolite porphyry	IG-63	Ttpp	F	51.87	0.77	20.15	3.70	2.50	0.20	2.03	6.21	4.50	5.06	0.37	2.33	99.69	0.02	2.08	0.04	0.2	8.2	6	116	1900
Quartz-latite porphyry	IG-43	Tqlp	F	62.40	0.38	17.00	2.74	0.85	0.06	0.86	3.14	5.06	3.96	0.42	1.70	98.57	0.50	0.96	<.02	0.1	<.5	13	12	1700
	OCN-8 249.5	Tqlp	F	62.72	0.41	16.79	2.40	1.30	0.06	0.74	2.97	4.73	4.36	0.15	2.46	99.09	0.84	1.08	0.03	0.2	1.1	36	40	1700
	OCN-10 431	Tqlp	F	64.23	0.41	17.43	2.15	0.90	0.08	0.51	3.12	6.19	3.60	0.14	0.46	99.22	0.02	0.33	0.03	0.2	0.7	10	40	1700
Quartz-trachyte porphyry	DJ-78	Tqtp	S	65.90	0.22	16.90	1.28	0.20	0.05	0.25	2.23	4.79	4.29	0.41	2.60	99.12	1.55	0.99	<.02	0.1	0.9	<2	15	1400
	DJ-102	Tqtp	W/B	68.80	0.20	16.80	0.40	0.15	0.02	0.15	1.32	5.13	4.66	0.25	0.60	98.48	0.02	0.61	<.02	0.1	0.9	9	12	1900
	IG-96	Tqtp	W	67.76	0.25	17.26	0.95	0.25	0.06	0.05	0.46	6.61	4.89	0.04	0.91	99.49	<.02	0.77	<.02	0.2	3.2	2	46	1800
Quartz monzonite	IG-46	Tqmd	F	64.36	0.42	16.30	2.17	1.20	0.08	1.18	4.00	4.72	2.40	0.32	0.60	97.75	<.02	0.60	<.02	0.1	<.5	<2	<10	1300
	IG-47	Tqmd	F	59.00	0.78	16.70	3.34	2.05	0.19	2.08	6.02	4.04	1.75	0.65	0.70	97.30	0.09	0.52	<.02	0.5	<.5	<2	<10	1400
	IG-48	Tqmd	F	60.90	0.70	16.70	3.53	2.20	0.14	2.12	5.53	3.76	2.56	0.54	0.50	99.18	<.02	0.45	<.02	0.1	0.9	<2	11	1200
	IG-62	Tqmd	F	62.26	0.70	17.01	3.45	1.65	0.16	1.50	4.97	4.06	2.17	0.27	0.85	99.05	<.02	0.35	0.03	0.2	1.4	4	59	1200
	IG-69	Tqmd	F	60.62	0.89	16.52	4.30	1.95	0.11	2.16	5.58	4.32	2.64	0.34	0.61	100.04	<.02	0.49	<.02	0.2	0.7	3	56	1100
	IG-93	Tqmd	F	58.74	1.02	16.42	4.10	2.25	0.15	2.43	6.46	3.96	2.40	0.34	0.82	99.09	0.21	0.58	<.02	0.2	0.5	3	55	1000
Latite porphyry	IG-92	Tlp	F	61.82	0.33	19.29	2.15	0.50	0.11	0.11	1.93	5.42	7.13	0.04	0.45	99.28	<.02	0.37	<.02	0.2	0.7	<2	52	3100
	OCN-11 409.5	Tlp	F	61.35	0.49	18.29	3.20	0.40	0.08	0.41	2.81	6.38	4.78	0.14	0.93	99.26	0.14	0.65	<.02	0.1	1.5	10	49	1800
Foid-bearing trachyte porphyry	OC-27 2087.6	Tftp	H	59.80	0.17	19.00	1.65	0.70	0.06	0.17	3.63	7.28	3.72	0.23	2.50	99.11	1.84	0.84	0.02	1.3	3.9	<2	305	540
	OC-41 2249.5	Tftp	H	60.10	0.19	18.90	2.42	0.65	0.05	0.25	2.63	6.11	4.84	0.22	2.00	98.36	1.31	0.38	0.67	0.6	4.3	<2	121	990
	OC-27 2224.8	Tftp	M	60.90	0.17	19.60	1.62	0.70	0.34	0.11	1.22	8.31	5.09	0.35	0.70	99.11	0.09	0.62	0.06	3.5	30.0	<2	191	80
	OC-41 2238	Tftp	M	61.00	0.20	18.90	2.11	0.90	0.07	0.18	2.45	6.13	4.85	0.21	1.60	98.60	0.82	0.01	0.05	0.6	8.3	<2	53	560
Latite-trachyte porphyry	OC-40 314.5	Tltp	B/S	56.50	0.81	20.90	3.63	0.50	0.07	1.52	1.15	5.51	4.20	0.52	3.40	98.71	<.02	2.11	<.02	1.1	70.1	12	36	1400
	OC-45 404	Tltp	B/S	51.30	0.73	18.60	3.54	4.55	0.29	1.75	0.69	4.19	5.13	0.50	6.90	98.17	1.93	4.64	2.31	1.1	41.0	17	42	1600
	OC-53 465.5	Tltp	B/S	56.30	0.81	19.90	4.02	0.50	0.13	2.03	1.22	5.28	3.60	0.49	3.90	98.18	<.02	2.08	0.02	0.1	65.1	<2	28	1300
	IG-32	Tap	F	61.60	0.46	17.20	1.45	2.75	0.13	1.60	5.19	4.34	1.94	0.40	1.40	98.46	0.16	1.07	0.11	0.1	<.5	2	10	1300
	IG-66	Tap	F	59.98	0.98	17.32	3.45	1.75	0.19	1.51	5.17	4.67	3.59	0.31	1.00	99.92	0.14	0.59	0.02	0.2	2.1	3	59	1400
	IG-91	Tap	F	63.70	0.48	17.77	2.25	1.55	0.12	0.99	4.03	5.23	2.52	0.18	1.01	99.83	0.09	0.78	0.02	<.1	1.1	<2	54	1400
	IG-94	Tap	F	58.80	0.81	16.78	3.55	1.95	0.16	1.75	5.68	3.82	2.67	0.31	3.17	99.45	0.26	2.43	0.02	0.2	0.8	3	48	1200
	IG-95	Tap	F	61.96	0.78	16.47	1.21	2.95	0.13	1.23	4.70	4.61	3.50	0.22	1.25	99.01	0.15	1.09	0.17	0.2	<.5	3	46	1400
	IG-97	Tap	F	61.15	0.69	17.43	3.00	1.70	0.07	1.65	5.46	4.75	2.42	0.27	0.96	99.55	<.02	0.71	<.02	0.2	0.8	5	35	1200
	DJ-17	Tap	P	59.70	0.55	17.20	1.53	2.20	0.07	2.27	6.82	3.78	1.51	0.38	1.90	97.91	0.56	1.10	<.02	0.1	2.0	91	<10	1100
	DJ-34	Tap	P	64.40	0.49	16.80	2.62	1.55	0.03	1.46	2.79	4.62	2.24	0.54	1.70	99.24	0.03	1.34	<.02	0.7	<.5	<2	<10	1200
	DJ-117	Tap	P	58.30	0.70	17.30	1.09	4.90	0.15	2.22	7.02	3.57	1.52	0.39	1.20	98.36	0.05	1.07	0.16	0.1	11.0	<2	<10	900
	OC-13 1066.6	Tap	P	63.40	0.46	16.70	0.70	2.70	0.07	1.41	4.02	4.79	2.71	0.38	1.00	98.34	0.41	0.51	0.27	0.3	7.4	<2	15	1300
	OC-12 377	Tap	P	57.90	0.60	16.60	1.20	4.30	0.18	2.24	5.10	4.66	3.16	0.44	1.60	97.98	1.00	0.62	0.20	0.1	1.4	<2	12	1700
	OC-12 471	Tap	P	63.10	0.38	17.10	0.55	3.40	0.09	0.89	3.11	4.95	2.96	0.31	0.70	97.54	<.02	0.60	0.18	0.3	1.5	<2	14	1600
	OC-16 471.7	Tap	P	59.20	0.71	17.10	0.93	4.75	0.14	1.67	5.00	3.78	2.61	0.46	1.60	97.95	0.01	1.00	0.09	0.7	8.0	<2	<10	1400
	OC-31 564	Tap	P	63.80	0.32	14.40	0.38	2.05	0.09	0.84	3.49	4.48	3.54	0.44	4.40	98.23	3.25	1.14	0.25	0.0	42.0	4	35	710
	OC-40 661.7	Tap	P	64.80	0.32	16.10	0.54	2.05	0.07	0.83	2.67	4.82	3.28	0.33	2.80	98.61	1.62	1.08	0.12	0.1	6.2	<2	19	1800

	Sample ID	Rock Type	Altera-tion	SiO2 %	TiO2 %	Al2O3 %	Fe2O3 %	FeO %	MnO %	MgO %	CaO %	Na2O %	K2O %	P2O5 %	LOI %	Totals %	CO2 %	H20+ %	S %	Ag (ppm)	As (ppm)	Au (ppb)	B (ppm)	Ba (ppm)
Andesite porphyry	OC-50 1488.8	Tap	P	65.10	0.32	15.70	0.15	1.40	0.08	1.01	2.00	5.46	3.27	0.29	3.40	98.18	2.62	0.47	0.15	0.1	2.6	6	19	1500
	DJ-13	Tap	B	57.80	0.70	17.00	2.99	2.70	0.17	1.99	6.17	3.68	1.85	0.44	3.30	98.79	1.69	1.52	0.03	0.3	1.6	10	14	1600
	OC-4 498.3	Tap	B	62.80	0.57	16.60	0.83	4.00	0.08	1.62	2.88	5.15	2.53	0.39	1.20	98.65	0.02	1.03	0.33	0.1	1.5	<2	14	1300
	OC-17 831	Tap	B	58.10	0.61	16.70	0.89	6.95	0.18	1.77	0.90	4.66	4.36	0.54	2.40	98.06	0.07	2.07	0.14	0.7	2.3	9	14	1600
	OC-34 111.8	Tap	B	63.40	0.85	19.00	0.46	0.25	<.02	0.20	0.68	3.76	6.94	0.41	2.00	97.95	<.02	1.45	<.02	1.4	10.0	16	27	2600
	OC-41 1501	Tap	B	63.90	0.44	16.50	0.74	3.10	0.05	1.30	3.58	4.16	2.81	0.36	1.60	98.54	0.76	0.48	0.32	0.1	<.5	<2	15	1500
	OC-49 99.5	Tap	B	62.90	0.42	16.60	0.96	3.40	0.06	1.17	3.00	4.72	2.73	0.35	1.70	98.01	0.30	0.80	0.29	0.1	5.6	<2	15	1300
	OC-67 782	Tap	B	64.00	0.56	16.70	1.77	3.45	0.06	1.62	4.03	4.11	1.93	0.37	1.00	99.60	0.08	0.68	0.05	0.1	1.8	<2	15	820
	OC-33 216	Tap	S/A	70.90	0.53	18.24	0.66	0.30	<.02	0.29	0.34	3.72	4.08	0.40	2.30	101.76	<.02	1.70	0.03	0.1	70.7	<2	75	1700
	OC-36 3349.7	Tap	S/A	67.40	0.48	19.50	0.15	0.20	<.02	0.14	0.62	3.32	3.76	0.37	3.30	99.24	<.02	2.70	0.06	1.5	5.2	<2	33	1800
	OC-36 608.2	Tap	S/A	66.00	0.57	17.50	1.37	0.15	0.03	0.33	0.54	6.06	3.55	0.39	1.80	98.29	<.02	1.47	0.12	0.7	3.5	49	30	950
	OC-44 107	Tap	S/A	69.00	0.42	17.50	0.16	0.25	<.02	0.22	0.18	4.34	3.06	0.24	2.50	97.87	<.02	2.09	0.77	1.1	119.0	160	42	1100
	OC-27 1514.7	Tap	S/C	61.10	0.46	17.00	0.74	4.25	0.12	0.79	1.04	3.52	2.84	0.40	5.50	97.76	2.17	2.63	0.29	0.3	2.5	5	28	1700
	OC-27 2227.6	Tap	S/C	65.20	0.33	16.60	1.99	0.30	0.02	0.18	2.25	7.04	1.97	0.28	2.10	98.26	1.44	1.32	1.57	0.1	512.0	28	19	720
	OC-36 850.8	Tap	S/C	66.70	0.32	16.10	0.60	1.40	0.07	0.59	1.06	4.82	4.10	0.29	2.50	98.55	1.54	0.99	0.19	0.1	113.0	40	34	1500
	OC-41 1056.4	Tap	S/C	64.70	0.49	18.40	0.53	0.75	0.02	0.74	1.36	2.70	4.40	0.37	4.30	98.76	1.04	2.33	0.11	0.1	0.6	17	51	1500
	OC-12 291	Tap	A	67.03	0.32	16.50	0.33	2.25	0.25	0.73	0.48	3.79	3.49	0.33	2.30	97.80	0.09	2.39	0.06	0.1	11.0	<2	40	970
	OC-16 594	Tap	A	59.10	0.57	17.40	2.86	3.45	0.26	0.40	0.67	7.87	0.30	0.41	4.90	98.19	0.04	4.55	1.60	2.1	86.2	31	19	<20
	OC-33 406.9	Tap	A	68.70	0.34	16.80	1.61	0.15	<.02	0.16	0.28	4.80	3.93	0.31	1.70	98.78	0.09	1.42	1.16	0.6	1180.0	130	35	960
	OC-34 371	Tap	A	66.30	0.80	18.70	0.04	0.20	<.02	0.15	0.69	5.01	4.43	0.44	1.40	98.16	<.02	1.04	0.04	0.7	15.0	6	35	2000
	OC-36 122.4	Tap	A	63.20	0.85	19.70	0.59	0.45	<.02	0.17	0.88	2.95	5.32	0.45	3.60	98.16	<.02	2.48	<.02	6.6	15.0	21	45	2400
	OC-50 1517	Tap	A	65.00	0.40	19.90	0.04	0.15	<.02	0.23	0.57	7.48	3.69	0.32	0.70	98.48	<.02	0.75	<.02	0.1	2.9	<2	11	1600
	OC-13 1058	Tap	A/C	62.60	0.55	17.10	1.35	1.80	0.05	1.02	2.48	3.36	4.07	0.40	4.40	99.18	2.29	1.36	0.38	0.3	1.6	<2	90	1200
	OC-45 1301.8	Tap	A/C	58.90	0.78	17.70	0.90	2.00	0.09	1.89	2.66	2.76	3.80	0.45	6.00	97.93	3.55	2.13	0.54	0.1	5.2	<2	73	330
	OC-41 1270	Tap	K	65.30	0.48	17.40	0.47	0.75	0.03	0.45	1.05	3.35	7.45	0.34	1.70	98.77	1.04	0.48	0.05	0.1	21.0	17	32	2300
	OC-41 1703.8	Tap	K	64.80	0.41	16.66	0.82	0.65	0.03	0.59	1.83	6.17	3.96	0.34	2.30	98.56	1.97	0.01	0.51	0.1	593.0	84	40	1700
	OC-50 1378	Tap	K	66.40	0.38	17.60	1.78	1.40	<.02	0.10	0.55	6.54	6.15	0.46	0.50	101.86	0.09	0.31	0.05	0.1	0.7	<2	11	2000
	DJ-32	Tap	TM	59.40	0.66	18.20	0.52	1.40	0.05	1.90	10.10	3.74	0.22	0.44	1.10	97.73	0.05	0.56	0.02	0.3	<.5	<2	<10	100
	DJ-61	Tap	TM	67.30	0.33	16.70	0.60	0.40	0.02	0.50	3.08	4.10	4.62	0.29	0.40	98.34	0.02	0.46	<.02	0.3	<.5	2	<10	1500
Augite monzonite & hornblende-augite monzodiorite	IG-50	Tamd	F	55.23	1.24	18.10	4.67	2.10	0.17	2.30	7.54	4.25	2.92	0.51	0.30	99.33	<0.02	0.26	<.02	1.1	<.5	<2	<10	1300
	IG-54	Tamd	F	56.10	0.91	18.30	3.47	2.40	0.15	1.78	6.04	4.58	3.55	0.49	0.70	98.47	<0.02	0.60	<.02	0.7	<.5	<2	19	1600
	IG-64	Tamd	F	58.56	0.86	18.57	3.75	1.45	0.21	1.25	5.58	5.30	3.59	0.26	0.48	99.86	<0.02	0.24	<.02	0.2	2.9	5	65	2300
	IG-44	Tam	F	54.10	1.11	18.60	4.00	2.65	0.21	2.03	7.19	4.61	3.49	0.55	0.30	98.84	<0.02	0.26	<.02	1.1	3.3	<2	38	2000
	IG-55	Tam	F	54.50	1.07	18.90	3.47	2.40	0.21	1.72	6.60	4.72	3.72	0.48	0.30	98.09	0.02	0.24	<.02	1.3	2.3	<2	26	2300
	IG-90	Tam	F	55.89	0.89	19.41	3.55	2.10	0.24	1.36	5.81	5.04	4.41	0.27	0.67	99.64	0.05	0.40	<.02	0.2	4.2	11	84	2000
	IG-101	Tam	F	53.85	0.88	18.93	3.60	2.25	0.21	1.63	4.50	5.72	4.88	0.37	2.68	99.50	0.17	2.48	0.02	0.2	7.5	<2	59	1900
Phonotephrite porphyry & phonotephrite	IG-98	Tptp	F	50.51	0.86	19.14	3.50	3.20	0.19	2.40	6.80	4.42	4.42	0.39	3.47	99.30	0.09	3.07	0.02	0.2	5.0	<2	52	1900
	IG-99	Tpt	F	47.16	1.77	18.32	5.40	2.95	0.21	2.48	8.08	4.41	4.21	0.60	3.47	99.06	<.02	3.33	<.02	<.1	5.8	<2	38	2800
	IG-100	Tpt	F	47.65	1.75	18.26	4.30	3.85	0.21	2.49	7.99	4.57	4.01	0.59	3.75	98.82	0.09	3.60	0.02	<.1	6.1	4	47	2900

APPENDIX I. Major oxide a

	Sample ID	Be (ppm)	Bi (ppm)	Br (ppm)	Cd (ppm)	Ce (ppm)	Co (ppm)	Cr (ppm)	Cs (ppm)	Cu (ppm)	Eu (ppm)	Fe (%)	Fe (ppm)	Hf (ppm)	Hg (ppb)	Ir (ppb)	La (ppm)	Li (ppm)	Lu (ppm)	Mn (ppm)	Mo (ppm)	Na (%)	Nb (ppm)	Ni (ppm)	Pb (ppm)
Trachytic latite porphyry	OC-49 722	4	<2	<2	<1	110	5	29	4.1	<1	1	0.8	510	5	<5	<50	71	6	1.1	600	4	3.17	52	3	20
	OC-49 763.7	3	<2	<2	<1	110	5	41	5.1	1	<1	1.1	510	5	<5	<50	65	8	1.0	533	3	2.00	48	1	18
	OC-58 714.5	3	<2	<2	<1	110	3	19	4.1	<1	1	0.8	290	5	10	<50	70	4	0.9	702	<1	2.64	49	<1	<2
	OC-55 136	3	<2	<2	<1	110	3	19	4.1	<1	<1	<.2	290	5	<5	<50	71	57	0.9	15	<1	3.19	57	<1	13
	DJ-62	5	<2	<2	<1	120	11	13	1.9	69	1	1.7	790	5	10	<50	51	46	1.5	1261	4	3.10	88	7	78
	DJ-82	4	<2	<2	<1	92	5	7	2.7	37	1	1.0	1100	7	<5	<50	55	38	1.7	740	6	2.67	86	<1	21
Trachyte porphyry	OC-12 506.8	3	<2	<2	<1	170	1	9	5.6	9	1	0.9	380	8	<5	<50	130	26	2.6	1673	<1	1.90	105	<1	28
	OC-27 2158	5	8	2.2	<1	290	5	19	5.4	13	2	1.0	430	19	<5	<50	170	9	9.0	135	<1	2.90	150	3	59
	OC-36 1927	2	<2	<2	<1	110	1	51	3.9	1	<1	0.6	120	9	<5	<50	77	12	1.7	282	3	1.50	54	1	27
	OC-44 85	4	<2	2.5	<1	66	13	33	3.8	274	1	1.8	420	7	<5	<50	30	16	1.4	99	54	2.94	87	5	256
	OC-45 152.6	2	<2	<2	<1	150	5	17	4.3	61	<1	0.4	460	8	<5	<50	84	12	1.8	89	<1	2.55	125	3	97
Tephri-phonolite porphyry	IG-63	4	3	2.1	<1	93	25	57	14.0	97	2	---	720	5	5	<50	65	43	<.2	---	5	----	56	29	47
Quartz-latite porphyry	IG-43	2	<2	<2	<1	73	5	61	1.0	155	<1	2.3	450	5	<5	<50	43	25	0.6	497	2	3.00	27	1	23
	OCN-8 249.5	3	3	<2	<1	76	7	53	3.9	129	2	---	850	6	5	<50	47	24	<.2	---	117	----	30	11	13
	OCN-10 431	3	3	<2	<1	79	7	47	2.0	15	2	---	520	6	<5	<50	50	16	<.2	---	10	----	31	13	21
Quartz-trachyte porphyry	DJ-78	2	<2	<2	<1	86	1	39	1.2	13	<1	1.0	700	6	<5	<50	53	9	0.6	485	1	2.68	39	1	26
	DJ-102	3	<2	<2	<1	76	1	41	1.8	13	<1	0.3	480	5	<5	<50	56	11	0.6	131	1	3.02	34	<1	18
	IG-96	2	7	<2	<1	92	3	33	1.1	5	<1	---	130	9	<5	<50	67	8	0.3	---	1	----	45	1	2
Quartz monzonite	IG-46	2	<2	<2	<1	65	7	55	0.9	21	<1	2.1	360	4	<5	<50	31	9	0.5	545	<1	2.78	25	9	14
	IG-47	2	2	<2	<1	91	13	53	1.3	33	<1	3.8	570	6	<5	<50	44	8	0.6	1307	2	2.50	28	5	29
	IG-48	2	<2	<2	<1	61	15	31	2.4	31	1	3.4	450	4	<5	<50	35	24	0.3	1042	<1	2.18	27	<1	67
	IG-62	2	3	<2	<1	73	17	67	0.7	17	<1	---	470	5	5	<50	43	7	0.3	---	1	----	22	21	25
	IG-69	2	5	<2	<1	88	31	97	0.5	37	<1	---	610	6	<5	<50	56	8	0.4	---	7	----	30	29	31
	IG-93	2	3	<2	<1	95	23	120	1.2	31	3	---	610	6	5	<50	55	9	0.5	---	1	----	27	25	21
Latite porphyry	IG-92	2	5	<2	<1	87	5	51	1.3	7	1	---	100	5	5	<50	47	5	0.3	---	1	----	47	7	17
	OCN-11 409.5	3	15	<2	<1	100	9	51	1.7	37	2	---	280	7	5	<50	65	7	0.4	---	9	----	33	13	3
Foid-bearing trachyte porphyry	OC-27 2087.6	14	<2	<2	<1	230	1	9	404.0	11	<1	1.4	4900	21	<5	<50	170	12	<5.4	392	<1	4.08	140	1	26
	OC-41 2249.5	13	<2	<2	<1	180	5	43	7.4	1	2	1.8	3900	17	<5	<50	130	11	<5.8	463	6	3.39	125	1	20
	OC-27 2224.8	22	<2	9.0	<1	230	<1	39	73.0	11	<1	1.3	3800	18	<5	<50	160	234	<8	2535	<1	4.53	150	<1	1409
	OC-41 2238	22	<2	<2	<1	180	3	37	8.6	19	<1	1.6	3600	16	<5	<50	1303	18	<5.9	503	6	3.61	125	3	70
Latite-trachyte porphyry	OC-40 314.5	5	<2	<2	<1	150	15	33	12.0	15	3	2.6	280	6	<5	<50	86	38	1.3	493	<1	3.12	77	15	27
	OC-45 404	3	9	<2	<1	190	23	29	6.5	214	1	4.8	1550	5	5	<50	120	868	1.8	1952	1	2.23	71	17	56
	OC-53 465.5	4	<2	<2	<1	130	17	55	4.7	7	2	3.1	670	6	<5	<50	67	29	1.2	981	2	3.21	77	15	18
	IG-32	2	<2	<2	<1	48	9	51	<.5	17	<1	3.0	310	4	<5	<50	26	16	0.4	911	1	2.71	17	1	9
	IG-66	3	7	<2	<1	120	19	59	1.7	13	2	---	740	8	<5	<50	71	9	0.4	---	1	----	35	17	23
	IG-91	2	3	<2	<1	65	13	73	<.5	7	2	---	32	5	<5	<50	37	7	0.3	---	1	----	21	15	2
	IG-94	2	3	<2	<1	87	17	31	2.2	15	1	---	560	4	5	<50	50	11	0.3	---	1	----	24	17	19
	IG-95	2	5	<2	<1	110	15	47	1.6	17	2	---	720	8	<5	<50	66	8	0.4	---	1	----	40	17	19
	IG-97	2	7	<2	<1	62	17	43	<.5	25	<1	---	440	5	5	<50	37	5	0.4	---	1	----	21	7	15
	DJ-17	2	<2	<2	<1	37	11	61	0.6	764	<1	2.4	530	3	20	<50	19	13	0.3	553	1	2.36	17	9	12
	DJ-34	2	<2	<2	<1	72	7	73	0.5	21	1	2.7	460	3	30	<50	38	14	0.5	199	<1	2.77	26	7	16
	DJ-117	2	<2	<2	<1	57	17	39	<.5	33	2	4.2	450	3	<5	<50	29	29	0.5	1070	1	2.17	13	7	14
	OC-13 1066.6	2	5	<2	<1	61	5	77	8.9	27	2	2.0	450	3	<5	<50	31	25	0.4	545	1	1.80	25	<1	69
	OC-12 377	3	<2	<2	<1	99	11	61	1.1	33	1	4.1	450	5	<5	<50	55	19	0.7	1363	2	2.83	31	13	31
	OC-12 471	2	<2	<2	<1	87	9	61	2.3	29	1	2.9	380	5	<5	<50	46	40	0.7	760	1	3.08	28	3	32
	OC-16 471.7	2	8	<2	<1	67	13	57	4.1	27	1	4.1	460	4	<5	<50	37	40	0.5	994	<1	2.24	21	3	20
	OC-31 564	1	<2	<2	<1	35	5	71	3.1	27	<1	1.4	290	3	<5	<50	20	23	0.2	702	1	2.20	21	9	15
	OC-40 661.7	1	<2	<2	<1	30	5	75	3.9	5	<1	1.6	180	3	<5	<50	20	31	0.4	553	<1	2.73	19	5	8

	Sample ID	Be (ppm)	Bi (ppm)	Br (ppm)	Cd (ppm)	Ce (ppm)	Co (ppm)	Cr (ppm)	Cs (ppm)	Cu (ppm)	Eu (ppm)	Fe (%)	Fe (ppm)	Hf (ppm)	Hg (ppb)	Ir (ppb)	La (ppm)	Li (ppm)	Lu (ppm)	Mn (ppm)	Mo (ppm)	Na (%)	Nb (ppm)	Ni (ppm)	Pb (ppm)
Andesite porphyry	OC-50 1488.8	2	<2	<2	<1	64	3	75	3.0	47	1	1.2	760	4	5	<50	31	8	0.3	591	4	3.22	22	9	<2
	DJ-13	2	<2	<2	<1	56	13	55	2.8	37	2	4.2	670	3	20	<50	33	37	0.4	1239	1	2.31	20	5	34
	OC-4 498.3	2	<2	<2	<1	65	11	73	6.9	41	<1	3.5	480	4	<5	<50	35	32	0.5	616	3	2.97	24	5	15
	OC-17 831	1	2	<2	<1	78	13	29	20.0	27	2	5.8	550	3	5	<50	43	41	0.5	1476	<1	2.74	26	3	30
	OC-34 111.8	1	4	<2	<1	73	9	49	2.7	43	<1	0.5	400	4	<5	<50	34	153	0.5	37	<1	2.05	30	1	27
	OC-41 1501	2	<2	<2	<1	65	7	59	10.0	23	<1	2.9	190	4	<5	<50	31	43	0.4	344	2	2.49	24	7	22
	OC-49 99.5	2	<2	2.4	<1	52	11	73	5.0	13	<1	2.7	470	3	<5	<50	29	25	0.4	467	<1	2.40	23	5	25
	OC-67 782	2	<2	<2	<1	66	9	69	8.9	56	<1	2.8	600	4	<5	<50	36	15	0.4	455	2	2.56	27	5	20
	OC-33 216	3	2	<2	<1	65	5	37	5.4	35	1	0.6	310	4	<5	<50	34	130	0.5	87	<1	2.13	29	1	18
	OC-36 3349.7	3	4	<2	20	51	11	41	2.9	11	1	<.2	190	5	5	<50	21	147	0.5	55	<1	2.01	27	5	512
	OC-36 608.2	2	<2	<2	9	63	13	63	3.0	69	<1	1.0	360	4	10	<50	33	11	0.4	292	3	3.58	25	7	312
	OC-44 107	2	4	<2	<1	54	7	57	2.9	161	<1	0.9	520	4	5	<50	27	36	0.4	29	1	2.54	15	3	1204
	OC-27 1514.7	3	<2	<2	<1	57	9	61	3.6	23	<1	3.7	290	3	<5	<50	31	44	0.4	921	4	2.15	24	7	21
	OC-27 2227.6	1	<2	4.8	<1	34	5	63	1.4	23	<1	1.3	260	3	<5	<50	14	6	0.6	197	2	4.27	22	<1	13
	OC-36 850.8	1	<2	<2	2	55	7	69	2.5	35	<1	1.4	290	2	<5	<50	28	12	0.3	541	2	2.94	18	9	130
	OC-41 1056.4	4	5	<2	<1	71	11	53	15.0	37	<1	1.0	900	4	<5	<50	35	258	0.7	378	2	1.50	29	13	18
	OC-12 291	1	2	<2	<1	42	9	39	3.5	15	<1	1.8	350	3	<5	<50	23	23	0.4	1741	4	2.30	20	5	18
	OC-16 594	2	8	<2	9	110	31	65	1.1	159	<1	4.1	380	5	30	<50	64	74	0.9	1747	85	4.28	30	5	233
	OC-33 406.9	1	4	10.0	<1	22	9	57	2.6	288	<1	1.2	170	<1	<5	<50	18	10	0.5	47	<1	2.53	20	5	292
	OC-34 371	2	<2	<2	<1	67	15	67	2.3	25	2	<.2	260	4	<5	<50	41	220	0.4	45	1	2.75	26	17	<2
	OC-36 122.4	2	4	<2	<1	120	9	23	3.7	115	2	0.9	450	4	<5	<50	61	30	0.7	59	<1	1.80	27	3	97
	OC-50 1517	2	<2	<2	<1	43	3	41	2.2	<1	<1	<.2	830	4	<5	<50	26	6	0.2	33	<1	4.45	26	1	<2
	OC-13 1058	4	<2	<2	<1	59	9	41	6.2	29	2	2.4	430	3	<5	<50	30	544	0.4	151	3	2.85	26	9	33
	OC-45 1301.8	5	<2	<2	<1	88	13	33	18.0	77	<1	1.7	2500	3	10	<50	52	64	0.5	758	7	1.40	23	5	6
	OC-41 1270	1	<2	<2	<1	56	7	39	4.2	37	<1	1.0	310	4	<5	<50	26	15	<.2	270	2	2.07	29	5	22
	OC-41 1703.8	2	7	5.6	<1	34	5	59	1.5	39	<1	1.1	260	2	<5	<50	11	6	0.4	240	3	3.48	20	5	102
	OC-50 1378	1	<2	<2	<1	26	1	43	2.1	<1	<1	<.2	220	4	<5	<50	10	2	0.4	39	3	3.66	24	5	<2
	DJ-32	2	<2	<2	<1	61	5	49	<.5	177	1	1.2	300	3	25	<50	30	12	0.6	364	1	2.19	23	9	6
	DJ-61	2	<2	<.2	<1	50	3	57	<.5	71	<1	0.4	140	3	20	<50	31	10	0.4	159	2	2.73	24	3	13
Augite monzonite & hornblende-augite monzodiorite	IG-50	2	11	<2	<1	100	21	33	1.7	29	2	4.6	730	6	<5	<50	54	31	0.6	1273	<1	2.58	36	5	35
	IG-54	4	<2	<2	<1	110	17	27	5.5	71	2	3.7	1050	7	<5	<50	63	27	0.9	1162	<1	2.61	43	3	48
	IG-64	3	3	<2	<1	120	17	65	6.1	17	<1	---	660	7	<5	<50	76	13	0.4	---	1	---	41	21	35
	IG-44	4	<2	<2	<1	120	21	41	6.3	55	1	4.4	700	5	<5	<50	64	25	0.9	1522	2	2.72	41	3	47
	IG-55	3	<2	<2	<1	110	19	37	5.7	63	1	3.4	900	5	<5	<50	59	28	0.7	1693	1	2.33	41	1	47
	IG-90	4	3	<2	<1	150	19	43	7.4	45	1	---	720	8	5	<50	91	13	0.5	---	1	---	60	17	43
	IG-101	4	7	<2	<1	150	21	19	15.0	61	<1	---	920	10	5	<50	92	18	0.4	---	3	---	66	19	47
Phonotephrite porphyry & phonotephrite	IG-98	4	3	<2	<1	110	25	35	13.0	99	3	---	820	5	<5	<50	72	27	0.2	---	1	---	50	27	41
	IG-99	3	5	<2	<1	140	37	17	9.3	75	2	---	820	7	<5	<50	82	13	0.3	---	3	---	63	25	47
	IG-100	3	7	<2	<1	140	37	17	12.0	85	3	---	820	6	5	<50	82	13	0.3	---	3	---	63	23	49

	Sample ID	Rb (ppm)	Sb (ppm)	Sc (ppm)	Se (ppm)	Sm (ppm)	Sn (ppm)	Sr (ppm)	Ta (ppm)	Tb (ppm)	Te (ppm)	Th (ppm)	Tl (ppm)	U (ppm)	V (ppm)	W (ppm)	Y (ppm)	Yb (ppm)	Zr (ppm)	Zn (ppm)
Trachytic latite porphyry	OC-49 722	330	0.6	1.3	2	6.0	<5	415	2.0	0.6	<.2	36.5	1.8	11.0	38	4	33	3	310	9
	OC-49 763.7	415	0.8	1.5	2	6.0	<5	435	2.0	0.7	<.2	36.0	2.3	11.0	36	3	44	3	290	9
	OC-58 714.5	350	0.4	1.7	1	5.9	7	400	1.9	0.7	<.2	34.3	1.8	9.4	40	1	39	3	290	7
	OC-55 136	240	0.4	1.5	<1	6.1	<5	470	1.9	0.7	<.2	37.4	1.5	10.0	33	<1	26	3	320	25
	DJ-62	195	1.7	2.0	<1	5.5	5	220	4.0	0.8	<.2	52.8	1.0	13.0	79	4	25	4	350	113
	DJ-82	175	1.4	1.0	1	5.9	6	260	4.5	0.9	<.2	56.2	1.1	16.0	33	4	25	4	400	15
Trachyte porphyry	OC-12 506.8	415	0.8	0.4	<1	5.3	6	145	4.1	0.5	<.2	110.0	1.8	26.4	17	1	41	5	570	19
	OC-27 2158	375	1.2	0.6	<1	5.9	6	265	2.0	0.8	<.2	222.0	1.0	92.9	21	4	62	11	1050	9
	OC-36 1927	465	0.6	0.5	<1	2.5	<5	335	1.1	<.5	<.2	55.8	1.5	17.0	3	<1	36	3	400	29
	OC-44 85	275	1.4	1.2	<1	3.6	<5	330	4.9	0.7	<.2	60.1	1.1	14.0	3	17	45	3	390	131
	OC-45 152.6	295	2.2	3.9	<1	7.8	9	235	7.0	1.1	<.2	95.9	1.1	19.0	7	8	45	6	530	45
Tephri-phonolite porphyry	IG-63	125	1.7	8.1	3	9.0	<5	1375	3.7	0.9	<.2	41.6	<.2	10.0	158	3	14	2	135	99
Quartz-latite porphyry	IG-43	105	0.2	3.6	2	6.1	<5	705	1.2	0.8	<.2	19.0	<.2	4.2	33	<1	17	3	160	77
	OCN-8 249.5	115	0.5	3.6	1	7.0	<5	680	1.6	0.9	<.2	46.0	<.2	10.0	56	3	11	<2	165	41
	OCN-10 431	84	0.3	3.4	1	8.3	5	735	1.9	1.0	<.2	22.0	<.2	5.3	52	4	10	2	160	71
Quartz-trachyte porphyry	DJ-78	140	0.9	0.8	<1	3.5	<5	320	1.5	<.5	<.2	18.0	1.1	4.4	8	<1	14	<2	295	51
	DJ-102	145	0.7	0.8	<1	2.3	<5	405	1.3	<.5	<.2	21.1	1.1	4.5	11	<1	9	<2	225	35
	IG-96	135	0.2	1.1	2	4.8	<5	470	2.3	<.5	<.2	21.2	0.4	4.4	24	<1	12	2	300	27
Quartz monzonite	IG-46	44	<.1	5.4	1	5.5	<5	815	1.7	0.9	<.2	7.9	<.2	2.2	43	2	16	2	135	51
	IG-47	33	<.1	9.5	<1	8.4	<5	785	1.8	1.1	<.2	8.2	<.2	2.3	92	1	26	4	160	91
	IG-48	70	0.2	10.0	<1	5.8	<5	565	1.1	0.9	<.2	11.0	0.2	1.6	94	<1	21	3	175	81
	IG-62	55	0.4	7.1	2	8.3	7	680	1.6	0.9	<.2	11.0	0.2	1.6	86	<1	11	2	135	75
	IG-69	69	0.2	11.0	<1	10.0	6	715	2.4	1.3	<.2	12.0	<.2	3.2	144	<1	14	3	160	65
	IG-93	48	0.2	13.0	2	11.0	<5	760	2.6	1.4	<.2	12.0	<.2	2.7	158	<1	18	3	160	63
Latite porphyry	IG-92	92	1.0	1.0	<1	7.1	<5	1070	2.5	0.8	<.2	20.3	<.2	3.0	64	<1	12	2	135	47
	OCN-11 409.5	101	0.3	2.5	2	10.0	8	795	1.9	1.2	<.2	26.5	0.2	4.6	72	<1	15	3	175	33
Foid-bearing trachyte porphyry	OC-27 2087.6	315	2.9	0.4	<1	3.4	5	245	2.5	0.8	<.2	231.0	0.4	56.4	17	5	55	11	1100	17
	OC-41 2249.5	3151	4.3	0.7	<1	2.6	<5	365	1.9	0.8	<.2	183.0	0.9	63.9	20	6	47	8	1030	27
	OC-27 2224.8	565	8.7	0.5	<1	2.6	<5	105	2.3	0.9	<.2	238.0	1.6	84.8	23	4	81	11	1085	210
	OC-41 2238	410	4.3	0.6	<1	2.5	<5	310	2.5	0.8	<.2	182.0	0.8	64.4	26	3	61	9	1000	41
Latite-trachyte porphyry	OC-40 314.5	195	1.7	7.2	<1	11.0	<5	535	4.6	1.2	<.2	55.0	0.6	14.0	17	6	37	5	340	527
	OC-45 404	275	5.2	6.1	2	9.1	5	255	4.0	0.6	<.2	47.8	1.2	19.0	136	50	28	4	315	573
	OC-53 465.5	165	1.4	10.0	<1	9.4	<5	460	4.2	1.2	<.2	53.0	0.6	11.0	134	8	31	4	320	399
	IG-32	43	0.1	6.4	<1	4.5	<5	810	0.8	0.7	<.2	6.4	<.2	1.8	56	<1	10	<2	97	65
	IG-66	81	0.8	7.0	1	13.0	5	820	3.3	1.5	<.2	19.0	0.2	3.0	130	<1	24	3	210	63
	IG-91	51	0.2	5.2	1	6.2	<5	1020	1.5	0.9	<.2	10.0	<.2	2.0	78	<1	<5	2	115	53
	IG-94	51	0.1	9.0	<1	9.4	<5	665	2.1	0.9	<.2	11.0	0.2	2.1	106	1	13	3	155	75
	IG-95	93	0.2	6.5	<1	11.0	5	800	3.5	1.3	<.2	17.0	0.3	2.0	82	2	19	3	200	57
	IG-97	24	0.2	8.3	1	7.5	6	710	1.5	0.9	<.2	8.7	<.2	1.9	100	2	8	3	135	39
	DJ-17	20	0.3	8.4	<1	4.2	<5	805	0.8	0.6	<.2	5.9	0.3	1.9	106	1	11	<2	95	67
	DJ-34	70	0.2	6.5	<1	6.4	<5	720	1.4	1.0	<.2	8.0	0.3	2.3	74	<1	21	2	140	33
	DJ-117	33	0.6	11.0	<1	5.9	<5	644	0.9	0.6	<.2	6.4	0.3	1.4	90	<1	20	3	145	79
	OC-13 1066.6	95	1.3	6.4	1	5.9	<5	760	1.1	0.7	<.2	7.7	0.6	2.3	46	13	16	3	140	87
	OC-12 377	70	1.3	7.0	<1	7.2	<5	820	1.5	1.0	<.2	23.1	0.4	5.6	116	1	17	2	155	85
	OC-12 471	81	0.8	3.7	<1	5.7	<5	855	1.1	0.7	<.2	19.0	0.6	5.2	53	<1	18	<2	160	63
	OC-16 471.7	65	1.1	7.4	<1	6.5	7	645	1.0	0.8	<.2	10.0	0.8	2.3	61	<1	21	3	150	145
	OC-31 564	175	0.7	3.6	1	3.8	<5	260	1.1	0.7	<.2	6.4	0.7	2.1	41	2	31	<2	140	27
	OC-40 661.7	105	0.6	3.8	<1	3.3	<5	625	1.1	<.5	<.2	6.3	0.8	2.3	21	<1	12	<2	120	43

	Sample ID	Rb (ppm)	Sb (ppm)	Sc (ppm)	Se (ppm)	Sm (ppm)	Sn (ppm)	Sr (ppm)	Ta (ppm)	Tb (ppm)	Te (ppm)	Th (ppm)	Tl (ppm)	U (ppm)	V (ppm)	W (ppm)	Y (ppm)	Yb (ppm)	Zr (ppm)	Zn (ppm)
Andesite porphyry	OC-50 1488.8	145	0.7	4.2	<1	4.3	<5	415	1.5	0.5	<.2	6.2	0.6	2.4	41	8	14	<2	140	29
	DJ-13	33	0.3	9.1	<1	7.1	<5	655	1.0	1.3	<.2	9.0	0.4	2.0	87	<1	15	4	140	149
	OC-4 498.3	96	1.1	7.5	<1	6.3	<5	690	1.7	1.2	<.2	8.4	0.9	2.5	70	<1	15	3	150	49
	OC-17 831	290	1.1	8.4	<1	7.6	7	335	1.8	0.9	<.2	10.0	1.8	2.4	82	<1	38	2	170	322
	OC-34 111.8	295	7.2	6.6	<1	6.1	<5	235	1.6	0.7	<.2	11.0	1.5	3.8	66	15	25	<2	210	101
	OC-41 1501	105	0.4	6.2	1	5.3	<5	780	1.2	0.7	<.2	7.8	0.8	2.1	29	<1	15	2	120	41
	OC-49 99.5	83	2.1	5.0	<1	5.6	9	675	1.2	0.7	<.2	8.5	0.8	3.0	59	<1	12	<2	140	63
	OC-67 782	120	0.4	7.0	1	5.9	<5	520	1.3	0.9	<.2	8.4	0.8	2.5	43	<1	21	3	170	41
	OC-33 216	205	1.0	6.2	<1	7.0	6	350	1.4	<.5	<.2	9.4	0.9	3.2	10	7	22	2	195	117
	OC-36 3349.7	155	2.1	7.0	<1	5.6	5	355	1.5	0.9	<.2	9.0	0.5	3.6	40	5	24	3	200	288
	OC-36 608.2	190	0.9	6.7	<1	5.1	6	240	1.4	0.9	<.2	8.5	0.5	3.1	35	13	22	<2	190	1375
	OC-44 107	165	4.4	5.0	2	4.1	<5	220	1.1	0.6	<.2	8.8	1.0	2.3	25	13	43	2	180	51
	OC-27 1514.7	105	0.6	6.6	<1	4.8	<5	575	1.0	0.8	<.2	7.9	0.6	3.2	57	22	10	<2	160	53
	OC-27 2227.6	93	0.8	2.7	<1	2.6	<5	290	0.5	<.5	<.2	13.0	0.4	4.2	23	4	9	3	175	33
	OC-36 850.8	195	0.9	4.1	<1	4.6	<5	390	1.1	0.6	<.2	6.3	0.8	2.1	21	6	21	<2	135	256
	OC-41 1056.4	195	0.5	6.6	<1	5.0	<5	220	1.4	0.9	<.2	7.7	1.0	5.8	66	26	22	3	195	37
	OC-12 291	190	0.8	4.2	<1	3.7	5	320	1.4	<.5	<.2	6.3	1.0	3.0	44	2	19	<2	150	861
	OC-16 594	22	3.8	4.1	<1	8.1	10	185	1.2	1.1	<.2	22.9	0.4	7.4	128	9	23	3	210	1281
	OC-33 406.9	150	1.6	3.4	<1	3.7	<5	335	0.5	<.5	<.2	6.0	0.8	1.8	47	8	30	3	149	81
	OC-34 371	190	1.2	5.0	<1	6.2	<5	315	1.1	0.7	<.2	11.0	0.8	3.7	87	10	19	2	200	272
	OC-36 122.4	195	3.4	8.2	<1	11.0	9	365	2.2	1.0	<.2	11.0	1.0	6.2	47	14	30	3	190	81
	OC-50 1517	185	0.3	3.4	<1	3.5	<5	340	1.6	<.5	<.2	6.9	0.6	1.9	40	9	8	<2	180	3
	OC-13 1058	230	0.6	7.0	2	5.4	<5	265	1.6	0.5	<.2	7.9	0.8	2.2	19	<1	27	2	185	47
	OC-45 1301.8	375	4.2	6.7	1	7.7	9	260	1.6	1.1	<.2	11.0	1.4	3.8	86	20	37	<2	190	59
	OC-41 1270	355	0.4	3.6	<1	3.4	<5	270	1.2	0.5	<.2	7.8	1.6	1.8	11	21	25	<2	175	17
	OC-41 1703.8	130	1.3	2.7	3	2.5	<5	560	0.6	<.5	<.2	11.0	0.8	3.1	15	11	14	<2	120	65
	OC-50 1378	260	0.2	1.8	<1	1.4	<5	350	0.7	<.5	<.2	12.0	1.1	3.2	12	4	20	<2	175	3
	DJ-32	25	<.1	8.7	<1	6.0	<5	490	1.0	0.9	<.2	8.4	0.2	2.5	114	2	18	3	170	45
	DJ-61	90	<.1	4.0	<1	4.1	<5	730	1.2	<.5	<.2	6.5	0.3	2.1	35	<1	10	<2	115	35
Augite monzonite & hornblende-augite monzodiorite	IG-50	68	0.1	9.4	1	10.0	<5	970	3.3	1.4	<0.2	16.0	0.3	3.7	171	<1	25	3	160	93
	IG-54	100	0.3	6.6	<1	9.0	<5	861	2.8	1.3	<.2	27.3	0.6	7.5	107	<1	27	4	230	81
	IG-64	83	0.8	4.7	2	12.0	<5	1230	3.4	1.2	<.2	27.5	0.2	6.4	122	1	17	2	130	35
	IG-44	85	0.6	7.4	<1	11.0	<5	1175	2.7	1.3	<.2	24.5	0.3	6.5	141	2	28	3	150	105
	IG-55	79	0.4	5.2	<1	10.0	5	1200	3.2	1.4	<.2	22.8	0.4	5.9	121	2	25	2	140	105
	IG-90	110	0.8	5.1	<1	16.0	<5	1300	5.4	1.6	<.2	29.7	<.2	7.0	134	<1	36	4	200	103
	IG-101	130	1.2	6.4	1	15.0	<5	1025	5.9	1.8	<.2	46.4	0.3	11.0	122	4	26	3	285	95
Phonotephrite porphyry & phonotephrite	IG-98	64	1.2	11.0	3	10.0	<5	1370	4.1	1.2	<.2	44.6	<.2	13.0	186	<1	15	2	145	79
	IG-99	72	0.6	11.0	<1	15.0	<5	1140	6.5	1.6	<.2	36.9	0.2	8.7	248	2	17	3	135	89
	IG-100	70	0.9	11.0	2	15.0	<5	1150	6.6	1.5	<.2	37.0	0.2	9.5	264	2	19	3	140	91